

**THE DESCRIPTION OF PHYSICO-CHEMICAL
PROCESSES IN COAL MINE SPOILS AND
ASSOCIATED PRODUCTION OF ACID MINE
DRAINAGE**

By

Petrus Johannes Fourie

Thesis

**Submitted in fulfilment of the requirements for the degree Magister Scientiae
in the Faculty of Natural Sciences and Agriculture, Department of
Geohydrology, University of the Free State, Bloemfontein, South Africa.**

Supervisor: Dr. B.H. Usher

MAY 2007

In the first place, there can be no living science unless there is a widespread instinctive conviction in the existence of an Order of Things, and, in particular, of an Order of Nature.

Alfred North Whitehead

ACKNOWLEDGEMENTS

I would hereby like to thank the following people/companies without whom this thesis would not be possible:

- My employer, JMA Consulting (Pty) Ltd, for providing me with all the field data in this study and for using their office facilities.
- Dr. Brent Usher, my study leader, with whom I had valuable discussions on various topics.
- Dr. John Molson, Research Associate from the Department of Civil, Geological and Mining Engineering at École Polytechnique in Montreal, Canada. The PYROX 3 model was kindly made available by Dr. Molson to use in this study.
- Prof. Rene Lefebvre from the Institut National de la Recherche Scientifique Centre Eau, Terre & Environnement in Québec, Canada who gave valuable insights into some aspects of this study through e-mail correspondence.
- My father, Johan Fourie Sr., who meticulously proofread the whole thesis and also Dr. Anneline Meij and Leana van Niekerk who proofread some parts.
- Special thanks to Anneline, Tertius, and my parents, Johan and Alet, for their love and support during this study.
- Thanks to the Lord, Creator of all things, for giving me loved ones and the ability to complete this study.

Table of Contents

1. Introduction	1-1
1.1 Objectives of study	1-1
1.2 Mine operations as a source of Acid Mine Drainage (AMD) in South Africa	1-3
1.2.1 Gold Mining	1-3
1.2.2 Coal Mining	1-4
1.3 The need for the prediction of AMD in South Africa	1-8
1.4 Conceptual model of the processes involved in AMD generation	1-11
1.5 References	1-14

PART I

Theoretical Description of the Physico-chemical Processes in Coal Mine Waste in the Generation of Acid Mine Drainage

2. Mineral reactions, kinetics and thermodynamics	2-1
2.1 Introduction	2-1
2.2 Thermodynamics in AMD chemistry and its application to geochemical modelling	2-2
2.2.1 Chemical potential and the activity of species	2-2
2.2.2 Equilibrium, the equilibrium constant and the saturation index	2-4
2.2.3 Types of equilibrium and geochemical model applications	2-6
2.3 Kinetic mineral dissolution	2-8
2.3.1 Classification of kinetic reactions	2-8
2.3.2 The kinetic rate law	2-9
2.4 Relative mineral activity	2-12
2.5 The classification of the geochemical environment	2-13
2.6 Pyrite	2-17
2.6.1 Morphological forms of pyrite in coal	2-17
2.6.2 The coal deposition environment and formation of syngenetic pyrite	2-19
2.6.3 Pyrite and siderite stability	2-22
2.6.4 Pyrite oxidation reactions	2-28
2.6.5 Kinetic rate of pyrite oxidation	2-32
2.7 Carbonate minerals	2-34
2.7.1 Calcite and dolomite stability and formation in the coal environment	2-34
2.7.2 CO ₂ species and carbonate mineral neutralization reactions	2-37
2.7.3 Reaction Rate of Carbonate Minerals	2-41

2.8	Silicate mineral buffering	2-42
2.8.1	The silicate mineral buffering mechanism	2-42
2.8.2	Silicate mineral dissolution reactions	2-43
2.8.3	Silicate mineral dissolution rates	2-47
2.9	Secondary minerals	2-48
2.10	Final remarks and conclusions	2-50
2.11	References	2-54

3. Oxygen migration into coal mine waste material **3-1**

3.1	Introduction	3-1
3.2	The oxygen diffusion process	3-2
3.2.1	Background	3-2
3.2.2	Thermodynamics of oxygen diffusion	3-3
3.2.3	Flux of molecular diffusion and change of concentration over time	3-8
3.2.4	Fick's Laws in porous material	3-10
3.2.4.1	Incorporating effective diffusivity and porosity into Fick's Laws	3-10
3.2.4.2	The effective diffusion coefficient of oxygen	3-12
3.2.4.3	The diffusion coefficient of oxygen in the pure gaseous and water phases	3-15
3.3	The advective movement of oxygen in coal mine waste material	3-18
3.3.1	Background	3-18
3.3.2	Mechanisms of advection	3-19
3.3.2.1	Convection of air	3-19
3.3.2.2	Barometric pumping due to changes in atmospheric pressures	3-20
3.3.2.3	Varying water saturation in pores	3-21
3.3.2.4	Infiltration of water from the surface	3-21
3.3.3	The Darcy Equation of advective airflow	3-21
3.4	Combining advective and diffusive flow of oxygen in porous media	3-23
3.5	Final comments and conclusions	3-24
3.6	References	3-26

4. Heat flow in coal mine waste material

4.1	Introduction	4-1
4.2	Heat conduction	4-1
4.2.1	Fourier's Law	4-2
4.2.2	Thermal conductivity	4-3
4.2.3	Heat capacity	4-6
4.3	Other heat transfer processes	4-7

4.4	The heat continuity equation for coal mine waste material	4-8
4.5	Spontaneous combustion of coal	4-9
4.6	Final comments and conclusions	4-10
4.7	References	4-11

PART II

Research and Applications to the South African Coal Mine Environment

5 Properties and production of coal discard in South Africa 5-1

5.1	Introduction	5-1
5.2	Coal discard production	5-2
5.2.1	Coal discard as a by-product of coal beneficiation	5-2
5.2.2	Coal discard production and dumping	5-5
5.3	Qualities of discard and potential to generate AMD	5-7
5.3.1	General sulphur and ash content of discard	5-7
5.3.2	Discard mineralogy and acid generation potential	5-8
5.3.3	Mineralogical changes in discard subjected to spontaneous combustion	5-12
5.4	Final remarks and conclusions	5-15
5.5	References	5-18

6 Mineralogy, geochemistry and Acid Base Accounting of coal mine spoils in South Africa 6-1

6.1	Introduction	6-1
6.2	Laboratory tests and analytical methods	6-2
6.2.1	X-Ray Diffraction (XRD) Analysis	6-2
6.2.2	X-ray Fluorescence (XRF) Spectrometry Analyses and Instrumental Neutron Activation Analysis (INAA)	6-3
6.2.3	Acid Base Accounting (ABA) analyses	6-3
6.3	Mineralogy and Acid Base Accounting (ABA) data of coal bearing strata	6-8
6.3.1	Sampling distribution	6-8
6.3.2	Summary of XRD and ABA results	6-9
6.3.3	Interpretation and discussion of results	6-12
6.4	Elemental composition of coal	6-29
6.5	Conclusions	6-37
6.6	References	6-40

7 Case study – Geochemical modelling of Acid Mine Drainage (AMD) from a rehabilitated open-cast colliery	7-1
7.1 Introduction	7-1
7.1.1 Objectives	7-2
7.1.2 Methodology	7-3
7.2 Geology, geomorphology and geohydrology of the mining area	7-4
7.2.1 Regional geology and geomorphology of the Klip River Coalfield	7-4
7.2.2 Local geomorphology and geology	7-9
7.2.3 Groundwater level information	7-14
7.2.4 Background groundwater chemistry	7-17
7.2.4.1 Classification of samples taken from the OBH boreholes	7-21
7.2.4.2 Background groundwater chemistry of the Karoo aquifer	7-26
7.3 Hydrological and hydro-chemical assessment of AMD seepage	7-29
7.3.1 Soil moisture distribution and AMD seepage volume from the unsaturated zone	7-29
7.3.2 Hydro-chemistry of generated AMD	7-31
7.4 Conceptual model, input and assumptions of the geochemical model	7-41
7.4.1 Introduction and objectives	7-41
7.4.2 Conceptual model and methodology	7-41
7.4.3 Model input and assumptions	7-45
7.4.3.1 Oxygen fugacity and pyrite oxidation rate	7-45
7.4.3.2 Pyrite and carbonate mineral content in mine spoils	7-46
7.4.3.3 Silicate minerals	7-50
7.4.3.4 CO ₂ buffer	7-52
7.4.3.5 Model and residence time	7-52
7.4.3.6 Inflowing water quality	7-53
7.4.3.7 Modelling temperature	7-53
7.4.3.8 Secondary minerals	7-54
7.5 Modelling of the oxygen diffusion through the unsaturated zone and the pyrite oxidation rate using PYROX 3	7-55
7.5.1 Objective	7-55
7.5.2 Model Code	7-55
7.5.3 The model input file	7-55
7.5.4 Model calibration and results	7-56
7.6 Geochemical mass model	7-59
7.6.1 The Geochemist’s Workbench (GWB)	7-59
7.6.2 Setup of the geochemical mass model	7-60
7.6.3 Modelling results	7-64

7.7	Conclusions of the geochemical modelling	7-89
7.8	References	7-92
8	Conclusions	8-1
8.1	Overall conclusions of the study	8-1
8.2	Summary of the data required for geochemical modeling of the physico-chemical processes in coal mine waste in future studies	8-5
8.3	Recommendations for future studies	8-8
8.4	References	8-8

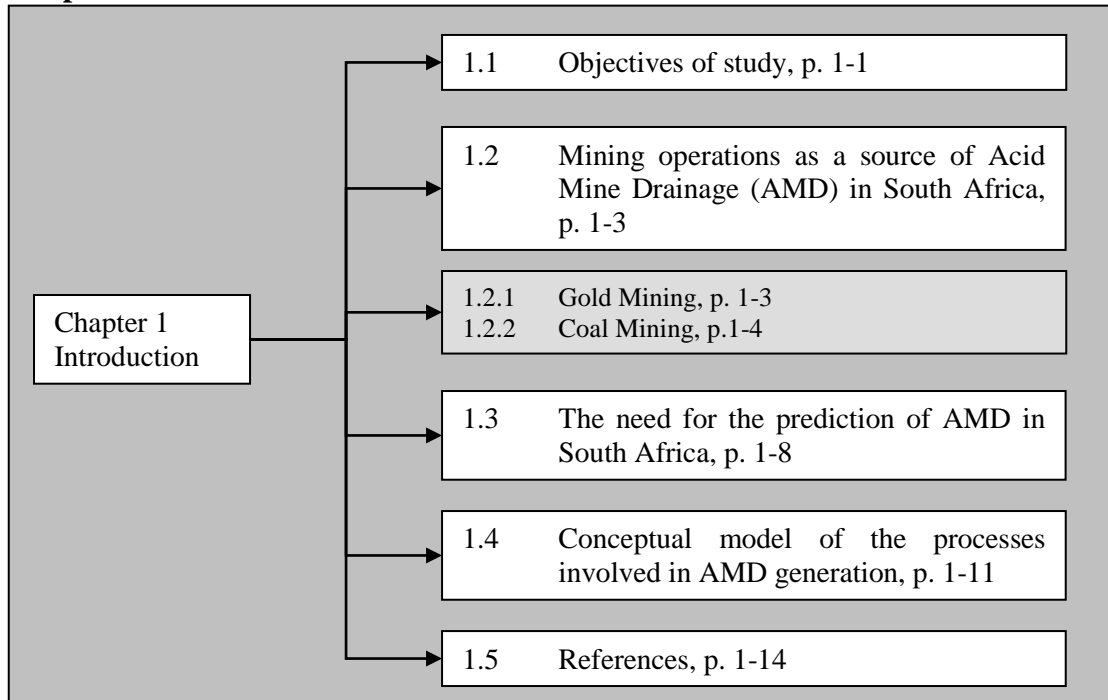
Abstract

Opsomming

Keywords

1 Introduction

Chapter Structure



1.1 Objectives of study

This study comprises of the description, conceptualizing and numerical modelling of the physico-chemical processes in the production of Acid Mine Drainage (AMD) in coal mine waste. Although the thesis title indicates that the AMD processes are described for coal mine spoils, the study was broadened to also include coal mine discard. Both spoils and discard are generally partly in contact with the atmosphere and have similar AMD processes which are described in this study. In general, coal mine spoils make out the largest volume of coal mine waste.

The definition of coal mine spoils (or waste rock) in this study will be limited to *waste rock* that is backfilled into the open-cast pits. Coal discard is defined as the *coarse and fine material discarded from the coal beneficiation process* which is usually dumped on surface or sometimes backfilled together with spoils into open-cast pits. The collective term coal mine waste will be used to refer to both *coal mine spoils* and *coal discard*.

The thesis is separated into two main sections as discussed below:

- PART I (entitled: “*Theoretical description of the Physico-chemical Processes in Coal Mine Waste in the Generation of AMD*”) includes all the literature research done in this study on the physico-chemical processes in coal mine waste including governing mineral reactions, mineral kinetics, thermodynamics, gas migration and heat flow.

- PART II (entitled: “*Research and Applications to the South African Coal Mine Environment*”) includes the description of coal discard and spoil quality in South Africa and the application of modelling techniques.

Objectives of study

The objectives for this study are stipulated below:

- *Conceptual understanding of the physical processes involved in the generation of AMD.*

It is important to conceptualize the most important processes involved directly or indirectly in AMD generation before proceeding to the theoretical description of some of these processes in the proceeding chapters. A conceptual model of the physical processes involved in AMD generation is given in **Section 1.4** below. The conceptual model does not only illustrate the internal processes present in a coal mine waste pile that influence AMD generation, but also the role of the site specific external variables.

- *Description of the physico-chemical processes in the generation of AMD.*

The physico-chemical processes in AMD, as well as their interaction with one another, are described in **Chapter 2 - 4**. In **Chapter 2** the thermodynamics and mineralogical reactions in AMD generation and neutralization, as well as the mineral dissolution kinetics, are described. The aim is to give a thorough description of the interaction of the mineralogy with the gas and water phases. In **Chapter 3** the oxygen migration (diffusion and advection) processes into coal mine waste are described as well as the parameters controlling these processes. In **Chapter 4** heat generation and heat flow through coal mine wastes are discussed. All the processes in AMD generation that are influenced by heat flow are examined.

- *Investigation on the production and quality of coal mine waste in South Africa and its AMD generation potential.*

Geochemical analyses of samples collected from coal discard and coal bearing strata in South African coalfields are discussed in **Chapter 5** and **Chapter 6**, respectively. Whole rock and Acid Base Accounting analyses results of spoils and discard are presented in order to show the potential of coal mine wastes to generate AMD.

- *Simulation of the AMD process through the application of geochemical modelling techniques.*

The physico-chemical processes of AMD are simulated through modelling of the acidic decant at a defunct coal mine in the KwaZulu-Natal province. **Section 7.2** describes the geological, geomorphical and geohydrological background information of the mine. The contaminated water generated by the mine and the seepage volume in the unsaturated zone are assessed in **Section 7.3**. A geochemical model of the mine comprised of various modelling scenarios is given in **Section 7.4 – 7.6**. The model aims to simulate the interaction between the gas, mineral and water phases in the production of the observed AMD from the coal mine. The different modelling scenarios illustrate the sensitivity of the AMD in terms of certain variables

An important part of the case study is to show *how* to apply data to the geochemical model. Furthermore, the shortcomings of the data in the case study will be identified and recommendations will be made for future AMD geochemical modelling studies. This objective is summarized as part of the overall conclusions of the study in **Chapter 8**.

1.2 Mining operations as a source of Acid Mine Drainage (AMD) in South Africa

South Africa has a large and diversified mineral reserve base and the mining industry has been the cornerstone of the country's economy since the late 1800's. The country has more than a third of the world's reserves of alumino-silicates, chromium, gold, manganese, platinum group metals (PGM), vanadium and vermiculite. For these commodities and for antimony, fluorspar, phosphate rock, titanium, zirconium, diamonds, zinc and coal, South Africa is among the world's top five countries in terms of its reserve base (Ringdahl and Oosterhuis, 1998).

Exploitation of the national mineral resource resulted in employment, foreign-exchange earnings, national tax revenues, national infrastructure development and also stimulated the country's secondary industry (Pulles, 2003; Ringdahl and Oosterhuis, 1998).

However, there is also a negative aspect to mining - its impact on the environment. Since South Africa is not a water rich country and is dependent on groundwater for 60% of its water supply, the impact of mining on the country's water resource is of a major concern. AMD plays the most important role in mine water pollution. The largest contributors to AMD in South Africa are the gold and coal mining industry as discussed below (with emphases placed here on coal mining).

1.2.1 Gold Mining

Pulles (1992) states that gold mines discharge 432 000 m³ of mine water daily towards surface and groundwater resources. For example, in the Vaal Barrage catchment it is estimated that gold mining contributes an additional salt load of

398 400 t/a towards the Vaal River (DWAF, 1995). According to Pulles (2003) the contribution to the total salt load of the Vaal River from gold mines can be estimated to be in the order of 60% to 70%.

Gold tailings dumps do not only have a large impact on water and dust pollution but also have a large negative visual impact. According to Robb and Robb (1998) gold tailings dumps cover a total of 40 000 ha in the Witwatersrand basin. Except for the impact on river systems a large environmental concern is the effect of gold mining on the dolomite aquifers of the Transvaal Super Group, which often overlies the gold bearing Witwatersrand Super Group.

The impact on the main river systems and on sensitive aquifers shows that AMD from gold mines are considered to be of an immense concern in South Africa.

1.2.2 Coal Mining

Coal production

South Africa is the fifth largest coal-producing country, with a production of 247 Mt in 2004. About 98% of energy production is through coal combustion, and at the same time, the country is the fourth largest exporter of coal, behind Australia, Indonesia and China in 2005 (DME, 2005).

Almost one third of coal production is destined for foreign markets and virtually all of this is handled through the Richards Bay Coal Terminal (RBCT) which is the world's largest coal export facility. With the implementation of the Sand Duned Coal Terminal (SDCT) an additional export capacity of 20 Mt/a is foreseen that will increase the export capacity in 2008 to 92 Mt/a (DME, 2005). In 2004 South African coal was exported to 34 countries of which 82% to the European Community (DME, 2005).

In 2004 the respective contribution of mined coal by the different coalfields were as follows: Witbank 56.31%, Highveld 19.85%, Waterberg 11.39%, Free State 7.49%, Ermelo 4.23%, Utrecht 0.03%, Nongoma 0.26%, Vryheid 0.26%, Soutpansberg 0.13%, Kangwane 0.01% and Kliprivier 0.03%. The coalfields in South Africa as well as the distribution of operating collieries are shown in **Figure 1.2.2(A)** below.

The Witbank Coalfield is the predominant producer and in spite of the large amount of producing mines located in this coalfield, it still has not reached its production peak (DME, 2005). Most of the large producers, as well as small ones, are viewing this coalfield as offering the most potential for future projects (DME, 2005).

During 2004 open-cast mines provided 52% of the run-of-mine (ROM) production. The remaining 48% was produced by bord-and-pillar (37%), longwall (6%) and stooping (5%) (DME, 2005).

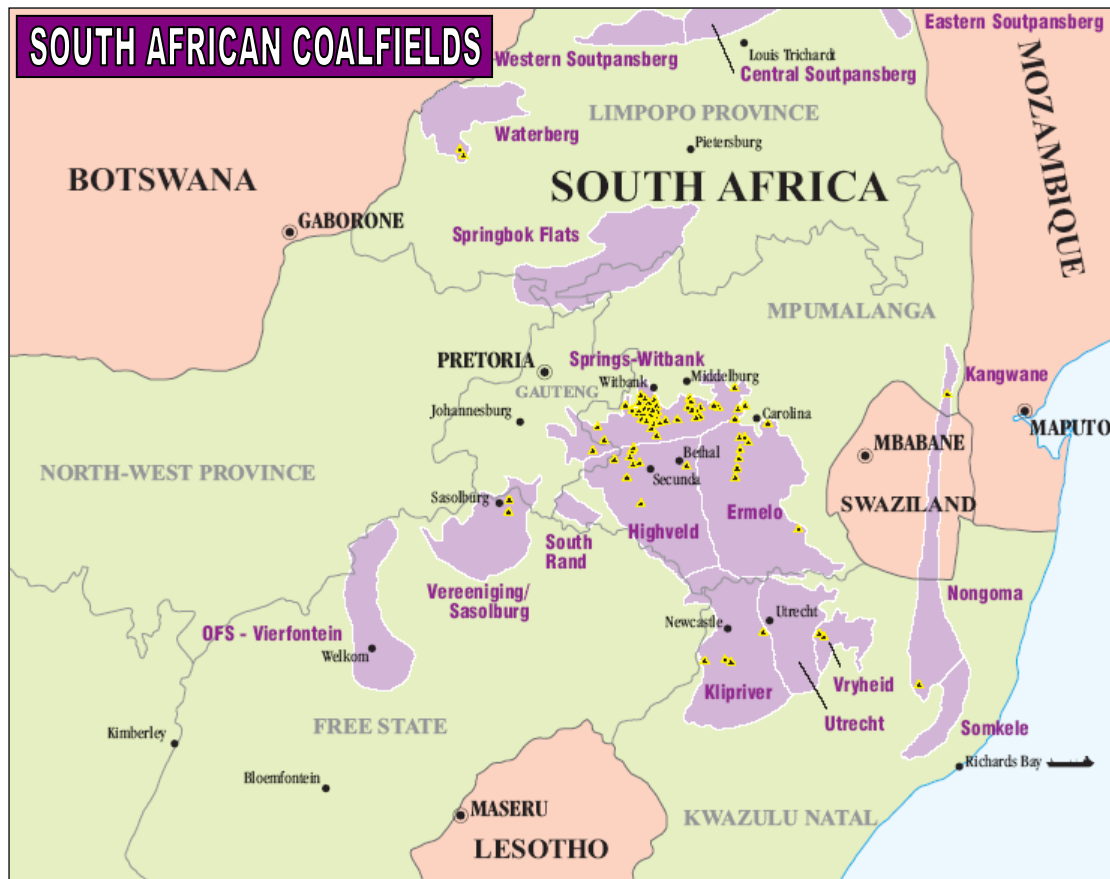


Figure 1.2.2(A). Coalfields in South Africa and location of operating coal mines (indicated as dots) (DME, 2006).

The coals produced in South Africa are of Gondwana type, sometimes with high levels of inherent ash, but low sulphur content (<1% sulphur) (Budge et al., 2000). Quoted coal reserves in South Africa are of bituminous rank and include coals with ash content of >45% (Budge et al., 2000).

Coal mine waste production and areas affected

According to Pulles (2003) the following catchments are the primary areas of coal mining related water pollution:

- 1) The Olifants River catchment in Mpumalanga.
- 2) The Vaal River catchment (upper reaches and Vaal Barrage) in Mpumalanga, Gauteng and the Free State Province.
- 3) The catchments of the Tugela, Mfolozi, Mkuze and Pongola rivers in Kwazulu Natal.

The major active coal mining at present is in the Witbank and Highveld regions that impact primarily on the Olifants River and upper reaches of the Vaal River. Most of the AMD problems in the Kwazulu Natal region stem from defunct mining operations from the last century (Pulles, 2003).

In the Witbank Dam catchment a total sulphate production of 45 – 90 t/d (average 70 t/d) is produced by open-cast mines (Hodgson and Krantz, 1998). Extrapolation of this to include future opencast mines can escalate the sulphate load to an anticipated value of 120 t/d. This translates into a sulphate concentration in the Witbank Dam of 450 mg/l (Hodgson and Krantz, 1998).

The overall water balance for the South African coal mining industry indicates that on average 133 liter water is used for each ton of coal that is mined (Pulles et al., 2001). Pulles et al. (2001) reports that a generic coal mine water balance indicates that daily approximately 200 000 m³ of water is either evaporated or discharged to the surface and groundwater environment.

AMD is generated by coal mine wastes which include 1) spoils backfilled into open-cast mines and 2) coarse and fine coal discard produced from coal beneficiation plants.

Spoil material

A large volume of carbonaceous waste rock material with elevated pyrite content end up as spoils in backfilled open-cast mines. The amount of open-cast mines have increased over the last few decades as it has become economically viable to mine deeper open-cast, especially where multi coal seam mining is possible. Open-cast mining also have a larger water make than underground mining with the result that a larger volume AMD is produced. Respectively 33% and 21% of all operating collieries in 2006 were solely and partly mined open-cast (DME, 2006).

Coal discard

In 1996 there were 58 coal wash plants on different sites and, although a number of mines have shut since that date (e.g. Rietspruit), others have opened and this total is considered effectively correct in 1999 (Budge et al., 2000).

Traditionally, coal beneficiation in South Africa has been kept to the minimum (Budge et al., 2000). An overall higher level of coal beneficiation in South Africa is mostly a response to the demands of the increasingly important export market. Furthermore, in South Africa the largest open-cast mines are strip mined by means of dragline operations. The indirect result of this method (in contrast to selective truck and shovel operations and selective underground mining) is that a larger degree of beneficiation is often required. A higher level of coal beneficiation necessarily implies that a larger volume of discard is produced. The result of the beneficiation of South African coal is the generation of approximately 60 Mt/a of coal discard which is estimated to have already accumulated to more than 1 billion ton (DME, 2002). These large amounts of carbonaceous waste impact negatively on the environment, while it often contains significant amounts of usable coal (DME, 2002).

Coal discard and slurry is often dumped on surface or co-disposed with backfill in open-cast pits. Slurry may also be pumped into underground mines.

Water quality of AMD in South Africa

Discharge from coal mines is either acidic (pH 2.5 - 4.5) or near neutral (pH 5.5 - 8). Constituents often elevated in AMD drainage are Ca, Mg, Na, Fe, Al, Mn and SO₄, with the latter the major contributor to the total dissolved solids. The sulphate concentration from rehabilitated open-cast collieries is at about 2000 mg/l – 3000 mg/l (e.g. Hodgson and Krantz, 1998).

The concentration of sulphate in AMD is often limited by gypsum saturation (e.g. Van Tonder, 2003), and salt load calculations based on the sulphate concentration must be used with caution. Many researchers report a sulphate generation rate of 7 kg/ha/d from open-cast mines in the Witbank Coalfield (e.g. Hodgson and Krantz, 1998; Van Tonder, 2003).

Because of the higher pyrite content in coal discard dumps (see **Chapter 5**) sulphate in effluent from rehabilitated No. 2 coal seam dumps have been observed at average concentrations of 2500 mg/l - 4500 mg/l in the Witbank Coalfield. This, however, may vary from site to site as the discard is produced from different levels of beneficiation. Hodgson and Krantz (1998) reported pH-levels below pH 2.5 and sulphate in excess of 6000 mg/l from sites monitored by them. One dump in the Witbank Coalfield with discard originating from the No. 5 coal seam produce sulphate values in excess of 15 000 mg/l.

Metals elevated in AMD are mostly Fe, Al and Mn with Cd, Cu and Zn also occasionally elevated as described by Hodgson and Krantz (1998). Both Pulles (2003) and Hodgson and Krantz (1998) mention Mn as a persistent element in mine drainage as it may be elevated even in neutral to alkaline drainage.

Low to moderate elevation of Fe, Mn and Al can, however, not be used as definite indicators of AMD since they are often present at high concentrations in the clastic coal bearing strata. Elevation of sulphate is rather used as a more accurate indicator of AMD in South Africa.

Pulles (2003) states that significantly elevated Na is fairly isolated and only a few South African coal mines in certain geographical areas are experiencing elevated Na levels. Hodgson and Krantz (1998) state that Na is higher in the sedimentary rocks of the Highveld Coalfield compared to that in the Witbank Coalfield.

1.3 The need for the prediction of AMD in South Africa

A detailed assessment of prediction techniques of AMD was done by Usher et al. (2001) and the report can be ordered from the website of the Water Research Commission. Prediction techniques consist of 1) the collecting and interpretation of field data (monitoring), 2) laboratory and field experimental methods, and 3) numerical modelling.

The results of AMD prediction must be interpreted in light of the assumptions and limitations of the specific prediction technique. It is important that all experimental techniques and modelling exercises must be validated and calibrated to actual field conditions as far as possible. An assessment of the AMD conditions at adjacent mines (mining the same mineral resource) may give valuable insights into the future AMD conditions at the mine of concern.

Since South Africa is dependent on groundwater for 60% of its water supply, unmitigated pollution of groundwater could have dire consequences for the country's potable water supply. Pollution of water resources by mine water is considered to be one of the most serious and potentially enduring environmental concerns facing the mining industry. An environmental adviser for the South African Chamber of Mines, Mr. N. Lesufi, states in *Mining Weekly*: "*if pollution from mine workings are left unchecked, it could have a significant impact on water quality and be remembered as mining's most harmful legacy*" (Tyrer, 2006). According to Mr. M. du Plessis from the Water Research Commission (WRC) "*mines in a region should combine efforts and develop models and predictions that identify management options to reduce the potential for acid mine drainage as much as possible*" (Tyrer, 2006).

Pulles (2003) states that the issue of being able to reliably predict future water quality from mine operations is "*obviously*" not only for academic interest, but quite fundamental to the ability of mine management to make informed choices between options in terms of their water quality implications.

In practice, the management of AMD in the mining environment would be much more constructive if it could be predicted to a certain degree. Overall, qualitative and quantitative prediction of possible AMD generation has the following functions:

- *Understanding the geochemistry and hydro-chemistry of a system*

AMD prediction (including interpretation of monitoring data, experimental work as well as geochemical modelling) helps to understand the specific geochemical environment and the governing geochemical reactions that are taking place in the system.

- *Planning in the remediation of mining and discard dump areas*

A thorough understanding of the geohydrological and geochemical system is vital for remediation practices. Remediation consists of the following aspects:

- 1) The prevention of effluent from the AMD source as far as possible.
- 2) Control, treatment and reuse of the AMD effluent.
- 3) Rehabilitation of the possibly polluted pathway (e.g. aquifer) and receptor (e.g. surface water feature) from AMD products.

AMD prediction techniques, especially modelling, may help in assessing several remediation options as well as determining the scale of the remediation.

- Mine layout and discard dump footprint planning

Mine layout and discard dump planning must first comply with environmental laws and regulations. Prediction of the quality of AMD at a mine or dump facility together with flow and transport modelling will aid enormously to the placement of mine layouts and discard dumps optimally in terms of its impact on the following aspects:

- 1) Volumes of AMD generated in the mine.
- 2) The surrounding aquifer, including preferential flow zones (i.a. dykes, fault zones) and sensitive aquifers (e.g. dolomite).
- 3) Adjacent mine workings.
- 4) Rivers, streams and wetlands.

- Pollution control management and planning

Prediction of the mine water quality during the operational or post-closure phase of a mine aids in the planning of the necessary pollution control facilities and in constructing rehabilitation strategies. Proper rehabilitation will limit the amount of water infiltration into coal mine wastes and the volumes of AMD therefore generated.

Knowledge of the most probable mine or discard dump water quality range will indicate where a relaxed or a more stringent liner system is required for pollution storage and return water dams.

AMD problems may decrease significantly when sites are mined and reclaimed more rapidly. Rehabilitation results in lower rainfall recharge and also limits oxygen migration into spoils.

- Financial planning

Proof of financial procurement for pollution control is an integral part of the Environmental Management Program Report (EMPR) required by the Mineral and Petroleum Resources Development Act (Act 28 of 2002) for mines in South Africa. Prediction of the potential AMD (volume and quality) produced at a mine aids in the financial planning of the management measures required for water management during the operational and post-closure phases.

- *Scientific preparation of legal documents and impact assessments*

An assessment of the mining impact on the environment is part of several legal documentations required for mining and related water use activities. Prediction of potential AMD production is a fundamental part of the required impact assessment that needs to be performed for a future coal mine. Prediction of AMD will also help the environment consultant/official to assess the impact and to propose constructive mitigation measures.

If mitigation measures could be included in the AMD prediction model, an assessment of the viability and effectiveness of such mitigations could be determined.

Coal mining in South Africa is a mature industry and there is a large number of closed collieries in the country's major coalfields. The challenges faced in closing coal mines should not be underestimated as the potential of AMD generation from coal mines will persist for many years after mining has ceased. In South Africa the number of operating coal mines has declined from 112 in 1986, to 65 in 2004. The condition in which defunct collieries have been left varies greatly from best practice closure to abandonment, with most collieries in the latter category having closed some time ago (Limpitlaw et al., 2005).

The South African legislation requires environmental practices for mines particularly through the Mineral and Petroleum Resources Development Act (Act 28 of 2002), which specifically requires mitigation of the mining related impacts. Before this Act mineral development was governed by the Minerals Act (Act 50 of 1991). The Minerals Act provided the first basis for environmental management, and prior to its passing into law, many mining companies "*used irresponsible mining methods with no regard towards protecting the environment and had often shirked their responsibility towards environmental rehabilitation by leaving an area unrehabilitated prior to them being liquidated or leaving the country*" (Limpitlaw et al., 2005). Mine closures before 1956 were not subject to legislative closure requirements and are now the responsibility of the State (Limpitlaw et al., 2005).

The lag in stipulating environmental sound practices in the South African legislature was partly due to a lack of understanding pollution generated at mines and its implications. It is clear that the understanding and the prediction of AMD are essential in the South African coal mine industry.

1.4 Conceptual model of the processes involved in AMD generation

Before the physico-chemical processes in AMD generation are discussed in **Chapter 2 – 4**, a conceptual model of the physical processes involved in AMD generation is presented in this section.

In coal mine wastes pyrite is present that produces acid, iron species, sulphate and heat upon oxidation. Because the physical exposure of pyrite to oxidizing conditions is the principal limiting factor in the production of AMD, it is clear that several *site specific* physical processes are involved in AMD generation.

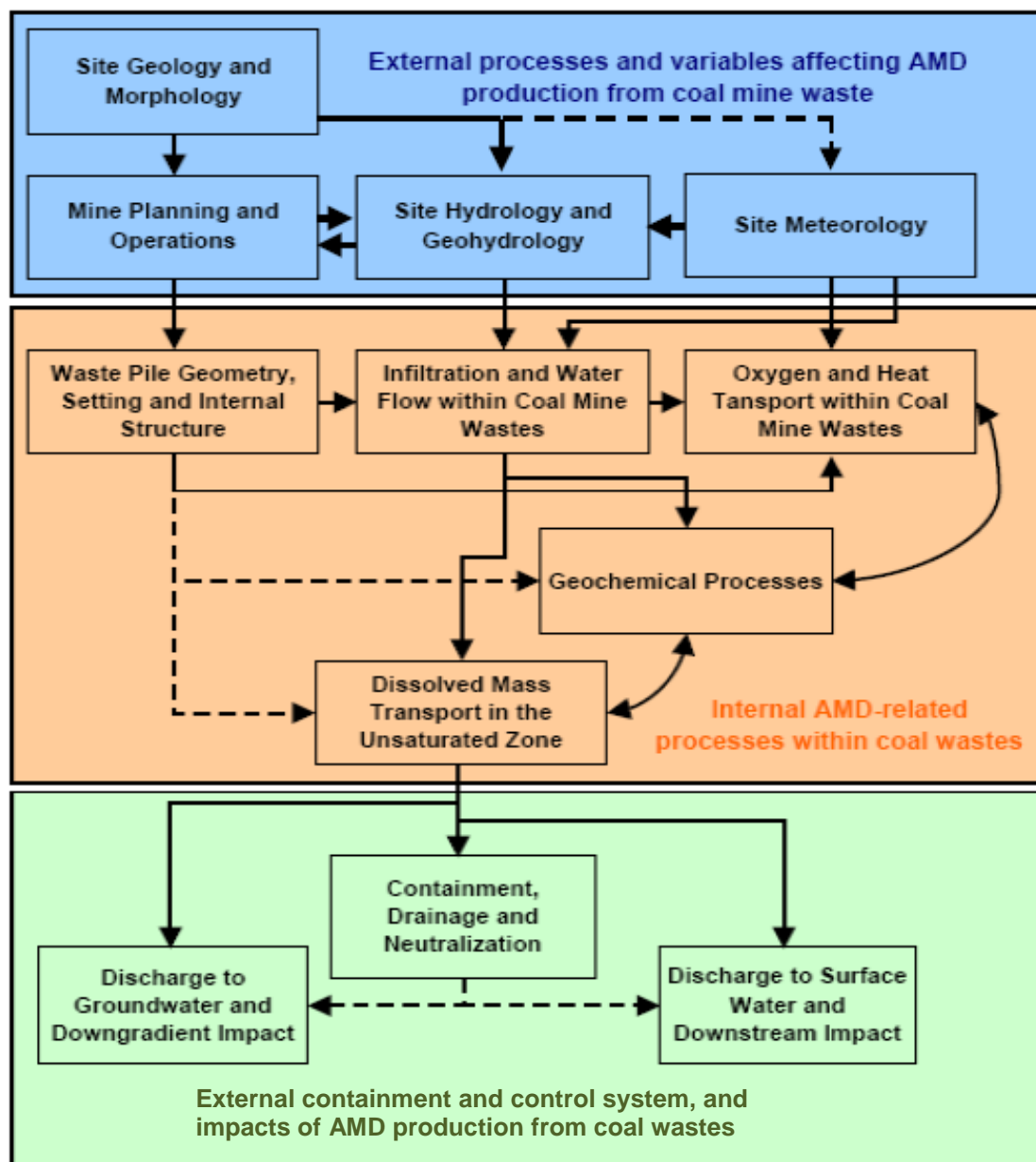


Figure 1.4(A). Coupling of processes affecting acidic drainage (AMD) from coal mine wastes (modified from Levevre et al., 2001, and Hockley et al., 1995).

Following Hockley et al. (1995) and Lefebvre et al. (2001), the physical processes involved in AMD generation can be grouped into three classes as shown in **Figure 1.4(A)** above:

- 1) External processes and variables acting upon coal mine waste.
- 2) Internal AMD-generation processes active within coal mine waste.
- 3) External containment and control systems aimed at the remediation or the limitation of the impact of AMD production from coal mine waste.

As indicated in **Figure 1.4(A)** the coupling between the processes may be one-way (single headed arrows), two-way (double headed arrows) or indirect (dashed arrows). The first part of this study describes the internal processes related to AMD-producing in coal mine waste (**Chapter 2 – 4**), while the case study (**Chapter 7**) elaborates on site specific external and internal processes.

Figure 1.4(B) represents a schematic vertical cross-section through a coal mine waste pile. The oxidation of pyrite results in heat generation that is transferred by conduction, fluid advection (liquid and gas) and diffusion. Latent heat is also generated by water phase changes.

The migration of oxygen can be enhanced by thermally driven gas convection, in addition to gaseous diffusion. Geochemical processes thus directly affect gas and heat transfer processes in coal mine waste piles, which in turn affect the rate of pyrite oxidation and other geochemical processes (Lefebvre et al., 2001); indicating a two-way coupling as shown in **Figure 1.4(A)**.

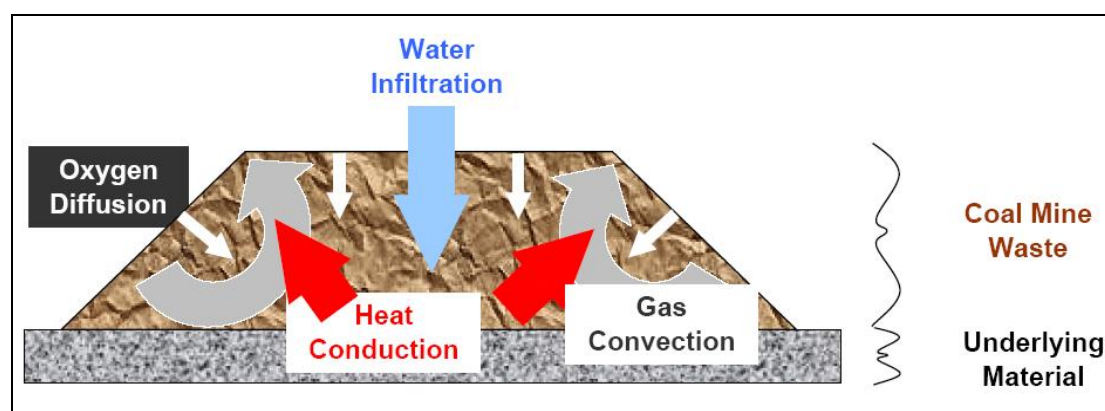


Figure 1.4(B). Conceptual model of the main physical processes acting within coal waste (Lefebvre et al., 2001).

Water entering coal mine waste is mostly rainwater recharge from the top of the waste pile or rehabilitated pit, while groundwater inflow through pit walls also occurs (e.g. Van Tonder et al., 2003; Hodgson and Krantz, 1998). As shown in **Figure 1.4(A)**, the rainfall at a site is slightly influenced by the country morphology whereas the rainfall has a direct influence on the hydrological conditions as well as the amount of infiltrating water on mine wastes which in turn affects the amount of saturation in the wastes. The latter has a direct effect on gas migration into and out of a pit. The

presence of rivers, wetlands and other hydrological features also directly influence mine planning as indicated in **Figure 1.4(A)**.

Typical rainfall recharge ranges in open-cast pits are given by Hodgson and Krantz (1998) in **Table 1.4(A)** below and is based on observations from nine collieries in the Witbank Coalfield:

Table 1.4(A). Recharge on open-cast mines (from Hodgson and Krantz, 1998).

Sources of inflowing water	Rainfall Recharge	
	Range	Suggested Average
Ramps and open cuts	20 – 100%	70%
Unrehabilitated spoils	30 – 80%	60%
Levelled spoils	18 – 37%	25%
Rehabilitated spoils	10 – 25%	18%

A large amount of the water in ramps and open-cuts will evaporate as the average evaporation in the semi-arid South African inland exceeds the average annual rainfall. Water that accumulates on ramps and voids are used for mining and excess water is pumped to evaporation ponds, dirty storm water dams or other pollution control facilities before its quality deteriorates in the pit. Unrehabilitated spoil heaps have a large water make and therefore impact on a large volume of water. Hodgson and Krantz (1998) state that unrehabilitated spoil heaps constitute a significant percentage of the disturbed areas within South African coal mines. A survey by Hodgson and Krantz (1998) of open-cast collieries in the Olifants River catchment (Witbank Coalfield) showed that rehabilitation lags 2 – 10 cuts behind the operating cut per dragline operation. They suggest that rehabilitation should follow within 2 cuts of the operating cut.

The rainfall recharge on coal discard dumps varies considerably due to differences in compaction and rehabilitation. Hodgson and Krantz (1998) state that “*ingress of water into the old dumps is almost unhindered...*” and “*...During rainfall events, very little run-off is observed from these dumps. At burning dumps, the cloud of steam that emanates from the dump is a tell-tale sign that water penetrates into the dumps*”. If coal fines are discarded, it is often pumped as slurry into the centre of a coal discard dump. The compacted discard forms a wall around the central slurry impoundment where excess water is drained through a penstock and returned to the beneficiation plant. Slurry is sometimes pumped onto the un-compacted discard coal resulting in a matrix, which does not require intensive compacting, to form a non-oxidising condition within the dump. If slurry is pumped to dump facilities it will contribute to the in-situ water make of the dump. Although a large amount of the water component

of the slurry is returned to the plant, a large amount will be contained in pores (\pm 40% porosity) and a large volume will leach to the underlying aquifer.

Hodgson and Krantz (1998) state that the groundwater inflow into an open-cast mine pit ranges from 2 – 15%, averaging at 10% of the total pit water make. Van Tonder et al. (2003) report the groundwater inflow into a rehabilitated open-cast mine in the Witbank Coalfield to be at 15% of the total pit water make. The amount of groundwater inflow into an open-cast pit is dependent on the mine layout geometry as well as on the geology (the surrounding aquifer) and is therefore very site specific (see **Figure 1.4(A)**). During the operational phase the groundwater inflow will initially form a large part (up to 30 – 60%) of the total pit water make due to the initial long influx length between the mine and the aquifer. As the mining progresses and a larger area is subjected to rainwater recharge, the groundwater component will decrease relative to the total mine water make to 10 – 20%.

Water that infiltrates into the coal mine waste interacts with the rock and is enriched in the AMD generation products. Mass transport in the liquid phase and geochemical processes are affecting each other and exhibit two-way coupling (Levebvre et al., 2001). The infiltrating water affects geochemical processes which in turn supply the mass transported by the infiltrating water. When saturated, secondary minerals will also precipitate from the infiltrating water.

The setting, geometry and properties of the coal mine waste have a direct impact on the magnitude of liquid, gas and heat transfer processes and therefore an indirect impact on the geochemical processes and the water quality in the coal mine waste.

Coal mine waste is therefore a complex system involving coupled physical processes: multiphase flow, heat transfer, and mass transfer in the liquid phase (advection) and in the gas phase (advection and diffusion) (Levebvre et al., 2001). In terms of modelling numerical simulation is required to handle all these processes and to understand their interaction.

1.5 References

Budge, G., Brough, J., Knight, J., Woodruff, D. and McNamara, L. (2000). *Review of the Worldwide Status of Coal Preparation Technology*. Report No. COAL R199. Department of Trade and Industry, UK.

Department of Minerals and Energy (2006). *Coal*. Internet: <http://www.dme.gov.za/energy/coal.stm>

Department of Minerals and Energy (2005). *South Africa's Mineral Industry 2004/2005*. 22nd Revised Edition, Directorate: Mineral Economics, Pretoria.

Department of Minerals and Energy (2002). *The national inventory discard and duff coal: 2001 summary report*. Directorate: Mineral Economics, Pretoria. Internet: http://www.dme.gov.za/energy/coal/coal_discard_report.pdf

Department of Water Affairs and Forestry (1995). *Impact of Witwatersrand gold mines on water quality in the Vaal Barrage catchment*. Phase 1: Preliminary situation analyses.

Hockley, D., Delaney, T. and Smolensky, J. (1995). *Modelling acid drainage from waste rock piles*. Steffen Robertson and Kirsten (Canada) Inc. Report S1202P9, MEND Program Report prepared for B.C. Ministry of Energy, Mines and Petroleum Resources and Environment Canada, October 1995.

Hodgson, F.D.I. and Krantz, R.M. (1998). *Groundwater Quality Deterioration in the Olifants River Catchment above the Loskop Dam with specialised investigation in the Witbank Dam Sub-Catchment*. WRC Report No. 291/1/98, Water Research Commission, Pretoria.

Lefebvre, R., Hockley, Smolensky, J. and Gelinas, P. (2001). *Multiphase transfer processes in waste rock piles producing acid mine drainage 1: Conceptual model and system characterization*. Journal of Contaminant Hydrology, 52: 137 – 164.

Limpitlaw, D., Aken, M., Lodewijks, H. and Viljoen, J. (2005). *Post-mining rehabilitation, land use and pollution at collieries in South Africa*. Presented at the Colloquium: Sustainable Development in the Life of Coal Mining, Boksburg, 13 July 2005.

Pulles, W. (2003). *The status of mine water pollution in South Africa*. 6th ICARD conference, Cairns, QLD, 12 – 18 July 2003.

Pulles, W., Boer, R.H. and Nel, S. (2001). *A generic water balance for the South African coal mining industry*. WRC Report no. 801/1/2001, Water Research Commission, Pretoria.

Pulles, W. (1992). *Water pollution: its management and control in the South African mining industry*. Journal of the Mine Ventilation Society of South Africa, 45(2): 17-36.

Ringdahl, P and Oosterhuis, W.R. (1998). *An overview of the South African minerals industry*. In: *Mineral resources of South Africa*. (Eds: M. G. C. Wilson and C. R. Anhaeusser), Handbook 16, Council for Geoscience, pp 689.

Robb, V.M. and Robb, L.J. (1998). *Mining in South Africa: Legislation and environmental considerations*. In: *Mineral resources of South Africa*. (Eds: M. G. C. Wilson and C. R. Anhaeusser), Handbook 16, Council for Geoscience, pp 689.

Tyrer, L. (2006). *Lack of action on mine-water pollution could cause environmental catastrophe*. Mining News, 2006/08/14.

Usher, B.H., Cruywagen, L-M., De Necker, N. and Hodgson, F.D.I (2001). *On-site and laboratory Investigations of Spoil in Opencast Collieries and the development of Acid-Base Accounting Procedures*. Water Research Commission, Pretoria.

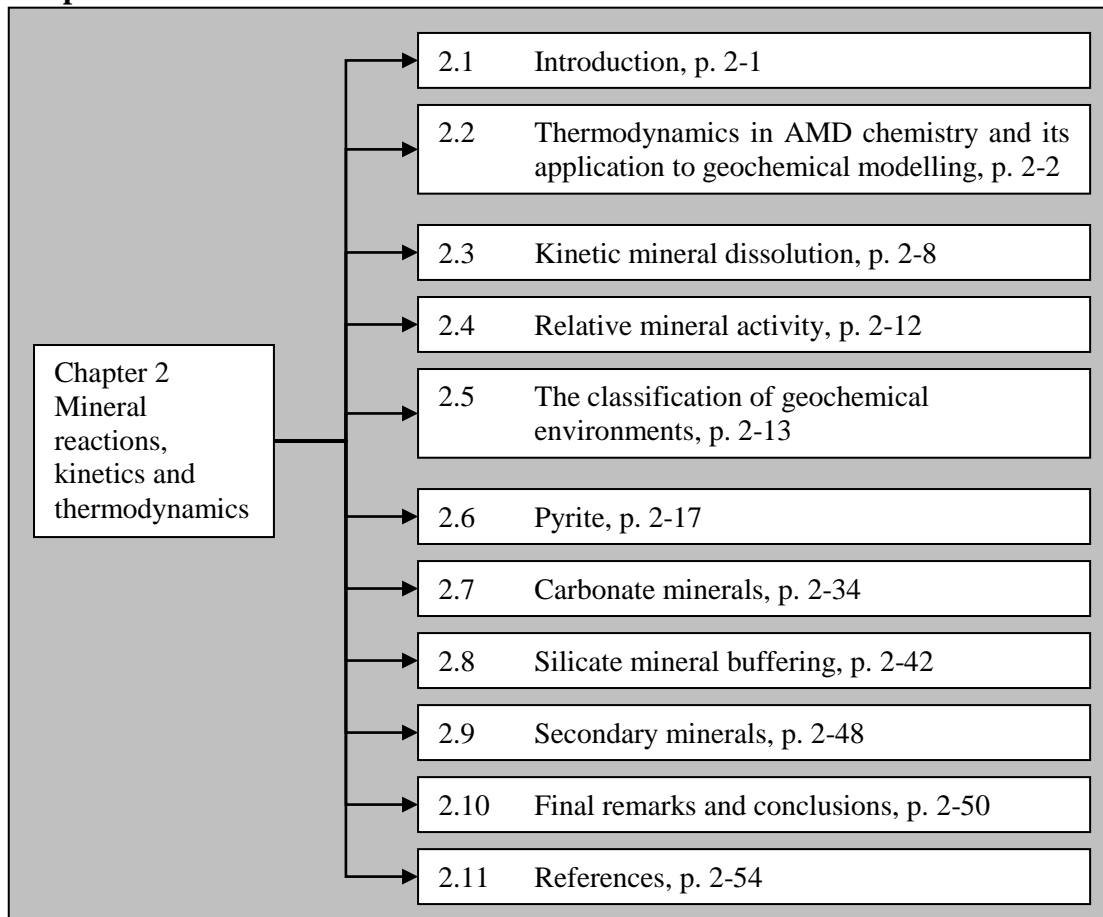
Van Tonder, G., Vermeulen, D., Cogho, V. and Kleynhans, J. (2003). *Initial prediction of the decant rate and sulfate concentration from rehabilitated open-cast coal mines in South Africa*. 6th ICARD Conference, Cairns, QLD, 12 – 18 July 2003.

PART I

Theoretical Description of the Physico-chemical
Processes in Coal Mine Waste in the Generation of
Acid Mine Drainage

2 Mineral reactions, kinetics and thermodynamics

Chapter Structure



2.1 Introduction

Coal mine waste is a heterogeneous system and consists of a solid, water and gas phase. Without one of these phases no AMD production and drainage is possible. In this chapter mineralogical reactions and interaction with the water and gas phases are reviewed.

The coal mine waste material (a solid phase) is the reactive part of the three phases and contains pyrite that reacts spontaneously with oxygen and water. Water and oxygen take part directly in the oxidation process of pyrite, and water also serves as a transport medium for the products of AMD. The water phase also serves as the medium in which dissolution of neutralizing minerals such as calcite and dolomite can take place. Consumption of oxygen leads to a gradient in oxygen fugacity in the coal mine waste pile that initiates oxygen diffusion. As the temperature in the waste rises with the oxidation of pyrite, differences in temperature leads to differences in gas pressure that initiate advection.

From the above discussion it is apparent that coal mine waste is a complex system with interdependent processes that create several challenges for geochemical

modelling. Numerical modelling of the interaction between the three phases that create (and neutralize) AMD rely heavily on thermodynamics. Kinetics is now also often included in thermodynamic models in order to model the reactions over the dimension of time. It depends on the modeller whether kinetic mineral reactions have to be included into the model. This will of course depend on the objective of the modelling exercise, the conceptualization of the problem by the modeller and, on the other hand, no model is unique and the same result may be obtained using different methods (Bethke, 1996).

Nordstrom and Munoz (1994) state: “*Thermodynamics is the study of energy and its transformations. Kinetics is the study of the rates and mechanisms of reactions. Thermodynamics tells us which geochemical processes are possible, whereas kinetics tells us which processes are the fastest*”.

2.2 Thermodynamics in AMD chemistry and its application to geochemical modelling

2.2.1 Chemical potential and the activity of species

Differences in chemical potential μ are the driving force behind chemical reactions. The change of the Gibbs free energy with temperature, pressure and constituents is given by the differential equation (Appelo and Postma, 1993):

$$d\Delta G = -\Delta SdT + \Delta VdP + \sum_i \mu_i dn_i \quad \text{Eq. 2.2.1(A)}$$

where ΔG is the Gibbs free energy that is liberated with each mole of i ($\text{J}\cdot\text{mol}^{-1}$) that reacts, ΔS is the entropy change of the reaction, T is absolute temperature (K), ΔV is the change in molar volume ($\text{cm}^3\cdot\text{mol}^{-1}$), P is pressure (atm), μ_i is the chemical potential of specie i ($\text{J}\cdot\text{mol}^{-1}$) and n_i is the moles of i .

The chemical potential indicates the change in the Gibbs free energy at a constant temperature and pressure if the amount of a constituent i varies while all the other constituents remain constant ($dT = 0$ and $dP = 0$):

$$\mu_i = \left(\frac{\partial \Delta G}{\partial n_i} \right)_{T,P,n_{j \neq i}} \quad \text{Eq. 2.2.1(B)}$$

In **Section 3.2** the following relation was derived from the ideal gas law and **Equation 2.2.1(A)**:

$$\mu_i = \mu_i^0 + RT \ln(P_i / P_i^0) \quad \text{Eq. 2.2.1(C)}$$

where R is the gas constant ($8.314 \text{ J}\cdot\text{K}^{-1}\cdot\text{mol}^{-1}$).

Equation 2.2.1(C) gives a simple relationship between chemical potential and gas pressure under isothermal conditions. The state of the gas at the reference pressure P^0 and reference chemical potential μ_i^0 is called the standard state. The convention is that $P^0 = 1$ atm and μ_i^0 is obtained from tabulated values of standard potential. Raoult's law states that the vapour pressure P_i of a gas in a mixture is proportional to its mole fraction X_i :

$$P_i = X_i P_i^0 \quad \text{Eq. 2.2.1(D)}$$

where P_i^0 is the vapour pressure of the pure component i .

The molecular interpretation of Raoult's Law is straightforward: a vapour pressure is a direct measurement of the escaping tendency of a gaseous component from a solution. Non-interaction between species forms the molecular framework for the ideal-solution concept: an ideal solution is defined as one that obeys Raoult's law for all compositions.

Combining **Equation 2.2.1(C)** and **Equation 2.2.1(D)** gives:

$$\mu_i = \mu_i^0 + RT \ln X_i \quad \text{Eq. 2.2.1(E)}$$

where X_i is the mole fraction of a gas or aqueous constituent under ideal conditions.

The standard state has been chosen such that the system behaves ideally and obeys the ideal law for gases and can be expressed simply in terms of the mole fraction of the liquid.

If the system is not ideal, a "fudge factor" called the activity coefficient, γ , is introduced (Zhu and Anderson, 2002):

For solid and liquid solutions:

$$a_i = X_i \gamma_{Ri}$$

For gaseous solutions:

$$a_i = \frac{P_i \gamma_{fi}}{f_i}$$

For aqueous solutions:

$$a_i = m_i \gamma_{Hi}$$

where a_i is the activity of any substance i , X_i is the mole fraction, P_i is the partial pressure, f_i is the fugacity and m_i the molality. The activity coefficients γ_{Ri} , γ_{fi} and γ_{Hi} are measures of the deviation from the ideal behaviour of a substance i from Raoult's law, the ideal gas law and Henry's law, respectively.

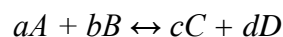
Equation 2.2.1(E) for the non-ideal state therefore becomes:

$$\mu_i = \mu_i^0 + RT \ln a_i \quad \text{Eq. 2.2.1(F)}$$

where a_i is the activity of substance i and μ_i^0 is defined as the standard state of a hypothetical one-molal solution in which activity and molality are equal and the species properties have been extrapolated to infinite dilution.

2.2.2 Equilibrium, the equilibrium constant and the saturation index

The chemical potential indicates the change in the free energy at a constant temperature and pressure of a constituent i as defined in **Equation 2.2.1(B)**. The chemical reaction:



is written in terms of **Equation 2.2.1(F)** as follows:

$$\begin{aligned} \Delta\mu_R - \Delta\mu_R^0 &= RT[c \ln a_C + d \ln a_D - a \ln a_A - b \ln a_B] \\ &= RT \ln \frac{a_C^c a_D^d}{a_A^a a_B^b} \\ &= RT \ln Q \end{aligned} \quad \text{Eq. 2.2.2(A)}$$

where

$$\begin{aligned} \Delta\mu_R^0 &= \Delta G_R^0 = c \mu_C^0 + d \mu_D^0 - a \mu_A^0 - b \mu_B^0 \\ \Delta\mu_R &= \Delta G_R = c \mu_C + d \mu_D - a \mu_A - b \mu_B \end{aligned}$$

and $Q = \frac{a_C^c a_D^d}{a_A^a a_B^b}$ is the reaction quotient.

It is evident that $RT \ln Q$ is a term which measures the difference between ΔG_R^0 , the tabulated or standard state Gibbs energy of reaction, and ΔG_R , the *real* Gibbs energy of the reaction.

A system is said to be in equilibrium when none of its properties change with time. From this definition it is obvious that no environmental system is in equilibrium.

However, the intuitive idea is that all systems will spontaneously lower their energy content to the lowest possible level. Zhu and Anderson (2002) compare chemical equilibrium to mechanical systems; just as mechanical systems spontaneously lower their potential energy, chemical systems spontaneously lower their free energy (Gibbs energy) – weights will fall until they can fall no further and reactions will proceed until they reach equilibrium.

The change in the free energy of the reaction $aA + bB \leftrightarrow cC + dD$ can be written as:

$$\Delta G_R = \Delta G_A + \Delta G_B - \Delta G_C - \Delta G_D \quad \text{Eq. 2.2.2(B)}$$

and is illustrated in **Figure 2.2.2(A)** below:

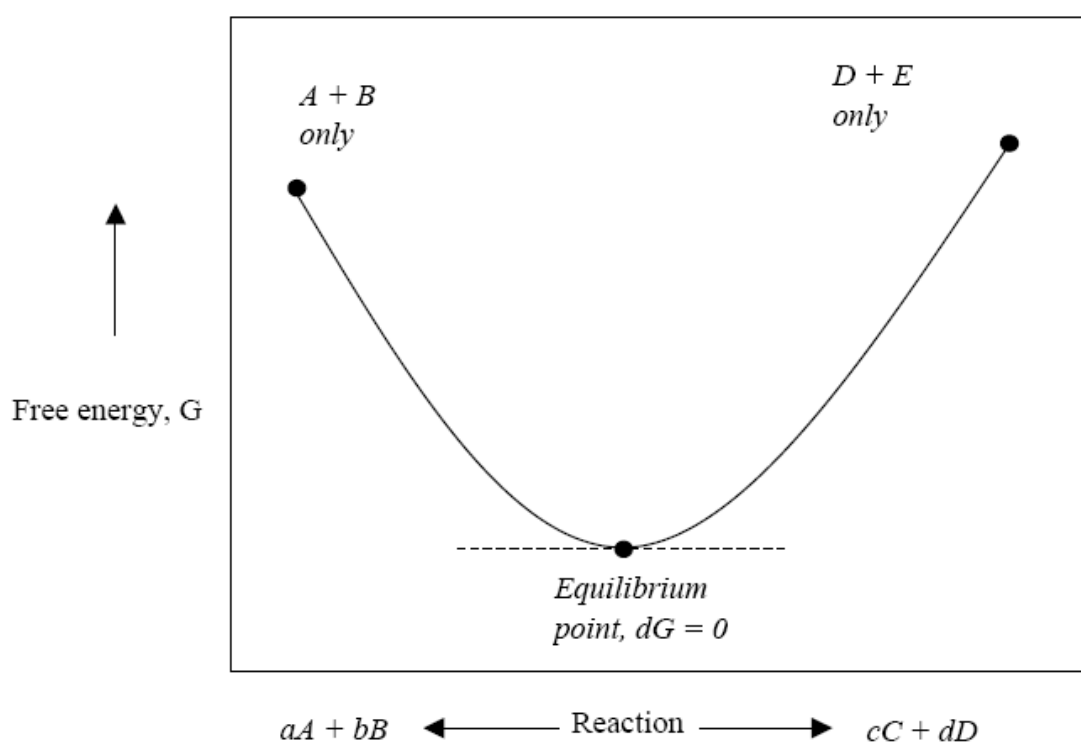


Figure 2.2.2(A). Variation in the free energy with reaction progress (edited from Bethke, 1996).

At the equilibrium point the change in the free energy of the reaction is zero:

$$\Delta G_R = \Delta G_A + \Delta G_B - \Delta G_C - \Delta G_D = 0 \quad \text{Eq. 2.2.2(C)}$$

and **Equation 2.2.1(F)** can be written as:

$$\begin{aligned} \Delta \mu_R^0 &= -RT \ln \frac{a_C^c a_D^d}{a_A^a a_B^b} \\ &= -RT \ln K \end{aligned} \quad \text{Eq. 2.2.2(D)}$$

where the equilibrium constant $K = \frac{a_C^c a_D^d}{a_A^a a_B^b}$ has replaced the reaction quotient Q at the equilibrium point $\Delta G_R = 0$.

The relation $Q/K = \Omega$ indicates in which direction a reversible chemical reaction will proceed in order to minimize the change in free energy of the reaction. If Q is smaller than K ($\Omega < 1$) the products will be favoured and if larger ($\Omega > 1$) the reactants; if $Q = K$ ($\Omega = 1$) then equilibrium is reached.

To indicate the precipitation or dissolution of a mineral the term saturation index SI is introduced and is expressed as $SI = \log \Omega$. Therefore, if SI is negative the mineral will dissolve, if positive, it will precipitate and if $SI = 0$, it is at equilibrium.

2.2.3 Types of equilibrium and geochemical model applications

A system is said to be in (complete) equilibrium when it occupies a specific region of space within which there is no spontaneous tendency for change to occur (Bethke, 1996). Because full equilibrium is seldom or never reached in nature, pseudo-equilibrium types are often conceptually defined as follow:

Types of pseudo-equilibrium (Bethke, 1996):

“A system is in *metastable equilibrium* when one or more reactions proceed toward equilibrium at rates that are vanishingly small on the time scale of interest. For instance the dissolution of a mineral (e.g. quartz) may be too slow to be in equilibrium with groundwater with a short residence time in an aquifer.”

“*Partial equilibrium* is where only a part of a system is in equilibrium. For example may a fluid in a sandstone aquifer be in equilibrium with itself, but not in equilibrium with the mineral matrix.”

“*Local equilibrium* is obtained when a small enough portion of a system is considered to be in equilibrium with itself. This idea is useful when the temperature, mineralogy or fluid chemistry varies across a system.”

What is the status of acid mine drainage in terms of equilibrium? How does a geochemical model that usually relies heavily on equilibrium tend to describe AMD systems?

Firstly, the source of the AMD production must be considered. Pyrite and carbonate mineral concentrations in the spoil material of a backfilled open-cast mine are highly variable. In a coal mine waste dump the pyrite and carbonate mineral content would also vary as the different parts of the waste dump represent different years of mining

and different parts of the mine. Within a single mine-site, the differences in mineral type and content relate to the lateral and vertical differences of the palaeo-environment. Some parts of the palaeo-basin (now the coal reserve) were typically more subjected to stable reducing conditions than shallower parts during peatification. Epigenetically deposition of minerals also shows high variance throughout a coal reserve.

Furthermore, different parts of the coal mine waste will be at different stages of AMD generation and buffering because of differences in 1) the age of the waste, 2) oxygen fugacity, and 3) the water saturation over the dimensions of the waste pile. Except for these differences over the larger mine-site (or waste rock pile), each pyrite grain may also be oxidized in its own microenvironment where bacteria are attached to pyrite surfaces and create their own conditions favourable to oxidation (see **Section 2.6.4**).

As seen from the above discussion, the heterogeneity in a coal mine waste varies both on the micro- and macro-scale. It is evident that due to the heterogeneity, *full chemical equilibrium is not possible* in coal mine waste; rather the *heterogeneity will initiate transient conditions*. The coal and the associated pyrite formed under sulphidic-anoxic conditions, therefore, the pyrite in the coal mine waste, is in disequilibrium with the oxidizing environment during and after mining. Because of this disequilibrium, the coal mine waste is reactive and the heterogeneous system will generate AMD. From a modelling perspective an *average* composition of the disequilibrium system is defined in an attempt to model the overall AMD generation.

In the *average* composition several types of (pseudo-) equilibrium states are modelled:

- Complete equilibrium with the water composition is often assumed for fast reacting minerals such as calcite, dolomite and secondary minerals such as gypsum and $\text{Fe}(\text{OH})_3$. (Calcite and dolomite may also be introduced as kinetic minerals as will be discussed in **Section 2.7** below).
- Very slow reacting or precipitating minerals are often not included or are *suppressed* (not introduced) in the geochemical model. It is therefore assumed that the system is in partial equilibrium excluding some minerals that remain in their metastable equilibrium state for long enough periods.
- A case of local equilibrium is also assumed: although the system is heterogeneous in its composition and therefore in its disequilibrium state over the waste extent, an *average* equilibrium is assumed and modelled. Coal mine waste is also open to infiltrating rain water or inflowing groundwater and modelling of the composition of the water flowing-through, also assumes local equilibrium.

Applying the above pseudo-equilibrium states solves many of the problems involved in the modelling of a system that is not in full equilibrium with its environment. One

problem still remains; that is the modelling of the minerals that 1) do not react fast enough to be in equilibrium with the water composition, or 2) do not react slowly enough to be excluded from the geochemical model. This includes important minerals such as pyrite that cannot comfortably be included into one of the pseudo-equilibrium schemes. For this purpose it is necessary to introduce kinetic rates for mineral reactions.

2.3 Kinetic mineral dissolution

2.3.1 Classification of kinetic reactions

Bethke (1996) states that in studying dissolution and precipitation, geochemists commonly consider that a reaction proceeds in five generalized steps:

- 1) Diffusion of reactant from the bulk fluid to the mineral surface.
- 2) Adsorption of the reactants onto reactive sites.
- 3) A chemical reaction involving the breaking and creation of bonds.
- 4) Desorption of the reaction products.
- 5) Diffusion of the products from the mineral surface to the bulk fluid.

The adsorption and desorption processes (steps 2 and 4) are almost certainly rapid, so two classes of rate limiting steps are possible: if the reaction rate depends on how quickly reactants can reach the surface by aqueous diffusion and how quickly the products can move away from it (steps 1 and 5) the reaction is said to be “transport controlled”; if, on the other hand, the speed of the surface reaction (step 3) controls the rate, the reaction is termed “surface controlled” (Bethke, 1996).

Brantley (2003) states that for dissolution or precipitation of silicates under ambient conditions, many authors assume that the surface reaction is rate-limiting in both the laboratory and in the field; however, others have suggested that transport control related to differences in hydrology, may explain slower rates observed in the field.

Where a reaction is rate-limited by the surface reaction, ion detachment is slow, and portions of the mineral surface may selectively dissolve, resulting in etch pits. Etch pits are considered by some to be evidence of a surface controlled reaction (Brantley, 2003). For such a condition, it is suggested that the concentration of solution at the mineral-solution interface is equal to that in the bulk solution because transport is fast compared to the surface reaction (Brantley, 2003).

Lüttge et al. (1999) mapped the breaking of bonds (Step 3) and the resultant formation of etch pits on an anorthite surface as shown in **Figure 2.3.1(A)** below:

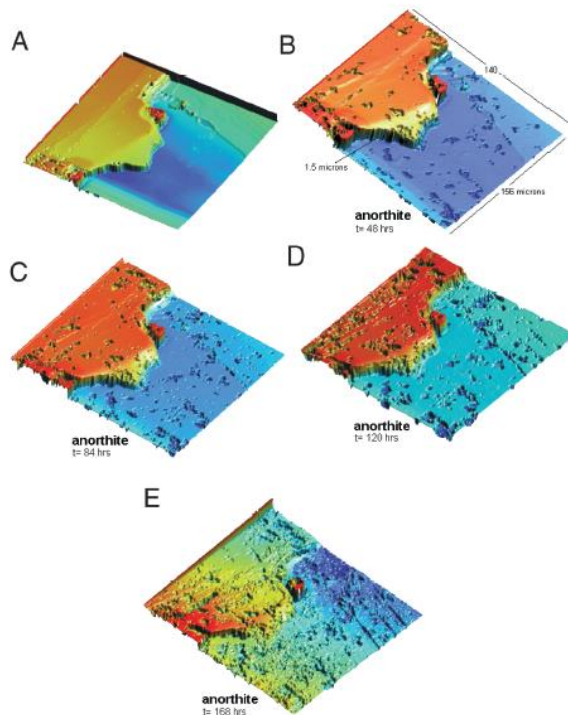


**Figure 2.3.1(A).
Dissolution on
anorthite surface and
the formation of etch
pits (from Lüttge et
al., 1999).**

In contrast, where reactions are rate-controlled by diffusion, mineral surfaces are expected to be rounded and devoid of etch pits, because the concentration at the mineral-solution interface is expected to approach equilibrium and only the highly energetic sites (e.g. corners, edges) should dissolve (Brantley, 2003). Although many authors have inferred surface control from the presence of etch pits, etch pits can form on minerals even when dissolved under conditions where rates of diffusion affect the rate of dissolution (Brantley, 2003). The presence or absence of etch pits may therefore not prove the rate-limiting step of dissolution. One distinguishing difference between transport and surface control of dissolution is the activation energy E_a of a reaction. The activation energy for a surface controlled reaction is much larger than for any transport controlled reaction.

2.3.2 The kinetic rate law

Surface controlled kinetic reactions are expressed by kinetic laws. Bethke (1996) states that, despite the apparent authority in its name, no single “rate law” describes how quickly a mineral precipitates or dissolves. Different parameters control a mineral dissolution reaction and the precise dependency on these parameters is difficult to measure and often varies from one laboratory to the next, and between the laboratory and the field (e.g. Brantley, 2003).

An appropriate rate law r_a for mineral a that is adequate for most geochemical modelling purposes is expressed as follows:

$$r_a = -A_s k_+ \prod (a_i)^n [I - \Omega] \quad \text{Eq. 2.3.2(A)}$$

where

A_s is the mineral surface area (cm^2);

k_+ is the forward rate constant ($\text{mol}\cdot\text{cm}^{-2}\cdot\text{s}^{-1}$);

a is the activity of basis species i to the power of n ; and

Ω is the ratio between the reaction quotient (Q) and the equilibrium constant (K).

The extent of disequilibrium is expressed by the term $[1 - \Omega]$. Thus, for undersaturation $1 - \Omega$ must range from near 1 ($Q \ll K$) to 0 ($Q = K$), but for saturation it can range from 0 ($Q = K$) to numbers substantially <-1 ($Q \gg K$) for supersaturation. For surface controlled reactions far from equilibrium, Ω often tends to be near zero for dissolution reactions.

The reactive surface area of a mineral is a large uncertainty when using kinetic data. According to Appelo and Postma (1993) estimation of the surface area for field situations has hardly passed the stage of reasonable guessing.

The geometric surface of a mineral can be estimated assuming that the mineral particles are smooth surfaced spheres. Geometric surface area is calculated using the following formula:

$$A_{s(\text{GEOM})} = 6/\rho \times d$$

where $A_{s(\text{GEOM})}$ is the geometric surface area ($\text{m}^2\cdot\text{g}^{-1}$), ρ is the grain density ($\text{g}\cdot\text{cm}^{-3}$) and d the grain diameter (μm).

The total surface area of a bulk sample could be determined by experimental methods using either gas adsorption in dry conditions (e.g. BET technique) or selective molecular absorption in aqueous suspensions. However, authors report variable success in using experimental determined surface areas for mineral kinetics. For instance Lüttge et al. (1999) states that using the experimental BET-determined surface area may be reasonably used for silicates and alumino-silicates, however, dolomite dissolution show less positive application of the BET surface area for carbonates.

BET determined surface areas are much higher than geometric surface areas due the inclusion of sub-microscopic surface roughness and crevices (Appelo and Postma, 1993).

The BET surface area can be expressed as

$$A_{s(\text{BET})} = \Omega \times A_{s(\text{GEOM})}$$

where $A_{s(\text{BET})}$ is the BET surface area ($\text{m}^2\cdot\text{g}^{-1}$) and Ω the surface roughness.

The surface area may actually increase during dissolution because of etching which will subsequently influence the kinetic rate of the mineral. The initial surface area of each primary mineral could be calculated by multiplying its volume fraction with the total surface area. From the total surface area, the surface area of a specific mineral i during any time of modelling could be calculated by the following equation:

$$A_s = A_s^o \left(\frac{V_f}{V_f^o} \right)$$

where

A_s is the mineral surface area (cm²);

A_s^o is the initial mineral surface area (cm²);

V_f is the volume fraction; and

V_f^o is the initial volume fraction.

The rate constant k can be related to temperature by the Arrhenius equation:

$$k = Ae^{-E_a/RT_k}$$

where

A is the pre-exponential or frequency factor (mol.cm⁻².s⁻¹),

E_a is the activation energy (J.mol⁻¹),

R is the gas constant (8.314 J. K⁻¹mol⁻¹), and

T_k is absolute temperature (K).

The rate constant k depends on the temperature, which can be explained by the Collision Theory. The Collision Theory assumes that for a reaction to occur, reactant molecules must collide with an energy greater than some minimum value and with the proper orientation (Ebbing, 1996). Ebbing (1996) states that the rate constant for a reaction is given as a product of three factors:

- 1) The collision frequency.
- 2) The fraction of collisions having energy greater than the activation energy.
- 3) The fraction of collisions that occur with the reactant molecules properly orientated.

The collision frequency increases only slightly with temperature, but the proper orientation of the reactant molecules is independent of temperature. The product of 1) and 3) is therefore the frequency of collisions with proper orientation and is called the frequency factor or the Arrhenius pre-exponential factor, A (mol.cm⁻².s⁻¹).

The fraction of collisions having energy greater than the activation energy of the reaction is highly dependent on the temperature and is related to the activation energy as e^{-E_a/RT_k} . The activation energy E_a is the minimum energy of collision required for

the molecules to react. Reactions with large activation energies have small rate constants and reactions with small activation energies have large rate constants.

Only the forward dissolution reaction of minerals is considered in this study. A large amount of kinetic data has been reported in literature for mineral dissolution, but not for precipitation reactions. Precipitation data do not exist for most minerals, because in mineral precipitation experiments, undesired metastable reaction products usually precipitate instead of the desired mineral (Palandri and Kharaka, 2004).

2.4 Relative mineral activity

For modelling purposes, mineral reactions rates fall into three groups (Bethke, 2003)

- 1) Reaction rates of minerals may be so slow relative to the time period of interest that the reaction can be ignored together.
- 2) Rates are fast enough to maintain equilibrium.
- 3) Mineral reaction rates that don't fall within one of the above groups. These minerals require a kinetic description if incorporated into the model.

A table of relative reactivity of neutralizing minerals (at pH 5) that has been widely quoted is that of Sverdrup (1990):

Table 2.4(A). Relative mineral reactivity at pH 5 (after Sverdrup, 1990, and Kwong, 1993a and 1993b).

MINERAL GROUP	TYPICAL MINERALS	RELATIVE REACTIVITY AT pH 5
Dissolving	Calcite, aragonite, dolomite, magnesite, brucite.	1.0
Fast weathering	Anorthite, nepheline, olivine, jadeite, leucite, spodumene, diopside, wollastonite.	0.6
Intermediate weathering	Epidote, zoisite, enstatite, hypersthene, augite, hedenbergite, hornblende, glaucophane, tremolite, actinolite, anthophyllite, serpentine, chrysotile, talc, chlorite, biotite.	0.4
Slow weathering	Albite, oligoclase, labradorite, montmorillonite, vermiculite, gibbsite, kaolinite.	0.02

Very slow weathering	K-feldspars, muscovite.	0.01
Inert	Quartz, rutile, zircon.	0.004

In **Chapter 6** the minerals typically found in the South African coalfields are discussed. Some minerals will play a more important role in directing acid generation or neutralization reactions because of their higher reactivity.

Kwong (1993a) has suggested that all of the minerals in the Dissolving, Fast Weathering and Intermediate groups (relative reactivity of 1.0, 0.6 and 0.4, respectively) listed in **Table 2.4(A)** can be considered as having practical neutralizing capability in the field.

AMD in the coal mine environment is the result of the oxidation of pyrite. The reactivity of pyrite cannot be classified into the above table as pyrite oxidation is dependent on the concentrations of ferric iron, acidity and oxygen in the surrounding solution. Pyrite activity must therefore be assessed in terms of the geochemical environment present.

2.5 The classification of the geochemical environment

The geochemical palaeo-environment varied laterally and vertically within the coal measures of a single mine-site. The minerals in coal originally formed in order to approach thermodynamical stability in the palaeo-environment. The formed minerals will often remain for millions of years thereafter in an approximate metastable state until the geochemical environment changes significantly and a transport medium (water) is available for dissolution. AMD is therefore a direct result of a difference between the palaeo-environment and the geochemical environment created by mining.

Reduction and oxidation processes play a major role in the distribution of oxygen, metal (e.g iron, manganese) species, sulphur, nitrogen, carbon and various other species in the natural environment. Sequences of important redox processes at pH 7 in natural systems are given in **Figure 2.5(A)** below:

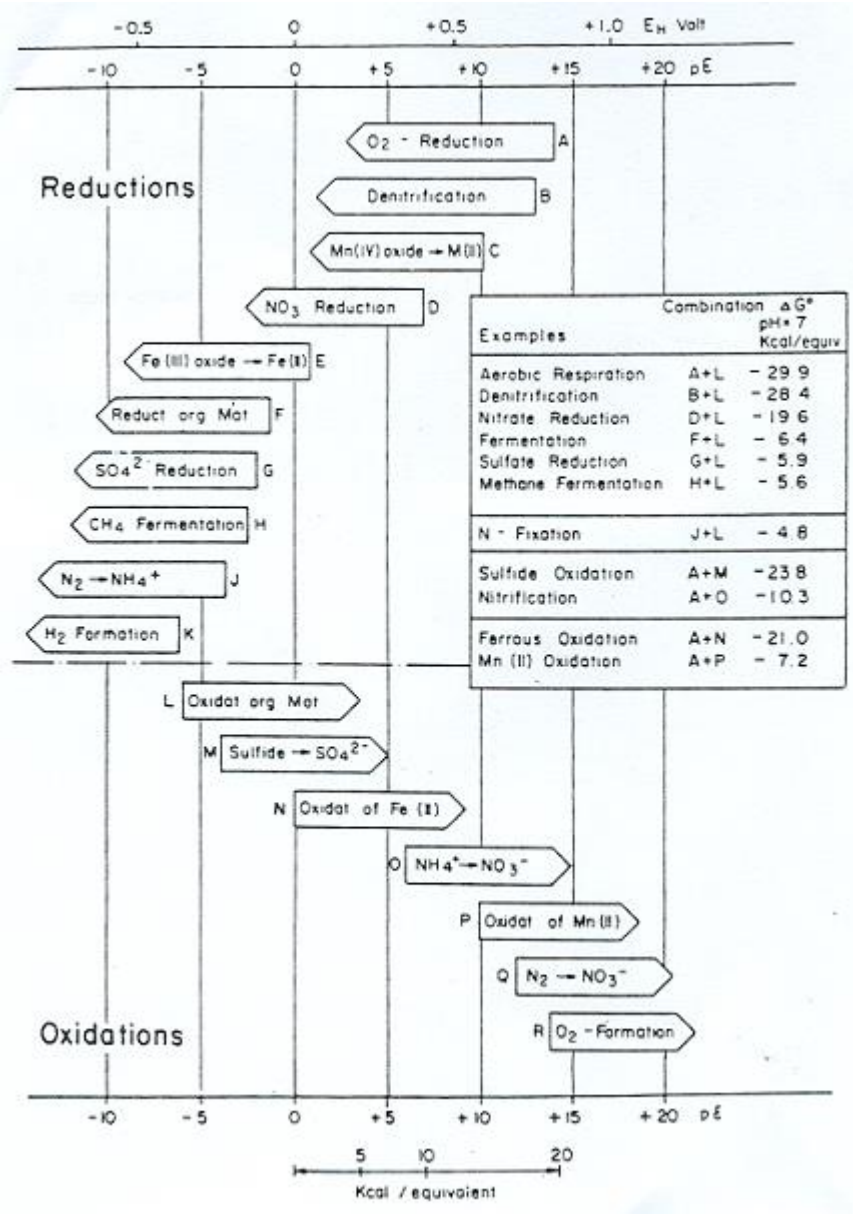


Figure 2.5(A). Sequences of redox reactions (at pH 7) in the natural environment (Stumm and Morgan, 1981).

In the above figure it is shown that oxygen reduces before manganese-oxides, which is followed by nitrate, iron-oxides, organic matter, sulphate etc.

The type of geochemical environment is critical in order to determine what redox mineral reactions are present in a system. Berner (1981) noted that dissolved O_2 and H_2S can be easily measured down to about 10^{-6} M. These two species are very useful in identifying the geochemical environment:

- They are very strongly tied to redox reactions.
- Their concentrations have significant effects on organisms.
- They exert a major amount of control on the formation of authigenic minerals.

- They cannot coexist: $\text{H}_2\text{S}(\text{aq}) + 2\text{O}_2(\text{aq}) \rightarrow \text{SO}_4^{2-} + 2\text{H}^+$.
- Bacteria divide neatly into aerobes (killed by H_2S) and anaerobes (killed by oxygen). (Under this classification, facultative bacteria are considered to be aerobes.)

The geochemical environment can therefore be separated firstly into the oxic ($\text{O}_2 \geq 10^{-6} \text{ M}$) and anoxic ($\text{O}_2 \leq 10^{-6} \text{ M}$) zones. The anoxic environment can further be subdivided into the anoxic-sulphidic zone ($\text{H}_2\text{S} \geq 10^{-6} \text{ M}$), the post-oxic zone ($\text{H}_2\text{S} < 10^{-6} \text{ M}$) and the anoxic-methanic zone (significant CH_4 , $\text{H}_2\text{S} < 10^{-6} \text{ M}$). A description of each geochemical environment is given in **Table 2.5(A)** below:

Table 2.5(A). Description of geochemical environments (modified from Appelo and Postma, 1993; based on Berner, 1981).

Geochemical Environment	Solid phases in sediments and typical reactions
<p style="text-align: center;">Oxic</p> <p style="text-align: center;">$\text{O}_2 \geq 10^{-6} \text{ M}$</p>	<p>Some solid phases added to sediments:</p> <p>Ferrihydrite, hematite, goethite, MnO_2-type minerals; no organic matter.</p> <p>Some typical reactions:</p> <p>$\text{O}_2 + \text{Organics}^* \rightarrow \text{H}_2\text{O} + \text{CO}_2 + \text{HNO}_3 + \text{H}_3\text{PO}_4$ Aerobic respiration.</p> <p>$3.75\text{O}_{2(\text{aq})} + \text{FeS}_2 + 3.5\text{H}_2\text{O} \rightarrow \text{Fe}(\text{OH})_3 + 2\text{SO}_4^{2-} + 4\text{H}^+$ $\text{O}_{2(\text{aq})} + 4\text{FeCO}_3 + 10\text{H}_2\text{O} \rightarrow 4\text{Fe}(\text{OH})_3 + 4\text{H}^+ + 4\text{HCO}_3^-$ Hematite form not directly at low temperature. When the ferrihydrite ($\text{FeOOH} \cdot \text{H}_2\text{O}$) later accumulates in soils and sediments under dry conditions, it may eventually dehydrate and recrystallize to form more thermodynamically stable goethite and hematite, especially when the temperature increases: $\text{Fe}(\text{OH})_3 \rightarrow \text{Goethite} + \text{H}_2\text{O}$ $2\text{Goethite} \rightarrow \text{Hematite} + \text{H}_2\text{O}$</p> <p>$\text{O}_{2(\text{aq})} + \text{MnS} \rightarrow \text{Mn}^{2+} + \text{SO}_4^{2-}$ Mn^{2+} is present in solution over a wide oxidation range under acidic to slightly alkaline pH conditions. $\text{O}_{2(\text{aq})} + 2\text{H}_2\text{O} + 2\text{Mn}^{2+} \rightarrow 2\text{MnO}_2 + 4\text{H}^+$ Under neutral to alkaline and strongly oxidizing conditions.</p>

<p>Anoxic-sulphidic</p> <p>$O_2 < 10^{-6} \text{ M}$ $H_2S \geq 10^{-6} \text{ M}$</p>	<p>Some solid phases added to sediments:</p> <p>Pyrite, marcasite, mackinawite, alabandite, chalcopyrite, rhodocrosite (stable over a wide Eh range), organic matter.</p> <p>Some typical reactions:</p> <p>Before sulphate reduction occurs, reduction of Mn-oxides, NO_3 (to N_2) and Fe(III)-(hydr)oxides take place within the post-oxic zone (below) that often precedes the anoxic-sulphidic zone if these oxidants are significantly present. Enough organic matter must remain for sulphate reduction through bacterial working:</p> $SO_4^{2-} + \text{Organics}^* \rightarrow H_2O + CO_2 + NH_4^+ + H_3PO_4 + H_2S$ $Fe^{2+} + H_2S(aq) \rightarrow FeS + 2 H^+ \text{ (fast)}$ $FeS + S^0 \rightarrow FeS_2 \text{ (slow)}$ $FeS(aq) + H_2S \rightarrow FeS_2 + H_2 \text{ (fast)}$
<p>(Anoxic non-sulphidic)</p> <p>Post-oxic</p> <p>(Low organics)</p> <p>$O_2 < 10^{-6} \text{ M}$ $H_2S < 10^{-6} \text{ M}$</p>	<p>Some solid phases added to sediments:</p> <p>Glauconite, and other Fe^{2+} and Fe^{3+} silicates; also some siderite, vivianite, rhodocrosite; no sulphide minerals; minor organic matter.</p> <p>Some typical reactions:</p> <p>The postoxic zone is dominated by the reduction of nitrate, Mn-oxides and Fe-oxides:</p> $NO_3 + \text{Organics}^* \rightarrow H_2O + CO_2 + N_2 \text{ (or } NH_4^+) + H_3PO_4$ $MnO_2 + \text{Organics}^* + H^+ \rightarrow Mn^{2+} + H_2O + CO_2 + N_2 \text{ (or } NH_4^+) + H_3PO_4$ $Fe(III)\text{-(hydr)oxides} + \text{Organics}^* + H^+ \rightarrow Fe^{2+} + H_2O + CO_2 + N_2 \text{ (or } NH_4^+) + H_3PO_4$ <p>Since the organic material is low, some oxidizing species remain in solution. If enough organic material remains then reduction of sulphate will proceed that will indicate the start of the anoxic-sulphidic zone. If no (or very little) sulphate is present in solution but enough organic matter remains, then the system will proceed into the anoxic-methanic zone.</p>
<p>(Anoxic non-sulphidic)</p> <p>Anoxic-Methanic</p> <p>(High organics)</p> <p>$O_2 < 10^{-6} \text{ M}$ $H_2S < 10^{-6} \text{ M}$</p>	<p>Some solid phases added to sediments:</p> <p>Siderite, vivianite, rhodocrosite, earlier formed sulphide minerals; organic matter.</p> <p>Some typical reactions:</p> $\text{Organics}^* \rightarrow H_2O + CO_2 + CH_4 + NH_4^+ + H_3PO_4 + H_2$ <p>e.g. $CH_3COOH \rightarrow CO_2 + CH_4$</p> $\text{Carbohydrates} + H_2O \rightarrow \text{formic acid} + H_2$ $4H_2 + CO_2 \rightarrow CH_4 + 2H_2O$ <p>Since the organic material is low, some oxidizing species remain in solution. If enough organic material remains all ferric iron will be used up and reduction of sulphate will proceed that will indicate the start of the anoxic-sulphidic zone. If no (or very little) sulphate is present in solution but enough organic matter remains, the system will proceed into the anoxic-methanic zone.</p>

*Where organic matter is approximately $(CH_2O)_{106}(NH_3)_{16}(H_3PO_4)$.

With regard to **Table 2.5(A)**, the following comments could be made:

- In sediments it is generally observed that redox processes proceed sequentially from the highest to the lowest energy as shown in **Table 2.5(A)** above. In the case where say both Mn- and Fe-oxides are reduced by organics, the produced Fe^{2+} would reduce Mn-oxide by a fast reaction and precipitate as $\text{Fe}(\text{OH})_3$. The overall process would therefore become MnO_2 reduction, until MnO_2 is exhausted and reduction of Fe-oxides takes over (Appelo and Postma, 1993).
- The sequence of redox reactions with a decreasing energy yield is also found for microbial mediated reactions; for example the sulphate reducing bacteria *Desulfovibrio* sp. is an obligate anaerobe which first becomes active when anoxic conditions have been reached (Appelo and Postma, 1993).
- Not all zones need to be necessarily present in a groundwater environment and the presence and absence of any zone is dependent on the presence or absence of the oxidants. For instance an aquifer is mostly devoid of any significant organic matter and will therefore not proceed past the post-oxic zone. In a wetland organic matter is high and sulphate reduction is often evident through the smell of H_2S gas. Now, if no Mn(IV) and Fe(III) are present, then the anoxic-sulphidic zone may directly follow below the oxic zone, however a small post-oxic zone is at least usually present. On the other hand, if no sulphate is present, then the anoxic-methanic zone may directly follow the postoxic zone.

2.6 Pyrite

2.6.1 Morphological forms of pyrite in coal

Pyrite occurs in several different morphological forms and grain sizes, from crystals invisible to the eye up to specimens of several inches. Two major forms of pyrite are distinguished: 1) framboidal pyrite, which is very fine grained, and 2) larger euhedral pyrite.

The term framboid, from the French *framboise*, refers to the characteristic raspberry-like morphology of the texture (Butler and Rickard, 2000). Essentially, a framboid is a spherical or sub-spherical structure composed of numerous (10^2 to 10^5) equidimensional microcrystals (Butler and Rickard, 2000). In sediments, framboids show a positively skewed size distribution with a modal size within the range 1 – 10 μm , and rare examples in excess of 50 μm in diameter.

Framboidal pyrite formed under high pyrite saturation conditions with the result that the pyrite nucleation was faster than crystal growth. Euhedral pyrite formed under lower pyrite saturation where crystal growth dominated over nucleation (Butler and Rickard, 2000) – see **Section 2.6.2** below.

The framboidal form is considered highly reactive and is characterized by a small grain size and large surface area (Caruccio et al., 1977). Euhedral pyrite has a much larger grain size of at least $>50\ \mu\text{m}$ in diameter with no apparent sub-grain structures and are therefore referred to as monolithic (Holuszko et al., 1992).

Disordered and ordered framboid pyrite as well as massive and disseminated euhedral pyrite is shown in **Figure 2.6.1(A) – (C)** below:

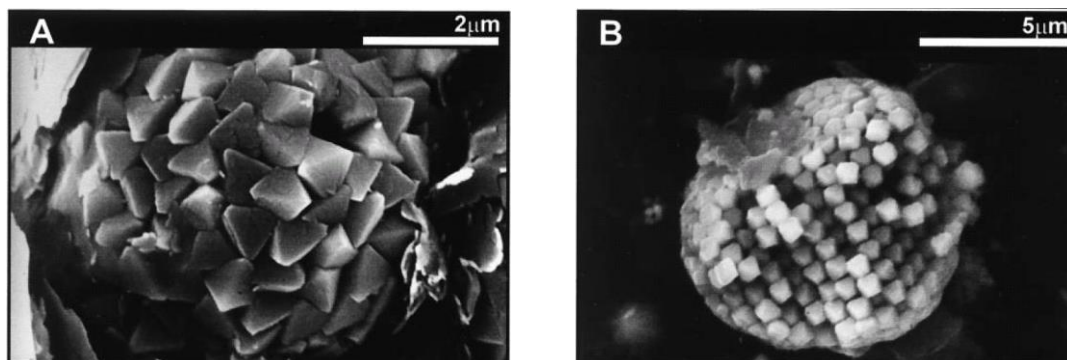


Figure 2.6.1. Disordered (A) and ordered (B) framboidal pyrite from the Chattanooga Shale, Upper Devonian, USA (Butler and Rickard, 2000). The general range of framboid morphology, and the diversity of environments in which they form, indicate a robust formation mechanism.



Figure 2.6.1(C). Massive and disseminated euhedral pyrite from the Leeuwpan Colliery, eastern Witbank Coalfield¹.

¹ Samples were obtained from Coert van Ryneveldt, geologist at Leeuwpan Colliery.

The large differences in pyrite morphology (crystal size, mass and surface area) within a single mine-site complicate beneficiation of coal, geochemical sampling and modelling. One of the primary uncertainties in geochemical modelling relates to the fact that only a few geochemical samples from a mine-site is taken that is thought to be representative of the whole mine.

2.6.2 The coal deposition environment and formation of syngenetic pyrite

pH status of the depositional palaeo-environment

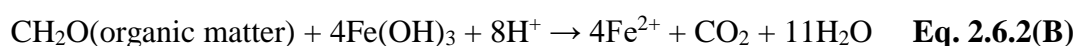
Except for low Eh conditions Renton and Bird (1991) state that coal is also deposited under low pH conditions with suppressed bacteriological working. Acidic conditions prevail in swamps due to the presence of humic/fulvic acids. However, Gondwana coal was deposited during colder climatic conditions than the Laurasian coal of the northern hemisphere. Cairncross and Cadle (1987) state that although low pH conditions were not present during the deposition of Witbank coal, the colder climate did ensure that bacteriological working was reduced.

Less acidic conditions, lowered water table, and the fact that plant material accumulated on a stable, passive margin that prevented subsidence and burial of the peat, led to the fact that most of the South African coal has a higher ash and inertinite content compared to the coal of the northern hemisphere (Cadle et al., 1990). The generally higher vitrinite content of the Natal coals is a function of the more distal setting of the peat swamps and accelerated rates of platform subsidence (sustaining higher water table levels) brought about by higher rates of differential compaction and proximity to the unstable edge of the Kaapvaal Craton (Cadle et al., 1990).

Overall, swamp water is acidic because of the presence of humic and fulvic acids that originate from decaying plant material. Because of a changing water level, plant material at the top of the accumulating peat mass undergoes some oxidation that also introduces carbonic acid into the swamp:



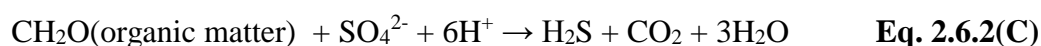
Reduction of ferric iron by Fe^{3+} -reducing bacteria would be required before SO_4 -reducing bacteria would be able to prevail over Fe-reducers as shown in **Table 2.5(A)**. Organic matter is used by microbial Fe-reducing bacteria to reduce $\text{Fe}(\text{OH})_3$ or other ferric compounds to produce ferrous iron in solution:



Experimental studies performed by Morse and Wang (1997) also found accelerated reaction of goethite with the introduction of organic matter.

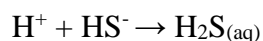
Sources of sulphur in the palaeo-environment

Organic sulphur is C-bonded (e.g. sulphate esters) or non-C-bonded (e.g. organic acids). Organic sulphur is quickly mineralised (conversion of organic S to inorganic forms) as microbes use or convert it. In an oxic environment plant material is oxidized and sulphur is released into solution. A stream (or sea, if the coal were deposited under shallow marine conditions) may also introduce sulphur-rich water into the swamp. After all oxygen is depleted organic matter and sulphur may further be used by S-reducing bacteria (e.g. *Desulfovibrio* sp.) as follows in an anoxic-sulphidic environment:



According to Holuszko et al. (1992) iron sulphides can only form in peat as a result of bacterial activity, since there is not enough energy for chemical reduction of sulphates to disulphide. Microbial activity becomes increasingly effective above a pH of approximately pH 4.5 which is necessary for disulphide formation.

In a reducing environment sulphur will be present as HS^- under neutral to alkaline conditions and as H_2S under acidic conditions. HS^- will also be converted to H_2S as the swamp water acidifies:

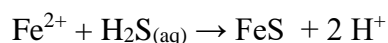


Pyrite crystallization

Pyrite will form in an anoxic-sulphidic environment as shown in **Table 2.5(A)**. Two major forms of pyrite are distinguished: 1) Framboidal pyrite, which is very fine grained, and 2) larger euhedral pyrite. The bulk of the pyrite in coal measures is usually made out by framboids which occur over a range of three orders of magnitude, from the least complex microframboids through framboids to polyframboids (Sawlowicz, 1993). The mechanism of framboidal self-organization remains unsolved and could only to a limited extent be reproduced in the laboratory (e.g. Ohfuji and Rickard, 2005). Bacterial working may play a role in the formation of pyrite itself. Folk (2005) states that many examples of sedimentary pyrite, ranging in age from Proterozoic to Recent, and in morphology from framboids to euhedral crystals, are made up of 30 – 50 nm spheroids. These are interpreted as fossils of the nanobacterial cells that precipitated the iron sulfide(s) according to Folk (2005). Field studies suggest that hydrogen sulphide can sulphidize amorphous FeS and form pyrite. Schoonen (2004) states that it is becoming increasingly clear that sulphate-reducing bacteria play a more important role than simply providing hydrogen sulphide for the reaction. Experiments by Schoonen (2004) with in-vitro cultures demonstrate the role of cell walls in directing and promoting the precipitation process of pyrite. Organic matter was found by Morse and Wang (1997) to inhibit pyrite formation probably because of the complexation of dissolved iron. Organic matter is however necessary for bacterial activity and the latter is important for H_2S production.

Experiments by Butler and Rickard (2000) showed that the form of pyrite is often controlled by the saturation state of the pyrite. Their experimental results showed that pyrite framboids preferably formed in a weakly acidic to weakly alkaline and slightly oxic solution ($E_h > -250$ mV, pH 6.0 in their experiments). Under such conditions, the solution is highly supersaturated with respect to pyrite and therefore the rate of nucleation becomes dominant over the rate of crystal growth (Butler and Rickard, 2000). In contrast, under lower E_h (-400 mV in their experiments) conditions (i.e. lower pyrite supersaturation), euhedral pyrite crystals formed dominantly, which suggests that the rate of crystal growth is greater than the nucleation rate under these conditions.

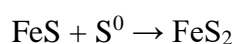
It is widely suggested in literature that FeS is an iron sulphide precursor. H_2S will react with Fe to precipitate FeS (mackinawite) in an anoxic environment:



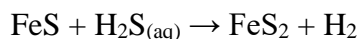
Some earlier reviews suggested that FeS converted to pyrite in a series of solid-state reactions, but such a process is difficult to implicate in framboid formation (Ohfuji and Rickard, 2005). Although pyrite has been synthesised from conditions of undersaturation with respect to mackinawite, framboids have not (Ohfuji and Rickard, 2005). However, aqueous clusters of FeS, both in the laboratory and in the natural environment, suggested that these clusters rather than FeS precipitates are involved in pyrite, and therefore framboid formation (Ohfuji and Rickard, 2005).

Greigite, a ferromagnetic iron sulphide (Fe_3S_4) has been suggested as a precursor phase (Ohfuji and Rickard, 2005), but magnetism is not universally observed in pyrite framboids so it seems unlikely that this is a fundamental attribute of framboids (Ohfuji and Rickard, 2005). Pyrite can be synthesised without greigite as an intermediary and framboids were also synthesised in the absence of greigite (Ohfuji and Rickard, 2005).

The role of oxidants (for the oxidation of FeS) in pyrite formation is equivocal and various experiments on pyrite employed different oxidizing agents. These include Fe(III), S^0 , H_2S and molecular O_2 (Ohfuji and Rickard, 2005). Fe(III) and O_2 are effectively considered to be absent in an anoxic environment. The reduction of Fe(III) to Fe(II) occurs before the formation of H_2S (see **Table 2.5(A)**) and it has been shown that O_2 and H_2S do not coexist (**Section 2.5**). Schoonen and Barnes (1991) noted that the zero-valent sulphur may be considered to represent any zero-valent sulphur species and the most reasonable candidate for such a reactant is polysulphide, $S_nS(aq)_2$ (Ohfuji and Rickard, 2005). The overall reaction of FeS with S^0 appears to be relatively slow at ambient temperatures with a rate constant at the order of $10^{-20} \text{ L}\cdot\text{mol}^{-1}\cdot\text{s}^{-1}$ at 25°C (Ohfuji and Rickard, 2005) and is given below:

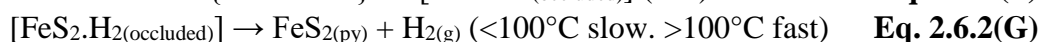
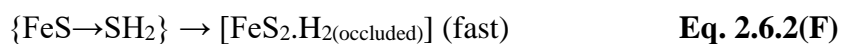
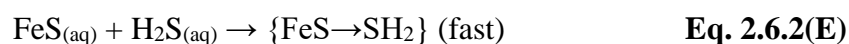
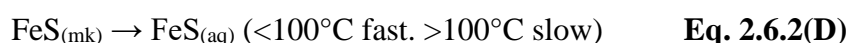


The most probable oxidant identified is H₂S (Ohfuji and Rickard, 2005) and the reaction to form pyrite is given as:



Guevremont et al. (1998) observed that the reaction of surface hydrogen to form gaseous hydrogen on the FeS₂ surface is not a simplistic process, and expected that the fate of hydrogen is to be incorporated into the pyrite lattice during growth (Ohfuji and Rickard, 2005).

Pyrite formation occurs via this pathway without the requirement for oxidised, reactive sulphur species which are present in nature at low concentrations. Thus, pyrite formation in strictly anoxic environments, and framboidal pyrite formation in many hydrothermal systems, can be accounted for. The mechanism of reaction proposed by Rickard and Luther (1997) is:



where FeS(aq) is an electroactive, dissolved species and represents cluster complexes of quantum-sized particles of FeS (Ohfuji and Rickard, 2005). This mechanism is important for pyrite formation since it involves a dissolved phase and therefore the pyrite microcrystals do not retain any textural memory of the precursor (Ohfuji and Rickard, 2005).

The oxidation of aqueous FeS by H₂S is by far the most rapid of the pyrite forming reactions hitherto identified (Rickard, 1997). The rate of pyrite formation by the dissolution of solid amorphous FeS and reaction with H₂S between 25 and 125°C is described by the equation (Rickard, 1997):

$$d\text{FeS}_2/dt = k(\text{FeS})(\text{H}_2\text{S}_{(\text{aq})})$$

and the second order rate constant k is 1.03 x 10⁻⁴ l.mol⁻¹.s⁻¹ at 25°C.

2.6.3 Pyrite and siderite stability

In order to illustrate the stability fields of pyrite, siderite, FeS and other iron minerals, Eh-pH diagrams were drawn (**Figure 2.6.3(A) – (X)**) for different Fe, TIC (Total Inorganic Carbon) and S activities using the Geochemist Workbench 6.0.3.

In **Figure 2.6.3(A) – (L)** all iron minerals were allowed to precipitate, whereas in **Figure 2.6.3(M) – (X)** pyrite was suppressed (excluded) in order to show the

stability of FeS which is the precursor of pyrite in the sedimentary environment as discussed in **Section 2.5** above. **Figure 2.6.3(A) – (F)** and **Figure 2.6.3(M) – (R)** were drawn for $a_{\text{Fe}} = 10^{-3}$ and **Figure 2.6.3(G) – (L)** and **Figure 2.6.3(S) – (X)** for $a_{\text{Fe}} = 10^{-5}$.

The conditions favourable for either pyrite or siderite formation is not so obvious when simply looking at a single pH-Eh diagram. Siderite and pyrite precipitation are not only dependent on the pH (and the carbonate activity), but is also strongly dependent on the sulphur activity. This is illustrated in **Figure 2.6.3(A) – (X)** where it is shown that the pyrite and FeS stability fields are strongly dependent on the activity of sulphur. Overall, it is seen that the stability field for FeS is smaller than that of the more thermodynamically stable pyrite.

Siderite can potentially form when there is enough Fe^{2+} in solution (indicating reducing conditions) and high carbonate activity. In **Table 2.5(A)** it is shown that some siderite can form in 1) the post-oxic zone before the transition to the sulphidic zone (and therefore the formation of pyrite), and in 2) the anoxic-methanic zone (after pyrite formation). Siderite can also form at near-neutral conditions under high TIC conditions before pyrite formation, e.g. **Figure 2.6.3(A) – (B)**, in anoxic conditions. However, with high sulphate content and under either more alkaline or acidic conditions, siderite would not form in the post-oxic zone and a quicker transition to the anoxic-sulphidic zone would be made where sulphate is reduced and pyrite is formed. When the sulphur is significantly depleted by pyrite formation, siderite will form again in the anoxic zone.

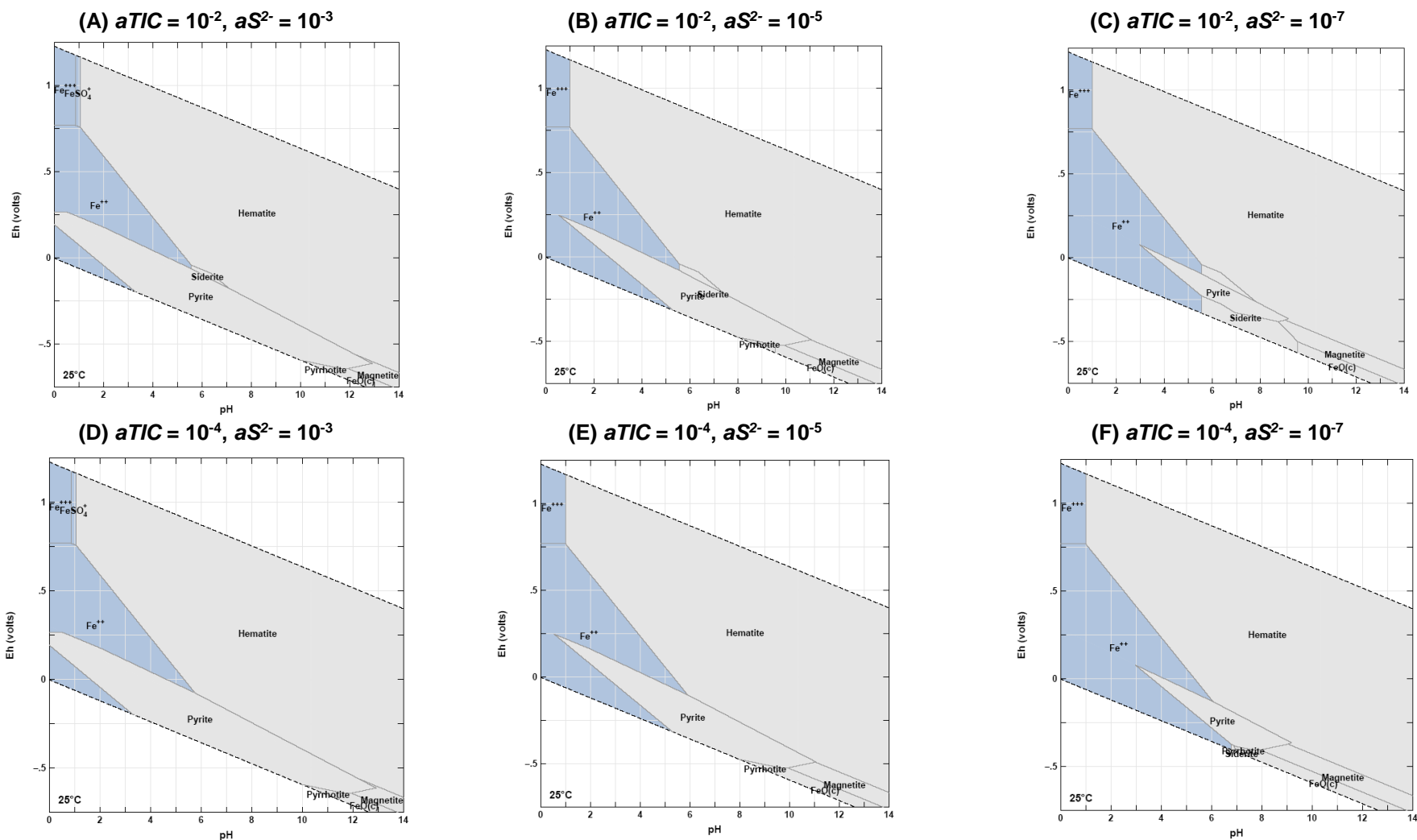


Figure 2.6.3(A) – (F). Eh-pH stability diagrams for the system Fe-H₂O-S-CO₂ at 25°C for $aFe^{2+} = 10^{-3}$.

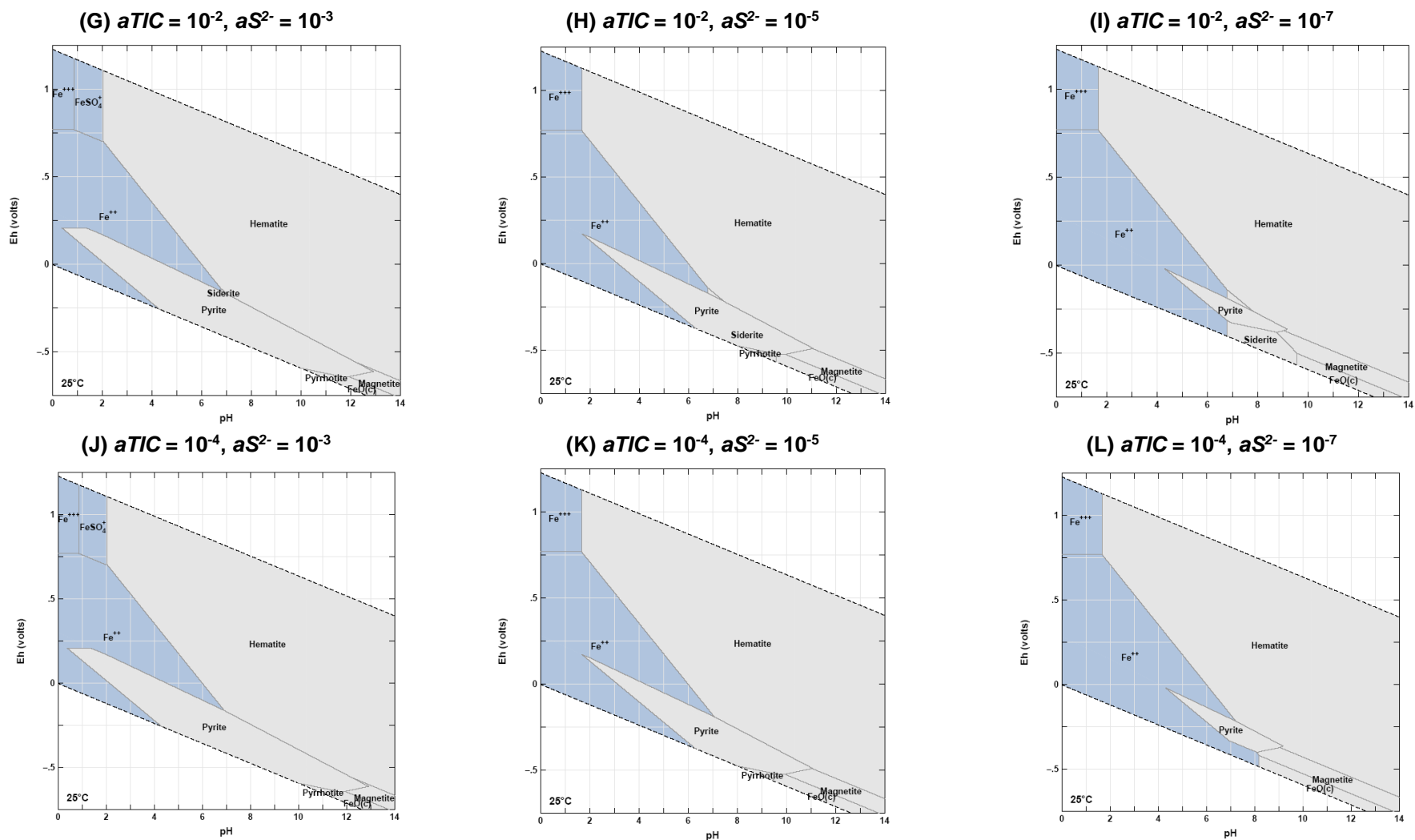
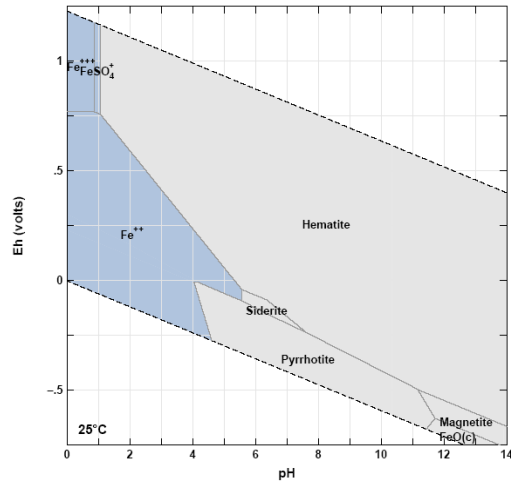
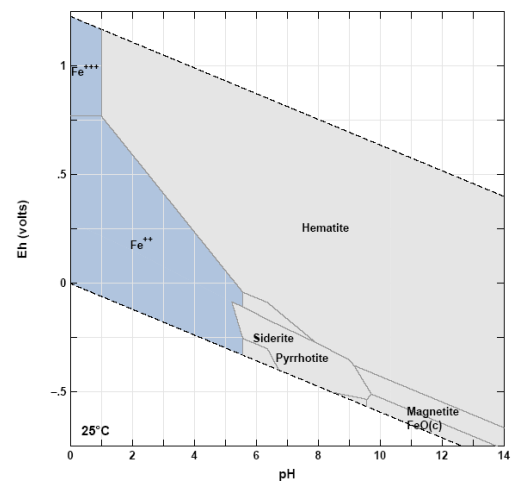


Figure 2.6.3(G) – (L). Eh-pH stability diagrams for the system Fe-H₂O-S-CO₂ at 25°C for $aFe^{2+} = 10^{-5}$.

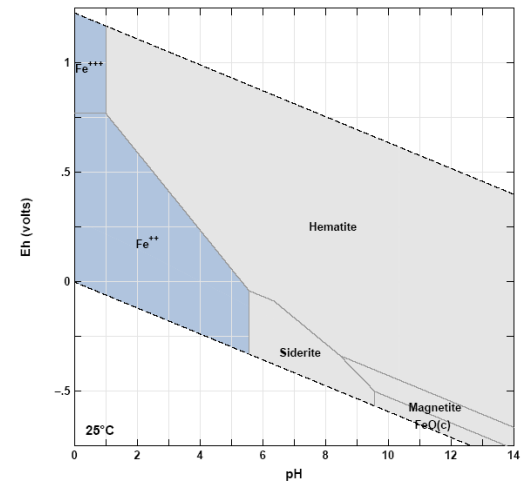
(M) (No FeS₂) $aTIC = 10^{-2}$, $aS^{2-} = 10^{-3}$



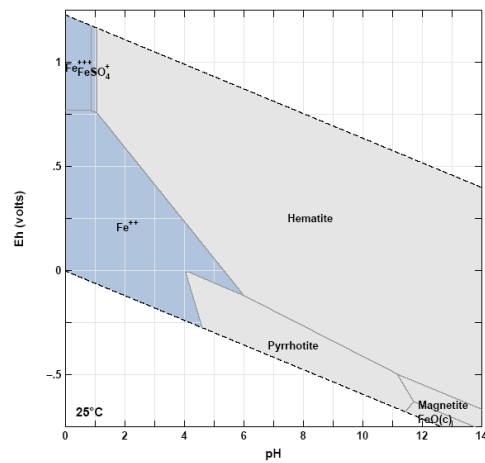
(N) (FeS₂ absent) $aTIC = 10^{-2}$, $aS^{2-} = 10^{-5}$



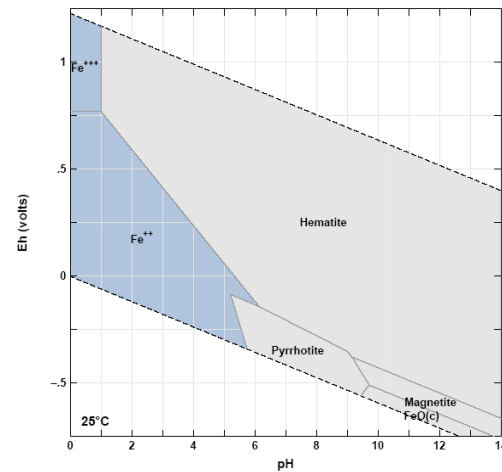
(O) (No FeS₂) $aTIC = 10^{-2}$, $aS^{2-} = 10^{-7}$



(P) (No FeS₂) $aTIC = 10^{-4}$, $aS^{2-} = 10^{-3}$



(Q) (No FeS₂) $aTIC = 10^{-4}$, $aS^{2-} = 10^{-5}$



(R) (No FeS₂) $aTIC = 10^{-4}$, $aS^{2-} = 10^{-7}$

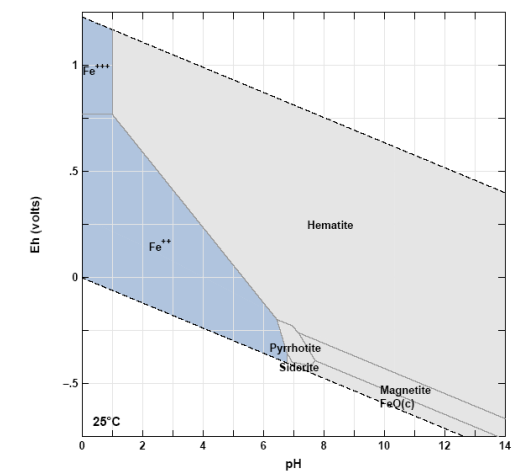
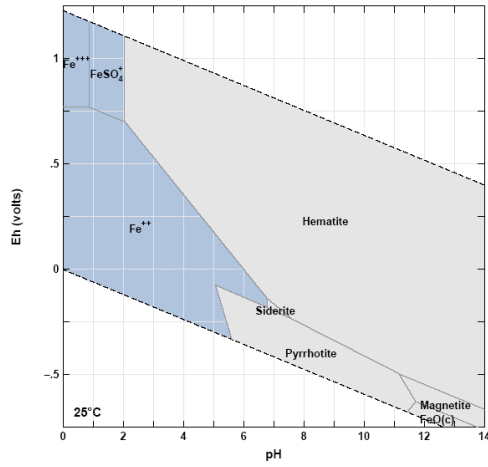
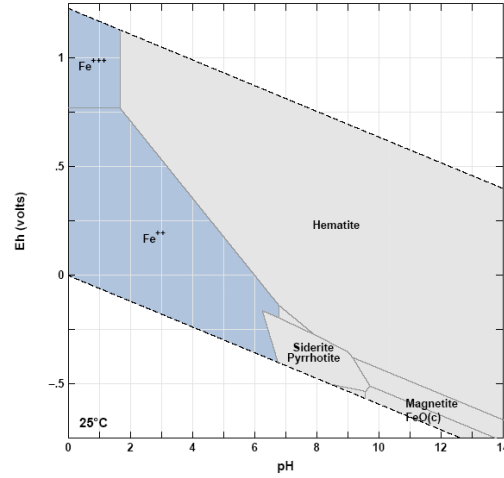


Figure 2.6.3(M) – (R). Eh-pH stability diagrams for the system Fe-H₂O-S-CO₂ at 25°C for $aFe^{2+} = 10^{-3}$ with suppression of pyrite.

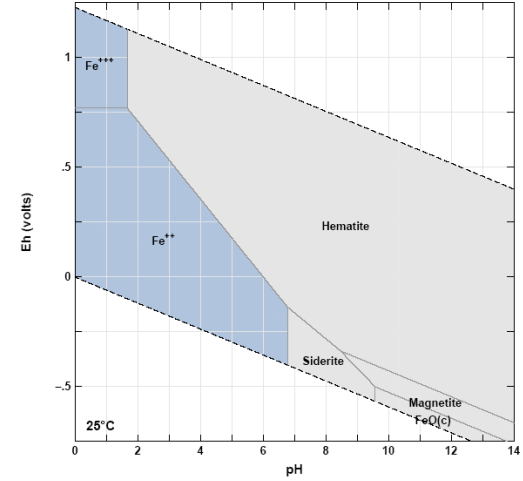
(S) (No FeS₂) $aTIC = 10^{-2}$, $aS^{2-} = 10^{-3}$



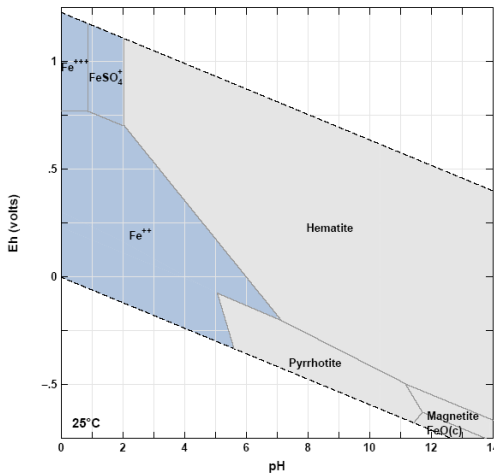
(T) (FeS₂ absent) $aTIC = 10^{-2}$, $aS^{2-} = 10^{-5}$



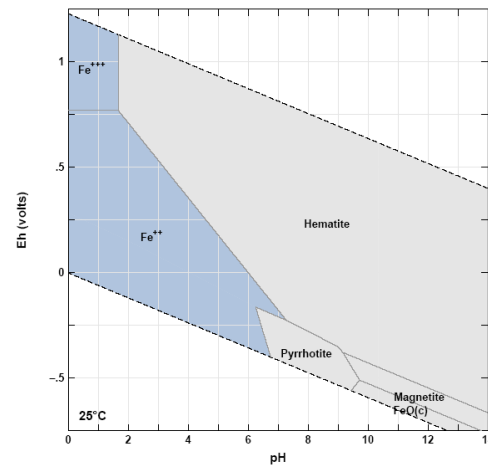
(U) (No FeS₂) $aTIC = 10^{-2}$, $aS^{2-} = 10^{-7}$



(V) (No FeS₂) $aTIC = 10^{-4}$, $aS^{2-} = 10^{-3}$



(W) (No FeS₂) $aTIC = 10^{-4}$, $aS^{2-} = 10^{-5}$



(X) (No FeS₂) $aTIC = 10^{-4}$, $aS^{2-} = 10^{-7}$

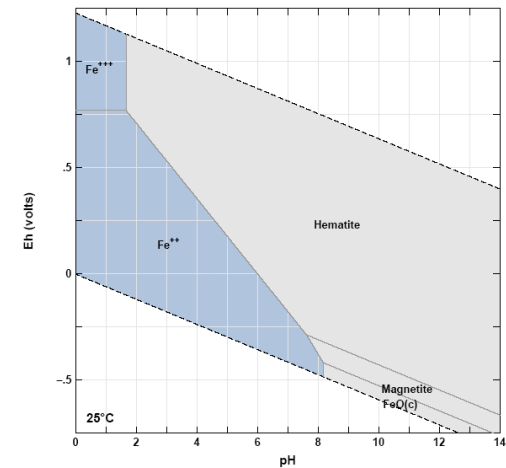


Figure 2.6.3(S) – (X). Eh-pH stability diagrams for the system Fe-H₂O-S-CO₂ at 25°C for $aFe^{2+} = 10^{-5}$ with suppression of pyrite.

To conclude, a significantly high Fe^{2+} and TIC content will not definitely lead to siderite formation, but a high Fe^{2+} and sulphur content would be very favourable for pyrite formation irrespective of the TIC content. Only with depletion of the sulphur content will siderite be formed significantly, but it is possible that most Fe^{2+} would then already be used up by the formation of pyrite.

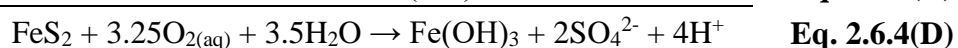
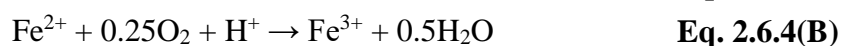
According to Renton and Bird (1991) sulphur would be more stable at very low pH conditions as H_2S than in pyrite. It is often observed in coal all over the world that pyrite is elevated in the top and bottom of the coal seam rather than in the centre. Holuszko et al. (1992) state that this is due to conditions becoming less acidic towards the top so that pyrite is more stable than H_2S and that with a further increase in pH, conditions become more favourable for siderite to form as a_{CO_3} increases as a result of faster plant material fermentation due to lowered water table levels.

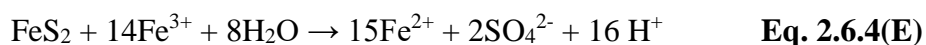
In South African coals pyrite and siderite formation are complex due to the variation of the water level during plant accumulation that leads to different coal bands in the same coal seam with variable qualities and ash contents. Often shale and siltstone partings and lenses also occur in the coal seam.

From **Section 6.3** it is observed that siderite in the South African coalfields is more frequent in carbonaceous clastic rocks than in the coal seams. Not only was the pH probably less acidic during the formation of the carbonaceous clastic rocks as described above, but the pyrite content is also observed to be much lower than in the coal seams (indicating lower sulphur activity). This correlates well with the stability fields of pyrite and siderite as illustrated by the Eh-pH diagrams.

2.6.4 Pyrite oxidation reactions

In **Table 2.5(A)** it is shown that pyrite can only form in an anoxic-sulphidic environment and it will oxidize in an oxic environment. Pyrite is also thermodynamically stable over a wider pH range than siderite and FeS , as shown in **Figure 2.6.3(A) – (X)**. Pyrite is relatively insoluble and previously formed pyrite will be metastable for long periods in other anoxic environments with low Fe^{2+} and H_2S in solution. The pyrite contained in coal mine wastes is not in equilibrium with the oxidizing environment and almost immediately begins to oxidize. The coal mine waste may be reactive over several decades. A complex series of chemical weathering reactions are spontaneously initiated when surface mining activities expose spoil materials to an oxidizing environment. The following equations show the generally accepted sequence of pyrite reactions in coal mine environments:





Step 1 – Equation 2.6.4(A)

In the initial step (**Equation 2.6.4(A)**), 1 mole of pyrite reacts with oxygen and water to produce 1 mole of ferrous iron, 2 moles of sulphate and 2 moles of hydrogen ions. The pyrite sulphur is therefore oxidized in this reaction while the iron remains in the same oxidation state.

Nordstrom (1982) and Kleinmann et al. (1981) state that any biotic oxidation of pyrite is dominantly by bacteria attached to the surface of pyrite grains. Oxidation of pyrite through bacterial working is often called the “direct mechanism” as Boon (2001) states: “*In the traditional idea about the direct mechanism, bacteria consume pyritic sulphur*”. The direct mechanism entails that the attached bacterial cells use dissolved oxygen as the electron acceptor and biologically oxidize pyrite sulphur by an enzyme system (Gleisner et al., 2006).

The effect of sulphur oxidizing bacteria attached to the pyrite grain that promote the oxidation of pyrite *via* a direct enzymatic attack is, however, much disputed by some researchers who suggest that the reaction is totally abiotic (Schoonen, 2004). The reaction has also been abiotically performed in experiments (e.g. Williamson and Rimstidt (1994) and Moses and Herman (1991)).

Step 2 – Equation 2.6.4(B)

The second step (**Equation 2.6.4(B)**) involves the conversion of ferrous iron to ferric iron whereby 1 mole of hydrogen is consumed. This reaction has been termed the "rate determining" step for the overall O₂ oxidation sequence (**Equation 2.6.4(D)**). This step must also take place in order for **Equation 2.6.4(E)** to proceed, which shows the importance of the presence of oxygen for the oxidation of pyrite by Fe³⁺.

At near neutral conditions this reaction will occur abiotically. Below pH 3 microbial activities is high and oxidation of Fe²⁺ occurs through bacterial catalysis whereas the abiotic oxidation of Fe²⁺ is slow. At pH 6 the "half-life" of Fe²⁺ in an aerated solution at 25°C is about 7 hours, but at pH 4 or less the abiotic "half-life" is about 8 years (Singer and Stumm, 1970).

In acid mine waters, the most prevailing bacteria are acidophiles. Most of these are autotrophs, such as the well known sulphur and iron oxidizer *Acidithiobacillus ferrooxidans* (formerly known as *Thiobacillus ferrooxidans*), the sulphur oxidizers *At. thiooxidans* and *At. albertensis* and the iron oxidizer *Leptospirillum ferrooxidans* (Gleisner, 2005). There are also heterotrophes in minor amounts, such as *Ferromicrobium acidophilus* and *Acidiphilium* species (Kelly and Wood, 2000). However, only a minor fraction of all bacteria species have been able to be cultivated in laboratory which implies that the named species mentioned above might not be the most important in reality (Gleisner, 2005).

In experiments *At. ferrooxidans* has been shown to increase the ferrous iron conversion reaction rate by a factor of hundreds to as much as one million times (Singer and Stumm, 1970). Olson (1991) presented an interlaboratory comparison which showed that the rate of pyrite oxidation by dissolved O₂ (pH 2, 28°C, [DO] = 241 μM) increased with a factor of 34 in the presence of *At. ferrooxidans*. Gleisner (2005) states that in mine tailings hot-spots of high bacterial concentration are often found with high bacterial diversity and activity even in anoxic zones. This shows that the microbial community and processes in a mine waste deposit are far more complex than simple, strictly-controlled laboratory experiments (Gleisner, 2005). This implies that the extremely high rate of pyrite oxidation observed in bacterial inoculated experiments cannot be directly extrapolated to field conditions.

At. ferrooxidans is acidophilic (acid loving, capable of surviving at low pH's), autotrophic and requires only dissolved CO₂, O₂, a reduced form of Fe or S and minor N and P, for their metabolism (Cravotta, 1994). **Figure 2.6.4(A) – (C)** below show the effect of dissolved O₂, pH and temperature, respectively, on *At. ferrooxidans* as reported by Jaynes et al. (1984). Dissolved oxygen is important for their growth as *At. ferrooxidans* obtains energy from the oxidation of ferrous iron and elemental or reduced sulphur compounds (e.g. metal sulphides), using dissolved oxygen as the electron acceptor under oxidizing conditions. The optimum pH levels are 2.0-3.5, but they can survive from 0.5 up to 5.5 (Goodman et al., 1981; Ledin and Pedersen, 1996). *At. ferrooxidans* is also mesophilic and their optimum growth temperature is in the range of 25-35°C, where the upper limit is about 42°C, and the lower range has not been well-defined (Ahonen and Tuovinen, 1989).

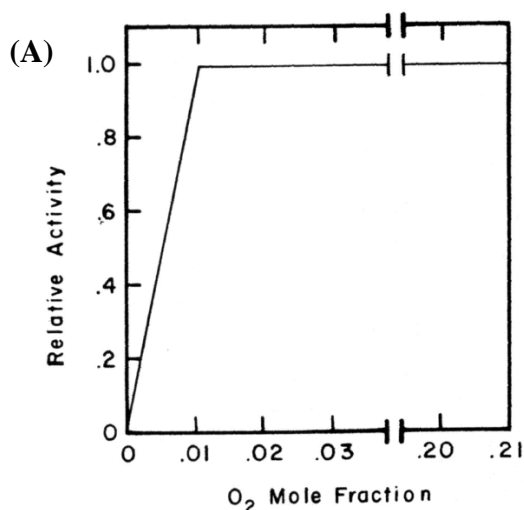


Figure 2.6.4(A). The effect of dissolved oxygen on *At. ferrooxidans* activity (Jaynes et al., 1984).

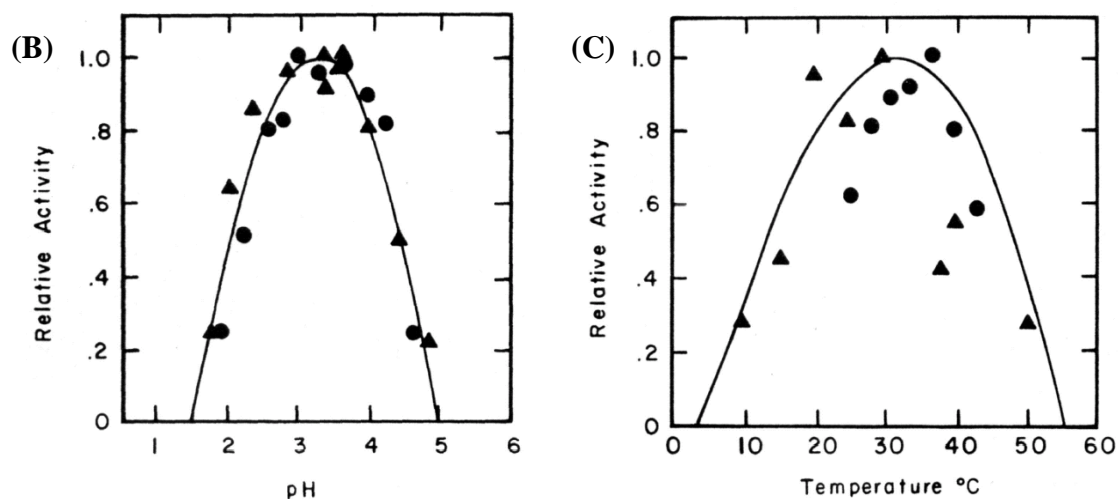


Figure 2.6.4(B) and (C). The effect of pH and temperature on *At. ferrooxidans* activity (Jaynes et al., 1984).

Reaction 3 – Equation 2.6.4(C)

The third step involves the hydrolysis of ferric iron with water to form ferrihydrite and the release of additional acidity. This third reaction is pH dependent. Under very acid conditions of less than about pH 3.5, the precipitate does not form and iron will remain in solution. At higher pH, ferrihydrite will form, commonly referred to as "yellowboy."

When the ferrihydrite later accumulates in soils and sediments under dry conditions, it may eventually dehydrate and recrystallize to form more thermodynamically stable goethite and hematite:



Sum of Steps 1, 2 and 3 – Equation 2.6.4(D)

The sum of Steps 1, 2 and 3 is given in **Equation 2.6.4(D)** and describes the overall oxidation of pyrite by oxygen and also the fate of Fe^{2+} at slightly acidic to neutral conditions. The evidence of this reaction is seen in many mining environments as ferrihydrite is colouring the water orange-red.

Step 4 – Equation 2.6.4(E)

The fourth step involves the oxidation of pyrite by ferric iron. The ferric iron is generated by the oxidation reaction in Step 2 (**Equation 2.6.4(B)**) and is used for pyrite oxidation (**Equation 2.6.4(E)**) where ferric iron is reduced to ferrous iron. Pyrite oxidation by ferric iron at low pH conditions takes place rapidly (more quickly

than the oxidation of pyrite by oxygen) and the oxidation continues until the supply of ferric iron or pyrite is exhausted. Oxygen supply through the coal mine waste may become the rate limiting step as oxygen is required for the ferric iron production. However, where high concentrations of oxygen are available, the oxidation of ferrous to ferric iron will be the rate limiting step (**Equation 2.6.4(B)**).

Although Fe^{3+} is formed rapidly at conditions with pH larger than pH 4, Fe^{3+} is relatively insoluble under these conditions and tends to form $\text{Fe}(\text{OH})_3$ or other solids, so that little Fe^{3+} remains in solution to oxidize pyrite (Cravotta and Rose, 1994). At pH conditions of about below pH 3, the concentration of Fe^{3+} becomes high enough so that Step 4 becomes the main mechanism for acid production, with bacterial reoxidation of Fe^{2+} providing the Fe^{3+} (Nordstrom, 1982; Kleinmann et al., 1981).

2.6.5 Kinetic rate of pyrite oxidation

Many factors determine the rate of AMD generation from pyrite oxidation, including bacterial activity, pH, pyrite chemistry, the presence of iron on the pyrite surface and in solution, surface area, temperature and oxygen concentration. The interactions of these factors are complex. In the case where sufficient oxygen is present, the kinetic rate of pyrite oxidation is surface controlled. In a high waste rock pile, the rate of pyrite oxidation will be dependent on the diffusion rate of oxygen towards the pyrite surface. Even when the oxidant is Fe(III) and the oxidation process is catalyzed by bacterial metabolism, oxygen is still necessary for the production of Fe(III) and furthermore, anaerobic bacteria need oxygen for their survival (see **Figure 2.6.4(A)**).

The oxidation rate of pyrite by oxygen (**Equation 2.6.4(A)**) and ferric iron (**Equation 2.6.4(E)**) and the oxidation of ferrous iron (**Equation 2.6.4(B)**) at different pH conditions are shown in **Figure 2.6.5(A) – (B)** below:

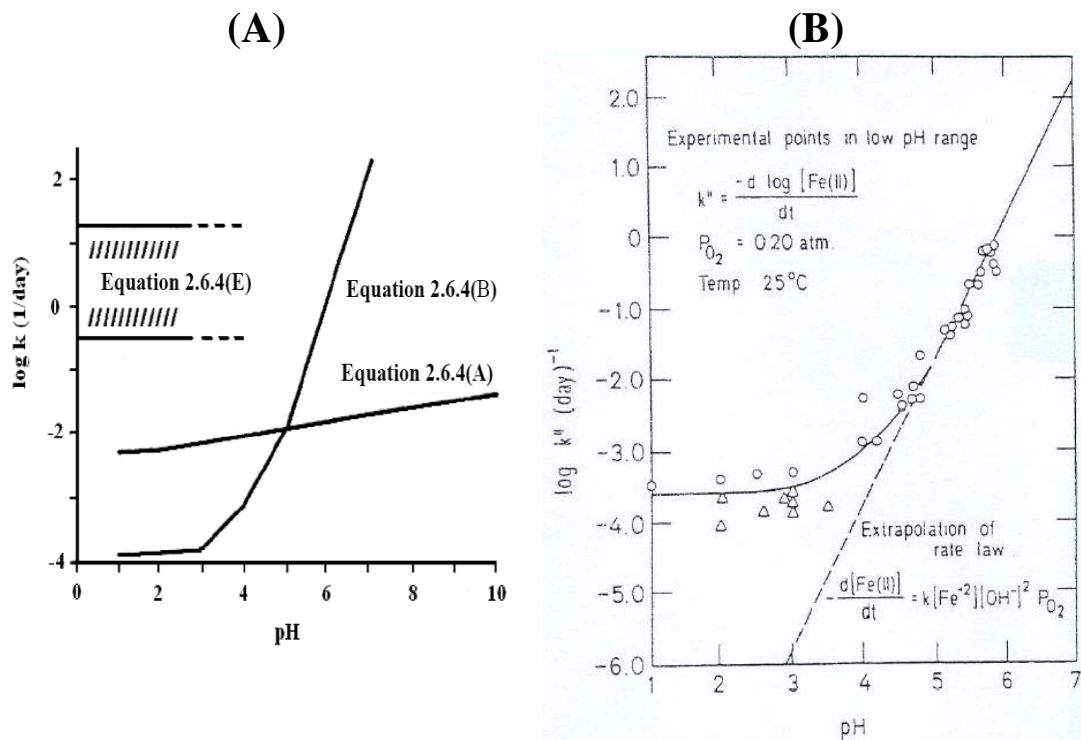


Figure 2.6.5(A). The oxidation rate of pyrite by oxygen and ferric iron and the oxidation of ferrous iron at different pH conditions from Evangelou (1995); **(B)** The oxidation of ferrous iron at different pH conditions from Singer and Stumm (1970).

From experimental studies on the oxidation of pyrite, the following rate parameters shown in **Table 2.6.5(A)** have been determined for the rate law expressed in **Equation 2.3.2(A)**:

Table 2.6.5(A). Rate law parameters determined for pyrite oxidation at 25°C.

$\log k_+$ (mol.m ⁻² .s ⁻¹)	n_{H^+}	n_{O_2}	$n_{Fe^{3+}}$	$n_{Fe^{2+}}$	Reference	Valid pH range
-8.58	-0.32	-	0.30	-0.47	Williamson and Rimstidt (1994)	pH 0.5 – 3 (No O ₂ , Purged with N ₂)
-6.07	-	-	0.93	-0.40	Williamson and Rimstidt (1994)	pH 0.5 – 3 (In the presence of O ₂)
-8.19	-0.11	0.50	-	-	Williamson and Rimstidt (1994)	pH 2 - 10

From **Figure 2.6.5(A)** and **(B)** and **Table 2.6.5(A)** above the following observations could be made:

- The oxidation of pyrite by oxygen (**Equation 2.6.4(A)**) and Fe³⁺ in the absence of O₂ (**Equation 2.6.4(E)**), decreases with increases in H⁺ activity. Therefore, as the H⁺ concentration increases, the oxidation reaction of pyrite (**Equation**

2.6.4(D) – (E)) will be slower towards the right. The oxidation rate of pyrite by oxygen and Fe^{3+} (the latter in the absence of O_2) is exponentially dependent on the H^+ activity by exponents of -0.11 and -0.32, respectively.

- In the presence of O_2 , the oxidation rate of pyrite by Fe^{3+} is not dependent on the H^+ activity.
- The oxidation of pyrite by oxygen is exponentially dependent on the dissolved oxygen activity by an exponent of 0.50.
- The oxidation of pyrite by Fe^{3+} is exponentially dependent on the Fe^{3+} activity by an exponent of 0.30, in the absence of O_2 , and an exponent of 0.93, in the presence of O_2 . The oxidation rate is negatively dependent on the presence of Fe^{2+} because ferrous iron may accumulate on the pyrite surface and block the surface reaction sites (Moses and Herman, 1991).

2.7 Carbonate minerals

2.7.1 Calcite and dolomite stability and formation in the coal environment

In some South African coal measures it was found that siderite is more frequent in carbonaceous clastic rocks than in coal seams or in non-carbonaceous clastic rocks. Calcite and dolomite were found to be generally more frequent in coal seams than in clastic rocks (see **Section 6.3** in **Chapter 6**). The stability of siderite has been discussed in **Section 2.6.3** above.

Carbonates can form both syn- and epigenetically. During the fermentation of organic material the activity of the CO_2 increases as shown in **Equations 2.4.2(A) – (C)** with resultant increase in carbonate precipitation when the right pH conditions is reached. Epigenetically, carbonates are often present as cleat infillings in coal as described by Ward (2002).

Acidic conditions prevail in swamps due to the presence of humic/fulvic acids. However, it is possible for the carbonates that formed in the sedimentary environment not to react with these acids. Compton and Sanders (1993) made the interesting observation that in equilibrated acidic solutions, humic acids had no influence on calcite dissolution rates; if fresh sodium salts of humic acid were added significant inhibition of dissolution occurred (Morse and Arvidson, 2002).

The decay of organic material and root respiration is the major source of CO_2 in soils (Appelo and Postma, 1993). It is shown in **Table 2.4.1(A)** that CO_2 is produced from the reduction of organic matter in all the geochemical environments - from oxic to anoxic environments. In the anoxic-methanic environment CO_2 is also used for methane production.

In some South African coal measures it was found that siderite is more frequent in carbonaceous clastic rocks than in coal seams or in non-carbonaceous clastic rocks. Calcite and dolomite were found to be generally more frequent in coal seams than in clastic rocks (see **Section 6.3** in **Chapter 6**). The stability of siderite has been discussed in **Section 2.6.3** above.

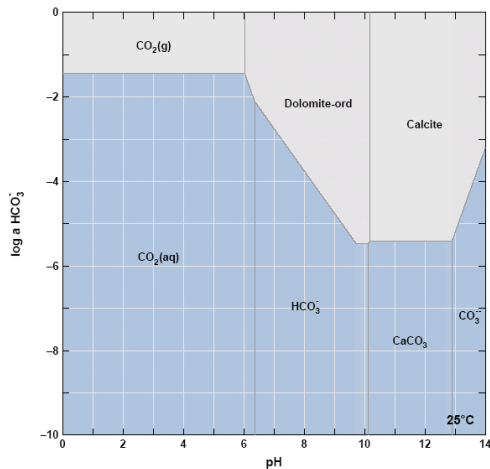
Figure 2.7.1(A) – (F) below show the stability fields of dolomite and calcite under different pH conditions and HCO_3^- activity at either 25°C or 100°C.

The typical reactions of carbonate minerals formation and dissolution are given in **Section 2.7.2** below.

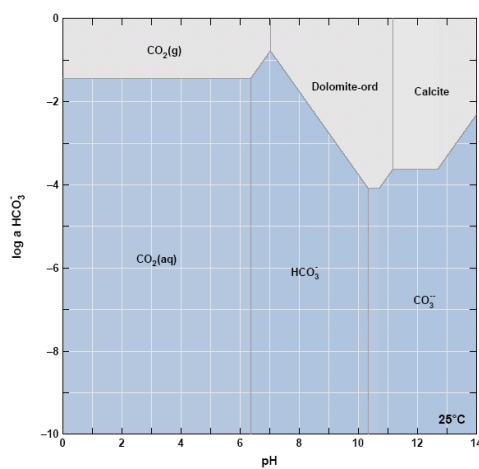
From **Figure 2.7.1(A)** and **(C)** it is observed that at 25°C and with equal activities of Ca and Mg (either 10^{-3} or 10^{-5}) calcite will only form under alkaline conditions of respectively $> \text{pH } 10$ and $> \text{pH } 11$; dolomite will form under near neutral conditions respectively between $\text{pH } 6 - 10$ and $\text{pH } 7 - 11$. For illustration of the effect of temperature on carbonates, the same diagrams were drawn for a temperature of 100°C and are shown as **Figure 2.7.1(B)** and **(D)**. From these figures it is evident that the calcite field grows in stability with temperature increase. These figures illustrate that calcite and dolomite not only form syngenetically under low temperatures but also epigenetically at higher temperatures during early diagenesis.

Figure 2.7.1(E) was drawn for Ca and Mg activities of respectively 10^{-3} and 10^{-5} , and *vice versa* in **Figure 2.7.1(F)**. With Ca activity at 10^{-5} and Mg activity at 10^{-3} the stability of both dolomite and calcite decreases drastically, however with Ca activity at 10^{-3} and Mg activity at 10^{-5} the stability of dolomite disappear and the calcite is stable down to $\text{pH } 6$.

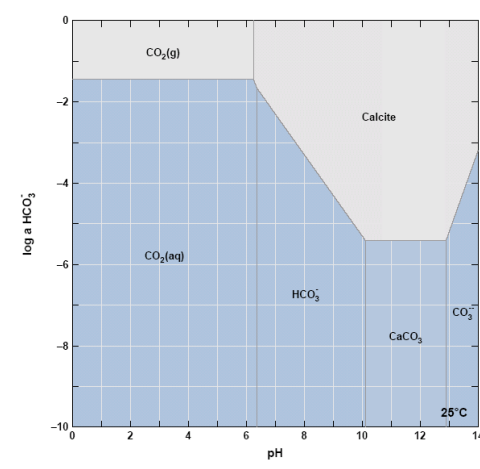
(A) $a_{Mg} = 10^{-3}$, $a_{Ca^{2+}} = 10^{-3}$, $T = 25^\circ\text{C}$



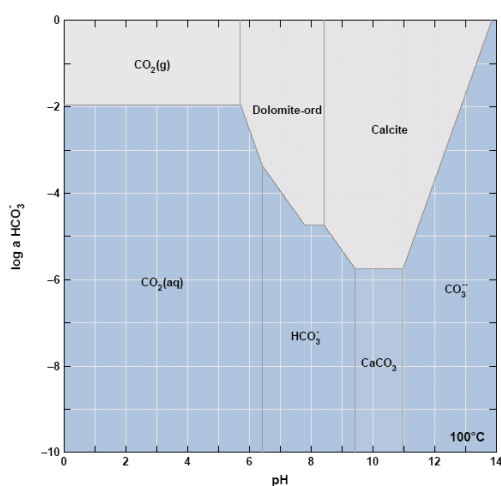
(C) $a_{Mg} = 10^{-5}$, $a_{Ca^{2+}} = 10^{-5}$, $T = 25^\circ\text{C}$



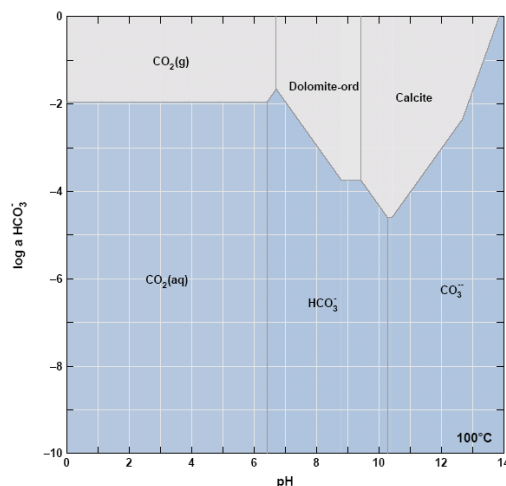
(E) $a_{Mg} = 10^{-5}$, $a_{Ca^{2+}} = 10^{-3}$, $T = 25^\circ\text{C}$



(B) $a_{Mg} = 10^{-3}$, $a_{Ca^{2+}} = 10^{-3}$, $T = 100^\circ\text{C}$



(D) $a_{Mg} = 10^{-5}$, $a_{Ca^{2+}} = 10^{-5}$, $T = 100^\circ\text{C}$



(F) $a_{Mg} = 10^{-3}$, $a_{Ca^{2+}} = 10^{-5}$, $T = 25^\circ\text{C}$

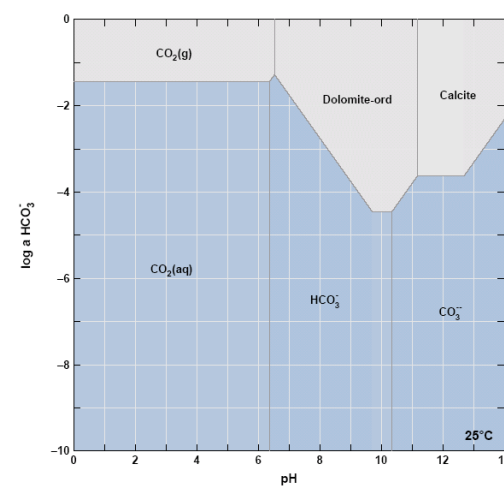


Figure 2.7.1(A) – (F). Log activity of HCO_3^- against pH for the system Ca-Mg-H₂O-CO₂.

2.7.2 CO₂ species and carbonate mineral neutralization reactions

CO₂ species in solution

The netto neutralization reaction of calcite under acidic conditions is as follows:

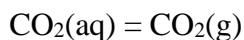


The H₂CO₃ largely decomposes to CO₂(aq) (where the solution has a pH < 6.4):



Appelo and Postma (1993) state that at 25°C CO₂(aq) is about 250 times more abundant in solution than H₂CO₃(aq).

If a gas phase is present, the CO₂(aq) will equilibrate with CO₂(g):



If the atmosphere is in full contact with the solution (open system), the CO₂(g) will serve as a buffer and equilibrate with CO₂(aq) where the average log fugacity of CO₂(g) in the atmosphere is -3.5.

In the unsaturated zone CO₂ may also be added to solution by the decomposition of organic matter (see **Equations 2.6.2(A) – (C)**).

For more convenient calculations CO₂(aq) is often included in H₂CO₃, and H₂CO₃* is used to express the sum of the dissolved carbon dioxide and the carbonic acid (Appelo and Postma, 1993):



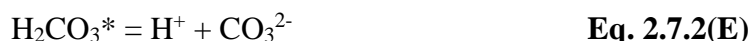
H₂CO₃* is dominant in solutions with pH values of below pH 6.4. Carbonic acid is diprotic and dissociates in two steps. The first step at pH conditions of 6.4 < pH < 10.3 gives bicarbonate and acid:



The second step where pH > 10.3 gives carbonate and acid:

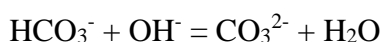
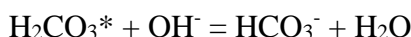


The overall step from carbonic acid to carbonate is obtained by adding **Equation 2.7.2(C)** and **(D)**:



HCO_3^- and CO_3^{2-} are the conjugate bases of respectively H_2CO_3^* and HCO_3^- and will buffer water against pH changes brought by AMD. HCO_3^- is a slightly above average base (and its conjugate acid H_2CO_3^* is a slightly below average acid) whereas CO_3^{2-} is a fairly strong base (and its conjugate acid HCO_3^- is a fairly weak acid). A buffered solution is one that resists a change in its pH when hydrogen ions (H^+) or hydroxide ions (OH^-) are added. The reverse proceeding of **Equation 2.7.2(C)** and **2.7.2(D)** describes the buffering of a solution against added acidity.

Buffering against added base in solution occurs as hydroxide ions are consumed by carbonic acid and bicarbonate:



The above reaction can be obtained by adding the dissociation reaction of water ($\text{OH}^- + \text{H}^+ = \text{H}_2\text{O}$) to **Equation 2.7.2(C)** and **2.7.2(D)**.

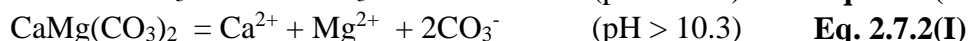
Carbonate alkalinity

The carbonate system is by far the most important buffer for water systems in nature. This is because carbonate minerals is 1) widely present in sedimentary rocks and 2) carbonate is considered as a fairly soluble mineral when undersaturated (see **Table 2.4(A)**).

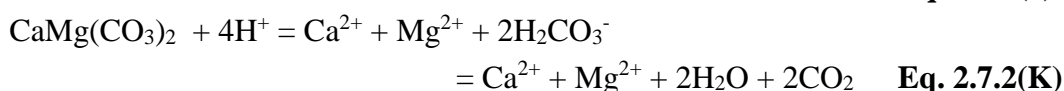
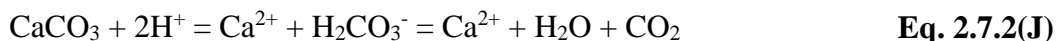
Alkalinity is the ability to consume or neutralize acidity. The sum of all the concentrations of acidity (H^+) consuming (inorganic) ions namely hydroxide [OH^-], carbonate [CO_3^{2-}], and bicarbonate [HCO_3^-] is known as Carbonate Alkalinity:

$$\text{Carbonate Alkalinity} = [\text{HCO}_3^-] + 2[\text{CO}_3^{2-}] + [\text{OH}^-] - [\text{H}^+]$$

The carbonate minerals calcite (CaCO_3) and dolomite ($\text{CaMg}(\text{CO}_3)_2$) are the main minerals providing alkalinity:

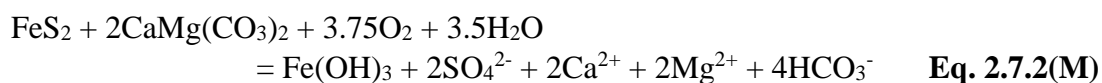
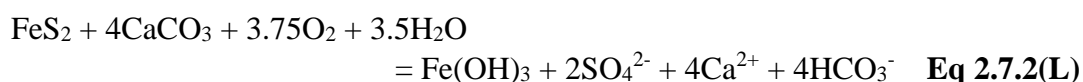


The overall neutralization reactions of calcite and dolomite can be obtained by combining **Equation 2.7.2(F)** and **2.7.2(G)** with **Equation 2.7.2(C)**:

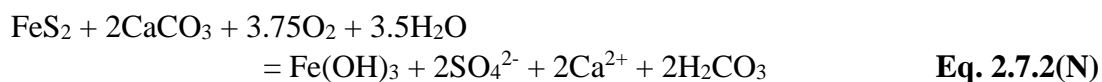


Neutralization of acid by calcite and dolomite in a closed system

With the commencement of pyrite oxidation in mine wastes and subsequent acid (H^+) production, the pH of the mine water is still neutral with pH values larger than pH 6.3 but usually smaller than pH 10.3. At these pH conditions, if there is no contact with a gas phase, HCO_3^- will be the main carbonate specie in solution, as shown in the above reaction equations and also depicted in the carbonate stability diagrams **Figure 2.7.1(A) – (F)**. Under these conditions one mol calcite consumes one mol of H^+ and one mol of dolomite two moles of H^+ to produce HCO_3^- . In order to neutralize the acidity produced by the oxidation of 1 mol of pyrite with oxygen (**Equation 2.6.4(D)**), 4 moles of calcite (**Equation 2.7.2(F)**) or 2 moles of dolomite (**Equation 2.7.2(G)**) is required:



If mine drainage with a pH smaller than pH 6.3 is introduced into a calcite containing matrix, the neutralization of calcite will produce two moles of H_2CO_3 :



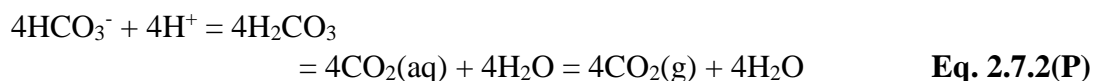
The produced carbonic acid will, however, react with calcite to equilibrate with bicarbonate:



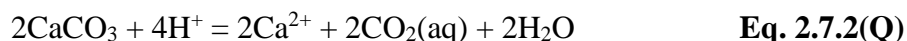
Therefore under *closed acidic conditions* ($< \text{pH } 6.3$) **Equation 2.7.2(N)** and **(O)** can be combined that will again give **Equation 2.7.2(L)** for calcite neutralization and through a similar approach, **Equation 2.7.2(M)** can be obtained for dolomite neutralization.

Neutralization of acid by calcite and dolomite in an open system

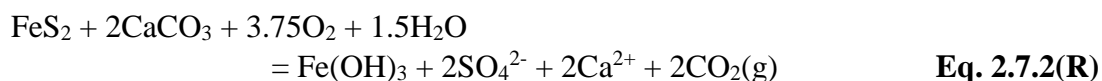
Under near neutral conditions ($6.4 < \text{pH} < 10.3$), if the solution is in contact with the atmosphere (that serves as a constant CO_2 buffer), 4 additional moles of H^+ is consumed by 4 moles of HCO_3^- in **Equation 2.7.2(L)** in order to equilibrate with the gas phase:



which can be written in terms of calcite neutralization:



Equation 2.7.2(Q) can be combined with **Equation 2.7.2(L)** to give:



where $\text{CO}_2(\text{g})$ exsolves into the atmosphere. Therefore, under a complete open system no carbonic acid will persist that will produce additional acidity as under closed conditions.

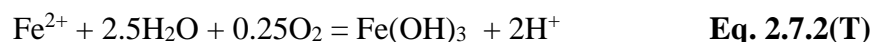
Under open acidic conditions HCO_3^- will not form first (as under neutral to alkaline conditions – **Equation 2.7.2(L)**) but rather carbonic acid will form (**Equation 2.7.2(N)**) that will equilibrate with $\text{CO}_2(\text{g})$ to give **Equation 2.7.2(R)**.

Siderite

One mole of siderite (FeCO_3) will consume 2 moles of H^+ :



However, with oxidation of Fe(II) to Fe(III) (**Equation 2.7.2(S)**), acidity is produced:



Combining **Equation 2.7.2(S)** and **(T)** gives



which shows that the netto reaction consumes no acid.

Therefore, although it is possible that siderite constitutes a temporary neutralizing agent, it is not effective overall. Most natural siderite is actually a solid solution containing some Ca, Mg and Mn in addition to Fe. Dissolution of siderite can produce elevated concentrations of Mn in groundwater at mines (e.g. Larsen and Mann, 2005). The presence of MnS and MnCO_3 in South African coal bearing strata has not been described and therefore it is possible that Mn may be present in siderite. To the extent that siderite contains Ca and Mg in solid solution, its dissolution will contribute some net alkalinity, analogous to reaction of the CaCO_3 or MgCO_3 component in the siderite.

2.7.3 Reaction Rate of Carbonate Minerals

In **Section 2.3.1** it was stated that the activation energy E_a of a reaction can be used to distinguish between transport and surface control of dissolution. The activation energy for a surface controlled reaction is much larger than for any transport controlled reaction.

In literature a fairly wide range (about 8–60 k.J.mol⁻¹) of activation energies was reported (Morse and Arvidson, 2002) for the dissolution reactions of calcite. However, probably the most reliable values in dilute solutions are close; 8.4 k.J.mol⁻¹ by Plummer et al. (1978) and 10.5 k.J.mol⁻¹ by Sjöberg (1978).

Gutjahr et al. (1996) found high activation energy (35 k.J.mol⁻¹) in the near equilibrium region confirming that the calcite dissolution reaction is surface controlled in this region of saturation (Morse and Arvidson, 2002).

The effect of temperature and pH on carbonate dissolution is illustrated in **Figure 2.7.3(A)** below:

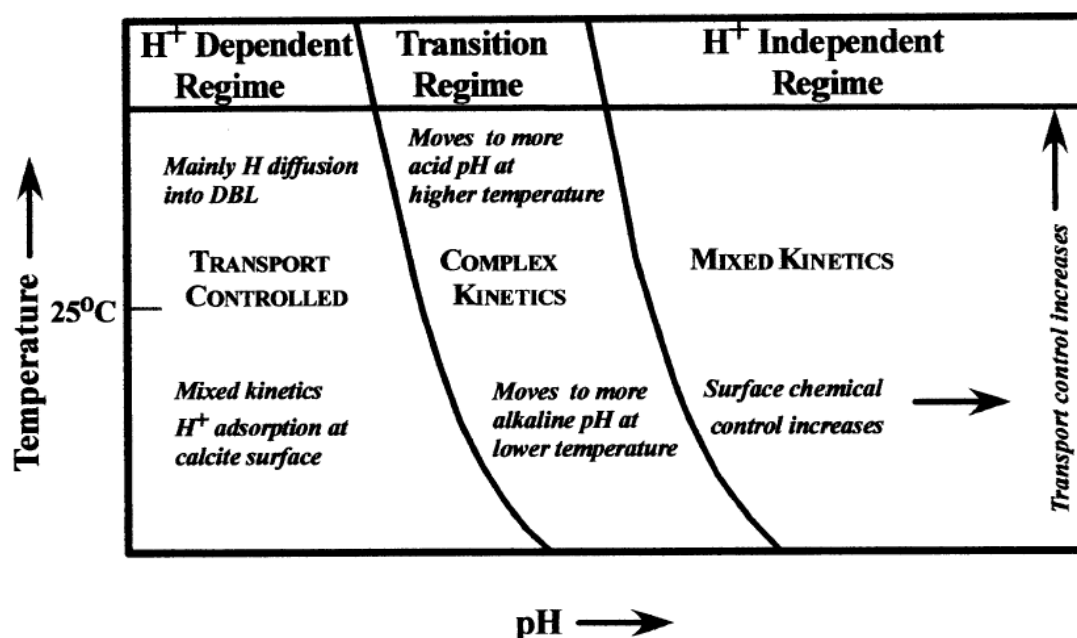


Figure 2.7.3(A). The dissolution kinetics of major sedimentary carbonate minerals (Morse and Arvidson, 2002).

From experimental studies on the dissolution of carbonate minerals, the following rate parameters in **Table 2.7.3(A)** have been determined for the rate law expressed in **Equation 2.3.2(A)** below:

Table 2.7.3(A). Rate parameters of calcite and dolomite dissolution at 25°C.

$\log k_+$ (mol.m ⁻² .s ⁻¹)	n_{H^+}	$n_{P(CO_2)}$	Reference	Valid pH range
Calcite				
-0.30	1.00	-	Plummer et al. (1978) and Talman et al. (1990) referenced in Palandri and Kharaka (2004)	Acid Mechanism
-5.81	-	-		Neutral Mechanism
-3.48	-	1.00		Carbonate Mechanism
Sedimentary (Disordered) Dolomite				
-3.19	0.50	-	Busenberg and Plummer (1982) referenced in Palandri and Kharaka (2004)	Acid Mechanism
-7.53	-	-		Neutral Mechanism
-5.11	-	0.50		Carbonate Mechanism

From **Figure 2.7.3(A)** and **Table 2.7.3(A)** the following observations could be made:

- With temperature increase the solubility of carbonate minerals will decrease and the H⁺ ion dependence of carbonate mineral dissolution will increase.
- At high pH and higher temperature, carbonate minerals will be closer to saturation and therefore surface control will increase.
- At lower pH ranges and lower temperature carbonate mineral dissolution will not be controlled at the mineral surface but mineral bonds will break easily because the mineral is undersaturated. The dissolution rate of the mineral will therefore become more dependent on the transport rate of H⁺ to the mineral surface.
- Because of the higher rate of carbonate dissolution far from saturation (where the dissolution rate is transport controlled) the carbonate minerals may be set to equilibrate with the water composition in geochemical modelling. If however the carbonate dissolution near saturation is modelled, the dissolution could be set to a kinetic rate law.

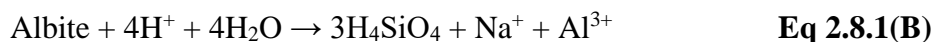
2.8 Silicate mineral buffering

2.8.1 The silicate mineral buffering mechanism

Silicate minerals consume acid as they dissolve because of the hydrolysis of silica tetrahedral consuming acid. The silicate dissolution reaction is essentially an exchange of protons for counterions from the silicate structure. For example, in the dissolution of albite, the counterions Na⁺ and Al³⁺ in the silicate structure go into solution as follows:

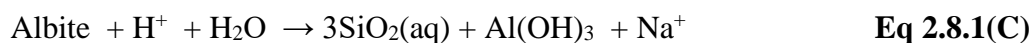


In an aqueous solution $\text{SiO}_2(\text{aq})$ can be presented by its hydrated form H_4SiO_4 and **Equation 2.8.1(A)** can be rewritten as follows:



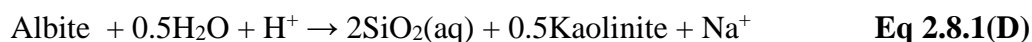
Equation 2.8.1(B) indicates that H^+ binds to the silicate ion as it dissolves. The lower the Si/O ration in the silicate structures, the higher the charge on the silicate tetrahedral. This greater charge is counterbalanced by counterions which in turn are replaced by more protons. Therefore, the lower the Si/O ratio of the silicate mineral, the greater the potential to neutralize acid.

Al and Fe may be important constituents of the silicate structure and will affect acid buffering. Al and Fe tend to hydrolyze in solution, producing acid. Therefore, minerals with Al and Fe in octahedral sites will have lower buffering capacities than a similar mineral where no hydrolyzes of produced Al and Fe is possible. For instance **Equation 2.8.1(A)** will be valid only for fairly low pH conditions. Except for low or very high pH conditions, the dissolution of albite in terms of Al hydrolysis can be written as follows:



Equation 2.8.1(C) is also an example of incongruent silicate dissolution. That is, albite only dissolves partially and form a secondary weathering product $\text{Al}(\text{OH})_3$. **Equation 2.8(A)** and **(B)** are examples of congruent dissolution where the silicate mineral dissolves completely to form ions in solution. If silicate minerals dissolve congruently, they will generally consume more acid than weathering in an incongruent process.

Another example of incongruent dissolution and a more probable product of weathering of silicates is clay minerals. For instance kaolinite ($\text{Al}_2\text{Si}_2\text{O}_5(\text{OH})_4$) can be produced as follows from albite dissolution:



The kaolinite does not necessarily have to precipitate out of solution after complete dissolution of albite (**Equation 2.8(A)**) but according to Casey et al. (1993) clay and amorphous phases could also directly form by reconstruction of the weathered outer layers of the silicate mineral without a solution step.

2.8.2 Silicate mineral dissolution reactions

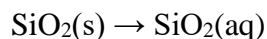
Quartz dissolution

Although quartz is a major to dominant mineral in the coal bearing strata of South African coal seams, quartz is not an important mineral in Acid Mine Drainage because of its extremely sluggish reaction kinetics. Appelo and Postma (1993) state

that quartz rarely controls the dissolved silica content. However, the stoichiometry of silica is briefly shown below as silica is often a product of silicate mineral dissolution.

Quartz precipitates in an acidic environment and only dissolves under high pH conditions. At low to neutral pH conditions the stable SiO_2 form is independent of pH, and quartz will only slowly dissolve to form $\text{SiO}_2(\text{aq})$ if undersaturated.

Quartz will dissolve to the aqueous form when undersaturated or under highly alkaline conditions:



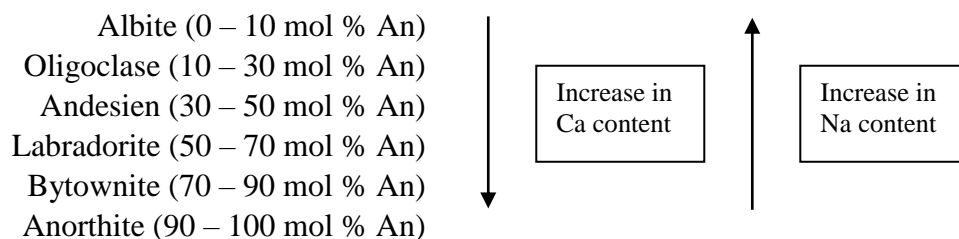
The hydrated form of $\text{SiO}_2(\text{aq})$, H_4SiO_4 , remains undissociated at pH values below pH 9 (Appelo and Postma, 1993) and the dissolution of quartz under these conditions can be written as:



Between pH 10 and pH 13 H_3SiO_4^- will be the stable specie and above pH 13 H_2SiO_4 will be the stable specie.

Feldspar dissolution

Plagioclase feldspar is frequently present as a minor mineral in the South African coal bearing strata (see **Chapter 6**) and have the general formula $(\text{Na,Ca})(\text{Al})_{1-2}(\text{Si})_{2-3}\text{O}_8$ with albite ($\text{NaAlSi}_3\text{O}_8$) and anorthite ($\text{CaAl}_2\text{Si}_2\text{O}_8$) as end-members. In the solid solution series Ca^{2+} replaces Na^{2+} and in order to keep electrochemical neutrality, an Al^{3+} atom will also replace a Si^{4+} atom. The percentage of an end-member (anorthite (An) or albite (Ab)) is often used to subdivide the solid solution series into a number of individual minerals:



The dissolution rate of plagioclase minerals increase with increasing An content and decreasing Ab content (Palandri and Kharaka, 2004). The reason for the increase in the rate of dissolution is related to the increase in Al content with higher anorthite content.

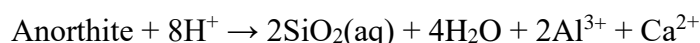
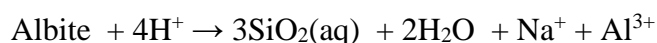
In silicate mineral dissolution, silicon-rich cation-depleted layers form as the slow step generally is the hydrolysis of the strong Si–O network bonds. Acceleration of

network hydrolysis occurs when metals like Al, which are bonded to the Si–O bridging bonds, are hydrolyzed and leached from the mineral surface.

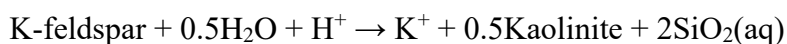
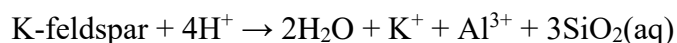
For example, the increase in dissolution rate observed above a threshold concentration of An 70–80 for plagioclase compositions has been attributed by Blum and Stillings (1995) to the lack of Si–O–Si linkages in compositions with high aluminum content. A mineral with a value of Al/Si approaching 1 is therefore hypothesized to dissolve by a different mechanism because aluminum is completely removed from the dissolving surface during dissolution, leaving only silicon atoms surrounded by nonbridging oxygens (Oelkers and Schott, 1995).

The average bond length of Si–O bonds within Al–O–Si linkages increases from 1.58 to 1.62 Å in the tetrahedral unit, suggesting that hydrolysis of Al–O–Si bonds in the plagioclase becomes easier as the Al/Si ratio increases. This observation is consistent with the increase in dissolution rate of plagioclase minerals as An content increases (Blum and Stillings, 1995).

Congruent and incongruent dissolution of feldspar minerals under acidic conditions are given below:

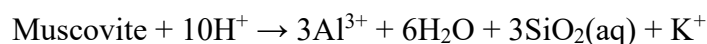


K-feldspar (KAlSi_3O_8) is often present as a minor mineral in the South African coal bearing strata. K-feldspar forms an incomplete solution series with albite, and K-feldspar will often contain small amounts of Na. The congruent and incongruent dissolution of K-feldspar under acidic conditions are given below:



Mica and clay dissolution

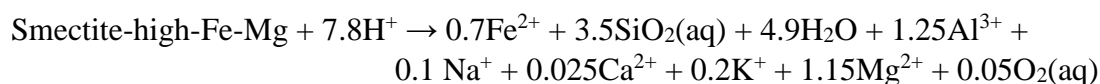
The congruent and incongruent dissolution of muscovite ($\text{KA}_3\text{Si}_3\text{O}_{10}(\text{OH})_2$) are given below:



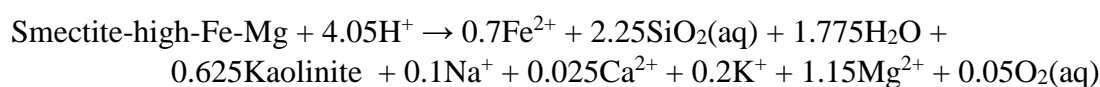
Glaucanite is often present in the Witbank and Highveld Coalfield coal bearing strata as markers on specific horizons indicating marine transgressions (see **Chapter 6**). Glaucanite is a member of the muscovite group and have the general formula of $(K,Na)(Fe^{3+},Al,Mg,Fe^{2+})_2(Si,Al)_4O_{10}(OH)_2$. The structure of glaucanite is essentially the same as muscovite. However, more Fe^{3+} than Al^{3+} is usually present in octahedral sites as well as significant amounts of Mg^{2+} and Fe^{2+} (Nesse, 1991). The charge deficiency resulting from the presence of divalent rather than trivalent cations in octahedral sites is balanced by substituting Si^{4+} for Al^{3+} in tetrahedral sites (Nesse, 1991). Due to the large amount of substituting in the glaucanite structure, glaucanite is more reactive and has a much higher reaction rate than muscovite as seen in **Table 2.8.3(A)** below.

Clays are produced from the weathering of feldspar, micas and other silicates. In the South African coal bearing strata kaolinite is much more frequent than smectite clays that include montmorillonite,.

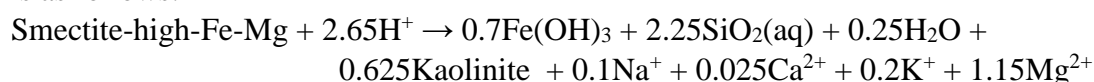
Montmorillonite has the general formula of $0.5(Ca, Na)_{0.67}(Al, Mg, Fe)_{4-6}(Si, Al)_8O_{20}(OH)_{4 \cdot n}(H_2O)$. For instance, smectite-high-Fe-Mg with the specific formula $Na_{0.1}Ca_{0.025}K_{0.2}Mg_{1.15}Fe_{0.7}Al_{1.25}Si_{3.5}O_{10}(OH)_2$ has the following congruent dissolution reaction:



The incongruent dissolution reaction of smectite-high-Fe-Mg to give kaolinite is as follows:

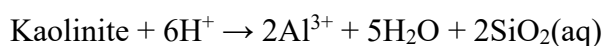


Incongruent dissolution reaction of smectite-high-Fe-Mg under oxidizing conditions is as follows:



Na^+ and Fe^{2+} in smectite are in exchangeable form and can be replaced by other species that compensate the charge. This reaction removes some Fe and acidity from the solution, and stores it in the solid phase. Cravotta and Rose (1994) report analogous Ca-Na exchange in AMD systems. In the latter case, by removing Ca^{2+} from solution, calcite dissolution was more extensive and alkalinity more extreme than otherwise possible. Because smectites are not generally stable in acid solutions, such reactions probably are of minor importance until alkaline conditions are reached.

The dissolution of kaolinite is given below:



Kaolinite is however stable over a wide pH and Al-activity range.

2.8.3 Silicate mineral dissolution rates

The dissolution rate of selected silicate minerals often present in coal mine drainage environments is given below:

Table 2.8.3(A). Selected silicate mineral dissolution rates at 25°C.

Minerals	Acid Mechanism		Neutral Mechanism	Base Mechanism	
	log k (mol.m ⁻² .s ⁻¹)	n _{H⁺}	log k (mol.m ⁻² .s ⁻¹)	log k (mol.m ⁻² .s ⁻¹)	n _{H⁺}
Quartz ^a	-	-	-13.99	-16.29	-0.500
Albite ^b	-10.16	0.457	-12.56	-15.60	-0.572
Oligoclase ^c	-9.67	0.457	-	-	-
K-feldspar ^d	-10.06	0.500	-12.41	-21.20	-0.823
Muscovite ^e	-11.85	0.370	-13.55	-14.55	-0.220
Glauconite ^f	-4.80	0.700	-9.10	-	-
Kaolinite ^g	-11.31	0.777	-13.18	-17.05	-0.472
Montmorillonite ^h	-12.71	0.220	-14.41	-14.41	-0.130
Smectite ⁱ	-10.98	0.340	-12.78	-16.52	-0.400

References
All reaction rate data cited by Palandri and Kharaka (2004):
^a Tester et al. (1994) (neutral mechanism) and Knauss and Wolery (1988) (base mechanism).
^{b & c & d} Derived parameters by Palandri and Kharaka (2004).
^e Nagy (1995).
^f Sverdrup (1990).
^g Carroll and Walther (1990).
^h Nagy (1995), montmorillonite composition K_{0.318}(Si_{3.975}Al_{0.025})(Al_{1.509}Fe_{0.205}Mg_{0.283})(OH)₂.
ⁱ Bauer and Berger (1998), smectite composition K_{0.04}Ca_{0.5}(Al_{2.8}Fe_{0.53}Mg_{0.7})(Si_{7.65}Al_{0.35})O₂₀(OH)₄.

From the above table the following remarks could be made:

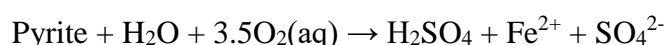
- Overall the dissolution of silicates is positively related to the $a\text{H}^+$ under acidic conditions and negatively related to $a\text{H}^+$ under alkaline conditions.
- In **Table 2.8.3(A)** no acid mechanism for quartz is reported as quartz is stable under acidic conditions.
- Oligoclase is more stable than albite under alkaline conditions.
- Glauconite has a much higher dissolution rate than muscovite under acidic conditions. This is because of less Si-O bonds in the glauconite structure than in muscovite.

2.9 Secondary minerals

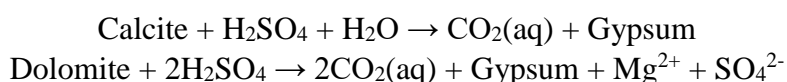
Gypsum

Some of the sulphate generated by pyrite dissolution will precipitate with the Ca released from calcite neutralization to produce gypsum ($\text{CaSO}_4 \cdot 2\text{H}_2\text{O}$). This will consume some of the sulphate and calcium from solution. Van Tonder et al. (2003) report that the precipitation of gypsum bound the average sulphate produced from several coal mines in South Africa.

Gypsum is formed by the reaction $\text{Ca} + \text{SO}_4^{2-} + \text{H}_2\text{O} \rightarrow \text{CaSO}_4 \cdot 2\text{H}_2\text{O}$. For every mole of pyrite that oxidizes, 1 mole of sulphuric acid forms:



One mole of respectively calcite or dolomite is necessary to neutralize respectively one and two moles of H_2SO_4 , which can again produce 1 mole of gypsum:



Gypsum is very soluble and the sulphate and calcium will be released into solution as soon as gypsum is undersaturated.

Other secondary minerals

Fe-hydroxides and several Fe-hydroxysulphates are often present in the AMD environment. Hematite (Fe_2O_3) is not formed directly at low temperature but rather ferrihydrite ($\text{FeOOH} \cdot \text{H}_2\text{O}$) is formed. When ferrihydrite later accumulates in soils and sediments under dry conditions, it may eventually dehydrate and recrystallize to form more thermodynamically stable goethite (FeOOH) and later hematite (Fe_2O_3).

Newly precipitated Fe is most likely to be ferrihydrite, schwertmannite ($\text{Fe(III)}_{16}\text{O}_{16}(\text{OH})_{12}(\text{SO}_4)_2$), or some other poorly crystalline phase (Cravotta, 1994).

A wide variety of Fe-sulphates may form in the AMD environment. Evaporation of AMD or oxidation of pyrite under humid conditions is usually the mechanisms that form these phases (Cravotta, 1994). At pH values below about pH 3.5, Fe(III) will mostly be present in solution as $\text{Fe}(\text{SO}_4)^+(\text{aq})$ and $\text{FeH}(\text{SO}_4)^{2+}(\text{aq})$. At high Fe concentrations in solution, particularly under evaporating conditions, several secondary sulphate phases can precipitate from solution or form on the surface of oxidizing pyrite in near-surface rock or mine spoil.

If appreciable K^+ or Na^+ is present, jarosite ($\text{KFe}_3(\text{OH})_6(\text{SO}_4)_2$) or natrojarosite ($\text{NaFe}_3(\text{OH})_6(\text{SO}_4)_2$) becomes stable under relatively acid conditions. Also, hydronium jarosite ($(\text{H}_3\text{O})\text{Fe}_3(\text{OH})_6(\text{SO}_4)_2$) of poorly defined character may occur in

solid solution with K- or Na-jarosite (Alpers et al., 1994). In South Africa little K and more Na is present in AMD.

Several hydrated acid sulphates are often observed in the AMD environment. An extensive list of possible sulphates is given below:

Fe(II), Mg and Mn containing hydrated acid sulphates:

Fe sulphates		Mg equivalent	Mn Equivalent
Szomolnikite	FeSO ₄ .H ₂ O	Kieserite	Szomikite
Rozenite	FeSO ₄ .4H ₂ O	Starkeyite	Ilesite
Siderotil	FeSO ₄ .5H ₂ O	Pentahydrate	Jokokuite
Ferrohexahydrate	FeSO ₄ .6H ₂ O	Hexahydrate	Chvaliteite
Melanterite	FeSO ₄ .7(H ₂ O)	Epsomite	Mallardite
		Magnesiocopiapite	
Copiapite	Fe(II)Fe(III) ₄ (SO ₄) ₆ (OH) ₂ .20(H ₂ O)	(with Mg replacing Fe(II))	-

Fe(II), Mg, Mn and Al containing hydrated acid sulphates where A(B)₂(SO₄)₄.x(H₂O):

Romerite	Fe ₃ (SO ₄) ₄ .14(H ₂ O)
Pickeringite	MgAl ₂ (SO ₄) ₄ .22(H ₂ O)
Halotrichite	Fe(II)Al ₂ (SO ₄) ₄ .22(H ₂ O)
Apjohnite	MnAl ₂ (SO ₄) ₄ .22(H ₂ O)
Bilinite	Fe(II)Fe(III) ₂ (SO ₄) ₄ .22(H ₂ O)

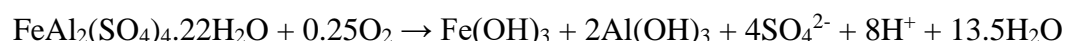
Fe(III) and Al containing hydrated acid sulphates where (A)₂(SO₄)₃.x(H₂O):

Lausenite	Fe(III) ₂ (SO ₄) ₃ .6(H ₂ O)
Kornelite	Fe(III) ₂ (SO ₄) ₃ .7(H ₂ O)
Coquimbite	Fe(III) ₂ (SO ₄) ₃ .9(H ₂ O)
Paracoquimbite	Fe(III) ₂ (SO ₄) ₃ .9(H ₂ O)
Quenstedtite	Fe(III) ₂ (SO ₄) ₃ .10(H ₂ O)
Alunogen	Al ₂ (SO ₄) ₃ .17(H ₂ O)
Meta-alunogen	Al ₄ (SO ₄) ₆ .27(H ₂ O)

Some of the commonly observed phases in literature include melanterite (FeSO₄.7H₂O), rozenite (FeSO₄.4H₂O), szomolnikite (FeSO₄.H₂O), copiapite (Fe(II)Fe(III)₄(SO₄)₆(OH)₂.20H₂O), and coquimbite (Fe₂(SO₄)₃.9H₂O) (Nordstrom, 1982; Alpers et al., 1994; Dixon et al., 1982; Bayless and Olyphant, 1993, all cited in (Cravotta, 1994). Cravotta (1991) and Cravotta (1994) have observed the above phases plus roemerite (Fe(II)Fe(III)₂(SO₄)₄.14H₂O), pickeringite (MgAl₂(SO₄)₄.22H₂O) and halotrichite (Fe(II)Al₂(SO₄)₄.22H₂O) in coal mine spoil in Pennsylvania, USA.

The formation of these hydrous sulphate minerals can be significant because they represent "stored acidity" (Alpers et al., 1994). The "stored acidity" is released when the minerals are dissolved by recharge or runoff and when the Fe or Al undergoes hydrolysis. The secondary minerals are generally relatively soluble and will

disappear with time except for goethite (Appelo and Postma, 1993) and hematite. For example, the dissolution of halotrichite:



or coquimbite:



shows this effect (Cravotta, 1994). The storage and release of acidity by these mechanisms can cause considerable temporal variability in water quality or, alternatively, can cause acid drainage to continue even after pyrite oxidation has been curtailed.

Secondary mineral dissolution rate

The mineral dissolution rate of selected secondary minerals is given in **Table 2.9(A)** below:

Table 2.9(A). Selected secondary mineral dissolution rates.

Minerals	Acid Mechanism		Neutral Mechanism
	log k (mol.m ⁻² .s ⁻¹)	<i>n</i> _{H⁺}	log k (mol.m ⁻² .s ⁻¹)
Gypsum^a	-	-	-2.79
Goethite^b	-	-	-7.94
Hematite^c	-9.39	1.000	-14.60
References			
All reaction rate data cited by Palandri and Kharaka (2004):			
^a Raines and Dewers (1997).			
^{b & c} Ruan and Gilkes (1995).			

Precipitation reaction rate data of secondary minerals would be valuable for application in geochemical modelling. However, precipitation data do not exist for most minerals, because in mineral precipitation experiments, undesired metastable reaction products usually precipitate instead of the desired mineral (Palandri and Kharaka, 2004).

2.10 Final remarks and conclusions

With regard to the overall mineral reactions in AMD as discussed in this chapter, the following general conclusions could be made:

Pyrite

- Pyrite was precipitated in an anoxic-sulphidic geochemical environment during coal formation. Because of mining, pyrite is exposed to the oxic environment

where it oxidizes and produces acid. The overall pyrite reaction series is among the most acid-producing of all weathering processes in nature (Cravotta and Rose, 1994).

- Pyrite oxidation by dissolved oxygen (**Equation 2.6.4(A)**) produces acidity, sulphate and ferrous iron. Some authors regard this reaction to be purely abiotic and it was also successfully repeated under abiotic conditions in the laboratory. Others regard the oxidation reaction to be intermediated by bacterial working through a direct mechanism. The direct mechanism occurs with bacterial cells attached to the grains, where the cells use dissolved O₂ as the electron acceptor and biologically oxidize pyrite sulphur by an enzyme system.

Because of the presence of oxygen, the produced ferrous iron will be oxidized to ferric iron that will hydrolyse to form iron(III)-hydroxides. With abundant supply of oxygen, ferrous iron oxidation to ferric iron is the rate limiting step of the oxidation of pyrite by oxygen that produces iron(III)-hydroxides and sulphate.

- Pyrite oxidation by ferric iron is more rapidly than oxidation by oxygen and produces acidity, ferrous iron and sulphate. Oxygen is however required for the oxidation of ferrous iron to form ferric iron. Where oxygen is readily available, the oxidation of ferrous to ferric iron (**Equation 2.6.4(B)**) will be the rate limiting step.
- The rate of ferric iron production depends on whether it is catalysed by iron-oxidizing bacteria. The indirect mechanism occurs when the ferric iron that oxidizes pyrite (**Equation 2.6.4(E)**) is produced by Fe-oxidation bacteria that catalyse the oxidation of ferrous iron (**Equation 2.6.4(B)**).
- The pyrite containing material is often not in full contact with the atmosphere and oxygen migration to the pyrite surface may actually become the rate limiting step in coal mine waste instead of ferric iron production. Oxygen is also required by the bacteria that mediate pyrite oxidation reaction through the *direct* or *indirect* mechanisms

Carbonate Minerals

- The carbonate system is by far the most important buffer for water systems in nature. This is because carbonate minerals are 1) widely present in sedimentary rocks and 2) carbonate is considered as a soluble mineral when undersaturated.
- In a complete open system no carbonic acid will form that will produce additional acidity as under closed conditions.

- Although it is possible that siderite constitutes a temporary neutralizing agent, it is not effective overall.
- Where siderite is more frequent in carbonaceous clastic rocks than in coal seams or in non-carbonaceous clastic rocks, calcite and dolomite is generally more frequent in coal seam samples than in clastic rocks.
- The largest component of water inflow into coal mine waste is rainwater that contains almost no alkalinity (alkalinity is defined as the capacity to neutralize acid). Groundwater from the surrounding Karoo aquifer that flows into spoils of rehabilitated open-cast mines contains low to moderate amounts of alkalinity (<300 mg/l CaCO₃) which are insufficient for acid mine drainage neutralization.
- In-situ carbonate minerals play the most important role in the neutralization of acid mine drainage from coal mines in South Africa.¹ In the Karoo Super Group (that contains all South African coal) carbonate minerals are present in-situ in the coal bearing strata (see **Section 6.3**).

Silicate Minerals

- Silicate minerals consume acid as they dissolve because of the hydrolysis of silica tetrahedral consuming acid.
- The lower the Si/O ration in the silicate structures, the higher the charge on the silicate tetrahedral. This greater charge is counterbalanced by counterions, which in turn are replaced by more protons. Therefore, the lower the Si/O ratio of the silicate mineral, the greater the potential to neutralize acid.
- Al and Fe tend to hydrolyze in solution, producing acid. Silicate minerals with Al and Fe in octahedral sites will have lower buffering capacities than similar minerals where no hydrolysis of Al and Fe are possible.
- Congruent dissolution occurs where the silicate mineral dissolves completely to form ions in solution. Upon incongruent dissolution, secondary minerals form such as gibbsite, ferrihydrate or kaolinite. If silicate minerals dissolve congruently, they will generally consume more acid than weathering in an incongruent process.

¹ In contrast with the sedimentary coal bearing strata of South Africa, the (slightly metamorphosed) gold bearing strata of the Witwatersrand Super Group contain no in-situ neutralization capacity. Because dolomite aquifers of the Transvaal Super Group often overly the Witwatersrand Super Group, infiltrating dolomite water helps to neutralize acid generating in the underlying gold mines. However, the large quantities of inflowing water from the dolomite aquifer often complicate mining and the re-mining of old flooded mines; the further partial dewatering of dolomite aquifers is also of great concern as they are classified as primary aquifers in a water poor South Africa.

Secondary Minerals

- Some of the sulphate generated by pyrite dissolution will precipitate with the Ca released from calcite neutralization to produce gypsum ($\text{CaSO}_4 \cdot 2\text{H}_2\text{O}$). This will consume some of the SO_4 and Ca from solution. Van Tonder et al. (2003) report that the precipitation of gypsum bound the average SO_4 produced from several coal mines in South Africa.
- Hematite (Fe_2O_3) is not directly formed at low temperature but rather ferrihydrite ($\text{FeOOH} \cdot \text{H}_2\text{O}$) is formed. When ferrihydrite later accumulates in soils and sediments under dry conditions, it may eventually dehydrate and recrystallize to form more thermodynamically stable goethite (FeOOH) and hematite (Fe_2O_3).
- A wide variety of Fe-sulphates may form in the AMD environment. Evaporation of AMD or oxidation of pyrite under humid conditions is usually the mechanisms that form these phases (Cravotta, 1994).
- If appreciable K^+ or Na^+ is present, jarosite ($\text{KFe}_3(\text{OH})_6(\text{SO}_4)_2$) or natrojarosite ($\text{NaFe}_3(\text{OH})_6(\text{SO}_4)_2$) becomes stable under relatively acid conditions.
- The formation of hydrous sulphate minerals can be significant because they represent "stored acidity". The "stored acidity" is released when the minerals are dissolved by recharge or runoff, and when the Fe or Al undergoes hydrolysis. The secondary minerals are generally relatively soluble and will disappear with time except for goethite and hematite.

Practical application to geochemical modelling

- Assuming pseudo-equilibrium states solve many of the problems involved in the modelling of a system that is not in full equilibrium with its environment.
- Kinetic rate laws could be defined for the dissolution of minerals that do not react or precipitate fast enough to be in equilibrium with the water composition, or do not react slowly enough to be excluded or suppressed in the geochemical model.
- Pyrite is included as a kinetic mineral in geochemical models and the oxidation rate of pyrite oxidation by oxygen must include the dependence on the oxygen fugacity and the hydrogen activity.
Although Fe^{3+} is formed rapidly at conditions with pH larger than pH 4, Fe^{3+} is relatively insoluble under these conditions and tends to form $\text{Fe}(\text{OH})_3$ or other solids, so that little Fe^{3+} remains in solution to oxidize pyrite. At pH conditions of about below pH 3, the concentration of Fe^{3+} becomes high enough so that oxidation of pyrite by Fe^{3+} becomes the main mechanism for acid production, with bacterial reoxidation of Fe^{2+} providing the Fe^{3+} .

Modelling of the kinetic oxidation rate of pyrite by ferric iron must include dependence on the hydrogen activity and the ferrous and ferric iron activity.

However the oxidation rate is negatively dependent on the presence of Fe^{2+} because ferrous iron may accumulate on the pyrite surface and block the surface reaction sites (Moses and Herman, 1991).

- At high pH and higher temperature, carbonate minerals will be closer to saturation and therefore surface control will increase. At low pH ranges and low temperature, carbonate mineral dissolution will not be controlled at the mineral surface but mineral bonds will break easily because the mineral is undersaturated. The dissolution rate of the mineral will therefore become more dependent on the transport rate of H^+ to the mineral surface. Carbonate minerals far from saturation (where the dissolution rate is transport controlled) will have a higher rate of dissolution and may be set to equilibrate with the water composition in geochemical modelling. If however the carbonate dissolution near saturation is modelled, the dissolution rate could be modelled using a kinetic rate law.
- Precipitation reaction rate data of secondary minerals would be valuable for application in geochemical modelling. However, precipitation data do not exist for most minerals, because in mineral precipitation experiments, undesired metastable reaction products usually precipitate instead of the desired mineral (Palandri and Kharaka, 2004).

2.11 References

Ahonen, L. and Tuovinen, O.H. (1989). *Microbiological oxidation of ferrous iron at low temperatures*. Applied and Environmental Microbiology, 55, 312-316.

Alpers, C.N., Blowes, D.W., Nordstrom, D.K. and Jambor, J.L. (1994). *Secondary minerals and acid mine-water chemistry*. In: *Environmental geochemistry of sulfide mine-wastes* (eds. D.W. Blowes, and J.L. Jambor). Short Course Handbook, vol. 22, Mineralogical Association of Canada, pp. 247-270.

Appelo, C.A.J. and Postma, D. (1993). *Geochemistry, groundwater and pollution*. Balkema, 536 p.

Bauer, A. and Berger, G. (1998). *Kaolinite and smectite dissolution rate in high molar KCl solutions at 35° and 80°C*. Appl. Geochem., 13, 905-916.

Bayless, E.R. and Olyphant, G.A. (1993). *Acid-generating salts and their relationship to the chemistry of groundwater and storm runoff at an abandoned minesite in southwestern Indiana, USA*. Journal of Contaminant Hydrology, 12, 313-328.

- Berner, R.A. (1981). *A new geochemical classification of sedimentary environments*. J. Sed. Petrol., 51(2), 359-365.
- Bethke, C.M. (1996). *Geochemical reaction modelling*. Oxford, 397 p.
- Blum, A.E. and Stillings, L.L. (1995). *Feldspar dissolution kinetics*. In: *Chemical Weathering Rates of Silicate Minerals* (eds. A. F. White and S. L. Brantley). Mineralogical Society of America, Washington, D.C. pp. 291-351.
- Boon, M. (2001). *The mechanism of 'direct' and 'indirect' bacterial oxidation of sulphide minerals*. Short communication, Hydrometallurgy, 62, 67-70.
- Brantley, S.L. (2003). *Reaction kinetics of primary rock-forming minerals under ambient Conditions*. *Fresh Water Geochemistry, Weathering, and Soils* (ed. Drever, J.I.). In: *Treatise on Geochemistry* (eds. Turekian, K.K. and Holland, H.D.), 5, 73-118.
- Busenberg, E. and Plummer, L.N. (1982). *The kinetics of dissolution of dolomite in CO₂-H₂O systems at 1.5 to 65°C and 0 to 1 atm P(CO₂)*. Am. J. Sci. 282, 45-78.
- Butler, I.B. and Rickard, D. (2000). *Framboidal pyrite formation via the oxidation of iron (II) monosulfide by hydrogen sulphide*. Geochim. Cosmo. Acta, 64(15), 2665-2672.
- Cadle, A.B., Cairncross, B., Christie, A.D.M. and Roberts, D.L. (1990). *The Permian-Triassic coal-bearing deposits of the Karoo Basin, Southern Africa*. Information Circular No. 218, Economic Geology Research Unit, University of the Witwatersrand, Johannesburg.
- Cairncross, B. and Cadle, A.B. (1987). *A genetic stratigraphy for the Permian coal-bearing Vryheid Formation in the east Witbank Coalfield, South Africa*. S. Afr. J. Geol., 90(3), 219-230.
- Carroll, S.A. and Walther, J.V. (1990). *Kaolinite dissolution at 25°, 60°, and 80°C*. Am. J. Sci., 290, 797-810.
- Caruccio, F.T., Ferm, J.C., Horne, J., Geidel, G. and Baganz, B. (1977). *Paleoenvironment of coal and its relation to drainage quality*. Report No. R-802597-02, U.S. Environmental Protection Agency.
- Casey, W.H., Westrich, H.R., Banfield, J.F., Ferruzzi, G. and Arnold, G. W. (1993). *Leaching and reconstruction at the surfaces of dissolving chain-silicate minerals*. Nature 366(6452), 253-256.
- Compton, R.G. and Sanders, G.H.W. (1993). *The dissolution of calcite in aqueous acid: the influence of humic species*. J. Colloid Interface Sci., 158, 439-445.

Cravotta, C.A. (1991). *Geochemical evolution of acidic groundwater at a reclaimed surface coal mine in western Pennsylvania*. In: *Proceedings of the 1991 National Meeting of the American Society of Surface Mining and Reclamation, May 14-17, 1991, Princeton*. American Society for Surface Mining and Reclamation, pp. 43-68.

Cravotta, C.A. (1994). *Secondary iron-sulfate minerals as sources of sulfate and acidity: The geochemical evolution of acidic groundwater at a reclaimed surface coal mine in Pennsylvania*, In: *Environmental geochemistry of sulfide oxidation* (eds. Alpers, C.N. and Blowes, D.W.). American Chemical Society Symposium Series, Washington, D.C., vol. 550, pp. 345-364.

Cravotta, C.A. and Rose A.W. (1994). *Geochemistry of coal mine drainage*. In: *Coal Mine Drainage Prediction and Pollution Prevention in Pennsylvania*. Pennsylvania Department of Environmental Protection.

Internet: <http://www.dep.state.pa.us/dep/deputate/minres/districts/cmdp/main.htm>.

Dixon, J.B., Hossner, L.R., Senkayi, A.L. and Egashira K. (1982). *Mineralogical properties of lignite overburden as they relate to minespoil reclamation*. In: *Acid sulfate weathering* (eds. J.A. Kittrick, D.S. Fanning, and L.R. Hossner). Soil Science Society of America, pp. 169-191.

Ebbing, D.D. (1996) *General chemistry*. 5th Edition, Houghton Mifflin Company, Boston.

Evangelou, V.P. (1995). *Pyrite oxidation and its control*. CRC Press, Boca Raton, Florida.

Folk, R.L. (2005). *Nannobacteria and the formation of framboidal pyrite: Textural evidence*. *J. Earth Syst. Sci.*, 114(3), 369-374.

Gleisner, M. (2005). *Quantification of mineral weathering rates in sulfidic mine tailings under water-saturated conditions*. PhD thesis. Department of Geology and Geochemistry, Stockholm University, Sweden.

Gleisner, M., Herbert, R.B. and Kockum, P.C.F (2006). *Pyrite oxidation by Acidithiobacillus ferrooxidans at various concentrations of dissolved oxygen*. *Chemical Geology*, 225(1-2), 16-29.

Goodman, A.E., Khalid, A.M. and Ralph, B.J. (1981). *Microbial ecology of Rum Jungle, Part I. Environmental study of sulphidic overburden dumps, experimental heap-leach piles and tailings dam area*. Report AAEC/E531, Australian Atomic Energy Commission.

Guevremont J.M., Strongin D.R., and Schoonen M.A.A. (1998). *Thermal chemistry of H₂S and H₂O on the (100) plane of pyrite: Unique reactivity of defect sites*. Am. Mineral. 83, 1246-1255.

Gutjahr, A., Dabringhaus, H. and Lacmann, R. (1996). *Studies of the growth and dissolution kinetics of the CaCO₃ polymorphs calcite and aragonite: I. Growth and dissolution rates in water*. J. Cryst. Growth, 158, 296-309.

Hodgson, F.D.I. and Krantz, R.M. (1998). Groundwater Quality Deterioration in the Olifants River Catchment above the Loskop Dam with specialised investigation in the Witbank Dam Sub-Catchment. *Report to the WRC, Report 291/1/98*, Water Research Commission, Pretoria.

Holuszko, M.E., Matheson, A. and Grieve, D.A. (1992). *Pyrite occurrences in Telkwa and Quinsam coal seams*. In: *Geological Fieldwork 1992*. British Columbia Geological Survey Branch, pp. 527-536.

Jaynes, D.B., Rogowski, A.S. and Pionke, H.B. (1984). *Acid Mine Drainage from reclaimed coal strip mines. I. Model description*. Water Research Resources, 20, 233-242.

Kelly, D.P. and Wood, A.P. (2000). *How microbes mobilize metals in ores: A review of current understandings and proposal for further research*. Minerals and Metallurgical Processing, 19, 220-224.

Kleinmann, R.L.P., Crerar, D.A. and Pacelli, R.R. (1981). *Biogeochemistry of acid mine drainage and a method to control acid formation*. Mining Engineering, 33, 300-303.

Knauss, K.G. and Wolery, T. J. (1988). *The dissolution kinetics of quartz as a function of pH and time at 70°C*. Geochim. Cosmochim. Acta, 52, 43-53.

Kwong, Y.T.J. (1993a). *Minesite acid rock drainage assessment and prevention – a new challenge for a mining geologist*. Proc. Int. Mining Geology Conf., Kalgoorlie, pp 213-217.

Kwong, Y.T.J. (1993b). *Prediction and prevention of Acid Rock Drainage from a geological and mineralogical perspective*. MEND Report 1.32.1, Ottawa.

Larsen, D. and Mann, R. (2005). *Origin of high manganese concentrations in coal mine drainage, eastern Tennessee*. Journal of Geochemical Exploration, 86, 143-163.

Ledin, M. and Pedersen, K. (1996). *The environmental impact of mine wastes – Roles of microorganisms and their significance in treatment of mine wastes*. Earth-Science Reviews, 41, 67-108.

Lüttge, A., Bolton, E.W. and Lasaga, A.C. (1999). *An interferometric study of the dissolution kinetics of anorthite: the role of reactive surface area*. Am. J. Sci., 299, 652–678.

Morse, J.W. and Arvidson, R.S. (2002). *The dissolution kinetics of major sedimentary carbonate minerals*. Earth-Science Reviews, 58, 51-84.

Morse, J.W. and Wang, Q. (1997). *Pyrite formation under conditions approximating those in anoxic sediments: II. Influence of precursor iron minerals and organic matter*. Marine Chemistry, 57, 187-193.

Moses, C.O. and Herman, J.S. (1991). *Pyrite oxidation at circumneutral pH*. Geochim. Cosmo. Acta, 55, 471-482.

Nagy K.L. (1995). *Dissolution and precipitation kinetics of sheet silicates*. In: *Chemical Weathering Rates of Silicate Minerals* (eds. A. F. White and S. L. Brantley). Mineralogical Society of America, Washington, D.C., pp. 173-233.

Nesse, W.D. (1991). *Optical mineralogy*. 2nd Edition, Oxford, New York.

Nordstrom, D.K. (1982). *Aqueous pyrite oxidation and the consequent formation of secondary iron minerals*. In: *Acid sulfate weathering* (eds. Kittrick, J.A., Fanning, D.S. and Hossner, L.R.), Soil Science Society of America, pp. 37-63.

Nordstrom, D.K. and Munoz, J.L. (1994). *Geochemical Thermodynamics*. 2nd Edition, Blackwell, Boston.

Ohfuji, H. and Rickard, D. (2005). *Experimental syntheses of framboids – a review*. Earth-Science Reviews, 71, 147-170.

Oelkers, E.H. and Schott, J. (1995). *Experimental study of anorthite dissolution and the relative mechanism of feldspar hydrolysis*. Geochim. Cosmochim. Acta, 59, 5039-5053.

Olson, G.J. (1991). *Rate of Pyrite Bioleaching by Thiobacillus ferrooxidans: Results of an Interlaboratory Comparison*. Applied and Environmental Microbiology, 57, 642-644.

Palandri, J.L. and Kharaka, Y.K. (2004). *A compilation of rate parameters of water-mineral interaction kinetics for application to geochemical modelling*. USGS Open file report 2004-1068, United States Geological Survey, California.

Plummer, L.N., Wigley, T.M.L. and Parkhurst, D.L. (1978). *The kinetics of calcite dissolution in CO₂-water systems at 5° to 60°C and 0.0 to 1.0 atm CO₂*. Am. J. Sci., 278, 179-216.

- Renton, J.J. and Bird, D.S. (1991). *Association of coal macerals, sulphur, sulphur species and the iron disulphide minerals in Three Column of the Pittsburgh Coal*. Int. J. Coal Geol. 17, 21-50
- Rickard, D. (1997). *Kinetics of pyrite formation by the H₂S oxidation of iron(II)monosulphide in aqueous solutions between 25°C and 125°C: The rate equation*. Geochim. Cosmochim. Acta, 61, 115-134.
- Rickard, D. and Luther, G.W. (1997). *Kinetics of pyrite formation by the H₂S oxidation of iron (II) monosulphide in aqueous solutions between 25°C and 125°C: The mechanism*. Geochim. Cosmochim. Acta, 61, 135-147.
- Raines, M.A. and Dewers, T.A. (1997). *Mixed transport/reaction control of gypsum dissolution kinetics in aqueous solutions and initiation of gypsum karst*. Chem. Geol., 140, 29-48.
- Ruan, H.D. and Gilkes, R.J. (1995). *Acid dissolution of synthetic aluminous goethite before and after transformation to hematite by heating*. Clay Minerals, 30, 55-65.
- Sawlowicz, Z. (1993). *Pyrite framboids and their development: a new conceptual mechanism*. Int. J. Earth Sci., 82(1), 148-156.
- Schoonen, M.A.A. (2004). *Mechanisms of sedimentary pyrite formation*. Special Paper 379: Sulfur Biogeochemistry - Past and Present, 379, 117-134.
- Schoonen, M.A.A. and Barnes, H.L. (1991). *Reactions forming pyrite and marcasite from solution via FeS precursors below 100°C*. Geochim. Cosmochim. Acta, 60, 115-134.
- Singer, P.C. and Stumm, W., 1970. *Acid mine drainage: The rate-determining step*. Science, 167, 1121-1123.
- Sjoberg, E.L. (1978). *Kinetics and mechanism of calcite dissolution in aqueous solutions at low temperatures*. Stockholm Contrib. Geol., Vol. 32, 92 pp.
- Stumm, W. and Morgan, J.J. (1981). *Aquatic chemistry, An introduction and emphasizing chemical equilibria in natural waters*. 2nd Edition, Wiley, New York.
- Sverdrup, H.U. (1990). *The kinetics of base cation release due to chemical weathering*. Lund University Press, Lund, 246 p.
- Talman S. J., Wiwchar B. and Gunter W. D. (1990). *Dissolution kinetics of calcite in the H₂O-CO₂ system along the steam saturation curve to 210°C*. In: *Fluid-Mineral Interactions: A Tribute to H. P. Eugster* (eds. R. J. Spenser and I.-M. Chou). Lancaster Press, San Antonio, pp. 41-55.

Tester, J.W., Worley, W.G., Robinson, B.A., Grigsby, C.O., and Feerer, J.L. (1994). *Correlating quartz dissolution kinetics in pure water from 25 to 625°C*. Geochim. Cosmochim. Acta, 58, 2407-2420.

Van Tonder, G., Vermeulen, D., Cogho, V., Kleynhans, J. (2003). *Initial prediction of the decant rate and sulfate concentration from rehabilitated open-cast coal mines in South Africa*. 6th ICARD conference, Cairns, QLD, 12 – 18 July 2003.

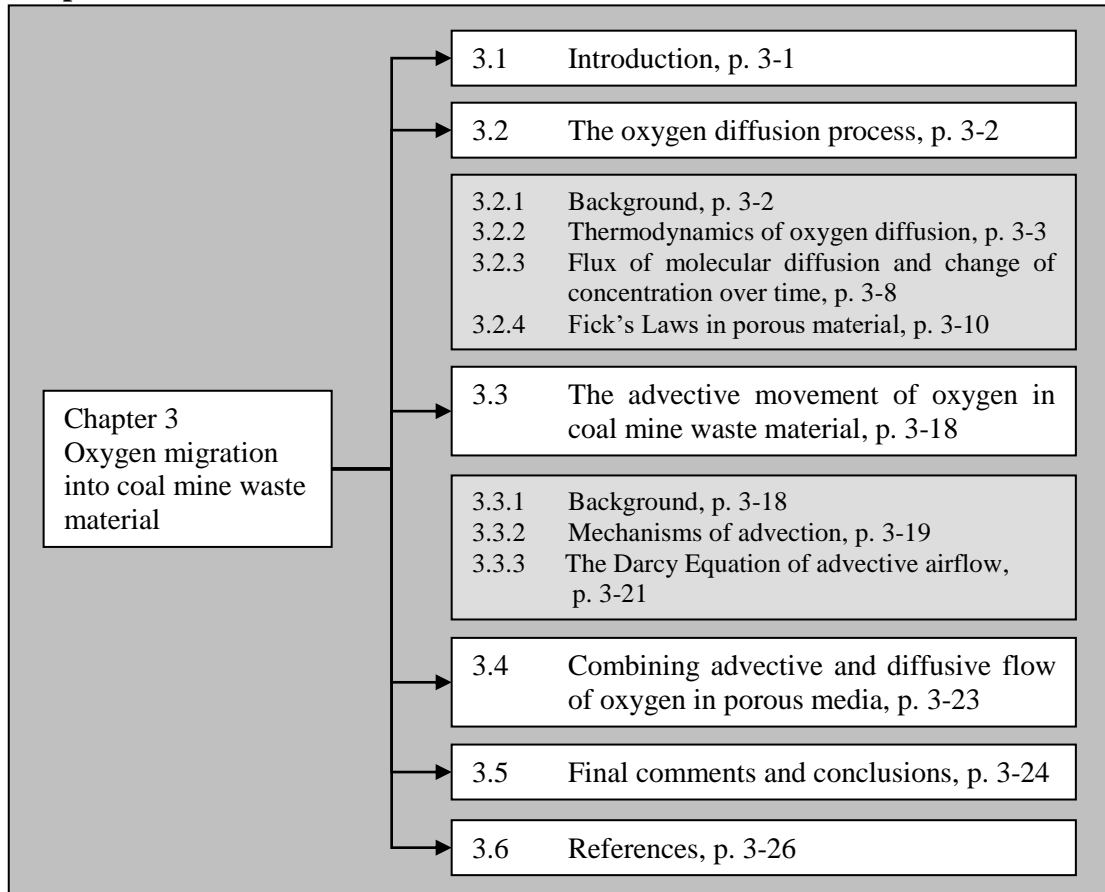
Ward C.R. (2002). *Analysis and significance of mineral matter in coal seams*. Int. J. Coal Geol., 50, 135-168.

Williamson, M.A. and Rimstidt, J.D. (1994). *The kinetics and electrochemical rate-determining step of aqueous pyrite oxidation*. Geochim. Cosmo. Acta, 58, 5443-5454.

Zhu, C. and Anderson, G.M. (2002). *Environmental applications of geochemical modeling*. Cambridge, 284 p.

3 Oxygen migration into coal mine waste material

Chapter Structure



3.1 Introduction

In unsaturated coal mine waste, pyrite will be oxidized by oxygen that spontaneously migrates into the coal mine waste materials. Experimental data of Williamson and Rimstidt (1994) and Gleisner (2005) and field data of Morin (1993) also indicate that oxidation of pyrite with Fe(III) is only significant in oxic conditions. Furthermore, acidophilic bacteria that mediate pyrite oxidation (below pH 3) can also only survive if oxygen is available. Oxygen is therefore an absolute necessity for the AMD generation process. The oxidation mechanisms of pyrite are discussed in more detail in **Chapter 2**.

In the first few meters of fresh coal mine waste, oxygen consumption is generally fast enough in order that oxygen is not readily available to the deeper parts of the waste. The supply of oxygen to pyrite grains is therefore an important rate limiting step in the production of Acid Mine Drainage (AMD). This chapter discusses the migration of oxygen into coal mine waste material emphasizing the critical variables that influence oxygen migration directly and AMD therefore indirectly.

3.2 The oxygen diffusion process

3.2.1 Background

Diffusion is defined as the movement of molecules or ions from a region of higher to one of lower solute concentration as a result of their random thermal movement (Allaby and Allaby, 2003). Chemical diffusion occurs in both the fluid (gas, liquid) and solid phases.

Gaseous diffusion is the main process providing oxygen within waste rock dumps after their initial placement and diffusion remains active thereafter as long as the oxidation process contributes to the depletion of the oxygen concentration in the gas phase within the pile (Wels et al., 2003). Mbonimpa et al. (2003) states that diffusion in porous media occurs predominantly in the air phase or at least when the degree of saturation is below about 85 – 90%, whereafter the air filled porosity is discontinuous.

Coal mine waste are voluminous and end up as coal discard dumps on surface or as waste rock material in open cast pits. Large parts of coal mine waste material are unsaturated:

- A rehabilitated open cast mine will be flooded after a few decades up to the surface decant elevation. However, depending on the geometry of the mine, a large part, if not most of the open cast mine coal mine waste material, will be present above the mine water decant elevation in the unsaturated zone.
- Large parts of a coal discard dump on surface will be unsaturated and only the bottom of the dump is situated below the water level.

In the unsaturated zone both an aqueous and a gaseous phase are present between the solid grains. The availability of oxygen is an important control on the rate of pyrite oxidation and the subsequent production of AMD. The atmosphere surrounding the waste rock is a constant source of oxygen with a P_{O_2} of 0.2 atm.

In the coal mine waste material oxygen is consumed by the oxidation of pyrite. An oxygen concentration gradient is therefore created between the gas phase within the pile and the surrounding atmosphere. The oxygen gradient drives the atmospheric oxygen to the interior of the waste material pile. However, resistance to diffusion exists between molecules and between the molecules and the solid phase. When referring to the resistance to diffusion, a distinction must be made between the two types of diffusion, namely: molecular diffusion and Knudsen diffusion.

The resistance to diffusion is defined by Thorstenson and Pollock (1989) as follows:

- Molecular diffusion: *“Gas molecules collide with other gas molecules. These collisions may occur between like or unlike molecules. The diffusive flux*

depends on the molecular weights and temperature of the gases in the capillary tube but is unaffected by the physical nature of the pore walls.”

- Knudsen diffusion: *“The phenomenon known as Knudsen diffusion occurs when pore size or capillary diameter is sufficiently small, or the pressure is sufficiently low, so that the molecules will collide only with the walls (the particles in a porous medium are considered as giant molecules) and never experience collision with other gas molecules. The Knudsen diffusive flux depends upon the molecular weight, the temperature of the gas and the radius of the capillary tube but is independent on the number and different species of molecules.”*

Knudsen diffusion will not be considered further in this study, since a practical approach will rather be followed by introducing the concept of effective diffusivity. In **Section 3.2.4.2** a review of the different semi-empirical equations that exist in literature is given which models the *effective* resistance to diffusion in porous material that includes the tortuous path the molecules have to take when migrating through porous material.

3.2.2 Thermodynamics of oxygen diffusion

As with chemical reactions, difference in chemical potential μ is the driving force behind diffusion. The change of the Gibbs free energy with temperature, pressure and constituents is given by the differential equation (Appelo and Postma, 1994):

$$d\Delta G = -\Delta SdT + \Delta VdP + \sum_i \mu_i dn_i \quad \text{Eq. 3.2.2(A)}$$

Where ΔG is the Gibbs free energy that is liberated with each mole of i ($\text{J}\cdot\text{mol}^{-1}$) that reacts, ΔS is the entropy change of the reaction, T is absolute temperature (K), ΔV is the change in molar volume ($\text{cm}^3\cdot\text{mol}^{-1}$), P is pressure (atm), μ_i is the chemical potential of specie i ($\text{J}\cdot\text{mol}^{-1}$) and n_i is the moles of i .

The chemical potential indicates the change in the Gibbs free energy at a constant temperature and pressure if the amount of a constituent i varies, while all the other constituents remain constant ($dT = 0$ and $dP = 0$):

$$\mu_i = \left(\frac{\partial \Delta G}{\partial n_i} \right)_{T,P,n_{j \neq i}} \quad \text{Eq. 3.2.2(B)}$$

In coal mine waste material a gradient in the chemical potential of oxygen was illustrated in **Figure 3.2.2(A)**. At constant total temperature and pressure, for the transferring of dn_{O_2} moles of O_2 from Zone B to the reactive surface of the unoxidized pyrite core of Zone A, the free energy change must be the sum of the free energy changes for both of these zones:

$$dG = dG^A + dG^B = \mu_{O_2}^A dn_{O_2}^A + \mu_{O_2}^B dn_{O_2}^B$$

If mass transferred from Zone B to Zone A, then by the conservation of mass $dn_{O_2}^A = -dn_{O_2}^B$. With substitution:

$$dG = (\mu_{O_2}^A - \mu_{O_2}^B) dn_{O_2}^A$$

At equilibrium between Zone A and Zone B, the sum of the free energy changes for each of the phases will be zero, $dG = 0$, which requires that

$$\mu_{O_2}^A = \mu_{O_2}^B$$

At equilibrium $dG = 0$, and so with the spontaneous transfer of dn_i moles from B to A:

$$\mu_{O_2}^A < \mu_{O_2}^B$$

Similarly it could be shown that the chemical potential is higher in every subsequent zone:

$$\mu_{O_2}^A < \mu_{O_2}^B < \mu_{O_2}^C < \mu_{O_2}^D < \mu_{O_2}^E .$$

Because of the consumption of O_2 at the pyrite surface, a gradient in the chemical potential of O_2 will therefore exist from the contact with Zone A (the reactive surface of the unoxidized pyrite core), through Zone B (the non-reactive oxidized pyrite shell), Zone D and C (the pore space) towards Zone E (the atmosphere). Because of different diffusive rates in every zone (e.g. the rate of diffusion is smaller in the aqueous phase than through the gaseous phase) it must be noted that the gradient throughout the coal mine waste material will vary among the different coal mine waste materials. **Figure 3.2.2(A)**,

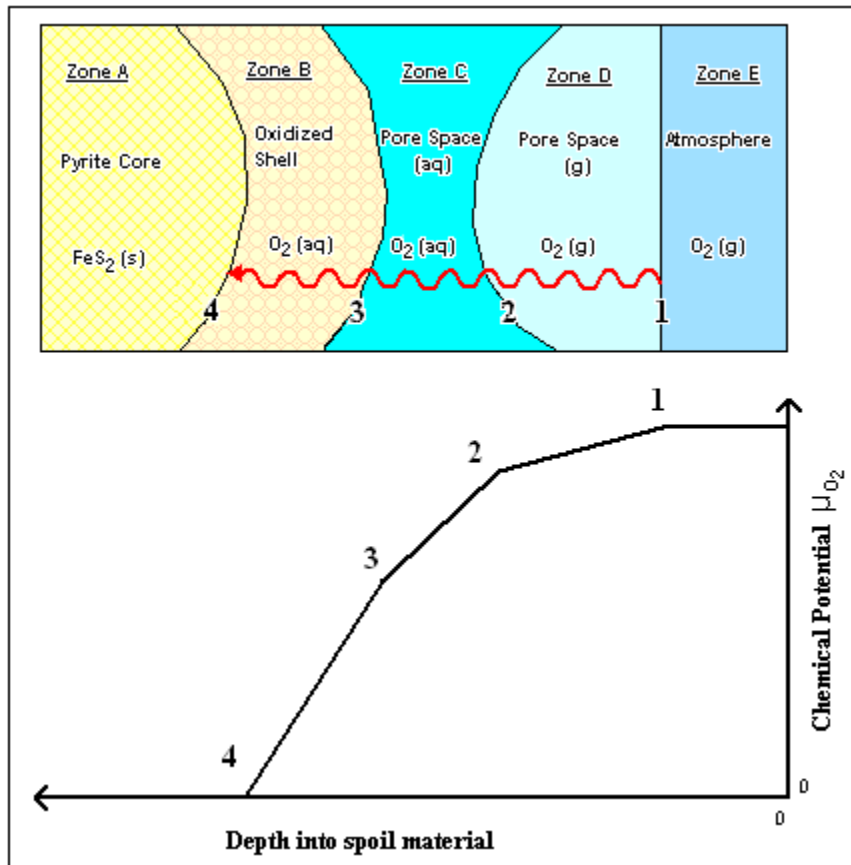


Figure 3.2.2(A). Oxygen diffusion from the pore space through the oxidized shell towards the pyrite core surface.

Defining the chemical potential for a gas

The physical meaning of the chemical potential is not obvious. It must have the units of energy per mole to be consistent with **Equation 3.2.2(B)**, and a relation with concentration can be expected (Appelo and Postma, 1994). Concentration is the density of atoms/molecules, which is related to the partial pressure of the specific gas in the system per unit volume.

The function of the chemical potential for an ideal gas could be derived that describes the chemical potential of the gas in terms of its partial pressure as shown below (after Appelo and Postma, 1994):

For a perfect gas, the following equation describes the relation between pressure, volume and the number of moles of an ideal gas:

$$PV = n_i RT \quad \text{Eq. 3.2.2(C)}$$

where R is the gas constant ($8.314 \text{ J.K}^{-1}.\text{mol}^{-1}$).

From **Equation 3.2.2(A)**, at a constant temperature and mass of constituents ($dT = 0$ and $dn_i = 0$), it could be shown that the pressure effect is given by:

$$\Delta V = \left(\frac{\partial \Delta G}{\partial P} \right)_{T, n_i} \quad \text{Eq. 3.2.2(D)}$$

A function for μ_{O_2} of an ideal gas, using the gas law as defined by **Equation 3.2.2(C)**, could be derived. Differentiating **Equation 3.2.2(A)** twice gives the following:

$$\left(\frac{\partial}{\partial P} \left(\frac{\partial \Delta G}{\partial n_i} \right) \right)_{T, n_{j \neq i}} = \left(\frac{\partial}{\partial n_i} \left(\frac{\partial \Delta G}{\partial P} \right) \right)_{T, n_{j \neq i}} \quad \text{Eq. 3.2.2(E)}$$

Combining **Equation 3.2.2(B)** and **Equation 3.2.2(D)** with **Equation 3.2.2(E)** leads to:

$$\left(\frac{\partial V}{\partial n_i} \right)_{T, n_{j \neq i}} = \left(\frac{\partial \mu_i}{\partial P} \right)_{T, n_{j \neq i}} \quad \text{Eq. 3.2.2(F)}$$

Substituting the Gas Law, **Equation 3.2.2(C)**, into **Equation 3.2.2(F)**, the following could be obtained:

$$\left(\frac{\partial V}{\partial n_i} \right)_{T, n_{j \neq i}} = \left(\frac{\partial \left(\frac{nRT}{P} \right)}{\partial n_i} \right)_{T, n_{j \neq i}} = \left(\frac{RT}{P} \right)_{T, n_{j \neq i}}$$

and

$$\frac{d\mu}{dP} = \frac{RT}{P} \quad \text{Eq. 3.2.2(G)}$$

which shows that the chemical potential of an ideal gas at constant temperature depends on the partial pressure of the gas.

A reference level can be defined, where $\mu = \mu^0$ when $P = P^0$. Going from this reference pressure to the actual conditions in the container where gas pressure of gas i is P_i means integrating **Equation 3.2.2(G)**:

$$\int_{\mu_i^0}^{\mu_i} d\mu = \int_{P_i^0}^{P_i} \frac{RT}{P_i} dP_i \quad \text{Eq. 3.2.2(H)}$$

which gives:

$$\mu_i = \mu^0 + RT \ln(P_i / P_i^0) \quad \text{Eq. 3.2.2(I)}$$

With **Equation 3.2.2(I)** a simple relationship between chemical potential and gas pressure under isothermal conditions has been obtained. The state of the gas at the reference pressure P^0 is called the standard state, and the convention is that $P^0 = 1$ atm. From **Equation 3.2.2(H)** it is shown that the chemical potential of a perfect gas is a logarithmic function of the relative pressure of the gas. This relative pressure is the activity of the gas molecules and is expressed as:

$$[i] = P_i / P_i^0$$

The activity is dimensionless and a perfect gas has activity $[i] = 1$ when the pressure is equal to the standard state ($P_i = 1$ atm).

Chemical potential is a function of the relative pressure of gas, and therefore, the differences in partial pressure of oxygen are the driving force behind the diffusion of its molecules. Because of its kinetic energy (KE) a molecule spontaneously moves in random directions if no differences in partial pressure exists. It will however spontaneously migrate towards a zone where fewer collisions (a zone of lower relative pressure) between molecules occur. The pressure of an ideal gas could be expressed in terms of the kinetic energy of the gas:

$$PV = \frac{2}{3} N(KE)_{av}$$

where N is the number of molecules and $(KE)_{av}$ is the average kinetic energy of the molecules of the specific gas that is a function of the temperature of the system ($(KE)_{av} = \frac{2}{3} k_b T$, where $k_b = 1.3806 \times 10^{-23}$ J.K⁻¹ is the Boltzmann's Constant).

The following summarizes the thermodynamics of diffusion:

- A gradient in oxygen concentration exists towards sulphide grains in coal mine waste material and therefore a gradient in the chemical potential is present.
- In the spontaneous process of diffusion, oxygen is distributed in such a way as to decrease the chemical potential (J.mol⁻¹) of the oxygen. The chemical potential is a function of the partial pressure of the gas.
- Because of its kinetic energy (KE) a molecule spontaneously moves in random directions if no differences in partial pressure exists. It will however spontaneously migrate towards a zone where fewer collisions (a zone of lower relative pressure) between molecules occur.
- Thermodynamics explains both the process and direction of chemical diffusion.

3.2.3 Flux of molecular diffusion and change in concentration over time

A gradient in chemical potential leads to the diffusion of molecules and a flux will exist from parts of the system with high chemical potential to other parts of the system with a lower chemical potential until the free energy is at its minimum.

Fick's Law states that flux is directly proportional to the gradient across a surface and inversely proportional to the resistances to flow (Baum, 1997). This was named after Adolf Fick, a German physiologist (Fick also first fitted contact lenses to the human eyes) who published a paper in 1855 entitled "*Uber Diffusion*" in which he described the molecular diffusion process and derived his law (Baum, 1997; Smith, 2003). In Adolf Fick's own words: "*The diffusion of the dissolved material...is left completely to the influence of the molecular forces basic to the same law...for the spreading of warmth in a conductor and which has already been applied with such great success to the spreading of electricity*" (Smith, 2003). In other words diffusion can be described on the same mathematical basis as Fourier's Law for heat conduction, Ohm's Law for electrical conduction (Smith, 2003) or Darcy's equation for groundwater flow.

Fick's First Law for diffusional solute transport in one dimension, x (m), is given by:

$$F = -D \frac{\partial C}{\partial x}$$

where F is flux ($\text{mol.m}^{-2}.\text{s}^{-1}$), D ($\text{m}.\text{s}^{-1}$) is the molecular diffusion coefficient and C is the concentration (mol.m^{-3}). The diffusion coefficient expresses the resistance to diffusion.

Activities instead of concentrations should be used to calculate the gradient since differences in the chemical potential ($\mu = \mu^\circ + RT \ln[\eta]$) are the driving force for diffusion just as for chemical reactions (Appelo and Postma, 1994).

If the conditions dictate that a steady state is not occurring, Fick's First Law can no longer be used and the concentration is differentiated with respect to time to give the equation known as Fick's Second Law.

When the diffusive flux varies with distance through a three-dimensional volume, say a cube, the change in concentration can be found from flux differences over the sides of the cube as shown in **Figure 3.2.3(A)**. An example from Appelo and Postma (1994) is used:

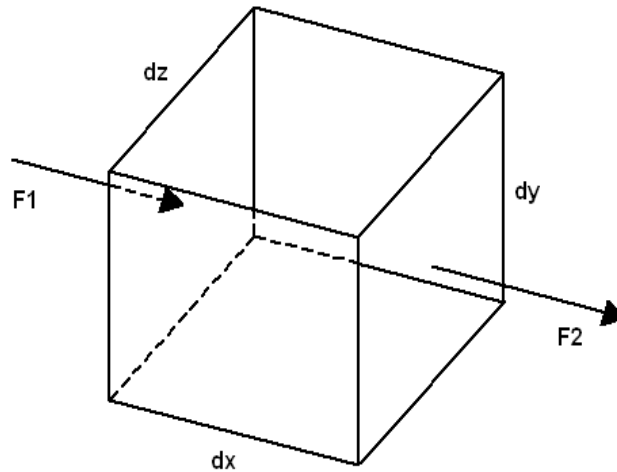


Figure 3.2.3(A). Concentration changes in a cube as a result of diffusion (Appelo and Postma, 1994).

The areal flux through the left side (at right angles to the gradient) is:

$$F_1 = -D \, dzdy \, \frac{\partial C}{\partial x}$$

and through the right side:

$$F_2 = -D \, dzdy \left(\frac{\partial C}{\partial x} + \frac{\partial}{\partial x} \frac{\partial C}{\partial x} dx \right)$$

The change in number of moles n in the cube is:

$$\frac{\partial n}{\partial t} = F_1 - F_2 = -D \, dzdy \, \frac{\partial C}{\partial x} + D \, dzdy \, \frac{\partial C}{\partial x} + D \, dzdy \, \frac{\partial^2 C}{\partial x^2} dx$$

$$\frac{\partial n}{\partial t} = F_1 - F_2 = D \, dzdy \, \frac{\partial^2 C}{\partial x^2} dx$$

which gives a change in concentration: $\delta C = \delta n / (dzdydx)$.

We therefore obtain:

$$\frac{\partial C}{\partial t} = D \, \frac{\partial^2 C}{\partial x^2}$$

which is known as Fick's Second Law.

Fick's Second Law describes the change in the concentration of a substance over time during the diffusion process. However, the cube in **Figure 3.2.3(A)** is perfectly homogeneous in terms of its oxygen diffusion rate and material properties. Fick's Second Law must therefore be modified to accommodate the diffusion process

through pyrite containing porous media that include water and air in their pores and a sink (pyrite) in the matrix.

3.2.4 Fick's Laws in porous material

3.2.4.1 Incorporating effective diffusivity and porosity into Fick's Laws

Fick's Laws describe the flux of molecular diffusion and in order to apply it to oxygen diffusion in porous media, it has to compensate for 1) the tortuous path the oxygen molecules have to take through the material, 2) the total porosity (ϕ), and 3) the water (θ_w) and air (θ_a) filled porosity.

In porous media, the following form of Fick's First Law describes the molar diffusive flux F ($\text{mol}\cdot\text{m}^{-2}\cdot\text{s}^{-1}$) of oxygen from the atmosphere into the interior of the coal mine waste pile in one dimension, x :

$$F(x,t) = -D_e(x,t) \frac{\partial C_{O_2}(x,t)}{\partial x}$$

Fick's Law states that the mass flux of oxygen is proportional to the effective diffusion coefficient D_e ($\text{m}\cdot\text{s}^{-1}$) and the oxygen concentration gradient ($\text{mol}\cdot\text{m}^{-3}\cdot\text{m}^{-1}$).

The effective diffusion coefficient, D_e , differs from the molecular diffusion coefficient D^o ($\text{m}\cdot\text{s}^{-1}$) of oxygen in a free fluid (gas, liquid) because of the presence of solids hindering diffusion by increasing the tortuosity of the transport pathways (Wels et al., 2003).

To describe the concentration change of a substance over time during the diffusion process, the aqueous and gaseous phases as well as effective diffusivity are incorporated into Fick's Second Law as follows:

$$\theta_a(x,t) \frac{\partial C_a(x,t)}{\partial t} + \theta_w(x,t) \frac{\partial C_w(x,t)}{\partial t} = D_e(x,t) \frac{\partial^2 C(x,t)}{\partial x^2}$$

Eq. 3.2.4.1(A)

where $\theta_a(x,t)$ and $\theta_w(x,t)$ are respectively the air and water content ($\text{m}^3\cdot\text{m}^{-3}$) of the pores.

To describe how the concentration of a substance will change over time during the diffusion process through a porous pyrite-containing medium, a sink term $q(x,t)$ ($\text{mol}\cdot\text{m}^{-3}$) is added to **Equation 3.2.4.1(A)**:

$$\theta_a(x,t) \frac{\partial C_a(x,t)}{\partial t} + \theta_w(x,t) \frac{\partial C_w(x,t)}{\partial t} = D_e(x,t) \frac{\partial^2 C(x,t)}{\partial x^2} - \frac{\partial q(x,t)}{\partial t}$$

Eq. 3.2.4.1(B)

The bulk oxygen concentration in the subsurface, $C_T(x,t)$ (mol.m^{-3}), is defined as the sum of the oxygen concentration in the air phase and water phase of the pore space as described in Romano et al. (2003):

$$C_T(x,t) = \theta_w(x,t) C_w(x,t) + \theta_a(x,t) C_a(x,t)$$

where C_w and C_a are the concentrations of oxygen in water and air, respectively, which are related through Henry's Law:

$$C_w(x,t) = HC_a(x,t) \quad \text{Eq. 3.2.4.1(C)}$$

which assumes equilibrium between the air and water phase. This assumption is adequate considering that the time scale of oxygen consumption by sulphide oxidation is slow in comparison to the time scale of mass transfer processes between the gas phase and the aqueous phase (Davis and Ritchie, 1986).

The temperature dependency of Henry's Law constant, H , could be expressed by the Vann't Hoff equation (Appelo and Postma, 1994):

$$H = K_H R(T(x) + 273.15)$$

and

$$\text{Log}K_H = \text{Log}K_{H(25^\circ\text{C})} - \frac{\Delta H_r^o}{2.303 R} \left(\frac{1}{T(x) + 273.15} - \frac{1}{298.15} \right)$$

where K_H is Henry's Law constant ($K_{H(25^\circ\text{C})} = 10^{-2.8996} \text{ M.atm}^{-1}$ at 25°C), R is the universal gas constant ($8.314 \text{ J.K}^{-1}\text{mol}^{-1}$), ΔH_r^o is the reaction enthalpy for the dissolution of oxygen in water (-10 kJ.mol^{-1}), and T is temperature ($^\circ\text{C}$).

Adding **Equation 3.2.4.1(B)** to **Equation 3.2.4.1(C)** leads to the following form of Fick's Law that describes the change of the concentration of a substance over time during the diffusion process in both the air and water phase of a pyrite containing porous medium:

$$\underbrace{(\theta_a(x,t) + H \theta_w(x,t))}_{\text{Storage Term}} \frac{\partial C_a(x,t)}{\partial t} = \underbrace{D_e(x,t)}_{\text{Diffusion Term}} \frac{\partial^2 C(x,t)}{\partial x^2} - \underbrace{\frac{\partial q(x,t)}{\partial t}}_{\text{Sink Term}}$$

$$\text{Eq. 3.2.4.1(D)}$$

Equation 3.2.4.1(D) describes the diffusion process in both saturated and unsaturated porous media and it accounts for the oxygen reserved in the water phase.

3.2.4.2 The effective diffusion coefficient of oxygen

Since both aqueous and air phases are present in the subsurface, then by definition the effective diffusion coefficient must be a function of D_a^o and D_w^o , the diffusion coefficients of oxygen in the free air and water phases respectively, with some adjustment in terms of the porespace tortuosity (τ) and the degree of saturation (where $\frac{\theta_w(x,t)}{\phi(x,t)}$ = water saturation, and $\frac{\theta_a(x,t)}{\phi(x,t)}$ = air saturation).

Various semi-empirical and theoretical equations for the effective diffusion are found in literature which could be applied for the transport of various gases in porous media and compensates for the tortuosity and the degree of saturation. Selected equations found in literature are shown in **Table 3.2.4.2(A)** below:

Table 3.2.4.2(A). Selected models for the effective diffusion of oxygen in porous media cited in literature.

Equation	Reference	Equation ($m.s^{-1}$)*	Comments
3.2.4.2(A)	Pruess (1991); cited in Lefebvre et al. (2001)	$D_e(x,t) = \tau' D_a^o \theta_a(x,t)$	Theoretical; Linear relationship
3.2.4.2(B)	Penman (1940); cited in Moldrup et al. (2003)	$D_e(x,t) = 0.66 D_a^o \theta_a(x,t)$	Semi-empirical
3.2.4.2(C)	Marshall (1959); cited in Moldrup et al. (2001)	$D_e(x,t) = D_a^o \theta_a(x,t)^{1.5}$	Semi-empirical
3.2.4.2(D)	Currie (1960); cited in Lefebvre (2003)	$D_e(x,t) = D_a^o \phi(x)^{\frac{4}{3}} \left(\frac{\theta_a(x,t)}{\phi(x)} \right)^{\frac{10}{3}}$	Semi-empirical
3.2.4.2(E)	Lai et al. (1976); cited in Lefebvre (2003)	$D_e(x,t) = D_a^o \theta_a(x,t)^{\frac{5}{3}}$	Applicable to gas diffusion in moist soils of different textures (Nobre and Thomson, 1993) Semi-empirical

3.2.4.2(F)	Reardon and Moddle (1985); cited in Romano et al. (2003)	$D_e(x, t) = 3.98 \times 10^{-9} \times \left(\frac{\theta_a(x, t) - 0.05}{0.95} \right)^{1.7} \times (T(x) + 273.15)^{1.5}$	Semi-empirical; Unsaturated tailings
3.2.4.2(G)	Collin and Rasmuson (1988); cited in Elberling and Nicholson (1996)	$D_e(x, t) = \tau' D_a^o \left(\frac{\theta_a(x, t)}{\phi(x)} \right)^\alpha + \tau' HD_w^o \left(\frac{\theta_w(x, t)}{\phi(x)} \right)$	Semi-Empirical Fitting parameters in sandy tailings: $\alpha = 3.28 \pm 0.04$ $\tau' = 0.273 \pm 0.08$ (95% confidence interval)
3.2.4.2(H)	Elberling et al. (1993); cited in Romano et al. (2003)	$D_e(x, t) = \tau' D_a^o \left(\frac{\theta_a(x, t)}{\phi(x)} \right)^\alpha + HD_w^o \left(\frac{\theta_w(x, t)}{\phi(x)} \right)^\alpha$	Semi-Empirical Fitting parameters in sandy tailings: $\alpha = 3.28 \pm 0.04$ $\tau' = 0.273 \pm 0.08$ (95% confidence interval)
3.2.4.2(I)	Millington and Quirk (1959); cited in Jin and Jury (1996)	$D_e(x, t) = D_a^o \frac{\theta_a(x, t)^2}{\phi(x)^{2/3}}$	Semi-Empirical
3.2.4.2(J)	Millington and Quirk (1959); cited in Moldrup et al. (2000)	$D_e(x, t) = D_a^o \theta_a(x, t)^{4/3}$	Dry soil (Nobre and Thomson, 1993) Semi-Empirical
3.2.4.2(K)	Millington and Quirk (1961); cited in Lefebvre (2003)	$D_e(x, t) = D_a^o \phi(x)^{\frac{4}{3}} \left(\frac{\theta_a(x, t)}{\phi(x)} \right)^{\frac{10}{3}}$	Dry soil (Nobre and Thomson, 1993) Semi-Empirical
3.2.4.2(L)	Simunek and Saurez (1993) similar to Millington and Quirk (1961); cited in Romano et al. (2003)	$D_e(x, t) = D_a^o \frac{\theta_a(x, t)^{10/3}}{\phi(x)^2} + HD_w^o \frac{\theta_w(x, t)^{10/3}}{\phi(x)^2}$	Moist soil (Nobre and Thomson, 1993) Semi-Empirical
3.2.4.2(M)	Millington and Schearer (1971); cited in James (1997).	$D_e(x, t) = D_a^o \theta_a(x, t)^{2x_a} \left(\frac{\theta_a(x, t)}{\phi(x)} \right)^2 + HD_w^o \theta_w(x, t)^{2x_w} \left(\frac{\theta_w(x, t)}{\phi(x)} \right)^2$	Non-aggregated material (Collin, 1987) The exponents x_a and x_w is given by: $\theta_w(x)^{2x_w} + [1 - \theta_w(x)]^{x_w} = 1$ $\theta_a(x)^{2x_a} + [1 - \theta_a(x)]^{x_a} = 1$

3.2.4.2(N)	Moldrup et al. (1999); cited in Moldrup et al. (2003)	$D_e(x, t) = D_a^o \phi(x)^2 \left(\frac{\theta_a(x, t)}{\phi(x)} \right)^{2+3/b}$	<p>Semi-Empirical; Undisturbed soils</p> <p>b is the slope of the Campbell water retention function (b>0). If b is not known it could be estimated from the clay fraction: b = 13.5*V_c + 3.5, where V_c = clay fraction.</p>
<p>* Where</p> <p>D_e = Effective Diffusion Coefficient for oxygen (m.s⁻¹), D_a^o = Diffusion Coefficient of oxygen in the pure air phase (m².s⁻¹) ≈ 1.8x10⁻⁵ m.s⁻¹ (T = 0°C, P = 1 atm), D_w^o = Diffusion Coefficient of oxygen in the pure water phase (m².s⁻¹) ≈ 2.1x10⁻⁷ m.s⁻¹ (T = 0°C, P = 1 atm), T = Temperature (°C), τ = Tortuosity (dimensionless), H = Henry's Law Constant (dimensionless) = 0.03 at 20°C = $\frac{C_w(x, t)}{C_a(x, t)}$, φ = porosity (m³.m⁻³), θ_w = Water filled porosity (m³.m⁻³), θ_a = Air filled porosity (m³.m⁻³).</p>			

The semi-empirical equations for the diffusion coefficient above were derived from soils or tailings, and different writers found some equations more suitable to fit their experimental data.

Overall good correlation between the different models and experimental data is found, i.e. Moldrup et al. (2003). However, Moldrup et al. (2003) found **Eq. 3.2.4.2(I)** (which slightly underestimated observed D_e) to fit his data better than **Eq. 3.2.4.2(F)** and **Eq. 3.2.4.2(G)** for undisturbed volcanic ash soils. He found **Eq. 3.2.4.2(G)** (which overestimated observed D_e) fitted better than **Eq. 3.2.4.2(F)** (which underestimated observed D_e).

Jin and Jury (1996) also found that **Eq. 3.2.4.2(F)** underestimated the observed D_e in soils, and that **Eq. 3.2.4.2(G)** gives a better prediction of the observed D_e , especially in disturbed soils.

The Troeh et al. (1982) model $D_e = D_a[(\theta_a - u)/(1 - u)]^v$ has the flexibility to fit all of the experimental data when both of the model parameters were varied simultaneously; however, no obvious correlation was found between soil properties and the parameters in Jin and Jury (1996) and in Moldrup et al. (2003).

In **Table 3.2.4.2(A)**, the effective diffusion in some equations is given as the sum of the effective diffusion in both the air (first term) and water phases (second term). However, the effective diffusion in the water phase is often considered negligible and omitted from the D_e models in literature.

3.2.4.3 The diffusion coefficient of oxygen in the pure gaseous and water phases

At STP (Standard Temperature and Pressure, $T = 0^\circ\text{C}$ and $P = 1 \text{ atm}$) the diffusion coefficient of oxygen in air, D_a^o , and in water, D_w^o , are approximately $1.8 \times 10^{-5} \text{ m.s}^{-1}$ and $2.1 \times 10^{-7} \text{ m.s}^{-1}$ respectively (Flühler, 1973; cited in Elberling and Nicholson, 1996).

The diffusion coefficient of oxygen in water and air is not constant and are dependant on various parameters. The diffusion coefficient is the resistance to diffusive flow in Fick's Law (see **Section 3.2.3**) and any parameter (e.g. gas composition, pressure, temperature etc.) that may influence the activity of the molecules (will therefore influence the resistance to diffusive flux).

The effect of temperature and pressure

The Kinetic Energy (KE) of the gas molecules is related to the temperature (see **Section 3.2.2**) and the diffusion coefficient of the gas would therefore be increased by elevated temperature. Expressions to determine temperature-dependent oxygen diffusion coefficients in the pure phases (water and air) were determined by Glinski and Stepniewski (1985) (Romano et al., 2003):

$$D_w^o = (0.0559 T(x) + 0.9864) \times 10^{-9}$$

$$D_a^o = (0.0119 T(x) + 1.7764) \times 10^{-5}$$

These expressions are based on regression analysis of diffusion coefficients at various temperatures and are valid over a temperature range from $0 - 30^\circ\text{C}$ (Romano et al., 2003).

Except for temperature, the diffusion coefficient of oxygen would also be dependent on the pressure of the system. Lefebvre et al. (2001) gives the following relationship of temperature T ($^\circ\text{C}$) and pressure P (Pa) on the effective diffusion coefficient of oxygen in the air phase:

$$D_a^o = D_o \frac{P_o}{P} \left(\frac{T + 273.15}{273.15} \right)^{1.75} \quad \text{Eq. 3.2.4.3(A)}$$

where $D_o = 1.8 \times 10^{-5} \text{ m.s}^{-1}$ and $P_o = 101325 \text{ Pa}$.

The Wilke-Chang relationship for diffusion of species in solution

The kinetic theory for the diffusion in binary liquids is not as well developed or as simple as the kinetic theory of gases at low density. The Wilke-Chang relationship has been proposed as a means of estimating the diffusion coefficient of species in solution (Jacob et al. (1999) and Richard (2003)) where D_w^o is given by:

$$D_w^o = 7.4 \times 10^{-8} \frac{(\chi M)^{1/2} T}{\nu V^{0.6}}$$

where M is the molecular weight ($\text{kg}\cdot\text{mol}^{-1}$) of the solvent, V is the molal volume ($\text{m}^3\cdot\text{mol}^{-1}$) of the solute at normal boiling point ($2.56 \times 10^{-2} \text{ m}^3\cdot\text{kg}^{-1}$ for O_2), T is the temperature (K), ν ($\text{kg}\cdot\text{m}^{-1}\cdot\text{s}^{-1}$) is the dynamic viscosity of the solvent and χ is an association parameter equal to 2.6 in the case of water (Jacob et al., 1999).

The Wilke-Chang relationship is one of the most widely used empirical expressions (Jacob et al., 1999) as a derivative of the Stokes-Einstein equation (Richard, 2003) and is only used on very dilute solutions. For most of the systems studied, a correlation to within 10% of the experimentally determined diffusion coefficient was observed (Jacob et al. (1999) and Richard (2003)).

The presence of different gaseous species

Except for temperature and pressure, the composition of the air mixture will also have an influence on the diffusion coefficient of oxygen because of the interaction with other molecules with different molecular weights.

However, changes in the diffusion coefficient of oxygen in air as described above are small due to changes in the air composition. Abriola et al. (1992) reports that under a pressure gradient of $0.05 \text{ mbar}\cdot\text{m}^{-1}$, the single component and multi-component model gave virtually indistinguishable results for transport predictions in sandy soils (Massmann and Farrier, 1992).

The smaller the permeability of the porous medium, the higher the total pressure and the higher the molecular mass of the molecular species, the higher will the resistance be (more collisions between different molecules) on the molecular diffusion of oxygen (Massmann and Farrier, 1992). Multi-component diffusion will be much more important in landfills (with a large variety of gases and the presence of contaminant species e.g. volatile organic species with high molecular masses) than in coal mine waste material. In soil compost Richard (2003) stated that temperature, for instance, has a much bigger impact on the diffusion coefficient than the gas composition.

The composition of the air entering the coal mine waste material will change because some gases are consumed and others are produced in the coal mine waste material. Atmospheric air has the following general composition:

- Oxygen (21% by volume)
- Nitrogen (78% by volume)
- Water Vapour (>1%, varies regionally)
- Argon (>1%)
- Carbon Dioxide (>0.03%)
- Other Gases: e.g. ozone, helium, methane (traces)
- Suspended Particulates (traces)

The gaseous species typically present in the air phase of coal mine waste are nitrogen and oxygen from the atmosphere, water vapour (due to higher temperature created by pyrite oxidation and spontaneous coal combustion, humidity will increase in coal material), carbon dioxide (from carbonate minerals reactions and also from spontaneous coal combustion) and methane (released from coal).

The following equation from Bird et al. (1960) gives the multi-component molecular diffusion coefficient of oxygen in a free-air mixture with n -number of gaseous species excluding oxygen (Nastev et al., 2001):

$$D_a^o = \frac{(1 - X_a^{O_2})}{\sum_{\substack{k=1 \dots n \\ k \neq O_2}} \frac{X_a^k}{D_a^{O_2 k}}}$$

where D_a^o is the diffusion coefficient ($m^2 \cdot s^{-1}$) of oxygen in the free-air mixture, $x_a^{O_2}$ and x_a^k is the respective mole fraction of oxygen and the k^{th} gaseous specie of the mixture, and $D_a^{O_2 k}$ is the binary diffusion coefficient ($m \cdot s^{-1}$) of oxygen and the gaseous component k .

The binary diffusion coefficient ($m \cdot s^{-1}$) of oxygen and gas k , $D_a^{O_2 k}$, could be determined at pressure P (atm) and temperature T (K) from the equation of Chen and Othmer (1962); cited in Stein et al. (2001):

$$D_a^{O_2 k} = \frac{0.604 \times 10^{-8} \times T^{1.81} \left(\frac{1}{M_{O_2}} + \frac{1}{M_k} \right)^{0.5}}{P \times \left(T_{C,O_2} \times T_{C,k} \right)^{0.1405} \left(\left(V_{C,O_2} \right)^{0.4} + \left(V_{C,k} \right)^{0.4} \right)^2}$$

where M_{O_2} , M_k = molecular weight ($kg \cdot kmol^{-1}$) of both gases, T_{C,O_2} , $T_{C,k}$ is the respective critical temperature (K), and V_{C,O_2} , $V_{C,k}$ the respective critical volumes of the gases ($m^3 \cdot kmol^{-1}$).

Table 3.2.4.3(A) below gives values of the diffusion coefficients of various binary gas pairs at atmospheric pressure (Richard, 2003).

Table 3.2.4.3(A). Diffusion coefficients of binary gas pairs at atmospheric pressure (Richard, 2003).

Binary Pair	Temp (°C)	Diffusion Coefficient (m.s ⁻¹)
Oxygen – Carbon Dioxide	20	1.53x10 ⁻⁵
	60	1.93 x10 ⁻⁵
Oxygen – Water Vapour	20	2.40 x10 ⁻⁵
	60	3.39 x10 ⁻⁵
Oxygen – Nitrogen	20	2.19 x10 ⁻⁵
	60	2.74 x10 ⁻⁵

3.3 The advective movement of oxygen in coal mine waste material

3.3.1 Background

Advection of the oxygen molecules occurs with air or water movement (flow) into coal mine waste material. Diffusion of oxygen is related to the kinetic properties of oxygen molecules and their spontaneous movement along a concentration gradient, whereas the advection of oxygen is related to the movement of the whole air/water phase (which contains the oxygen molecules) along a pneumatic/hydraulic gradient. Advective movement of oxygen molecules is therefore passive in contrast with diffusive movement which is active and spontaneous.

Diffusion occurs along a concentration gradient and can easily be described analytically in comparison to advection which is highly non-linear because the three driving forces 1) temperature, 2) gas composition, and 3) air pressure are interdependent (Wels et al., 2003). For example, an increase in air temperature (due to pyrite oxidation) produces changes in the gas composition and internal air pressure thus producing more advective airflow (as well as oxygen) into the pile, which again produces internal heating (pyrite oxidation). This non-linear feedback mechanism leads to ‘self-acceleration’ of pyrite oxidation and acid rock drainage often observed in advection-dominated waste rock piles (Wels et al., 2003). Another non-linear aspect of advective airflow is the strongly non-linear dependency of the relative air permeability on water saturation (Wels et al., 2003).

Airflow is also highly affected by the internal structure and anisotropy of waste rock material making it difficult to estimate ‘effective’ parameters for calculations of oxygen mass flux or oxygen penetration (Wels et al., 2003). Fala (2002) provides a thorough review of waste rock construction methods, of their effect on the internal structure and their influence on water flow. Similar effects are likely to influence airflow (Wels et al., 2003).

3.3.2 Mechanisms of advection

Four processes play a major role in oxygen advection in coal mine waste material, namely convection, barometric pumping, varying water saturation in pores and infiltration of water from the surface.

3.3.2.1 Convection of air

The release of heat from the oxidation process drives temperature up within waste rocks or tailings leading to density (pressure) differences. The magnitude of airflow into or out of a waste rock pile by thermal convection depends on the difference in temperature within the pile relative to the atmospheric air temperature (Wels et al., 2003). The different transfer processes of heat in coal mine waste material are described in **Chapter 4** and are an integral part in the convection of gases.

Temperature and oxygen measurements in “Borehole 36” in a waste rock pile situated in Nordhale, Germany, are shown in **Figure 3.3.2.1(A)**. The pile shows indications of increased thermal convection during the winter months (higher temperature gradients; heat produced within the pile v. the atmospheric winter temperatures) as evidenced by higher oxygen concentrations (Smolensky et al. (1999); cited in Wels et al. (2003). During the late autumn and early winter at the site, when temperatures in the upper portions fall below the pile’s internal temperature, the oxygen profiles show an overall increase in concentrations within the lower ports, indicating the onset of thermal convection (Wels et al., 2003). This pattern is most marked in the boreholes closer to the edge of the pile, where oxygen concentrations at depth remain high throughout the winter months (Wels et al., 2003).

Temperature generation in the pit material leads to gas density differences. Kuo and Ritchie (1999) also proposed compositional changes in the gas phase as a significant contribution to gas convection (Wels et al., 2003). Two common processes that can lead to a change in the molar mass of the gas phase in waste rock piles include 1) oxygen consumption in the gas phase related to pyrite oxidation, as well as 2) the increase in water vapour in the gas phase caused by increased temperatures (Wels et al., 2003).

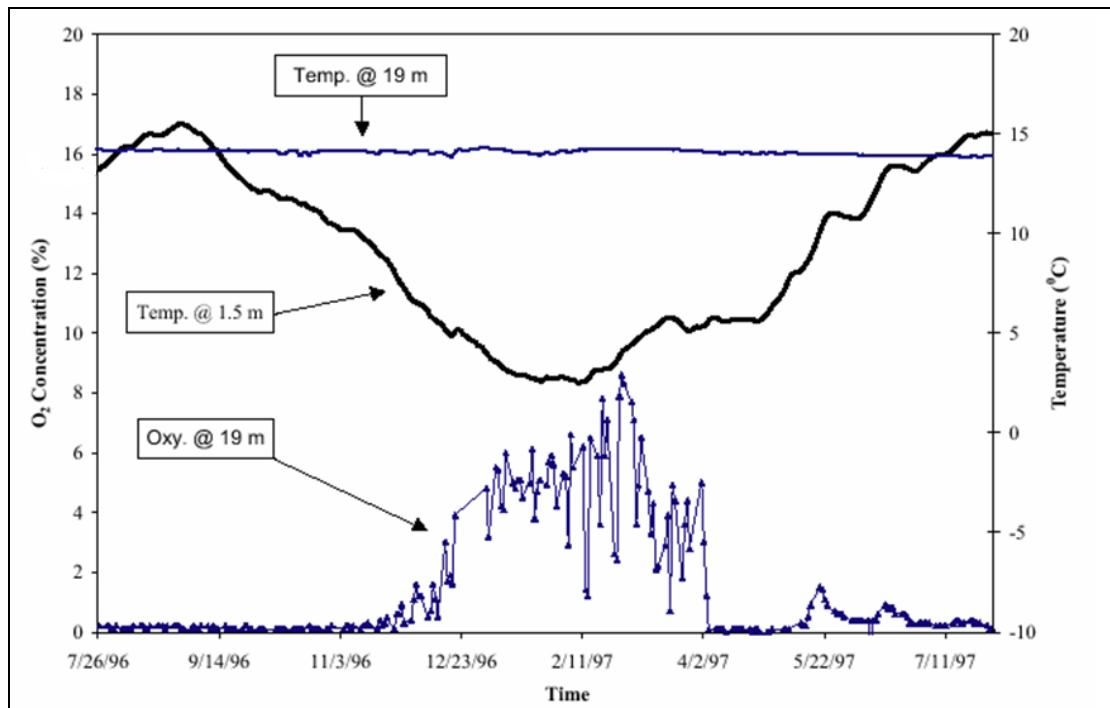


Figure 3.3.2.1(A). Relationship of oxygen concentrations in the 19 m port to temperatures in the 1.5 m and 19 m port for “Borehole 36”, Nordhale, Germany (from Smolensky et al. (1999); cited in Wels et al., (2003)).

3.3.2.2 Barometric pumping due to changes in atmospheric pressures

Increases in barometric pressures would enhance oxygen entry and decreases would tend to oppose gas flow within waste rock piles. No detailed study has yet been carried out to precisely determine the net effect of this potentially important oxygen supply process (Wels et al., 2003). Such effects would be more important for thicker unsaturated waste rock piles as shown by Massmann and Farrier (1992).

Anisotropy, however, may be capable of enhancing the local entry of oxygen in zones where waste rock material would locally be more permeable. Much remains to be understood on the net effect of barometric pumping on oxygen supply and ARD production in waste rock piles. Even though increases in barometric pressure would enhance oxygen entry, decreases in pressure would tend to oppose gas flow within waste rock piles.

The geometry and placement of coal mine waste material will play an important role in barometric pumping. For example, discarded material placed on surface exhibits a much larger surface area than waste that is backfilled into an open cast mine. The larger the surface area of the waste dump, the larger the interaction between atmospheric conditions and the conditions within the dump.

3.3.2.3 Varying water saturation in pores

An increase in the water content (a rising “waterlevel”) would drive out air, or *vice versa*, a decrease in water saturation would force air to fill the spaces and thus cause an influx of air into the pores. However, water saturation changes slowly and depends on dry and wet seasons. It has mostly a negligible effect on the replacement of air or influx of air into a dump.

Much more important will be the effect of changing saturation on gas diffusion and heat transfer. Diffusion is very sensitive for water saturation.

3.3.2.4 Infiltration of water from the surface

Water infiltrating the coal mine waste material will have a higher concentration of dissolved oxygen than the water within the coal mine waste material. Using Henry’s Law it could be calculated that water in direct contact with the atmosphere will have an oxygen concentration of 8.26 mg.l⁻¹ (0.26 m.mol.l⁻¹) at 25°C, increasing to 12.8 mg.l⁻¹ at 5°C (Appelo and Postma, 1994).

However, the quantity of oxygen dissolved in water entering the coal mine waste material is extremely small relative to the oxygen in the air entering the coal mine waste material. The migration of the gases in (or out) of the coal mine waste material is also much more dynamic and faster than water infiltration.

3.3.3 The Darcy Equation of advective airflow

In partially saturated porous media, the following equation could be used to describe the advective flux of gases in the direction x (m) where gas flow is driven by a potentiometric head $P(x,t)$ (Senevirathna and Achari, 2002):

$$q_g(x,t) = \frac{k}{\mu_g} \frac{\partial P(x,t)}{\partial x} \quad \text{Eq. 3.3.3(A)}$$

where k is the permeability (m²) of the porous medium, and μ_g the viscosity (kg.m⁻¹.s⁻¹) of the gaseous mixture.

The total viscosity of the gas phase μ_g could be expressed as a function of the viscosities of individual gases, as given below by Poling et al. (2001); cited in Senevirathna and Achari (2002):

$$\mu_g = \sum_{k=1}^n \frac{\mu_k}{1 + \sum_{l=1; l \neq k}^n \frac{x_l}{x_k}}$$

where

$$\varpi_{kl} = \frac{\left[1 + \left(\frac{\mu_l}{\mu_k} \right)^{0.5} \left(\frac{M_l}{M_k} \right)^{0.25} \right]^2}{\sqrt[8]{1 + \frac{M_l}{M_k}}}$$

and n is the number gaseous species, and k and l are two separate gases.

$P(x,t)$ is given in terms of density ρ (kg.m^{-3}) by Massmann and Farrier (1992) as $P'(x,t) = \rho g z(x,t) + P(x,t)$ and substituting into **Eq. 3.3.3(A)** yields:

$$q_g(x,t) = -\frac{k}{\mu} \frac{\partial}{\partial x} (\rho g z(x,t) + P(x,t)) \quad \text{Eq. 3.3.3(B)}$$

Where z is the elevation (m) relative to a reference level and g (m.s^{-2}) the acceleration due to gravity.

By substituting the Gas Law, **Equation 3.2.2(C)**, and the molar mass into density (mass/volume = moles/volume x mass/moles = $P/RT \times M$), we could obtain the following equation from **Eq. 3.3.3(B)** with some rearrangement:

$$q_g(x,t) = -\frac{k\rho g}{\mu} \frac{\partial}{\partial x} \left(z(x,t) + \frac{RT(x,t)}{gM} \cdot \ln \frac{P(x,t)}{P_o} \right) \quad \text{Eq. 3.3.3(C)}$$

where R is the universal gas constant ($8.314 \text{ J.K}^{-1}\text{mol}^{-1}$), T is temperature (K). $\frac{P(x,t)}{P_o}$ is the ratio of the gaseous pressure relative to a reference pressure (usually atmospheric pressure), and M is the molar mass (kg.mol^{-1}) of the oxygen.

From **Equation 3.3.3(C)** Darcy's Law can be written as follows:

$$q_g = -Ki(x,t) = -\frac{k\rho g}{\mu} \left(\frac{\partial h_g(x,t)}{\partial x} \right) \quad \text{Eq. 3.3.3(D)}$$

where K is the pneumatic conductivity (m.s^{-1}), i (dimensionless) is the pneumatic gradient, h_g is the pneumatic head (m) defined as $\frac{\partial}{\partial x} \left(z(x,t) + \frac{RT(x,t)}{gM} \cdot \ln \frac{P(x,t)}{P_o} \right)$ for a perfect gas (Lefebvre et al., 2001), and x is distance (m).

For the relatively small pressure changes with time that result from barometric pressure fluctuations, the pressure gradients in **Equation 3.3.3(A)** could also be partially differentiated to time.

3.4 Combining advective and diffusive flow of oxygen in porous media

The velocity v_g (m.s⁻¹) of the gas convective flow in one dimension (x) could be estimated from Darcy's Law (Massmann and Farrier, 1992):

$$v_g(x,t) = q_g(x,t) \left(\frac{\theta_a(x,t)}{\phi(x,t)} \right)_e^{-1} = - \frac{k\rho(x,t)g}{\mu} \left(\frac{\theta_a(x,t)}{\phi(x,t)} \right)_e^{-1} \frac{\partial h_g(x,t)}{\partial x}$$

or in terms of **Eq. 3.3.3(A)**

$$q_g(x,t) = - \frac{k}{\mu} \left(\frac{\theta_a(x,t)}{\phi(x,t)} \right)_e^{-1} \frac{\partial P'(x,t)}{\partial x}$$

where $\left(\frac{\theta_a(x,t)}{\phi(x,t)} \right)_e$ is the effective air porosity.

The advective-diffusion equation for gases could be described with a combination of gaseous flux and mass balance (Massmann and Farrier, 1992):

$$\frac{\partial C}{\partial t} = \nabla(D_d \nabla C) - v \nabla C - \frac{\partial q}{\partial t}$$

where D_d is the dispersion coefficient. In the classical approach the dispersion coefficient is given by

$$D_d = \alpha |v| + D_e$$

where the D_e is the effective diffusion coefficient, $|v|$ is the gas velocity, and α is the dispersivity. In many gas transport applications, diffusion is much more important than dispersion, and the dispersion coefficient D_d can be replaced by the effective diffusion coefficient D_e (Massmann and Farrier, 1992).

One dimensional diffusive-advective gas transport in the reactive porous medium could be written by adding Darcy's Equation for advective gas flow to **Equation 3.2.4.1(D)** (neglecting dispersion) to yield the following:

Storage Term	Diffusion Term	Advection Term	Sink Term
$\underbrace{(\theta_a(x,t) + H \theta_w(x,t)) \frac{\partial C_a(x,t)}{\partial t}}$	$\underbrace{= D_e(x,t) \frac{\partial^2 C(x,t)}{\partial x^2}}$	$\underbrace{- q_g(x,t) \left(\frac{\theta_a(x,t)}{\phi(x,t)} \right)_e^{-1} \frac{\partial C(x,t)}{\partial x}}$	$\underbrace{- \frac{\partial q(x,t)}{\partial t}}$

Eq. 3.4(A)

Equation 3.4(A) describes the diffusion and advective processes in both saturated and unsaturated porous media and it also accounts for the oxygen reserved in the water phase.

3.5 Final comments and conclusions

In **Section 3.2** and **3.3** general mathematical expressions of diffusive and advective flow of oxygen into coal mine waste material has been discussed as well as the parameters that influence them. The most important characteristics of diffusion and advection are discussed below. Several practical implications to coal mine waste material were also discussed.

Diffusion

- Diffusion is described by Fick's Law that states that flux is directly proportional to the gradient across a surface and inversely proportional to the resistances to flow.
- After their initial placement gaseous diffusion is the main process providing oxygen within coal mine waste rock. Diffusion remains active thereafter as long as the oxidation process contributes to the depletion of the oxygen concentration in the gas phase within the pile (Wels et al., 2003).
- Molecular diffusion is a spontaneous process and its rate increases with temperature. Diffusion is resisted in the unsaturated zone by the mineral matrix, the water-filled pores, other gas molecules and by bacteriological and pyrite consumption.

Advection

- Advection in coal mine waste material is described using Darcy's Equation of advective airflow. This equation is partially differentiated to the direction of the potentiometric gradient, but the dimension of time could also be included to compensate for barometric pressure.
- Advection is a passive mechanism of air migration into coal mine waste. Various processes play a role in gaseous advection in waste material:
 - Convection due to heat gradient.
 - Convection due to changes in gas composition.
 - Barometric pumping.
 - Change in saturation.
- Advection is highly non-linear because the three main driving forces, namely temperature, gas composition, and air pressure are interdependent (Wels et al.,

2003). For example, an increase in air temperature (due to pyrite oxidation) produces changes in the gas composition and internal air pressure thus producing more advective airflow into the pile, which in turn produces more internal heating. This non-linear feedback mechanism leads to ‘self-acceleration’ of pyrite oxidation and acid rock drainage, often observed in advection-dominated waste rock piles (Wels et al., 2003).

Practical implications for coal mine waste material

Various measures could be put into place to limit oxygen migration into coal mine waste material. The following general practical implications for coal mine waste material exist:

- Advective flow is highly dependant on the permeability of the material. The same general measures that would limit water ingress into coal mine waste, would also limit advective air flow.
- Both the oxygen diffusion and advection rates are accelerated by an increase in temperature. Spontaneous combustion of coal must therefore be prevented by proper rehabilitation of the dumps.
- A larger heat gradient will be present in coal discard dumps because of their higher pyrite content and because spontaneous combustion is often present in discard dumps. Therefore, convection will play a far more important role in discard dumps on surface than in backfilled open cast mines. Coal discard dumps also have a much larger contact area with the atmosphere than waste rocks in rehabilitated open cast mines.
- Water saturation limits oxygen diffusion into coal mine waste. Coal mine waste has a low field capacity and a thick topsoil cover would therefore be essential. The topsoil must enable plant growth which in turn would 1) stimulate bacteriological activity in the soil, and 2) would prevent erosion of the newly placed soil. Bacteriological working decreases oxygen migration. The soil cover must however not be too clayey and compacted as this will inhibit plant growth and limit water infiltration into the soil and will promote run-off. The underlying waste rock must still be allowed to be flooded with water in order to minimize pyrite oxidation as discussed below.
- Since oxygen supply is mostly limited to the unsaturated zone, it is preferable that pyrite containing rocks is kept under saturated conditions. For this purpose open pits could be left to be filled up with water. However, significant pyrite oxidation may occur before an open pit would become flooded. Therefore, it is recommended that a mining pit is backfilled with waste rock instead of leaving it on surface. With a general porosity of 20 – 35% the water storage capacity of the pit will decrease and the pit will fill up with recharging water more rapidly. It is important to place carbonaceous materials with higher pyrite

content at the bottom of the pit and also below the surface decant elevation in order for it to become saturated as soon as possible.

3.6 References

Abriola, L.M., Fen, C.S. and Reeves, H.W. (1992). *Numerical simulation of unsteady organic vapor transport in porous media using the dusty gas model*. In: Proceedings from the IAH conference on *Subsurface Contamination by Immiscible fluids*, Calgary, Alberta, April 18-20, 1991. International Association of Hydrogeologists, Arnhem, Netherlands, in press.

Allaby, A. and Allaby, M. (2003). *Dictionary of Earth Sciences*, 2nd Edition. Oxford University Press.

Appelo, C.A.J. and Postma, D. (1994). *Geochemistry, groundwater and pollution*. Balkema, 536 p.

Baum, S.K. (1997). *Glossary of Oceanography and the Related Geosciences with References*. Unpublished class notes, Texas A&M University. Internet: <http://stommel.tamu.edu/~baum/paleo/paleogloss/node15.html>

Bird, R.B., Stewart, W.E. and Lightfoot, E.N. (1960). *Transport Phenomena*. John Wiley & Sons, NY, 780 pp.

Collin, M. (1987). *Mathematical modelling of water and oxygen transportation in layered soil covers for deposits of pyritic mine tailings*. PhD Thesis, Royal Institute of Technology, Sweden.

Davis G.B. and Ritchie, A.I.M. (1986). *A model of oxidation in pyrite mine wastes, Equations and approximate solution*. *Appl. Math. Modell.*, 10, 314-322.

Elberling, B. and Nicholson, R.V. (1996). *Field determination of sulphide-oxidation rates in mine tailings*. *Water Resources Research*, 32: pp. 1773-1784.

Fala, O. (2002). *Study of unsaturated flows in waste rock piles using numerical simulations*. MSc thesis, École Polytechnique, Montreal (in French).

Gleisner, M. (2005). *Quantification of mineral weathering rates in sulfidic mine tailings under water-saturated conditions*. PhD thesis. Department of Geology and Geochemistry, Stockholm University, Sweden.

Glinski, J. and Stepniewski, W. (1985). *Soil aeration and its role for plants*. CRC Press, Boca Raton.

Jacob, S.R., Hong, Q., Barry, A.C. and Compton R.G. (1999). *Variable-Temperature Microelectrode Voltammetry: Application to Diffusion Coefficients and Electrode Reaction Mechanisms*. J. Phys. Chem. B., 103, 2963-2969.

James, A.R. (1997). *The prediction of pollution loads from coarse sulphide-containing waste material*. Report to the water research commission. WRC report no. 559/1/97.

Jin, Y. and Jury, W.A. (1996). *Characterizing the dependency of gas diffusion coefficient on soil properties*. Soil Sci. Soc. Am. J., 60, 66-71.

Kuo, E.Y. and Ritchie, A.I.M. (1999). *The impact of convection on the overall oxidation rate in sulfidic waste rock dumps*. Conference proceedings, Sudbury '99 – Mining and Environment, Paper AD2, vol 1, pp. 9-18.

Lefebvre, R., (2003). *Écoulement multiphase en milieux poreux*. Graduate course notes, 5th ed., Course GEO-9602/GLG-65146, Joint Earth Sciences Graduate Program, Université Laval/INRS, INRS-Eau, Terre et Environnement, 350 p.

Lefebvre, R., Hockley, D., Smolensky, J. and Gélinas, P. (2001). *Multiphase transfer processes in waste rock piles producing acid mine drainage - 1: Conceptual model and system characterization*. Journal of Contaminant Hydrology, 52, 137-167.

Massmann J. and Farrier, D.F. (1992). *Effects of atmospheric pressures on gas transport in the vadose zone*. Water Resources Research, 28(3), 777 – 791.

Mbonimpa, M., Aubertin, M., Aachib, M., and Bussiere, B. (2003). *Diffusion and consumption of oxygen in unsaturated cover materials*. A draft version submitted to the Canadian Geotechnical Journal, 57 p.

Moldrup, P., Yoshikawa, S., Oleson, T., Komatsu, T. and Rolston, D.E. (2003). *Gas diffusivity in undisturbed volcanic ash soils: Test of Soil-water-characteristic-based prediction models*. Soil Sci. Soc. Am. J., 67, 41-51.

Moldrup, P., Olesen, T., Komatsu, T., Schjønning, P. and Rolston, D.E. (2001). *Tortuosity, Diffusivity, and Permeability in the Soil Liquid and Gaseous Phases*. Soil Sci. Soc. Am. J., 65(3), 613-623.

Moldrup, P., Oleson, T., Gamst, T., Schjønning, P., Yamaguchi, T. and Rolston, D.E. (2000). *Predicting the gas diffusion coefficient in repacked soil: Water-induced linear reduction model*. Soil Sci. Soc. Am. J., 64, 1588-1594.

Morin, K.A. (1993). *Rates of sulfide oxidation in submerged environments: Implications for subaqueous disposal*. In: *Proceedings of the 17th Annual Mine Reclamation Symposium*, Port Hardy, British Columbia, May 4-7, 235-247. Mining Association of British Columbia.

Nastev, M., Therrien, R., Lefebvre, R. and Gelinas, P. (2001). *Gas production and migration in landfills and geological materials*. Journal of Contaminant Hydrology, 52, 187-211.

Nobre, R.C.M. and Thomson, N.R. (1993). *The effects of transient temperature gradients on soil moisture dynamics*. Journal of Hydrology, 152, 57-101.

Richard, T. (2003). *The Science and Engineering of Composting*. Unpublished online class notes, Cornell University. Internet:
<http://www.cfe.cornell.edu/compost/science.html>.

Romano, C.G., Mayer, K.U., Jones, D.R., Ellerbroek, D.A. and Blowes, D.W. (2003). *Effectiveness of various cover scenarios on the rate of sulfide oxidation of mine tailings*. Journal of Hydrology, 271, 171-187.

Senevirathna, D.G.M. and Achari, G. (2002). *A mathematical formulation to determine the errors in estimating gas emissions from landfills using closed flux chambers*. Article of Dept. of Civil Engineering, University of Calgary, presented at the CSCE/EWRI Environmental Engineering Conference, Niagara. Internet:
http://www.iranrivers.com/Electronic_Library/paper/Asce/41.pdf

Smith, P.J. (2003). *Multicomponent mass transport - Who is Adolf Fick?* Unpublished online class notes, University of Utah. Internet:
<http://opus.utah.edu/~smith/Classes/666/lectures/lecture4/fick.html>

Stein, V.B., Hettiaratchi, J.P.A. and Achari, G. (2001). *A numerical model for biological oxidation and migration of methane in soils*. ASCE Practice Periodical of Hazardous, Toxic, and Radioactive Waste Management, vol. 5, no. 4, pp. 225-234. Internet:
http://www.eng.ucalgary.ca/Civil/Hettiarachi/ANumericalModel_revisedPaper.pdf

Thorstenson, D.C. and Pollock, D.W. (1989). *Gas transport in unsaturated zones: Multicomponent systems and the adequacy of Fick's laws*. Water Resources Research, 25(3), 477-507.

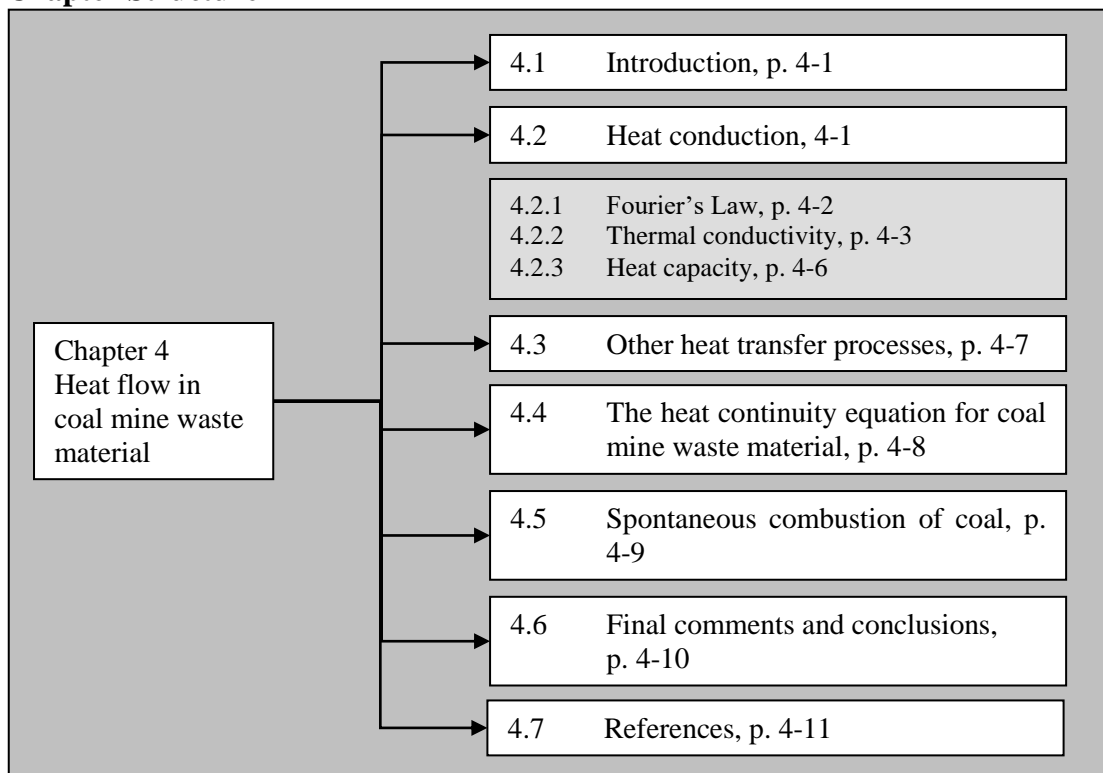
Troeh, F.R., Jabro, J.D. and Kirkham, D. (1982). *Gaseous diffusion equations for porous materials*. Geoderma, 27:239-253.

Wels, C., Lefebvre, R. and Robertson, A.M. (2003). *An overview of prediction and control of air flow in acid-generating waste dumps*. Paper in preparation for the 6th ICARD conference, 20p.

Williamson, M.A. and Rimstidt, J.D. (1994). *The kinetics and electrochemical rate-determining step of aqueous pyrite oxidation*. Geochim. Cosmochim. Acta, 58, 24, 5443-5454.

4 Heat flow in coal mine waste material

Chapter Structure



4.1 Introduction

Pyrite oxidation is an extremely exothermic reaction producing 1409 kJ of heat per mole (or 1.7×10^5 kJ/g pyrite) of pyrite oxidized (Wels et al., 2003). In coal discard heat is also produced from the spontaneous combustion of coal. The amount of heat produced during coal combustion depends on the calorific value of the coal which usually ranges between 23-35 kJ/g.

Heat has a direct or indirect influence on every physico-chemical process in Acid Mine Drainage (AMD) generation in coal mine waste. Temperature influences the gas migration into coal mine waste, the rate of chemical reactions as well as the microbial activity.

The distribution of heat within the waste pile influences the kinetic energy of gas molecules and therefore the gas diffusion rate. Differences in temperature within the waste pile also leads to density differences and resultant gas convection.

Heat flow occurs in coal mine waste material by means of conduction, convection, radiation and latent heat (Nobre and Thompson, 1993).

4.2 Heat conduction

The magnitude of conductive heat flux is related to the temperature gradient between the inside and the external boundaries of the piles as well as the heat transfer

properties of the waste rock material (Lefebvre et al., 2001). The external conditions are not constant and surface temperatures vary daily and seasonally. According to Lefebvre et al. (2001) the penetration of seasonal thermal waves within the waste rock piles is mostly limited to the upper 5 – 10 m layer near the surfaces exposed to the atmosphere.

Heat loss by conduction also occurs at the base of waste rock piles and Lefebvre (1994) showed that this heat loss affects the temperature distribution in the piles (Lefebvre et al., 2001). A change in water saturation affects heat conduction significantly because of the large difference between the thermal properties of water and air.

4.2.1 Fourier's Law

Heat conduction is the transfer of heat driven by temperature gradients through the bulk material as described by Fourier's Law, the First Law of heat conduction:

$$q_h = - k_h \frac{\partial T}{\partial x} \quad \text{Eq. 4.2.1(A)}$$

where q_h is the thermal energy flux ($\text{J}\cdot\text{s}^{-1}\cdot\text{m}^{-2}$); k_h ($\text{J}\cdot\text{s}^{-1}\cdot\text{m}^{-1}\cdot\text{C}^{-1}$) is the thermal conductivity; T is the temperature ($^{\circ}\text{C}$); and x is the distance (m).

Fourier's First Law is applicable to steady state conditions in one dimension. For transient thermal conductivity, the Second Law of heat conduction could be derived in a similar way Fick's Second Law has been derived in **Section 3.2.4** for transient diffusion of oxygen. Heat capacity ($\text{J}\cdot\text{m}^{-3}\cdot\text{C}^{-1}$) is added to compensate for the amount of heat absorbed or released by a unit volume of material in the transient state for a corresponding rise or fall of 1°C :

$$\frac{\partial T}{\partial t} = k_h / c_h \frac{\partial^2 T}{\partial x^2} \quad \text{Eq. 4.2.1(B)}$$

where T is the temperature (C), t is time (s), k_h ($\text{J}\cdot\text{s}^{-1}\cdot\text{m}^{-1}\cdot\text{C}^{-1}$) is the heat conductivity, c_h is the heat capacity ($\text{J}\cdot\text{m}^{-3}\cdot\text{C}^{-1}$), and x is the distance (m).

In **Equation 4.2.1(B)**, k_h/c_h is often replaced with D_h , where $D_h = k_h/c_h$ is the heat diffusivity ($\text{m}^2\cdot\text{s}^{-1}$).

In a similar way that porous media give resistance to molecular diffusion (as described in **Section 3.2**), it will also affect the heat conductivity k_h and heat capacity c_h . In porous media the variation in k_h is much bigger (hundred fold or more) than the variation in c_h (3 to 4 fold) relative to homogeneous media (Quinton, 2003).

The heat diffusivity $D_h = k_h/c_h$ is influenced by the heterogeneity of the porous media and is therefore a function of the heat diffusivity of the solids, the water and the air phase, with some correction for tortuosity.

4.2.2 Thermal conductivity

Various semi-empirical models exist in the literature for describing the relation of thermal conductivity to soil properties:

The Johansen (1975) semi-empirical model (cited in Geoslope, 2003)

The thermal conductivity could be expressed by the functions given by Johansen (1975) (Geoslope, 2003). Several software models like VADOSE/W Version 5, SoilCover use these relationships (Geoslope, 2003).

For dry, natural soils, the thermal conductivity k_h^{dry} ($\text{J.s}^{-1}.\text{m}^{-1}.\text{C}^{-1}$) can be estimated based on its dry density using the following equation:

$$k_h^{dry} = \frac{0.135\rho_d + 64.7}{2700 - 0.947\rho_d} \pm 20\%$$

where the dry density ρ_d is in kg.m^{-3} and the unit weight of soil particles could be taken as 2700 kg.m^{-3} .

For dry crushed rock materials, the thermal conductivity k_h^{dry} can be estimated based on its porosity ϕ using the following equation:

$$k_h^{dry} = 0.039\phi^{-2.2} \pm 25\%$$

For a saturated unfrozen soil, the thermal conductivity k_h^{sat} is estimated based on the thermal conductivities of its components and their respective volume fractions:

$$k_h^{sat} = (k_h^{solids})^{1-\phi} (k_h^{water})^{\phi}$$

where, k_h^{solids} is the thermal conductivity of the soil particles, and k_h^{water} is the thermal conductivity of the pore water.

For a saturated frozen soil containing some unfrozen water content, W_u , the thermal conductivity k_h^{sat} becomes:

$$k_h^{sat} = (k_h^{solids})^{1-\phi} (k_h^{water})^{\phi} W_u (k_h^{ice})^{W_u}$$

where, k_h^{solids} is the thermal conductivity of the solid particles, k_h^{ice} is the thermal conductivity of ice, and k_h^{water} the thermal conductivity of the unfrozen water.

For an unfrozen unsaturated soil, the thermal conductivity k_h^{unsat} is estimated based on its saturated conductivity k_h^{sat} , dry conductivity k_h^{dry} and degree of saturation $\frac{\theta_w}{\varphi}$ using the following equation:

$$k_h^{unsat} = (k_h^{sat} - k_h^{dry}) k_e + k_h^{dry}$$

where:

$$k_e = 0.7 \text{Log} \frac{\theta_a}{\varphi} + 1.0 \text{ for unfrozen coarse grained soil;}$$

$$k_e = \text{Log} \frac{\theta_a}{\varphi} + 1.0 \text{ for unfrozen fine grained soil;}$$

$$k_e = \frac{\theta_a}{\varphi} \text{ for frozen soil;}$$

$$\theta_w = \text{volumetric water content (m}^3\text{.m}^{-3}\text{);}$$

$$\varphi = \text{porosity (m}^3\text{.m}^{-3}\text{).}$$

The above equations may be used for a rough, general estimation of the thermal conductivity of a soil.

The De Vries (1966) Model

De Vries (1966) developed a procedure where the thermal conductivity k_h of a soil with ellipsoidal particles is calculated as the weighted average of the conductivities of the various soil constituents according to the formula (Ochsner et al., 2001):

$$k_h = \frac{\sum_{i=1}^n \kappa_i \theta_i k_h^i}{\sum_{i=1}^n \kappa_i \theta_i}$$

where k_h^i is the thermal conductivity ($\text{J.s}^{-1}\text{.m}^{-1}\text{.}^\circ\text{C}^{-1}$) and θ_i is the volume fraction of each constituent and n is the number of constituents. The weighting factors, κ_i , is the ratio of the space average of the temperature gradient in the soil grains of kind i and the space average of the temperature gradient in the continuous medium water or air. The factor κ_i is expressed as (De Vries, 1966; cited in Nobre and Thomson, 1993):

$$\kappa_i = \frac{2}{3} \left[1 + \left(\frac{k_h^i}{k_h^w} - 1 \right) g_i \right]^{-1} + \frac{1}{3} \left[1 + \left(\frac{k_h^i}{k_h^w} - 1 \right) (1 - 2g_i) \right]^{-1}$$

Eq. 4.2.2(A)

where g_i are the shape factors given in **Table 4.2.2(A)** along with the heat conductivity for various soil constituents.

Table 4.2.2(A). Shape factors and heat conductivity for parameters in Eq. 4.2.2(A) at 20°C (De Vries, 1966; cited in Nobre and Thomson, 1993).

Constituent	i	Shape factor g_i	k_h^i ($J.s^{-1}.m^{-1}.^{\circ}C^{-1}$)
Quartz	q	0.125	8.79×10^{-4}
Clay	c	0.125	2.93×10^{-4}
Organic matter	o	0.500	2.51×10^{-5}
Water	w	-	5.86×10^{-5}
Air (dry)	a	g_a^*	k_h^{a**}
*where g_a (Kimball et al., 1976)	$g_a = 0.013 + \left(\frac{0.022}{\theta_{wp}} + \frac{0.298}{\phi} \right) \theta_w$, when $\theta_w \leq \theta_{wp}$		
	$g_a = 0.035 + \frac{0.298}{\phi} \theta_w$, when $\theta_w > \theta_{wp}$		
**where k_h^a (Kimball et al., 1976)	$k_h^a = k_h^{DryAir} + D_a^{wv} L \frac{\partial \rho_v}{\partial T}$ <p>where</p> <p>k_h^{DryAir} = the conductivity of dry air = $2.57 \times 10^{-6} J.s^{-1}.m^{-1}.^{\circ}C^{-1}$;</p> <p>$D_a^{wv}$ = the diffusion coefficient of water vapour in air. Eq. 3.2.4.3(A) could be used to express the diffusion coefficient in terms of pressure and temperature where $D_o^{wv} = 2.2 \times 10^{-4} m^2.s^{-1}$ at 1 atm and 0°C;</p> <p>L = the latent heat of vaporization of water ($J.kg^{-1}$);</p> <p>ρ_v = the density of water vapour ($kg.m^{-3}$);</p> <p>T = temperature in °C.</p>		

Equation 4.2.2(A) applies as long as the water content is greater than a minimum value so that the liquid phase may still be regarded as continuous. For very dry conditions, when liquid flow becomes negligible, the same theory may be applied by substituting k_h^w with k_h^{DryAir} and considering air as the continuous phase (De Vries, 1966; cited in Nobre and Thomson, 1993).

Other semi-empirical models

Soil thermal conductivity (k_h) can be determined from the empirical equation (Bristow, 2002; cited in Hendrickx et al., 2003):

$$k_h = A + B\theta_w - (A - D)\exp[-(C\theta_w)^E]$$

where θ_w is the volumetric soil water content and A , B , C , D and E are soil dependent coefficients which are related to soil properties that are usually fairly readily available. The relationships are:

$$A = \frac{0.57 + 1.73\phi_q + 0.93\phi_m}{1 - 0.74\phi_q - 0.49\phi_m};$$

$$B = 2.8\phi_s; C = 1 + \frac{2.6}{m_c^{0.5}}; D = 0.03 + 0.7\phi_s^2; E = 4$$

where ϕ is the volume fraction of a specific component, subscripts “ q ”, “ m ”, and “ s ” indicate quartz, minerals other than quartz, and total solids; m_c is the clay mass fraction.

4.2.3 Heat capacity

The heat capacity c_h ($\text{J.kg}^{-1}.\text{°C}^{-1}$) of the porous medium is modelled as the weighted sum of the specific heat capacities of the soil components (Ochsner, 2001; Quinton, 2003):

$$c_h = \sum_i^n \rho_i \theta_i c_h^i$$

where: c_h = volumetric heat capacity ($\text{J.m}^{-3}.\text{°C}^{-1}$) of the porous media; c_h^i = specific heat capacity ($\text{J.kg}^{-1}.\text{°C}^{-1}$) of component i ; ρ_i the density (kg.m^{-3}) of component i ; θ_i is the volumetric content of component i ; and i = mineral matter, organic matter, water, air and ice.

Thermal properties for common soil components are given in **Table 4.2.3(A)** below:

Table 4.2.3(A). Thermal properties of soil constituents (Quinton 2003).

Substance	Density (kg.m ⁻³)	Specific Heat Capacity (J.kg ⁻¹ .C ⁻¹)	Specific Heat Capacity (J.m ⁻³ .C ⁻¹)
Water	1000	4185	4185000
Air	1.2	1010	1212
Ice	920	2120	1950400
Soil (Minerals)	1000 - 2650	890	1157000 - 2000000
Soil (Organic)	50-300	1920	75000 - 200000

4.3 Other heat transfer processes

Advection

During the heat advection process, heat is transferred by moisture in the 1) liquid, 2) vapour and 3) adsorbed phase (Nobre and Thompson, 1993). The thermal energy that is transferred with moisture flux is given by:

$$q_A = c_l (T - T_o) q_m$$

where

- q_A = advective thermal energy flux (J.s⁻¹.m⁻²);
- c_l = specific heat of liquid water (J.kg⁻¹.°C⁻¹);
- T = the temperature (°C);
- T_o = is a reference temperature (°C);
- q_m = moisture density flux (kg.s⁻¹.°C⁻¹).

The moisture density flux q_m consists of moisture flux in the liquid, vapour and adsorbed phase and is described in more detail by Nobre and Thompson (1993).

Latent heat

Latent heat (heat produced during phase change) is also transferred by vapour movements and could be expressed as follows:

$$q_L = - \rho_l (LD_\psi + gTD_{Ta}) \frac{\partial \psi}{\partial x}$$

where

- q_L = thermal latent energy flux (J.s⁻¹.m⁻²);
- T = temperature (°C);
- x = distance (m);

- ρ_l = liquid water density (kg.m^{-3});
 D_ψ = isothermal vapour diffusivity (m.s^{-1});
 g = gravitational acceleration (m.s^{-2});
 D_{τ_a} = coefficient related to the heat of wetting on the pressure field responsible for adsorbed liquid flow ($\text{m}^2.\text{s}^{-1}.\text{°C}^{-1}$);
 ψ = water pressure head (m).

The isothermal vapour diffusivity D_ψ ($\text{m}^2.\text{s}^{-1}$) is defined as follows (Nobre and Thompson, 1993):

$$D_\psi = \frac{D_a^{wv} g \rho_v}{\rho_l R T}$$

where

- D_a^{wv} = the diffusion coefficient ($\text{m}^2.\text{s}^{-1}$) of water vapour in air.
 ρ_v = liquid water density (kg.m^{-3});
 R = universal gas constant ($8.314 \text{ J.K}^{-1}\text{mol}^{-1}$);
 T = temperature (K).

Eq. 3.2.4.3(A) could be used to express the diffusion coefficient D_a^{wv} in terms of pressure and temperature where $D_o^{wv} = 2.2 \times 10^{-4} \text{ m}^2.\text{s}^{-1}$ at 1 atm and 0°C ;

The coefficient D_{τ_a} is related to the heat of wetting on the pressure field responsible for adsorbed liquid flow ($\text{m}^2.\text{s}^{-1}.\text{°C}^{-1}$). The coefficient for adsorbed liquid flow D_{τ_a} for clayey materials, as derived by Groeneveldt and Kay (1974), is $D_{\tau_a} = -0.0013/T(^\circ\text{C})$.

4.4 The heat continuity equation in coal mine waste material

In coal mine waste material pyrite will generate heat that will be transferred by the three major processes discussed above, namely 1) heat conduction, 2) advection and 3) latent heat generation.

The total amount of thermal energy that is stored in a unit volume of porous waste material is given as S_h in J/m^3 . The energy produced as a result of pyrite oxidation and coal combustion is given by $S_{\text{pyrite+combustion}}$ in J/m^3 .

The change in the thermal energy in coal mine waste material over time could be expressed as follows:

$$\begin{array}{ccccc}
 \text{Storage Term} & \text{Heat Conduction} & \text{Latent Heat} & \text{Advection Term} & \text{Source Term} \\
 \underbrace{\hspace{1.5cm}} & \underbrace{\hspace{1.5cm}} & \underbrace{\hspace{1.5cm}} & \underbrace{\hspace{1.5cm}} & \underbrace{\hspace{1.5cm}} \\
 \frac{\partial S_h}{\partial t} = \frac{\partial}{\partial x} \left[k_h \frac{\partial T}{\partial x} + \rho_l (LD_\psi + gTD_{Ta}) \frac{\partial \psi}{\partial x} - c_l (T - T_o) q_m \right] + \frac{\partial s_{\text{pyrite+coalcombustion}}}{\partial t}
 \end{array}$$

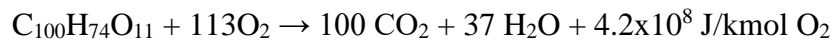
In the above equation radiative (radiation is the result of electromagnetic waves emitted by all matter) transfer and air phase convection is neglected as it would play a negligible role in coal mine waste material.

4.5 Spontaneous combustion of coal

Coal mine waste is considered as a porous medium where coal combustion and pyrite oxidation serve as sources of heat generation. The potential for spontaneous combustion of coal lies in its ability to react with oxygen at ambient temperature. This occurs through the absorption of oxygen at the surface of the coal which is an exothermic reaction. This absorption reaction generates small amounts of heat as shown below (Gangopadhyay and Kuntala, 2005):



The temperature of the coal will then start to rise. Coal is a relatively good thermal insulator and much of this heat can be trapped, increasing both the temperature and the rate of oxidation. In fact, the oxidation rate doubles for every rise of 8 – 11°C in coal. If the temperature reaches what is often called the ‘threshold’ temperature (somewhere between 80 – 120°C) a steady reaction resulting in the production of gaseous products such as carbon dioxide ensues (Gangopadhyay and Kuntala, 2005). The temperature of the coal will then almost certainly continue to rise until (somewhere between 230 and 280°C) the reaction becomes rapid and strongly exothermic – in other words, the coal reaches ‘ignition’ or ‘flash’ point and starts to burn (Gangopadhyay and Kuntala, 2005):



Other factors that accelerate the spontaneous combustion are methane released by coal and also latent heat generated by the wetting of coal which is an exothermic process.

Spontaneous combustion of coal discard dumps leads to a significant change in the mineralogy of the material. Mineralogical analysis has been performed on a burnt coal discard dump and the results are discussed in **Section 5.3.3**.

4.6 Final comments and conclusions

Spoils will have a much smaller heat generating potential than coal discard due to the following reasons:

- Higher concentration of carbonaceous material in coal discard dumps

Spoil are a mix of uneconomical coal, carbonaceous clastic rocks and clastic (sandstones, shales, siltstones) rocks. Coal discard contains a higher fraction of carbonaceous material than spoil material.

- Higher pyrite content in coal discard dumps

Pyrite oxidation contributes to heat generation in coal mine waste. Pyrite is much higher in coal discard dumps than in mined coal. In spoil material the average pyrite content is usually lower than that of the mined out coal.

- Higher heat conduction in waste rocks

As seen in **Table 4.2.3(A)** minerals have a much lower specific heat capacity than carbonaceous material. From **Table 4.2.2(A)** it is observed that minerals also have higher heat specific conductivity than carbonaceous material. Heat conductivity is proportional and heat capacity inversely proportional to heat conduction (see **Equation 4.2.1(B)**).

In coal mine waste material, heat generation has the following influence on physico-chemical and other processes:

- Water vapour movement

Increased heat in coal mine waste leads to an increase in the water vapour phase. Water vapour will in return influence gas migration.

- Gas migration

An increase in temperature leads to an increase in the kinetic energy of gas molecules and therefore in the rate of gas diffusion. Increased temperature leads to gas density differences with resultant advective gas flow.

- Mineralogy

Temperature generation in coal mine waste will at first have no effect on the mineralogy of the matrix; only when the temperature exceeds about 65°C slight changes will commence in clay mineralogy. Coal discard dumps that have undergone spontaneous combustion (>200 – 300°C) show extreme changes in mineralogy as discussed in **Section 5.3.3**.

- Bacteriological working

Active bacteriological working is present at 10°C and although a lower limit is not established it is generally accepted to be the freezing point of water. Optimal oxidation of sulphides by bacteria occurs between 25°C and 45°C. The upper temperature limit for bacterial mediated pyrite oxidation is 55°C and only abiotic oxidation occurs above this temperature (sees **Section 2.6.4**).

- Chemical reactions

The rate of all exothermic chemical reactions will increase with increased temperature (e.g. pyrite oxidation) and the opposite will be true for endothermic reactions. The general mineralogical reactions in AMD generation and neutralization are discussed in **Chapter 2**.

4.7 References

Bristow, K.L. (2002). *Thermal conductivity*. In: *Methods of soil analysis, Part IV, Physical Methods* (eds. Danc, D.H. and Topp, G.C.). Soil Science Society of America, Book Series No. 5, Madison, Wisconsin, pp. 1209-1226.

De Vries, D.A. (1966). *Thermal properties of soil*. In: *Physics of plant environment* (ed. Van Wijk, W.A.). North-Holland, Amsterdam, pp. 210-235.

Gangopadhyay, P.K. and Kuntala, L-D. (2005). *Detecting Coal fires with Remote Sensing: A Comparative Study of Selected Countries*. In: *Resource Management in Asia-Pacific Working Paper No. 58*. Research School of Pacific and Asian Studies, Resource Management in Asia-Pacific Program, The Australian National University, Canberra.

Geoslope Software (2003). *Estimating Thermal Conductivity for Soils*. VADOSE/W Version 5 online technical guide. Internet:

http://www.geo-slope.com/gsi_home/webhelp/vad/vadhlp.htm

Groeneveldt, P.H. and Kay, B.D. (1974). *On the interaction of water and heat transport in frozen and unfrozen soils II, The liquid phase*. Soil Sci. Soc. Am., 38(3), 400-404.

Hendrickx, J.M.H., Van Dam, R.L., Borchers, B., Curtis, J., Lensen, H.A. and Harmon, R.S. (2003). *Worldwide distribution of soil dielectric and thermal properties*. In: *Detection and remediation technologies for mines and minelike targets VIII*. Proceedings of the SPIE, Vol. 5089. Internet: <http://www.ees.nmt.edu/Hydro/landmine/publications.html>

Kimball, B.A., Jackson, R.D., Reginato, R.J., Nakayama, F.S. and Idso, S.B. (1976). *Comparison of field-measured and calculated soil-heat fluxes*. Soil Sci. Soc. Am., 40, 18-25.

Lefebvre, R. (1994). *Characterization and numerical simulation of acid mine drainage in waste rocks*. In French, PhD Thesis, Université Laval, Québec City, Canada, June 375 pp.

Lefebvre, R., Hockley, D., Smolensky, J. and Gélinas, P. (2001). *Multiphase transfer processes in waste rock piles producing acid mine drainage - 1: Conceptual model and system characterization*. Journal of Contaminant Hydrology, 52, 137-167.

Nobre, R.C.M. and Thomson, N.R. (1993). *The effects of transient temperature gradients on soil moisture dynamics*. Journal of Hydrology, 152, 57-101.

Ochsner, T.E., Horton, R. and Ren, T. (2001). *A new perspective on soil thermal properties*. Soil Sci. Soc. Am. J., 65, 1641-1647.

Quinton, W. (2003). *Soil temperature and heat flow*. Unpublished online class notes, Simon Fraser University. Internet:

http://www.sfu.ca/~bquinton/teaching/geog311/11_soilthermal.pdf

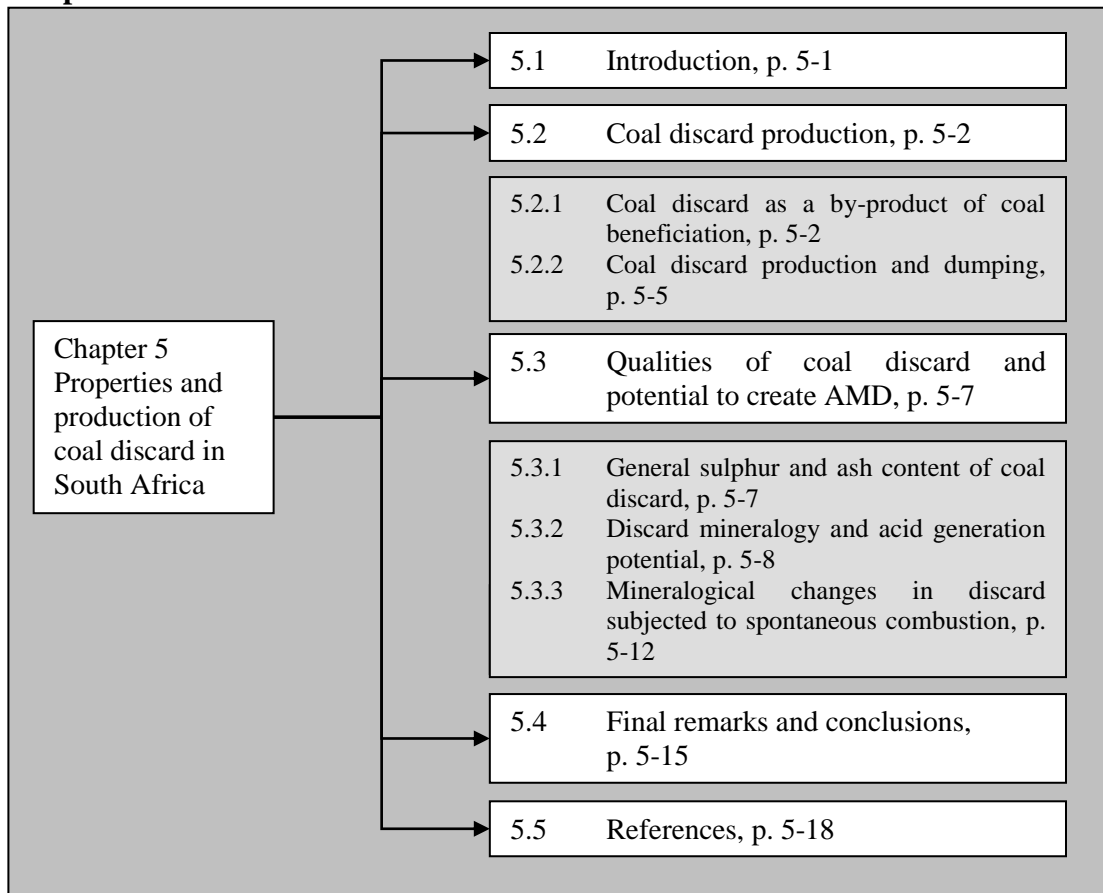
Wels, C., Lefebvre, R. and Robertson, A.M. (2003). *An overview of prediction and control of air flow in acid-generating waste dumps*. Paper in preparation for the 6th ICARD conference, 20p.

PART II

Research and Applications to the South African
Coal Mine Environment

5 Properties and production of coal discard¹ in South Africa

Chapter Structure



5.1 Introduction

In an area with a high occurrence of coal mines, Hodgson and Krantz (1998) state that “...*coal discard disposal is probably the second biggest environmental problem in the Olifants Catchment, after open-cast mining*”.

The result of the beneficiation of South African coals are the generation of approximately 60 Mt per annum of coal discard, which is estimated to have already accumulated to more than 1 billion ton. These large amounts of carbonaceous material impact negatively on the environment while it often contains significant amounts of usable coal (DME, 2006).

Coal discard is a by-product of the coal beneficiation process. Coal is beneficiated in order to improve the quality of the mined coal as specified by the consumer. Southern hemisphere coals, and notably those of South Africa, are characterized by lower proportions of vitrinite and exinite, and much higher proportions of inertinite and

¹ The term discard usually refers to any kind of coal discard, however, it is often used to refer to coarse coal discard and not fine discard or slurry, e.g. as in DME (2002). For the sake of clarity, in this chapter coal discard will be used as a collective term for both coarse and fine discard. The term discard as it refers to coarse discard, fine discard or slurry, will be called as such.

mineral matter, than their northern hemisphere counterparts. With the spread of open-cast mining the run-of-mine coals are tending to get dirtier with more stone bands included and a higher level of cleaning is often desired (Horsefall, 1993).

The only commercial viable type of coal beneficiation is physical coal cleaning. It involves the crushing of the coal and screening of it into differently-sized particles to separate out impurities that are not chemically bound to the coal. Water sprayed over the coal particles loosens the remaining mineral matter. Specific gravity differences are used to separate the coal from other constituents such as ash.

5.2 Coal discard production

5.2.1 Coal discard as a by-product of coal beneficiation

Coal discard in the South African coal chain

South Africa's energy economy is heavily dependent on coal. **Figure 5.2.1(A)** below shows the different end users of coal in the South African coal market:

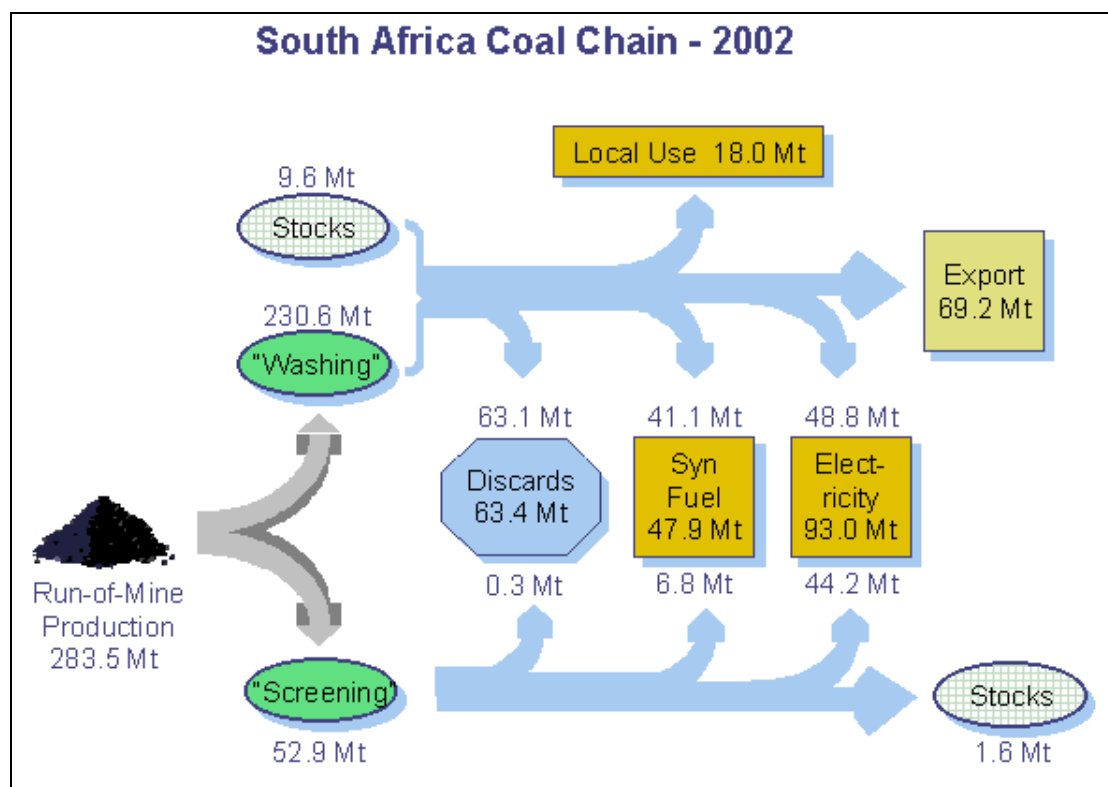


Figure 5.2.1(A). The South African coal chain (Coaltech 2020, 2006).

All users have different requirements for the coal product they are using whether it is for the generation of electricity, synthetic fuels or other uses such as for the metallurgical industry.

Washed coal end-products are distributed between export (39%), electricity (28%), synthetic fuels (23%) and local use (10%). Of the coal product delivered to local

power stations, respectively 47% and 53% went through screening and washing. Of the coal product used for synfuels, respectively 86% and 14% went through washing and screening. All export coal is washed in order to improve its quality.

Coal cleaning methods and coal discard products

Coal preparation technology covers a wide range of processes that can be used in many combinations to suit the needs of each particular application. Sometimes single products, such as power station fuel (PSF) or metallurgical coal, are produced, but often multi-products are required for a range of markets. Consequently, coal preparation plant designs are varied. Two major categories of plants have emerged: total washing and partial washing. In general, total washing is applied where a high-quality product is specified (e.g. metallurgical coal) or where total washing is necessary to produce a PSF of the required quality. For many power applications, however, it is not necessary to wash the whole of the run-of-mine (ROM) coal (Budge et al., 2000).

Coal discard differs slightly depending at what stage of coal cleaning it has been discarded. The basic commercial methods as well as environmental concerns in general are given in **Table 5.2.1(A)** below.

Table 5.2.1(A). Coal beneficiation and environmental concerns of the by- or end-product in South Africa.

Coal beneficiation*			Environmental concerns	
Level of cleaning	Product	Method** (Size limits of raw coal used as feed are given in brackets)	Production of coal discard	Pollution of the atmosphere and water resources***
I	Coal products not washed. (Almost 20% of ROM coal in South Africa).	Crushing and screening of coal.	No discard produced.	No discard produced and therefore no potential to create AMD. High amounts of CO ₂ and SO ₂ introduced into the atmosphere by end-users.
II	Large coal washed to +10/15 mm. Discard sometimes also rewashed to obtain middling product.	<u>Large coal (> 25 mm) washed using:</u> Baum Jig (0.5 to 150 mm), DMS bath (6 to 250 mm), DM cyclone (35 to 45 mm), Larcodems (up to 120 mm).	Coarse discard produced. No fines.	Coarse discard contains a high %S. Potential to create AMD. High amounts of CO ₂ and SO ₂ are introduced into the atmosphere by end-users.
III	Small coal cleaned to +0.5 mm.	<u>Small coal (> 3 mm) washed using:</u> The Batac jig, DM cyclone (0.5 to 13 mm).	Coarse and small discard produced.	Coarse discard contains a high %S. Fine discard contains lower %S than coarse discard. Potential to create AMD. Usually smaller amounts of CO ₂ and SO ₂ are introduced into the

IV	Fine coal cleaned to +0.1/0.2 mm using spirals or -0.1/0.2 mm using froth flotation.	<u>Fine coal (< 3 mm) washed using:</u> Spiral concentrators (3 to 0.1 mm), Froth flotation (-0.5 mm).	Coarse, small and fine discard produced.	atmosphere by end-users.
V	(Ditto)	Rewashing of coarse coal.	Coarse, small and fine discard produced.	

* Beneficiation information obtained from Horsefall (1993) and Budge et al. (2000).

** DMS – Dense Medium Separators, Larcodems – Large Coal Dense Medium Separators.

*** The amount of gases that are released from discard dumps are determined by the quality of the rehabilitation in order to prevent spontaneous combustion.

Coal product that is not washed, or only washed up to Level II, is typically used for PSF or synthetic fuels. At low levels of beneficiation, the coal product still contains a fair amount of sulphur. End-users of these products are typically power stations or other industries that eject a large amount of CO₂ and SO₂ into the atmosphere.

Mines supplying coal to power stations are now finding it economical to re-wash discard to produce a middling product for sale to the power-station, thereby reducing the amount of discard produced considerably (DME, 2002). Re-washing is normally carried out in jigs or in DMS plants. The discard is normally crushed to 30 mm in order to improve recoveries by liberating the coal from the shale and gangue material. Power stations benefit from this middling product which normally has the same heat value as the raw coal, but a lower abrasion index and more often than not, lower sulphur content, due to the re-washing process (DME, 2002).

Coal that is cleaned for metallurgical or export purposes are usually washed to Level III, IV or V. Treatment of slurry and the reclamation of slurry ponds for beneficiation by froth flotation are being carried out by a number of mines (DME, 2002). Product quality and recovery is normally good due to the better quality of the slurry when compared to coarse discard. Smaller amounts of CO₂ and SO₂ are introduced into the atmosphere because the end-users generally operate on a smaller scale and the coal products contain smaller amounts of sulphur.

Cleaning of coal up to these levels produces small to fine discard. In slurry ponds large volumes of water is collected by e.g. penstocks and returned to the plant. However, a large volume of slurry water also seeps towards the underlying aquifer creating large volumes of AMD. Fine discard contains smaller amounts of sulphur than coarse discard and the quality of the slurry water may not be as poor as seepage from coarse discard dumps. The more water saturated conditions created by slurry in coal discard dumps, also helps to minimize pyrite oxidation.

The coal discard dumps are rehabilitated by covering them with a revegetated soil layer. The volume of gas released from coal discard dumps is determined by the quality of the rehabilitation in order to prevent spontaneous combustion.

Frequent consumers of the country's coal products include the following (Horsefall, 1993):

- ESKOM: CV: 16 – 25 MJ/kg; Ash: 20 – 30%; Cleaned to Level I or II.
- SASOL I: CV: 18 – 19 MJ/kg; Ash: >30%; Cleaned to Level I or II.
- SASOL II&III: CV: 21 – 24 MJ/kg; Ash: 22 – 25%; Cleaned to Level I or II.
- Metallurgical, blend coking coal: CV: >28 MJ/kg; Ash: 10 – 15%; Cleaned to Level IV or V.
- Metallurgical, straight coking coal: CV: >27 MJ/kg; Ash: 10 – 17%; Cleaned to Level IV or V.
- General domestic industry: CV: 22 - 29 MJ/kg; Ash: 12 – 25%; Cleaned to Level III.
- Export power station: CV: 27 – 28.4 MJ/kg; Ash: 12.9 – 16.1%; %S: 0.42 – 0.59; Cleaned to Level III.
- Export metallurgical: CV: 30.7 – 31.2 MJ/kg; Ash: 6.8 – 7.6%; %S: 0.42 – 0.59; Cleaned to Level V.

5.2.2 Coal discard production and dumping

Annual discard production obtained from a DME (Department of Minerals and Energy) survey in 2001 was 42.5 Mt. Annual slurry production in 2001 was 11.3 Mt (DME, 2002). It is estimated that both these figures are 10 – 15% higher as a few collieries did not respond to the survey or are ownerless defunct collieries from Kwazulu-Natal. **Figure 5.2.2(A)** and **(B)** below shows typical annual tonnages of discard and slurry produced by the major collieries:

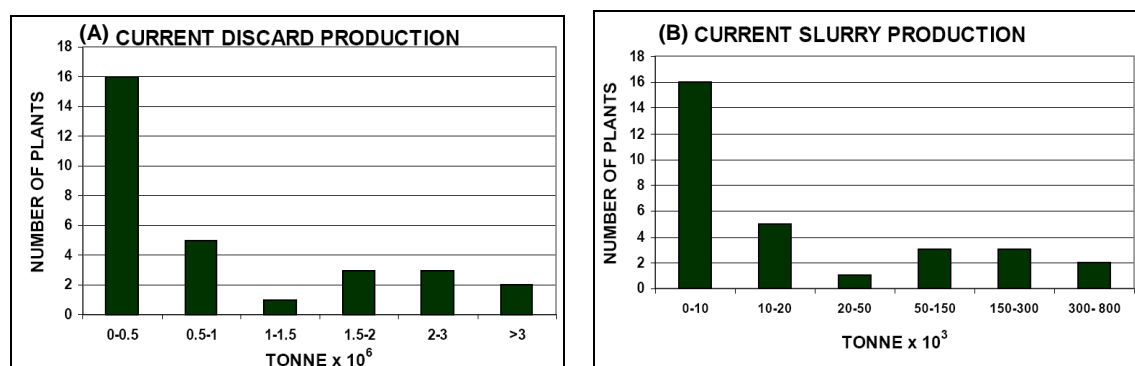


Figure 5.2.2(A) and (B). Annual tonnages of discard and slurry produced in 2001 (DME, 2002).

More than 1000 Mt of discard is present in the South African coalfields. The size of the discard dumps in the survey varied from 18 kt for the smallest dump to 32 Mt for the largest. A total of 52.8 Mt of dumped slurry is present in the South African coalfields. The size of the slurry ponds in the survey varied from 6 kt for a facility just started, to 5.7 Mt for the largest active slurry pond.

Since the 1985 DME inventory, annual coal discard production has increased from 43.6 Mt (1985) to 66.2 Mt (2001). It is not envisaged that the above-mentioned rates of coal discard deposition will be maintained because of the following reasons:

- Closure of a number of collieries including numerous very large producing collieries.
- The increase of raw coal being sent to utilities using this type of coal, namely ESKOM and SASOL.
- The production of a middling product to supply ESKOM and SASOL.
- The blending of discard, raw coal and slurry for the power generation sector.
- Reclamation of slurry ponds to supply ESKOM.

Figure 5.2.2(C) shows the area in hectares occupied by coal discard facilities in South Africa. The majority of the larger discard dumps are situated in Mpumalanga Province with a large number of smaller defunct dumps in KwaZulu-Natal Province. The total area covered by discard and slurry disposal facilities, amounts to 4,011 ha (DME, 2002).

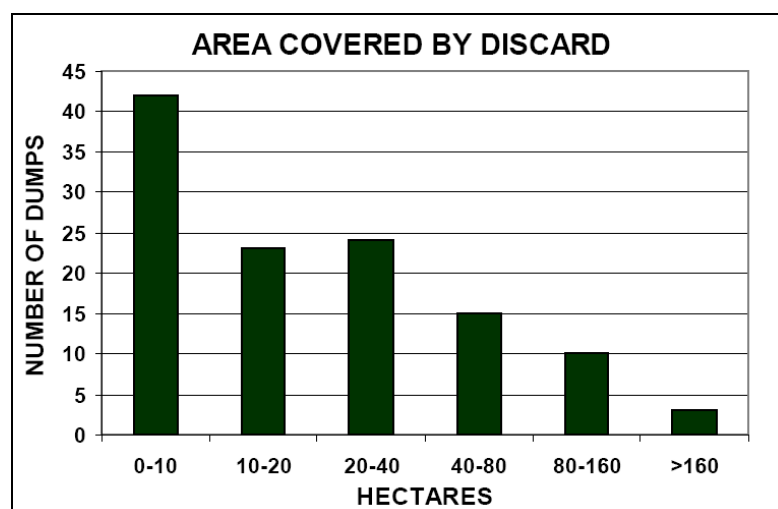


Figure 5.2.2(C). Area covered by disposal facilities in the South African coalfields (DME, 2002).

Coarse discard is most often dumped on surface but because of a lack of space in mining areas, the discard is sometimes tipped into open-cast voids or mixed with

open-cast overburden material to fill voids left by the mining operation. According to the 2001 DME survey, 14 mines co-dispose discard with spoils. The discard might also be used for road building inside the pit and dragline stability in the open cut. This discard is considered un-reclaimable.

With environmental laws becoming stricter, mines are paying greater attention to the methods of discard disposal. Discard is now being compacted and the discard dump clad with soil and vegetated. These rehabilitated dumps are potentially reclaimable, the discard being kept under non burning conditions. Numerous collieries are using compacted discard to cover or blanket old, smouldering or burnt-out discard dumps. Once the largest part of the discard dump is oxidized and subjected to long periods of spontaneous combustion, it becomes irreclaimable (DME, 2002).

Methods of slurry disposal have changed considerably. Slurry is now pumped into the centre of a dump, the compacted discard forming a wall around the central slurry impoundment. Slurry is sometimes pumped onto the un-compacted discard coal resulting in a matrix, which does not require intensive compacting, to form a non-oxidising condition within the dump. This method of slurry disposal is known as integrated coal discard disposal and will also affect the coal discard reclamation.

On numerous open-cast operations slurry has been pumped into the voids and once dry, covered with overburden; this slurry is considered un-reclaimable. Certain mines have however pumped slurry into well prepared, open-cast voids, this slurry being potentially recoverable. Slurry pumped into old underground workings as backfill is also considered un-reclaimable and this method of disposal helps to prevent surface collapse. (DME, 2002).

5.3 Qualities of discard and potential to generate AMD

5.3.1 General sulphur and ash content of discard

During coal beneficiation the ash content is lowered to the required range specified by the consumer. Coal discard therefore generally has a higher mineral content than the mined coal. The typical ash and sulphur contents of dumped coal discard and slurry in the South African coalfields are shown in **Figure 5.3.1(A) – (D)** below:

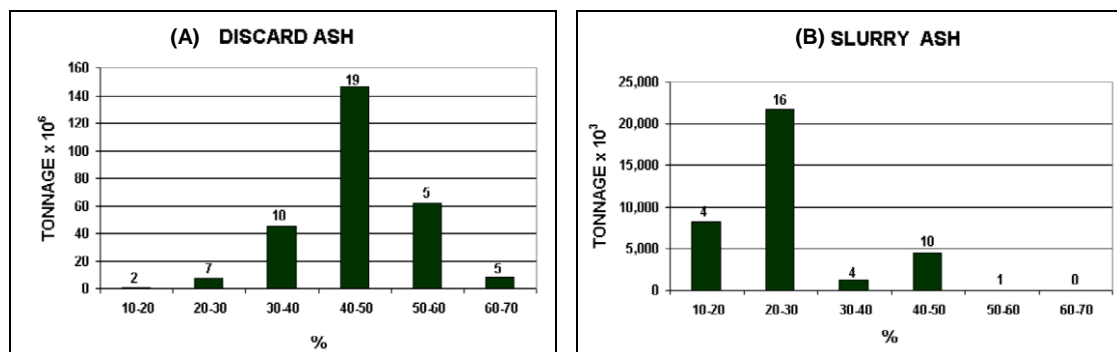


Figure 5.3.1(A) and (B). Ash content of discard and slurry (DME, 2002).

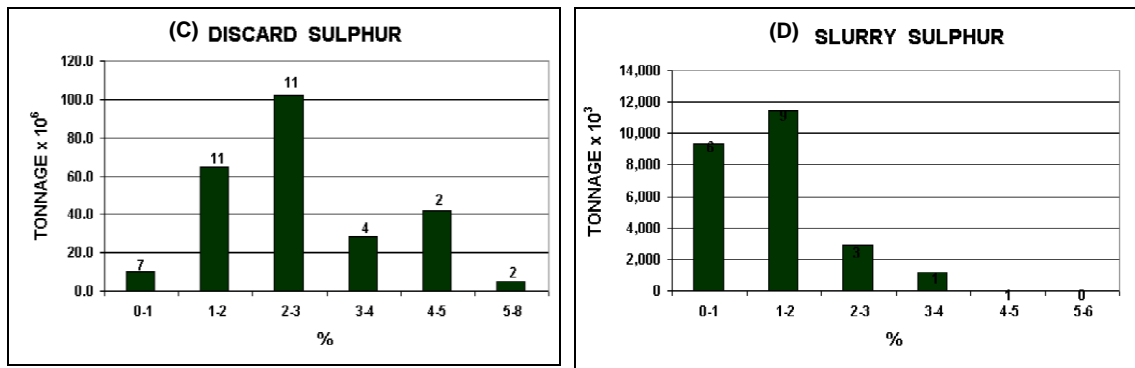


Figure 5.3.1(C) and (D). Sulphur content of discard and slurry (DME, 2002).

In general the slurry coal quality is higher than that of coarse discard; the slurry also contains a smaller amount of ash and sulphur. The ash and sulphur contents are a qualitative indication of the amount of mineral matter and pyritic sulphur present in carbonaceous material. The more sulphur, the higher the potential will be for the material to produce AMD.

Large volumes of slurry water may seep through slurry ponds, often situated on discard dumps, towards the underlying aquifer. Although slurry ponds may potentially increase the volume of AMD, fine discard contains however smaller amounts of sulphur and the quality of the slurry water may not be as poor as the AMD from the coarse discard. The increased water saturated conditions created by slurry in discard dumps, also helps to minimize pyrite oxidation.

In the 2001 DME survey it was found that some dumped coal discard have good enough qualities for it to be beneficiated and marketed. According to the survey 40.8 Mt of dumped discard can be reworked. All the slurry disposed of has a quality which will lend itself to beneficiation by froth flotation to produce power station feedstock or even an export product (DME, 2002). Slurry often has the potential to be utilized in its raw state provided the moisture content of the initial dried product can be reduced.

5.3.2 Discard mineralogy and acid generation potential

Acid-base accounting (ABA) is a static method used to predict the net acidification potential of rock containing pyrite. The ABA method used in this study is discussed in more detail in **Section 6.2.3**. X-ray diffraction (XRD) is used to identify the mineralogy of a rock and is discussed in **Section 6.2.1**. ABA was performed by Waterlab Pty (Ltd) based in Pretoria and XRD analyses by the Department of Geology, UP. The semi-quantitative mineralogical contents of the samples were determined using the Rietveld method.

In order to illustrate the differences between the mineralogy and the acid generation potential of raw coal and discard, XRD and ABA were performed on ROM (run-of-mine) coal and on discard samples obtained from a colliery in the northern Witbank Coalfield.

The XRD analyses done on clastic rocks, raw coal and discard from the mine are given in **Table 5.3.2(A)**. The coal are from the No. 1 and No. 2 coal seams.

Table 5.3.2(A). Identified minerals (wt%) in lithological units and discard from a mine in the north-eastern Witbank Coalfield.

Mineral	Sandstone and shale	Raw Coal (ash)	Discard (ash)
Calcite	0.48	1.02	3.00
Dolomite	1.12	1.73	2.33
Siderite	3.03	1.76	-
Pyrite	1.12	2.95	5.66
Anatase	0.46	0.56	-
K-feldspar	4.52	2.46	2.33
Plagioclase	1.27	0.76	-
Quartz	48.25	39.52	44.59
Mica	3.94	2.15	7.49
Kaolinite	35.80	47.09	36.61
Total	100.00	100.00	100.00

The following observations are made from **Table 5.3.2(A)**:

- The major minerals present in the mineral assemblages are quartz and kaolinite. All other minerals can be classified as minor, accessory or trace minerals (see **Section 6.1** for the classification of mineral quantities).
- The clastic rocks show higher siderite, K-feldspar and plagioclase content than the coal. The coal in turn shows higher calcite, dolomite and pyrite content than the clastic rocks.
- In the discard there is almost double the amount of calcite, dolomite and pyrite than in the coal.

Acid-base accounting (ABA) has been performed on the above samples in order to assess the acidification and neutralization potential thereof. The results are given in **Table 5.3.2(B)** and **(C)** below:

Table 5.3.2(B). Summary of the ABA results of lithological units from a mine in the north-eastern Witbank Coalfield.

Geochemical Unit		Total % S	Acid Generating Potential (kg CaCO ₃ /t)	Neutralization Potential (kg CaCO ₃ /t)	Net Neutralization Potential (kg CaCO ₃ /t)	Ratio NP:AP
Non-carbonaceous sandstone and shale	Min.	0.001	0.031	-9.250	-9.563	0.352
	Max.	0.091	2.844	18.750	16.188	29.600
	Ave.	0.045	1.403	3.575	2.172	7.855
Carbonaceous shale and sandstone	Min.	0.128	4.000	-2.000	-41.906	0.054
	Max.	1.773	55.406	23.250	17.375	3.957
	Ave.	0.321	10.031	5.263	-4.768	0.794
No. 1 and No. 2 coal seams	Min.	0.432	13.500	-10.000	-49.344	0.008
	Max.	1.619	50.594	29.000	-3.781	0.740
	Ave.	0.853	26.656	4.583	-22.073	0.315

Table 5.3.2(C). ABA results of discard from a mine in the north-eastern Witbank Coalfield.

Sample	Paste pH	NAG pH	Total S (%)	Acid Generating Potential (kg CaCO ₃ /t)	Neutralization Potential (kg CaCO ₃ /t)	Net Neutralization Potential (kg CaCO ₃ /t)	NP:AP Ratio
1	7.30	2.60	4.468	139.63	22.75	-116.88	0.163
2	8.00	2.59	1.357	42.41	14.00	-28.41	0.330
3	7.50	2.68	4.069	127.16	28.50	-98.66	0.224
4	7.60	2.46	4.601	143.78	17.00	-126.78	0.118
5	7.30	2.75	5.588	174.63	26.25	-148.38	0.150
6	7.30	2.61	4.889	152.78	17.50	-135.28	0.115
Minimum	7.30	2.46	1.357	42.41	14.00	-28.41	0.115
Maximum	8.00	2.75	5.588	174.63	28.50	-148.38	0.330
Average	7.50	2.62	4.162	130.06	21.00	-109.06	0.183

From these results the following could be concluded on the potential acidification potential of the discard:

- The %S is much higher in the discard than in the coal and clastic rocks. All discard samples have a %S of above 4.069 %S, except one sample which is at 1.357 %S. A higher %S is expected from the discard since it has been through

a process where its ash content has been concentrated. The average 4.162 %S relates to an average *pyrite content* in the discard of 7.79 wt% that is higher than the XRD-determined pyrite content of 5.66 wt%.

- The %S of the discard lead to subsequent higher Acid Generating Potential (AP), which ranges between 42.41 – 174.63 kg CaCO₃/t, averaging at 130.06 kg CaCO₃/t.
- The neutralization potential (NP) of the discard ranges between 14.00 – 28.50 kg CaCO₃/t, averaging at 21.00 kg CaCO₃/t. The NP gives an indication of the neutralization capacity of the rock that would neutralize acidic drainage. The NP of the discard are much lower than the AP and the Net Neutralization Potential (NNP) ranges between 28.41 – 148.38 kg CaCO₃/t, averaging at 109.06 kg CaCO₃/t.
- The discard shows a negative NNP and low NP:AP ratio (averaging at 0.183), and shows a resultant increase in acidic drainage potential relative to the raw coal.
- NP and AP are respectively 4.6 and 4.9 times higher in the discard than in the mined coal. The AP is not elevated much higher in the discard than the NP but the difference between NP and AP has increased 4.9 times. This makes a large difference in the acid drainage potential of the discard relative to the raw coal. The NNP increased from -22.07 kg CaCO₃/t in the raw coal to -109.06 kg CaCO₃/t in the discard.
- Based on the %S and the NP:AP ratio, the discard samples are all classified as “Likely Acid Generating” (see **Section 6.2.3** for ABA screening methods).
- The NAG (Net Acid Generating Potential) pH is another way of determining whether the drainage from a rock will turn acidic. The NAG pH is determined after oxidizing all sulphides with a standard amount of peroxide. The pH is measured after 48 h when all the carbonates have reacted. If the pH is between 3.5 and 5.5, the sample is classified as “Low Risk Acid-generating” and with a pH below 3.5 the sample is classified as “High Risk Acid-generating”. All six discard samples have NAG pH’s below 3. This proves the acid generation potential of the material, which is in agreement with the results of the ABA.

The results of this section cannot be quantitatively extrapolated to other sites because of differences in coal quality and beneficiation processes over the coalfield. However, the results show two important general properties of coal discard: it has 1) a higher mineral content as well as 2) a higher acidification potential than the ROM coal.

5.3.3 Mineralogical changes in discard subjected to spontaneous combustion

Mineralogical content

A total of 17 samples were taken from a discard dump in the central Witbank Coalfield from five auger-drilled holes. Bh No. 1 to 5 were drilled respectively 6 m, 8 m, 2 m, 3.5 m, and 4.2 m deep. The mineralogical content of the 17 samples was determined by XRD-analyses (by the Department of Geology, UP) and the results are summarized in **Table 5.3.3(A)** below:

Table 5.3.3(A). Mineralogical content of samples taken from a discard dump in the central Witbank Coalfield.

Sample No. and depth of sampling	Calcite	Dolomite	Pyrite	Hematite	Mullite	K-feldspar	Plagioclase	Quartz	Cristobalite	Tridymite	Gypsum	Anhydrite	Amphibole*	Kaolinite	Amorphous
Bh No. 1 2 m	5	4	4	-	-	-	-	8	-	-	-	-	-	78	-
Bh No. 1 4 m	9	4	3	-	-	-	-	18	-	-	-	-	-	66	-
Bh No. 1 6 m	5	3	3	-	-	-	-	9	-	-	-	6	-	75	-
Bh No. 2 2m	-	-	-	3	20	-	1	12	22	26	2	10	3	-	-
Bh No. 2 4m	-	-	-	6	23	-	1	9	34	16	1	9	2	-	-
Bh No. 2 6m	-	-	-	4	26	1	1	8	44	14	-	2	-	-	-
Bh No. 2 7m	-	-	-	4	24	-	1	10	50	7	-	3	-	-	-
Bh No. 2 8m	-	-	-	7	21	-	-	17	42	7	-	7	-	-	-
Bh No. 3 1m	-	-	-	-	24	4	5	16	16	16	9	9	-	-	*
Bh No. 3 2m	-	-	-	-	26	-	2	18	11	17	12	15	-	-	*
Bh No. 4 1m	-	-	-	-	31	1	1	4	33	13	13	-	3	-	-
Bh No. 4 2m	-	-	-	-	26	1	2	6	29	27	5	-	3	-	-
Bh No. 4 3m	-	-	-	-	30	-	5	2	30	28	4	-	2	-	-
Bh No. 5 1m	-	-	-	4	34	6	3	2	21	22	5	-	5	-	-
Bh No. 5 2m	-	-	-	2	29	3	3	1	35	21	3	-	3	-	-
Bh No. 5 3m	-	-	-	4	25	3	2	1	35	23	2	1	3	-	-

*Formula: $(W_{1-0}X_2Y_5Z_8O_{22}(OH)_2)$, W = (Na,K), X = (Ca, Mg,Fe, Na), Y = (Mg,Fe,Al), Z = (Si,Al)

The following observations are made from **Table 5.3.3(A)**:

- Sample Bh No. 1 shows typical ash-forming minerals that are present in the coal of the Witbank Coalfield, namely kaolinite, quartz, pyrite, calcite and dolomite.
- The mineral composition of the samples from boreholes Bh No. 2 to 5 is typical that of ash-forming material subjected to heat at a low pressure range. The first evidence that the material was subjected to heat (coal combustion) is shown by the presence of mullite ($\text{Al}(\text{Al}_{1+2x}\text{Si}_{1-x})\text{O}_{5-x}$) which is a rare mineral in nature, but frequently occurs in heated material (e.g. furnace slags and in a variety of ceramic and refractory materials). Based on the above information it could be concluded that the mullite originates from the alumino-silicates (especially kaolinite) in the coal discard prior to coal combustion.
- The second evidence of coal combustion is the presence of the quartz-polymorphs cristobalite and tridymite. The polymorphs were formed by the fusion of quartz grains during combustion. Recrystallization occurred under a much lower pressure than the original quartz crystals and a subsequent different crystal structure formed. Minerals with different crystal structures but with the same composition (SiO_2 in this case) are called polymorphs.
- The presence of hematite shows that oxidation took place. Hematite can be seen as a dehydrated recrystallized form of ferrihydrate and goethite (See **Section 2.5**).
- Amorphous material (likely silica glass, iron-sulphates or hydroxide minerals) are present in Bh No. 3. Other samples may also contain amorphous phases that were not detected by XRD analyses.
- Gypsum ($\text{CaSO}_4 \cdot 2\text{H}_2\text{O}$) is present in most samples that were subjected to heat. Gypsum precipitates from the interstitial water elevated in calcium and sulphate. Anhydrite (CaSO_4) formed from the dehydration of gypsum during heating.

Based on the above observation we conclude that the dump consists of two types of material:

- A fair amount of material was subjected to heat (coal combustion) and oxidation. The bulk of these materials now consists of minerals that are slow-reacting or basically inert and oxidized. The only abundant minerals in this material that are fairly reactive are gypsum and anhydrite. Seepage from this part of the dump will contain elevated sulphate.
- The absence of mullite, hematite and quartz-polymorphs in Bh No. 1 shows that some material has not been subjected to coal combustion. In these parts of

the dump not subjected to heat, minerals like dolomite and calcite are present which will partly neutralize acidic drainage. Pyrite is also detected in samples from this part of the dump. Pyrite at low concentrations may be present in the other samples, although it was not detected with XRD.

Acid-Base Accounting (ABA) and Net-Acid Generating (NAG) pH

The results of the ABA done on the above discard dump samples are summarized in **Table 5.3.3(B)** below:

Table 5.3.3(B). ABA analyses on discard dump samples.

Sample No. and depth of sampling	Paste pH	NAG pH	Total S (%)	Acid Generating Potential (kg CaCO ₃ /t)	Neutralization Potential (kg CaCO ₃ /t)	Net Neutralization Potential (kg CaCO ₃ /t)	NP:AP Ratio
Bh No. 1 2 m	7.64	2.40	2.575	80.47	13.75	-66.72	0.17
Bh No. 1 4 m	7.50	2.55	1.593	49.78	20.25	-29.53	0.41
Bh No. 1 6 m	7.72	2.75	1.548	48.38	17.50	-30.88	0.36
Bh No. 2 2m	6.67	4.07	1.171	36.59	6.00	-30.59	0.16
Bh No. 2 4m	5.91	3.82	1.112	34.75	4.00	-30.75	0.12
Bh No. 2 6m	6.01	3.02	0.196	6.13	2.25	-3.88	0.37
Bh No. 2 7m	5.15	3.05	0.345	10.78	0.75	-10.03	0.07
Bh No. 2 8m	5.84	3.31	1.117	34.91	1.75	-33.16	0.05
Bh No. 3 1m	7.93	2.29	2.352	73.50	10.75	-62.75	0.15
Bh No. 3 2m	6.00	2.25	3.008	94.00	3.75	-90.25	0.04
Bh No. 4 1m	3.52	3.10	2.828	88.38	0.00	-88.38	0.00
Bh No. 4 2m	5.32	4.22	0.851	26.59	7.25	-19.34	0.27
Bh No. 4 3m	4.38	3.45	0.847	26.47	4.25	-22.22	0.16
Bh No. 5 1m	4.17	3.33	1.001	31.28	0.00	-31.28	0.00
Bh No. 5 2m	4.26	2.91	0.755	23.59	0.00	-23.59	0.00
Bh No. 5 3m	5.49	4.01	0.345	10.78	4.00	-6.78	0.37
Bh No. 1 2 m	7.45	4.79	0.544	17.00	6.25	-10.75	0.37

Minimum	3.52	2.25	0.196	6.13	0.00	-90.25	0.00
Maximum	7.93	4.79	3.008	94.00	20.25	-3.88	0.41
Average	5.94	3.25	1.305	40.79	6.03	-34.76	0.18

The following observations are made from the ABA results in **Table 5.3.3(B)**:

- The paste pH's is near neutral to slightly acidic and four samples have paste pH-values lower than pH 4.
- The total %S is high with a resulting high Acid Potential (AP).
- The Neutralization Potential (NP) is moderate to low, indicating the limited acid neutralization potential of the samples.
- The Net Neutralization Potential (NNP) is calculated by subtracting the AP from NP. The NNP is negative in all the samples and averages at -34.76 kg/t , showing that the effluent from the discard dump will be potentially acidic.
- Based on the %S and the NP:AP ratio, the samples from the discard dump are classified as "Likely Acid Generation" (see **Section 6.2.3** for ABA screening methods).
- The NAG (Net Acid Generating Potential) pH is another way of determining whether the drainage from a rock will turn acidic. The NAG pH is determined after oxidizing all sulphides with a standard amount of peroxide. The pH is measured after 48 h when all the carbonates have reacted. If the pH is between 3.5 and 5.5, the sample is classified as "Low Risk Acid-generating" and with a pH below 3.5 the sample is classified as "High Risk Acid-generating". Five samples have NAG pH's between 3.5 and 5.5 and 12 have NAG pH's of below 3.5. This proves the acid generation potential of the material, which is in agreement with the results of the ABA.

The results of this section cannot be quantitatively extrapolated to other sites because of the differences in 1) coal discard dump age and 2) beneficiation processes over the coalfield. However, the results show important general properties of coal discard subjected to spontaneous combustion: 1) a significant change in mineralogy occur and 2) the discard maintain the potential for creating acidic drainage.

5.4 Final remarks and conclusions

With regard to coal discard production and its potential to generate AMD in South Africa, the following general conclusions could be made:

Coal discard production

- The production of coal discard is a direct result of the coal beneficiation process. The extent to which coal is cleaned is determined by the end-use of the coal.
- Crushing and screening of coal produces no coal discard. Crushing of the coal only to an appropriate top size is required for respectively 47% and 14% of the coal supplied for electricity generation and synthetic fuels in South Africa.
- Coarse discard is produced where low levels of coal washing are required. These low levels of beneficiation are responsible for 53% and 84% of the coal supplied for respectively power generation and synthetic fuels.
- Higher levels of beneficiation produce fine discard that is often pumped as slurry to impoundments. Metallurgical and export coal generally require higher levels of coal beneficiation, which generally entails the removal of shale and low quality coal.
- Since the 1985 DME inventory the annual total coal discard production has increased from 43.6 Mt (1985) to 66.2 Mt (2001). More than 1000 Mt of discard and a total of 52.8 Mt of dumped slurry are present in the South African coalfields. Annual discard and slurry production in 2001 were respectively 42.5 Mt and 11.3 Mt (DME, 2002).

General environmental impacts

- At low levels of beneficiation, the coal product contains a fair amount of sulphur. End-users of these products are typically power stations or other industries that eject a large amount of CO₂ and SO₂ into the atmosphere.

At high levels of beneficiation, the coal product contains less sulphur and smaller amounts of CO₂ and SO₂ are introduced into the atmosphere by end-users. These end-users also generally operate on a smaller scale.

- Old discard dumps in South Africa is one of the greatest polluters of the environment, polluting the atmosphere, rivers, groundwater and the esthetics of the countryside.
- Discard dumps subjected to spontaneous combustion eject a large amount of CO₂ and SO₂ into the atmosphere. It is difficult to rehabilitate burning dumps as machinery must be protected against the heat.
- Seepage from coal discard dumps will pollute the underlying aquifer and may also impact on surface water resources.

Potential to create AMD

- In the discard analyzed in this study, there is an increase in the pyrite and also carbonate mineral content. The results of this study cannot be quantitatively extrapolated to other sites because of differences in the coal quality and beneficiation processes over the coalfield. However, the results show two important general properties of coal discard: it has 1) a higher mineral content as well as 2) a higher acidification potential than the ROM coal.
- Significant mineralogical changes take place in coal discard that is subjected to spontaneous combustion. In this study no pyrite or carbonate minerals were identified by XRD in dump material subjected to spontaneous combustion. The implication is that although sulphides will oxidize in parts of the discard dump (with resultant release of sulphur as SO₂ to the atmosphere), discard subjected to heat also loses most of its neutralization capability as carbonate minerals are lost. In the data of this study NP was lower in the part of the dump that was subjected to spontaneous combustion. A high %S and a NAG pH of below pH 4 were still present in this part of the dump indicating net acidic drainage potential.
- Both NAG pH's and ABA proved the high net acid generation potential of discard, whether it was subjected to spontaneous combustion or not. It can be concluded that coal discard has a high potential to generate AMD.

General measures for atmospheric pollution and AMD mitigation

- Free-tipping of coarse discard must be minimized and be replaced by spreading of discard and compaction to eliminate the ingress of air into the dump.
- With rehabilitation, coal discard facilities must be covered with soil and vegetated to prevent atmospheric pollution and oxygen infiltration, thereby greatly reducing the chances of spontaneous combustion of discard on the dump.
- Dumps must be constructed with run-off paddocks to control storm water run-off from the top and sides of the dump.
- Storm water must be diverted around the dump and possible contaminated run-off must be collected in dirty storm water dams.
- Trenches must be constructed down gradient in order to intercept some of the seepage from the dump. The seepage trenches must be constructed as deep as is practical possible.

- The quality of groundwater in the surrounding aquifer and seepage from the dump must be monitored. Seepage must be collected in paddocks for re-use in the processing plant or gravitated to evaporation dams.
- Changes in environmental legislation and the mine's realization that coal discard is a valuable energy source has changed the way coal discard is now being considered (DME, 2002).

Implications for geochemical modelling

- A detailed assessment of the hydrology and air migration into the dump must be made for modelling purposes. The water balance of the dump could be modelled using a program such as HELP, which is an U.S. EPA model for predicting landfill hydrologic processes and testing the effectiveness of landfill designs.
- Detailed ABA and mineralogical and geochemical analyses must be performed on the coal discard material to establish the amount of pyrite and carbonate minerals present as well as the degree to which the material was subjected to heat. If it was not subjected to heat, then the incorporation of the mineralogy into the model is straightforward.
- If the coal discard material was subjected to heat, no carbonate minerals are present, and although it may be possible that no pyrite is present, the coal discard can still generate acidic drainage. The acid generation may come from secondary iron hydrous sulphate minerals that contain "stored acidity". The "stored acidity" is released when the minerals are dissolved by recharge or run-off, and when the iron or aluminium undergoes hydrolysis (see **Section 2.9**). The secondary minerals are generally relatively soluble except for goethite and hematite.

5.5 References

Budge, G., Brough, J., Knight, J., Woodruff, D. and McNamara, L. (2000). *Review of the Worldwide Status of Coal Preparation Technology*. Report No. COAL R199, Department of Trade and Industry, UK.

Coaltech 2020 (2006). *South Africa's coal chain*. Internet: <http://coaltech.csir.co.za/>

Department of Minerals and Energy (2006). *Coal*. Internet: <http://www.dme.gov.za/energy/coal.stm>

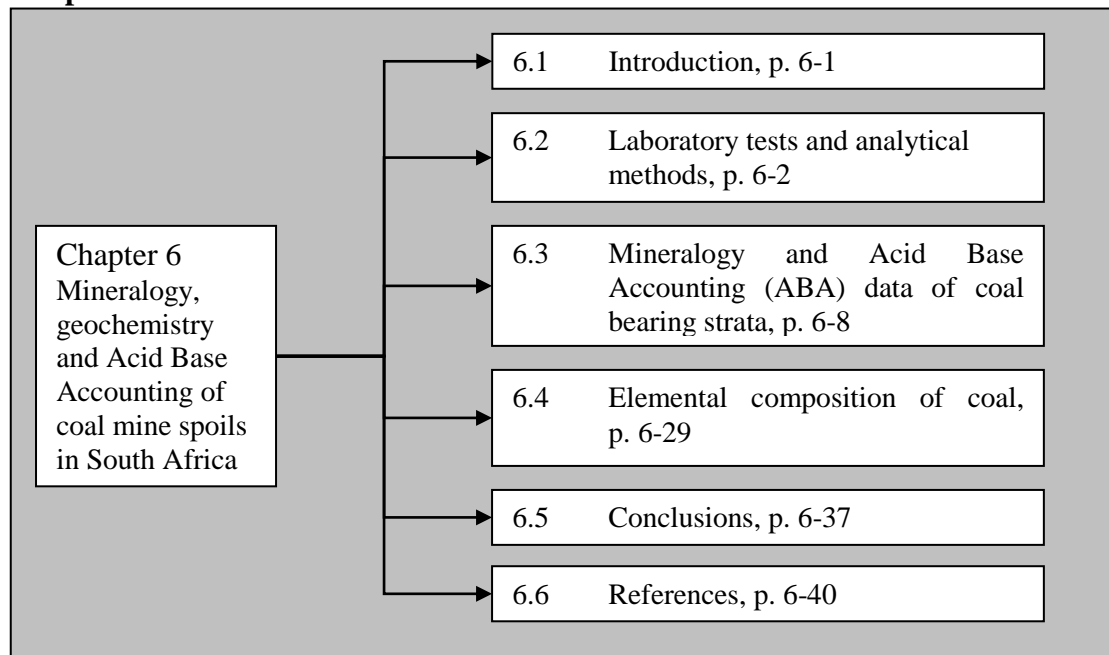
Department of Minerals and Energy (2002). *The national inventory discard and duff coal: 2001 summary report*. Directorate: Mineral Economics, Pretoria. Internet: http://www.dme.gov.za/energy/coal/coal_discard_report.pdf

Hodgson, F.D.I. and Krantz, R.M. (1998). *Groundwater Quality Deterioration in the Olifants River Catchment above the Loskop Dam with specialised investigation in the Witbank Dam Sub-Catchment*. Report to the WRC, Report 291/1/98, Water Research Commission, Pretoria.

Horsefall, D.W. (1993). *Coal preparation and usage – Coal processing for management*. Volume 1, Coal Publications.

6 Mineralogy, geochemistry and Acid Base Accounting of coal mine spoils in South Africa

Chapter Structure



6.1 Introduction

In open-cast mining, the soft overburden (soils and highly weathered rock), the hard overburden (unweathered rock) and some inter-burden (rock between coal seams) are removed in order to mine the coal. The over- and inter-burden are backfilled into the voids of the open-cast pit as mining progresses. The backfilled spoils are rehabilitated by compaction, topsoil covering and vegetation.

Coal mine spoils consist of carbonaceous and non-carbonaceous clastic rocks (sandstone, shale and siltstone), uneconomical coal seams, and a small part (<5%) of the economical coal seam left in the mine.

In **Chapter 1** it was stated that the Witbank and the Highveld Coalfields produce respectively 56% and 20% of all mined coal in South Africa. The description of the mineralogy and the geochemistry of the spoils were limited to these two coalfields. In order to describe the mineralogy and geochemistry of the coal mine spoils in the Witbank and Highveld Coalfields, the following rock material was included in the sampling program:

- Coal seams (No. 1 to No. 5 coal seams).
- Carbonaceous clastic rocks.
- Non-carbonaceous clastic rocks.

Soils and other parts of the soft overburden will not be described geochemically as these material are considered to be inert with relation to acid mine drainage production and in the neutralization thereof.

In this study the mineralogical content of the geological material was classified in terms of the relative mineralogical weight percentage (wt%):

- Dominant minerals (>40 wt%)
- Major minerals (10 – 40 wt%)
- Minor minerals (2 – 10 wt%)
- Accessory minerals (1 – 2 wt%)
- Trace minerals (0 – 1 wt%)

Research on the mineralogy and geochemistry of the coal seams from the Witbank and/or Highveld Coalfield includes studies by Gaigher (1980), Hart et al. (1982), Hart and Leahy (1983), Cairncross et al. (1990), Cadle et al. (1989), Bühmann and Bühmann (1988), Azzie (2002) and Pinetown (2003). Reference will be made to these studies in the discussion on the mineralogical analyses (**Section 6.3.3**) and the geochemistry of the rocks (**Section 6.4**) in the coalfields.

6.2 Laboratory tests and analytical methods

6.2.1 X-Ray Diffraction (XRD) Analysis

Whole rock samples obtained from JMA Consulting (Pty) Ltd were analyzed for its mineralogical content. All XRD analyses and semi-quantitative interpretations were performed by the Geology Department of the University of Pretoria.

Accessory and trace minerals are less accurately identified when using a whole rock sample. To represent the minerals identified by XRD analyses semi-quantitatively, further interpretation is needed using computer software or manual investigation. The accuracy of semi-quantitative results of the XRD analysis vary depending on the number of minerals present in a sample. Many correction techniques exist that have been applied with great success (Ward and Taylor, 1996). Interpretation of the XRD results in this study were done using the Rietveld procedure.

The XRD method entails the direction of an X-ray beam of known wavelength at a crystal. The beam is diffracted by planes of atoms in the crystals. By recording the angular positions of diffracted beams, the spacing between atomic planes can be determined. The procedure is repeated for various directions in the crystal and a model of its internal structure established (Allaby and Allaby, 2003).

6.2.2 X-ray Fluorescence (XRF) Spectrometry Analysis and Instrumental Neutron-activation Analysis (INAA)

Although no XRF or INAA analysis have been performed in this study, some reference will be made to relevant major and trace element analysis of other studies on South African coals.

XRF analysis is used to quantitatively determine a large amount of major, minor and trace elements present in rocks. INAA is an analytical technique that could very accurately determine some trace elements.

Cairncross et al (1990) applied both methods as certain elements can be more accurately determined by the one or the other. XRF determine Si, Al, Ti, Ca, Mg, P, V, Ni, Cu, Zn, Ga, Ge, Y, Zr, Ba, Pb more accurately than INAA. Other elements such as the rare earths, Th, U, Hf, Ta, Co, Cs, Br, Sb and As either occur at concentrations below detection limits for XRF or are more accurately determined by INAA.

The XRF Spectrometry method entails the use of an X-ray beam to excite atoms in a sample; electrons near the nucleus emit secondary or fluorescent X-rays on reversion to their original states. An element have a unique wavelength and the intensity of the radiation measured, relative to a standard, is proportional to the concentration of the element.

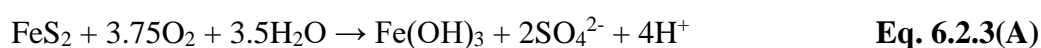
Neutron-activation Analysis entails the bombarding of a sample with fast moving neutrons in the core of a nuclear reactor. Neutrons are added to the nuclei of stable isotopes to form new radionuclides which decay, producing particles with characteristic energies that can be measured with a scintillation counter.

6.2.3 Acid Base Accounting (ABA) analyses

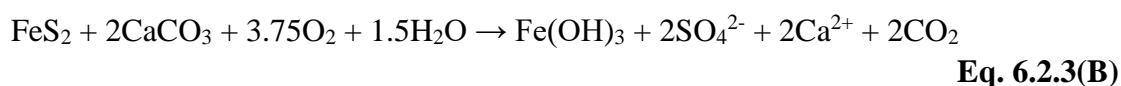
All ABA analyses in this study were done by Waterlab (Pty) Ltd using the Modified Sobek (Sobek et al., 1978, and Lawrence and Wang, 1997) procedure (therefore not correcting for the siderite content).

AP, NP and NNP

Coal mine spoils contain pyrite and have the potential of producing acidic drainage. In ABA the measure for the potential of acid generation by a rock is based on the stoichiometry of the oxidation of pyrite with oxygen as given below:



The neutralization potential of a rock, in an open system, is based on the following neutralization reaction of calcite with the acidity produced by the oxidation of pyrite:



Following **Equation 6.2.3(A) and (B)**, 1 mol of calcite is used to neutralize 2 mol of acid in an open system. Therefore, on a mass ratio basis, 3.125 g calcite is needed to neutralize 1 g of pyrite. When expressed in parts per thousand (ppt) of spoil, for each 10 ppt of sulphur present, 31.25 ppt calcite is required for acid neutralization.

It was shown in **Section 2.7.2** that in a closed system CO₂ would not be exsolved. Additional acidity would then be generated by carbonic acid and 2 additional moles of calcite would be needed to neutralize the acid. Therefore, for each 10 ppt of sulphur present, 62.50 ppt calcite is required for acid neutralization.

The %S of all samples were calculated in a Leco furnace at Waterlab (Pty) Ltd. AP is determined by multiplying the %S with a factor of 31.25, in an open system, and with 62.50 in a closed system. AP has the unit kg CaCO₃/t rock to indicate the theoretical amount of calcite that would be neutralized by the acid produced.

The NP (Neutralization Potential) is determined by first treating a sample with a known excess of standardized hydrochloric or sulfuric acid (the sample and acid are heated to ensure reaction completion), then back-titrated with standardized sodium hydroxide to determine the amount of unconsumed acid. NP is also expressed as kg CaCO₃/t rock as to represent the amount of calcite theoretically available to neutralize the acidic drainage.

NNP is determined by subtracting AP from NP. Therefore, a rock with NNP < 0 kg CaCO₃/t will have a net potential for acidic drainage, and a rock with NNP > 0 kg CaCO₃/t rock will have a net potential for the neutralization of acidic drainage. Because of the uncertainty related to the exposure of the carbonate minerals or the pyrite for reaction, the interpretation of whether a rock will actually be net acid generating or neutralizing is more complex. Usher et al. (2001) state that research has shown that a range from -20 kg CaCO₃/t to 20 kg CaCO₃/t exists that are defined as a “grey” area in determining the net acid generation or neutralization potential of a rock.

ABA Screening Methods

Screening criteria could be used that attempt to classify the rock further in terms of its net potential for acid production or neutralization. The following screening methods given in **Table 6.2.3(A)** below, as proposed by Price (1997), use the NP:AP ratio to classify the rock in terms of its potential for acid generation:

Table 6.2.3(A). Screening methods using the NP:AP ratio (Price, 1997).

Potential for Acid Generation	NP:AP screening criteria	Comments
Likely	< 1:1	Likely AMD generating.
Possibly	1:1 – 2:1	Possibly AMD generating if NP is insufficiently reactive or is depleted at a faster rate than sulphides.
Low	2:1 – 4:1	Not potentially AMD generating unless significant preferential exposure of sulphides along fracture planes, or extremely reactive sulphides in combination with insufficient reactive NP.
None	>4:1	No further AMD testing required unless materials are to be used as a source of alkalinity.

The following screening methods using the %S and the NP:AP ratio are proposed by Soregaroli and Lawrence (1998):

- Samples with less than 0.3% sulphide sulphur are regarded as having insufficient oxidisable sulphides to sustain long term acid generation.
- If the ratio of NP:AP is > 4:1 the material is considered to have enough neutralizing capability, while NP:AP between 2:1 and 1:1 are inconclusive.
- Material with AP:NP of <1:1 and with more than 0.3% sulphide sulphur, is potentially acid generating.

Validity of the assumptions of ABA to the South African coal mine environment

The assumptions made in ABA calculations, and its validity to the South African coal mine environment are discussed below:

Assumption 1: In ABA it is assumed that the total %S analyzed in the rock originate from pyrite.

Sulphur can be present in coal in both organic and inorganic form and inorganic sulphur can be present as sulphides or as sulphates. The Leco furnace determines the total %S whereas the peroxide method (the method is discussed in detail by Usher et al., 2001) excludes sulphate species but includes all sulphide and organic sulphur (if the sample is fully oxidized). Usher et al. (2001) found a regression of 0.92 between these two methods on 50 samples from coal bearing strata. The Leco analyzer generally determined the %S slightly higher than the peroxide method.

Organic sulphur content has been determined in the No. 2 coal seam samples from the Witbank Coalfield by Cadle et al (1989). The organic sulphur for most samples ranged between 0.01 - 0.60% and in samples with organic sulphur content of above 0.30%, organic sulphur shows a good positive correlation with the mineralogical %S content as shown in **Figure 6.2.3(A)** below.

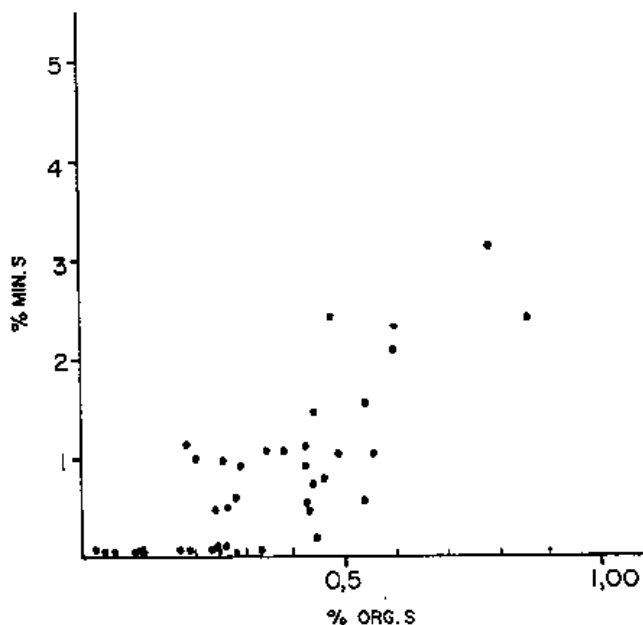


Figure 6.2.3(A). Correlation between mineral and organic sulphur in the No. 2 coal seam of the Witbank Coalfield after Cadle et al. (1989).

Cadle et al. (1989) states that the Witbank Coalfield coals have negligible sulphate content of up to 0.05%. Except for some outliers no minor to rare sulphate minerals have been identified analytically in this study. At one mine in the western Witbank Coalfield alunite ($\text{KAl}_3(\text{SO}_4)_2(\text{OH})_6$) has been identified in three No. 2 coal samples and also in four No. 4 coal seam samples. One sandstone sample at a mine in the northeastern Highveld Coalfield also contained alunite. A more complete discussion of the presence of alunite in the samples is given in **Section 6.3.3** below.

Assumption 2: Pyrite is the only sulphide mineral present and therefore all acid produced in the rock is from its oxidation.

Cadle et al. (1989) states that marcasite (FeS) and pyrothite (Fe_{1-x}S) are occasionally present in the coal seams of the Witbank Coalfield. However, neither their study nor other studies, i.e. Pinetown (2003) and Cairncross et al. (1990), has identified any other sulphides than pyrite by means of any analytical methods.

Assumption 3: Calcite is the only mineral present that would neutralize acid.

A half mole of dolomite ($\text{CaMg}(\text{CO}_3)_2$) would substitute the calcite in reaction **Equation 6.2.3(B)** above. Dolomite is frequently present in South African coal along

with calcite. Although dolomite has a slower reaction rate than calcite, the reaction time in most South African coal mines is long enough for dolomite to react completely. The residence time in most open-cast mines is often between 20 years and 60 years depending on the geometry of the mine. For underground mines the residence time is often a few hundred years. The Annandale mine in the case study (see **Chapter 7**) does however have a smaller residence time (< 10 years) because of the shallowness of the pit (12 m deep on average).

Ankerite ($\text{CaFe}(\text{CO}_3)_2$) will have a reduced acid neutralizing capacity because of the iron present – see **Equation 6.2.3(C)** below. Unfortunately, ankerite is not easily distinguished from dolomite by means of XRD analyses. Siderite (FeCO_3) is another carbonate mineral frequently present in South African coals. Siderite has no net neutralizing capacity since the carbonate is just adequate to neutralize the acid produced by the oxidation of the ferrous iron. The oxidation of 1 mole of ferrous iron will produce 2 moles of acid as shown in **Equation 6.2.3(C)** below:



Because siderite constitutes such a large quantity of the carbonate mineral content of the South African coalfields, the NP may often be overestimated. This is because the siderite will neutralize acid under laboratory conditions but the oxidation of Fe^{2+} takes longer and will not occur during the normal methods used for the estimation of NP. It is therefore recommended that the “Peroxide Siderite Correction for Sobek Method” is used when determining the NP of both coal and clastic rocks from the South African coalfields. Discussion of the method is found in Skousen et al. (1997) or in Mills (2003). The method involves the oxidation (with peroxide) of the Fe^{2+} (to produce acid) before the normal back-titration with acid. This method is seldom or never used in South Africa.

Most natural siderite is actually a solid solution containing some Ca, Mg and Mn in addition to Fe. To the extent that siderite contains Ca and Mg in solid solution, its dissolution will contribute some net alkalinity, analogous to the reaction of the CaCO_3 or MgCO_3 component in the siderite.

Most silicate minerals also neutralize acidic water as it consumes hydrogen in its dissolution reaction. Silicates however have much smaller reaction rates than carbonates. A more detailed description of mineral reactions in Acid Mine Drainage (AMD), as well as a discussion of mineral dissolution rates, is given in **Chapter 2**. Silicate minerals will not play a significant role in the neutralization of acidic drainage over the short term (during the life of the mine) but they would definitely play a role over the long term as was also shown in the case study in **Chapter 7**. Evidence for silicate mineral dissolution is found in elevated Si, Al or other cations in AMD. For instance, the precipitation of K- and Na-jarosite or alunite is often indirectly the result of the dissolution of Na or K silicate minerals, e.g. feldspar, mica or clay, under acidic conditions.

Silicates that do however show a significant dissolution rate and potential to neutralize acid over the short term are those originating mostly from ultra-mafic, mafic or Si-poor intermediate rocks, e.g. anorthite, nepheline, olivine, pyroxene and amphibole. Anorthite has often been wrongly introduced as the plagioclase mineral present in the South African coal bearing strata in geochemical models. However, this would be incorrect, as the plagioclase would be rather of oligoclase ($An_{10}Ab_{90}$ – $An_{30}Ab_{70}$) composition because of the felsic origin of the clastic rocks as described in Cairncross et al. (1990). The reason for the faster kinetic rate of anorthite (Ca-plagioclase) in contrast to albite (the Na end member) lies within its crystal structure as discussed in **Section 2.8**.

6.3 Mineralogy and Acid Base Accounting (ABA) data of coal bearing strata

Only samples on which XRD, NP and AP analyses were performed were included in the calculations. The paste pH was not determined on all the samples and it was therefore omitted from the calculations.

Samples were only collected from the Witbank and Highveld Coalfields as these two coalfields are currently the major coalfields producing about 75% of all mined coal in South Africa.

6.3.1 Sampling distribution

A total of 157 coal, roof and floor rock samples from the lower Vryheid Formation were taken by JMA Consulting (Pty) Ltd from 64 boreholes in the Witbank and Highveld Coalfields. The location of these boreholes is shown in **Figure 6.3.1(A)** below.

X-Ray Diffraction (XRD) and Acid Base Accounting (ABA) were performed on all the samples. The following samples were taken:

- 36 samples were taken from 17 boreholes in the north-eastern Witbank, from the No. 1 and No. 2 coal seams and the surrounding clastic rocks. 61 samples were taken from 28 boreholes in the western Witbank Coalfield, from the No. 2 to No. 5 coal seams and the surrounding clastic rocks.
- 60 samples were taken from 19 boreholes in the north-eastern Highveld Coalfield, from the No. 2 to No. 5 coal seams and the surrounding clastic rocks.

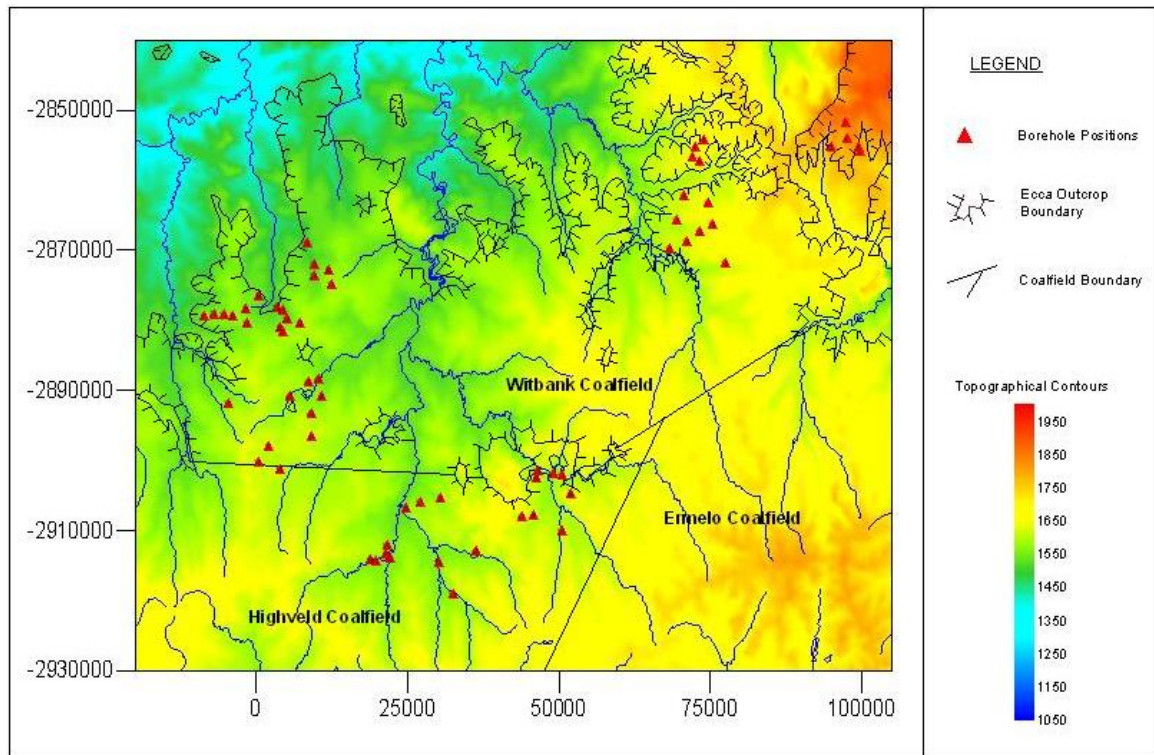


Figure 6.3.1(A). Location of sampling points in the Witbank and Highveld Coalfields.

6.3.2 Summary of XRD and ABA results

The mineralogy from the western and north-eastern Witbank Coalfield was comparable both in mineral occurrences and quantities. These two datasets were combined to form a single dataset of the Witbank Coalfield. The mineralogy of the Highveld Coalfield was slightly more distinct and treated separately. Not enough data existed in order to distinguish between the clastic rocks above the various coal seams.

A summary of the XRD and ABA results for the Witbank and Highveld Coalfields are given in **Table 6.3.2(A)** and **(B)** below:

Table 6.3.2(A). XRD analyses (wt% of mineralogical content) and ABA data (on total coal) for the Witbank Coalfield.

Mineral (average wt%)	No. 1 Coal Seam ash	Frequency	No. 2 Coal Seam ash	Frequency	No. 3 Coal Seam ash	Frequency	No. 4 Coal Seam ash	Frequency	No. 5 Coal Seam ash	Frequency	Carbonaceous Clastic Rocks	Frequency	Non-Carbonaceous Clastic Rocks	Frequency	Frequency in 97 samples
Quartz	34.13	4	34.02	26	31.00	1	29.81	14	34.00	2	44.57	31	46.40	19	97
K-feldspar	3.16	3	3.43	18	0.00	0	2.82	9	9.00	2	5.98	31	7.24	19	82
Plagioclase	0.00	0	0.88	4	0.00	0	0.00	0	5.00	1	0.54	6	0.87	4	15
Mica	2.00	1	2.04	10	0.00	0	2.05	6	5.00	2	4.99	27	4.01	11	57
Kaolinite	38.34	4	50.43	26	66.00	1	53.92	14	22.50	2	36.88	31	35.44	19	97
Illite/Smectite	0.00	0	0.30	3	0.00	0	1.05	2	3.00	1	0.58	6	0.08	1	13
Smectite	0.00	0	0.18	1	0.00	0	0.00	0	4.00	1	0.20	3	0.00	0	5
Pyrite	6.37	3	2.20	18	2.00	1	3.77	8	0.00	0	1.25	13	0.70	5	48
Hematite	2.00	1	0.65	4	0.00	0	1.12	5	10.50	2	0.65	5	0.00	0	17
Siderite	1.55	2	1.12	11	0.00	0	0.48	3	0.00	0	1.63	17	3.02	11	44
Calcite	3.79	3	2.11	12	1.00	1	1.81	6	4.00	2	1.85	11	0.39	7	42
Dolomite	7.79	4	1.76	12	0.00	0	1.32	6	1.50	1	0.49	6	0.85	5	34
Apatite	0.00	0	0.52	3	0.00	0	1.25	3	1.50	1	0.19	3	0.00	0	10
Anatase	0.86	2	0.17	4	0.00	0	0.00	0	0.00	0	0.07	3	0.40	9	18
Alunite	0.00	0	0.22	3	0.00	0	0.61	4	0.00	0	0.00	0	0.00	0	7
Clinopx*	0.00	0	0.00	0	0.00	0	0.00	0	0.00	0	0.15	2	0.60	2	4
Total Ash	100.00	4	100.00	26	100.00	1	100.00	14	100.00	2	100.00	31	100.00	19	97
NP (kg CaCO ₃ /t)	13.83	4	9.99	26	3.25	1	10.93	14	11.17	2	5.95	31	5.06	19	-
AP (kg CaCO ₃ /t)	31.25	4	27.63	26	26.09	1	37.80	14	21.53	2	18.18	31	4.10	19	-
NNP (kg CaCO ₃ /t)	-17.42	4	-17.64	26	-22.84	1	-26.87	14	-10.36	2	-12.23	31	0.96	19	-
%S	1.00	4	0.88	26	0.84	1	1.21	14	0.69	2	0.58	31	0.13	19	-
Pyrite (Calc)**	1.87	4	1.65	26	1.56	1	2.26	14	1.29	2	1.09	31	0.25	19	-

* Clinopx = Clinopyroxene.

** Pyrite calculated from %S.

Table 6.3.2(B). XRD analyses (wt% of mineralogical content) and ABA data (on total coal) for the Highveld Coalfield samples.

Mineral (average wt%)	No. 2 Coal Seam ash	Frequency	No. 4 Coal Seam ash	Frequency	No. 5 Coal Seam ash	Frequency	Pyrite Containing Clastic Rocks*	Frequency	Low Pyrite Containing Clastic Rocks	Frequency	Frequency in 60 samples
Quartz	54.04	3	44.03	14	31.89	7	39.55	24	38.88	12	60
K-feldspar	3.58	3	3.28	11	10.29	7	7.19	19	6.59	12	52
Plagioclase	0.00	0	2.06	7	5.31	6	6.20	19	8.07	9	41
Mica	1.04	1	3.38	9	8.48	7	8.68	22	7.60	8	47
Kaolinite	32.81	3	28.65	13	14.83	4	22.41	18	24.70	6	44
Illite/Smectite	3.53	2	4.04	5	13.25	5	1.33	7	3.84	4	23
Smectite	0.00	0	1.43	5	4.39	2	1.24	4	0.00	0	11
Chlorite	0.00	0	2.13	1	4.45	3	2.46	6	4.59	6	16
Pyrite	0.48	1	0.83	10	0.79	4	0.53	10	0.22	2	27
Hematite	0.00	0	0.00	0	0.00	0	0.00	0	0.13	1	1
Goethite	0.00	0	0.00	0	0.00	0	0.00	0	1.11	1	1
Siderite	0.31	1	1.09	4	4.16	3	5.53	14	0.35	3	25
Calcite	3.74	2	3.95	11	0.79	3	2.83	20	2.88	8	44
Dolomite	0.00	0	3.70	7	0.16	1	0.56	6	0.87	3	17
Anatase	0.46	1	1.24	4	0.15	1	0.15	5	0.16	2	13
Alunite	0.00	0	0.00	0	0.00	0	0.94	1	0.00	0	1
Clinopyroxene	0.00	0	0.21	1	1.05	1	0.41	1	0.00	0	3
Total	100.00	3	100.00	14	100.00	7	100.00	24	100.00	12	60
NP (kg CaCO ₃ /t)	13.17	3	18.98	14	4.82	7	17.58	24	7.92	12	-
AP (kg CaCO ₃ /t)	25.48	3	24.56	14	23.22	7	22.27	24	1.15	12	-
NNP (kg CaCO ₃ /t)	-12.31	3	-5.58	14	-18.40	7	-4.69	24	6.77	12	-
%S	0.82	3	0.79	14	0.74	7	0.71	24	0.04	12	-
Pyrite(Calc)**	1.53	3	1.47	14	1.39	7	1.33	24	0.07	12	-

* Includes pyrite containing clastic rocks (with S% > 0.1) and all carbonaceous clastic rocks.

** Pyrite calculated from %S.

In **Table 6.3.2(A)** and **(B)** the average mineral content and ABA results are given for both the coal seams and the clastic rocks in the Witbank and Highveld Coalfields. In the Witbank Coalfield the clastic rocks were separated into carbonaceous and non-carbonaceous rocks in order to distinguish between low- and high pyrite containing rocks. However, in the Highveld Coalfield it was found that not only do carbonaceous rocks contain a significant pyrite content, but also some non-carbonaceous sandstone, siltstone and shale. The pyrite in these non-carbonaceous clastic rocks is often euhedral and may have an epigenetic origin.

In **Table 6.3.2(A)** and **(B)** the column, “frequency”, refers to the number of times the mineral has been identified by means of XRD. Although a mineral may not be identified in all samples, it may still occur in trace amounts (<1 wt%) in the sample. The amount of samples analyzed is given at the bottom of the column “frequency” in the row “total”. Note that some minor coal seams have been infrequently sampled in the Witbank (No. 1, No. 3 and No. 5) and Highveld Coalfields (No. 2). A discussion of the XRD and ABA results are given in **Section 6.3.3** below.

6.3.3 Interpretation and discussion of results

NP, AP and NNP distribution in the Witbank and Highveld Coalfield samples

The definition of NP, AP and NNP and the screening methods of ABA has been discussed in **Section 6.2.3**. NP, AP and NNP have been determined on all the samples on which XRD was performed and the results are depicted in **Figure 6.3.3(A)** below.

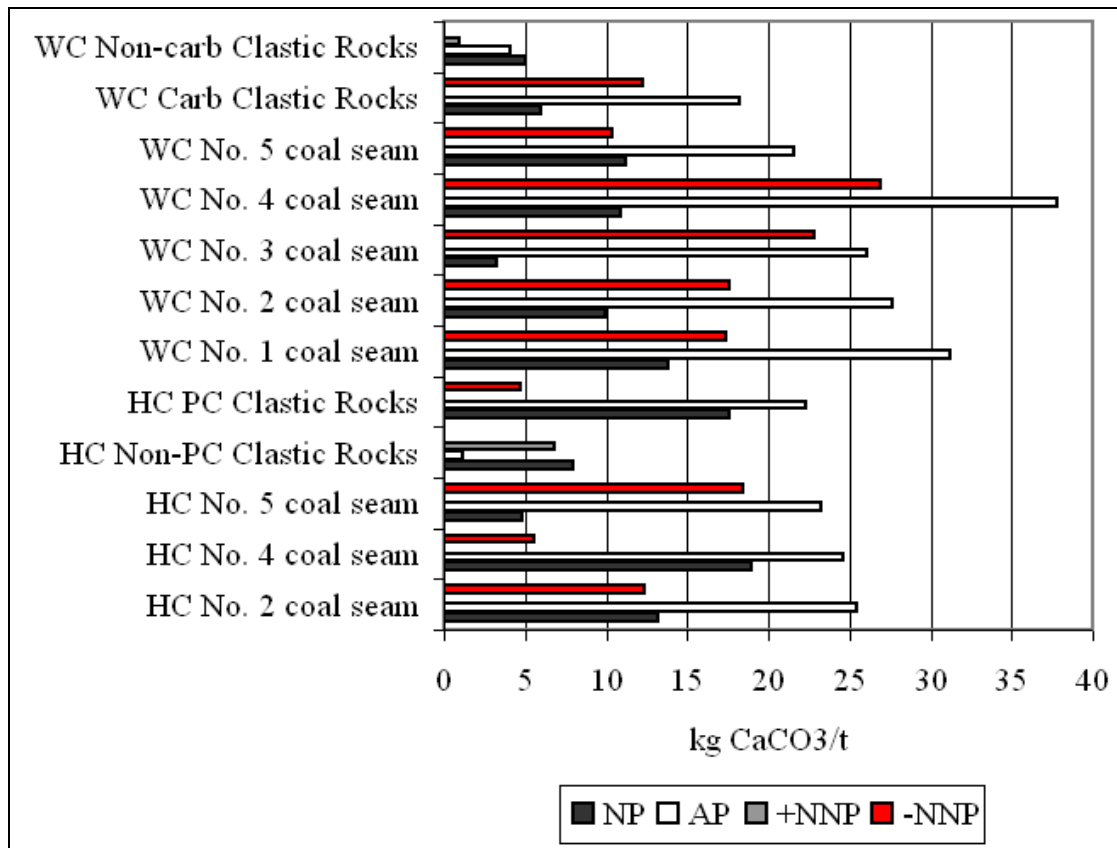


Figure 6.3.3(A). NP, AP and NNP in the Highveld Coalfield (HC) and Witbank Coalfield (WC) coal bearing strata (Carb = carbonaceous, PC = pyrite containing).

The following observations could be made from the distribution of NP, AP and NNP as depicted in **Figure 6.3.3(A)**:

- Non-carbonaceous clastic rocks show NP and AP values of below 10 kg CaCO₃/t. XRD analyses also show little pyrite and carbonate mineral content for these rocks. Non-carbonaceous clastic rocks are the only material that shows a positive NNP.
- Carbonaceous clastic rocks from the Witbank and Highveld Coalfield show a negative NNP, comparable with the NP of some of the coal seams. The average AP and NP for the carbonaceous and pyrite containing clastic rocks are higher in the Highveld Coalfield samples but the NNP is less negative than that of the Witbank Coalfield carbonaceous rocks.
- Generally the NNP increases in the coal seams upwards from the No. 1 to the No. 4 coal seams in the Witbank Coalfield. This has frequently been observed in literature, e.g. Pinetown (2003) and Usher et al. (2001). XRD analyses confirmed that the calcite and dolomite mineral content decreases from the No. 1 to the No. 4 coal seam. It was however observed that the siderite content increases from the No. 1 up to the No. 4 coal seam.

- Overall, both the AP and NNP are higher in the Witbank Coalfield samples than in the Highveld Coalfield. XRD analyses of the samples also show an average higher pyrite content for the Witbank Coalfield samples than for the Highveld Coalfield.

A more detailed comparison between NP and the carbonate mineral content and %S and the pyrite mineral content will be made further below.

Quartz

Quartz (SiO₂) is a major to dominant mineral in both coal and clastic rocks of the Vryheid Formation of the Witbank and Highveld Coalfields. Quartz was found in all samples taken from both the coal seams and the clastic rocks. In the samples from the Witbank Coalfield, quartz (in contrast to kaolinite) shows a higher average concentration in clastic rocks than in coal samples as shown in **Figure 6.3.3(B)** below. In the Witbank Coalfield the kaolinite is the dominant mineral in coal samples from the No. 1 to No. 4 coal seams. However, in the coal samples of the Highveld Coalfield quartz tends to be the dominant mineral instead of kaolinite.

Pinetown (2003) found that Si and Al show good positive correlation in the Witbank Coalfield coal seams. This could be expected from sedimentary rocks with a felsic mother rock (see **Section 6.4** below). Numerous dominant, major and minor aluminous silicate minerals are present such as kaolinite, K-feldspar, plagioclase, mica, smectite and illite. Cadle et al. (1989) found positive correlation between kaolinite and quartz in the No. 2 coal seam of the Witbank Coalfield at minor to major quartz and kaolinite content; however, most of their samples did not have a dominant quartz or kaolinite content. Cadle et al. (1989) do however state that in kaolinite-dominated samples that contained more than 43 wt% kaolinite the quartz/kaolinite ratio decreases.

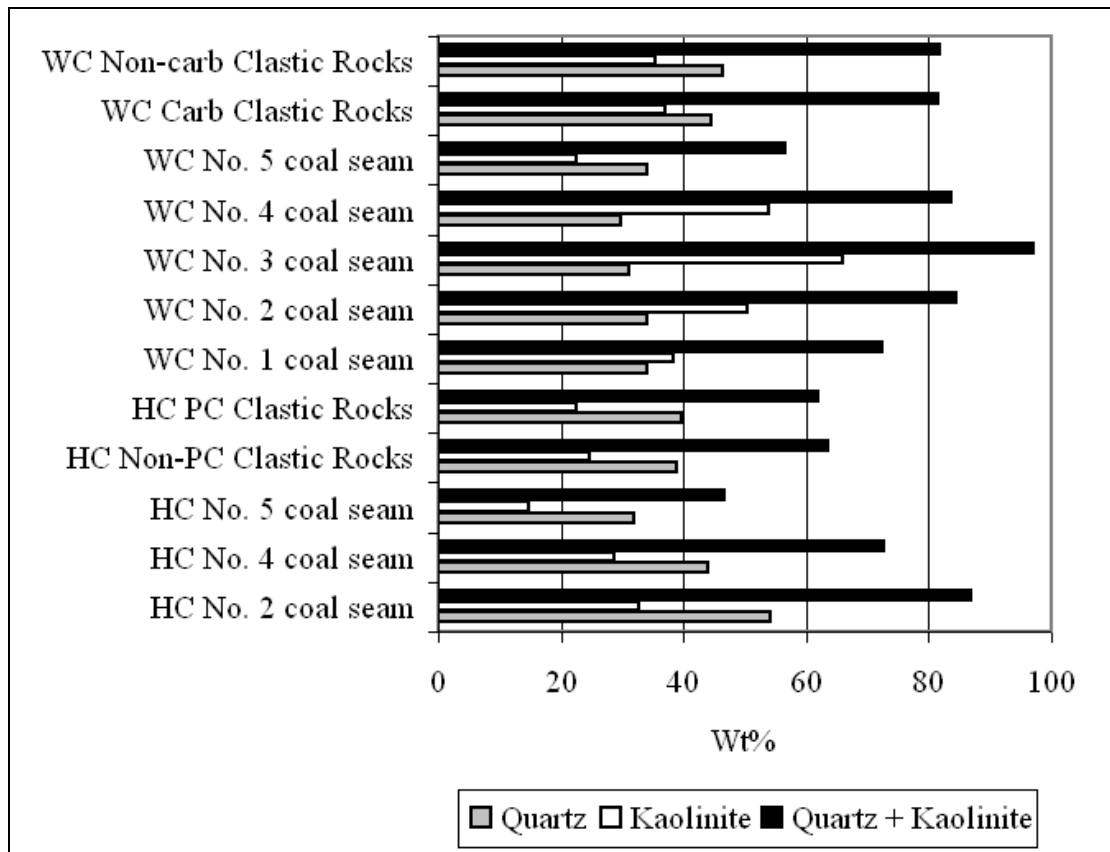


Figure 6.3.3(B). Quartz and kaolinite content in the Highveld Coalfield (HC) and Witbank Coalfield (WC) coal bearing strata (Carb = carbonaceous, PC = pyrite containing).

In this study a similar positive correlation has been found for all samples with major concentrations of both kaolinite and quartz below 35 wt% as shown in **Figure 6.3.3(C)**. However, most samples show either a dominant kaolinite or quartz content, and a negative correlation between kaolinite and quartz exist if one of these minerals became dominant as indicated in **Figure 6.3.3(C)** below. It was shown by Cadle et al. (1989) that the quartz content is positively correlated with the ash content of the No. 2 coal seam of the Witbank Coalfield as shown in **Figure 6.3.3(D)** below.

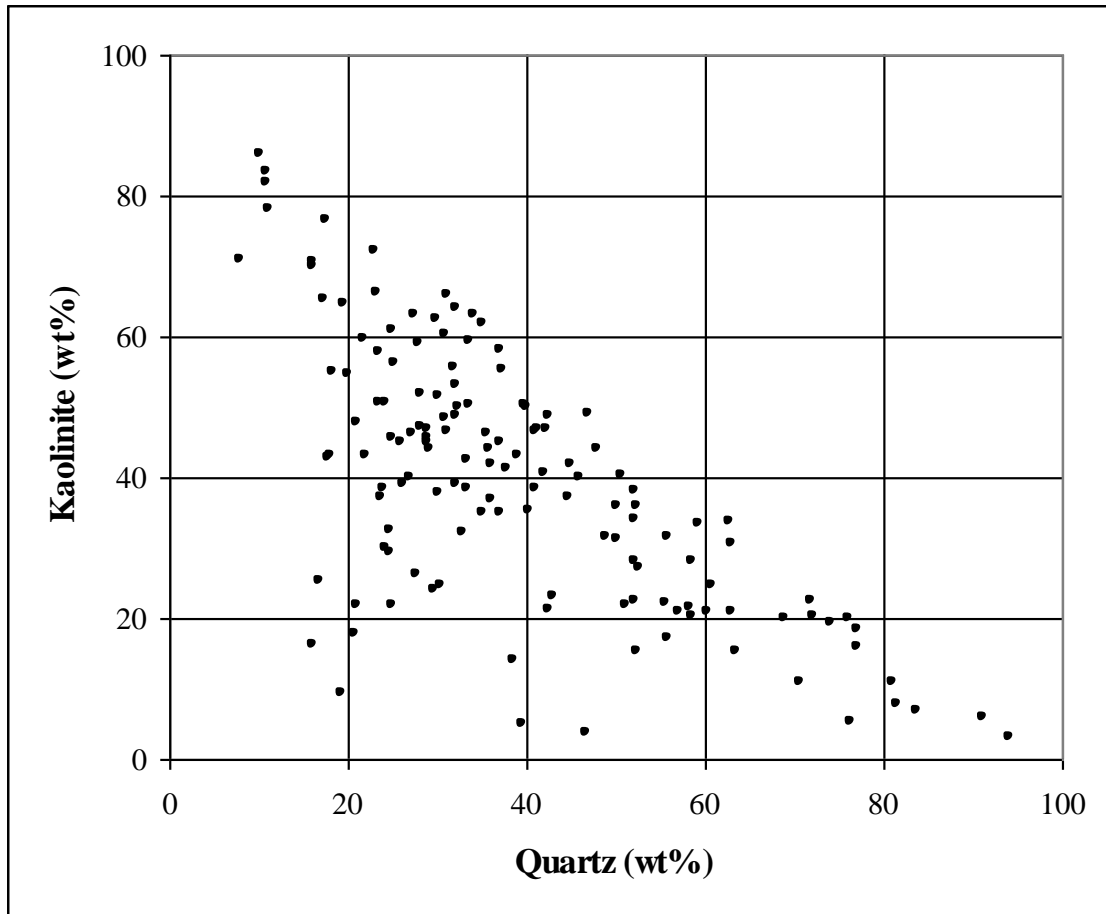


Figure 6.3.3(C). Kaolinite and quartz in coal and clastic rocks.

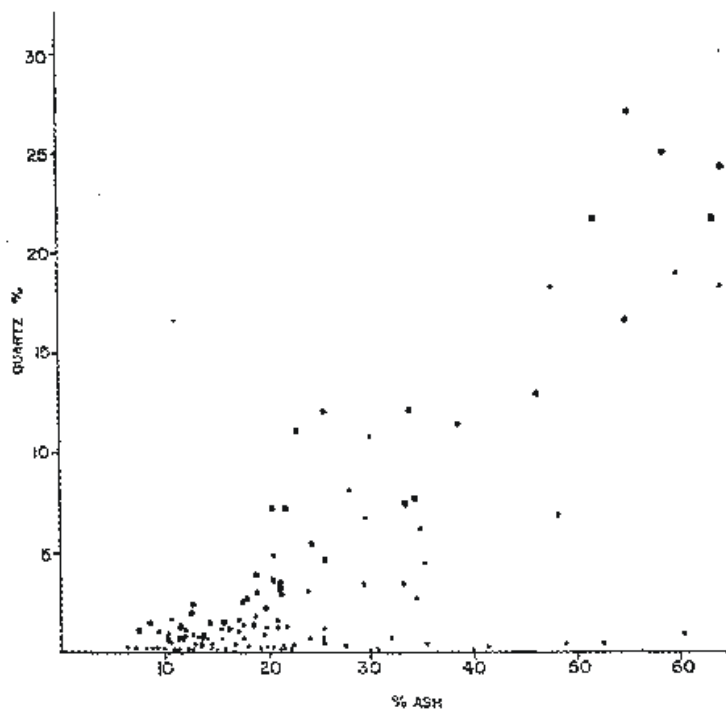


Figure 6.3.3(D). Relationship between the quartz and ash content in the No. 2 coal seam of the Witbank Coalfield after Cadle et al. (1989).

Ward (2002) states that in coal generally, quartz grains have a detrital origin, but are also commonly found as cell and pore infillings in the organic matter of coal, a mode of occurrence that clearly indicates an authigenic origin. In the case of South African coals most quartz is believed to be detrital, being provided from the felsic mother rock of the clastic sediments.

Phyllosilicates – clays and mica

Figure 6.3.3(E) below illustrates the average content of illite/smectite + smectite, mica and chlorite in the Witbank and Highveld Coalfield samples. The kaolinite content (together with quartz) of the samples was already illustrated in **Figure 6.3.3(B)**.

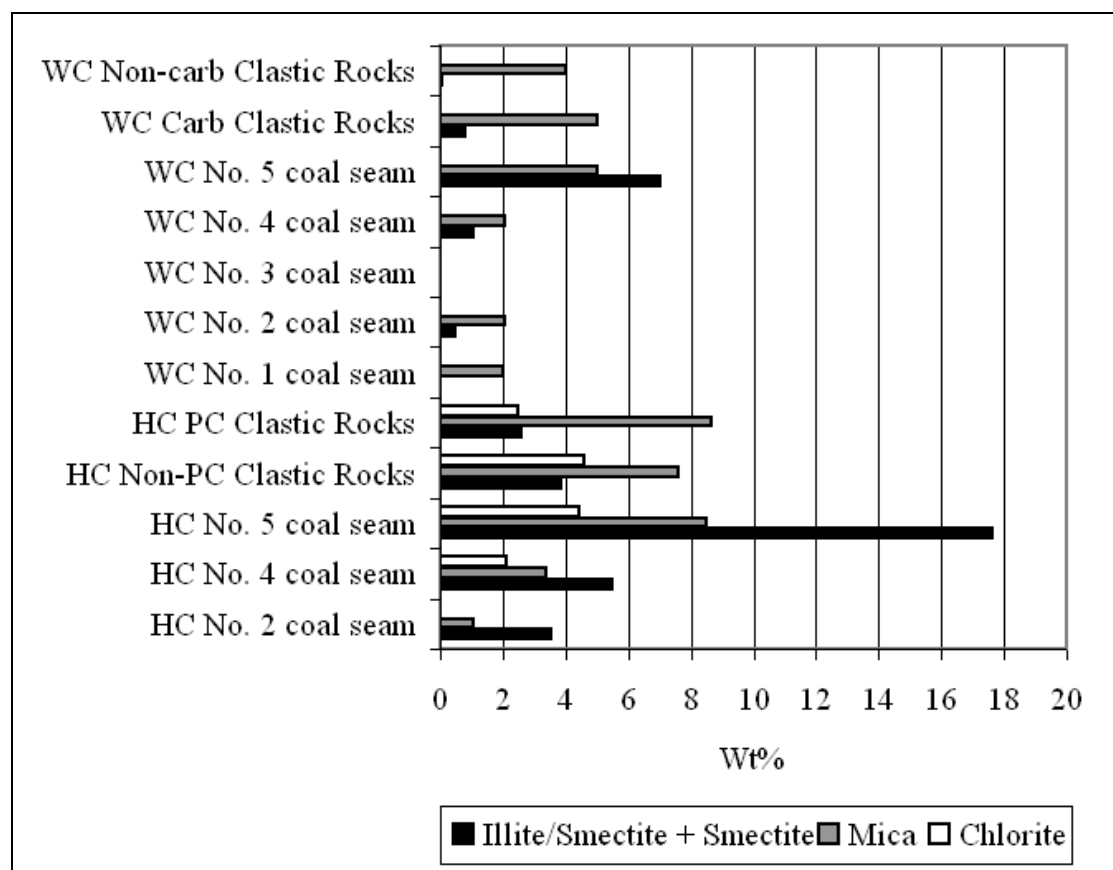


Figure 6.3.3(E). Average illite/smectite + smectite, mica and chlorite content in the Highveld Coalfield (HC) and Witbank Coalfield (WC) coal bearing strata (Carb = carbonaceous, PC = pyrite containing).

Kaolinite

Kaolinite ($Al_2Si_2O_5(OH)_4$) is present in all samples except in those containing chlorite. Kaolinite is present mostly as a major or dominant mineral in coal seams and clastic units. Kaolinite is the dominant mineral in most Witbank Coalfield coal seams and quartz was found to be the dominant mineral in Highveld Coalfield coal seams as

was illustrated in **Figure 6.3.3(B)**. Quartz is found to be the dominant mineral in all clastic rocks. It was shown above that if either kaolinite or quartz is dominant, these minerals show a negative correlation. However, these two minerals show a positive correlation when both are present in minor or major mineral quantities.

It was shown by Cadle et al. (1989) that the kaolinite content is positively correlated with the ash content of the No. 2 coal seam of the Witbank Coalfield as shown in **Figure 6.3.3(F)** below.

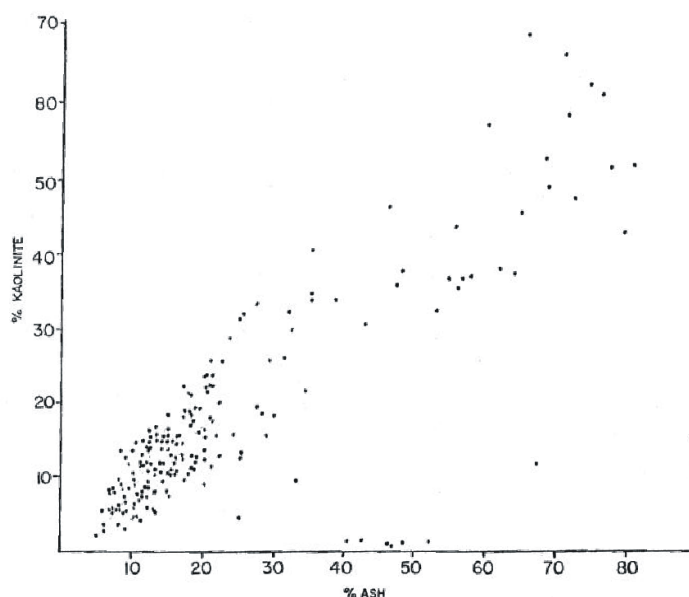


Figure 6.3.3(F). Relationship between kaolinite and the ash content in the No. 2 Witbank Coalfield coal seam after Cadle et al. (1989).

Kaolinite is ultimately precipitated by authigenic processes as described by Ward (2002). Al is soluble at low pH conditions and the higher solubility would allow the Al to be leached from any detrital material in the swamp by the organic acids (Ward, 2002). Movement of the Al in organometallic complexes to higher pH conditions would cause the Al to be precipitated first as bauxite-minerals (e.g. gibbsite and boehmite) and later interaction with Si in solution would lead to authigenic precipitation of kaolinite (Ward, 2002).

Smectite, illite and interlayered smectite minerals

Smectite and smectite/illite is more frequently found in the Highveld Coalfield samples as shown in **Figure 6.3.3(E)**. Smectite has been found in a total of 16 samples and Pinetown (2003) has identified montmorillonite $((\text{Na,Ca})_{0.3}(\text{Al,Mg})_2\text{Si}_4\text{O}_{10}(\text{OH})_2 \cdot n(\text{H}_2\text{O}))$ as the smectite mineral present in samples from the Witbank and Highveld Coalfield. Illite $((\text{K,H}_3\text{O})(\text{Al,Mg,Fe})_2(\text{Si,Al})_4\text{O}_{10}[(\text{OH})_2,(\text{H}_2\text{O})])$ is difficult to distinguish analytically from interlayered illite/smectite and is reported often without distinction as the latter. Illite/smectite has been identified in 36 samples. Both smectite and illite/smectite is present in coal and in clastic units, however illite/smectite is significantly higher in

coal (at average 10 wt%) than in clastic rocks (at average 5 wt%). This is in concurrence with the findings of Cadle et al. (1989) that indicates that illite is associated with low ash coals. It was shown above in **Figure 6.3.3(D)** and **(F)** that the quartz and kaolinite content increase with the ash content in the coal. A negative correlation between illite/smectite and quartz + kaolinite would therefore be expected. Illite/smectite was plotted against the sum of the quartz and the kaolinite content in **Figure 6.3.3(G)** below for all samples in which the former was identified.

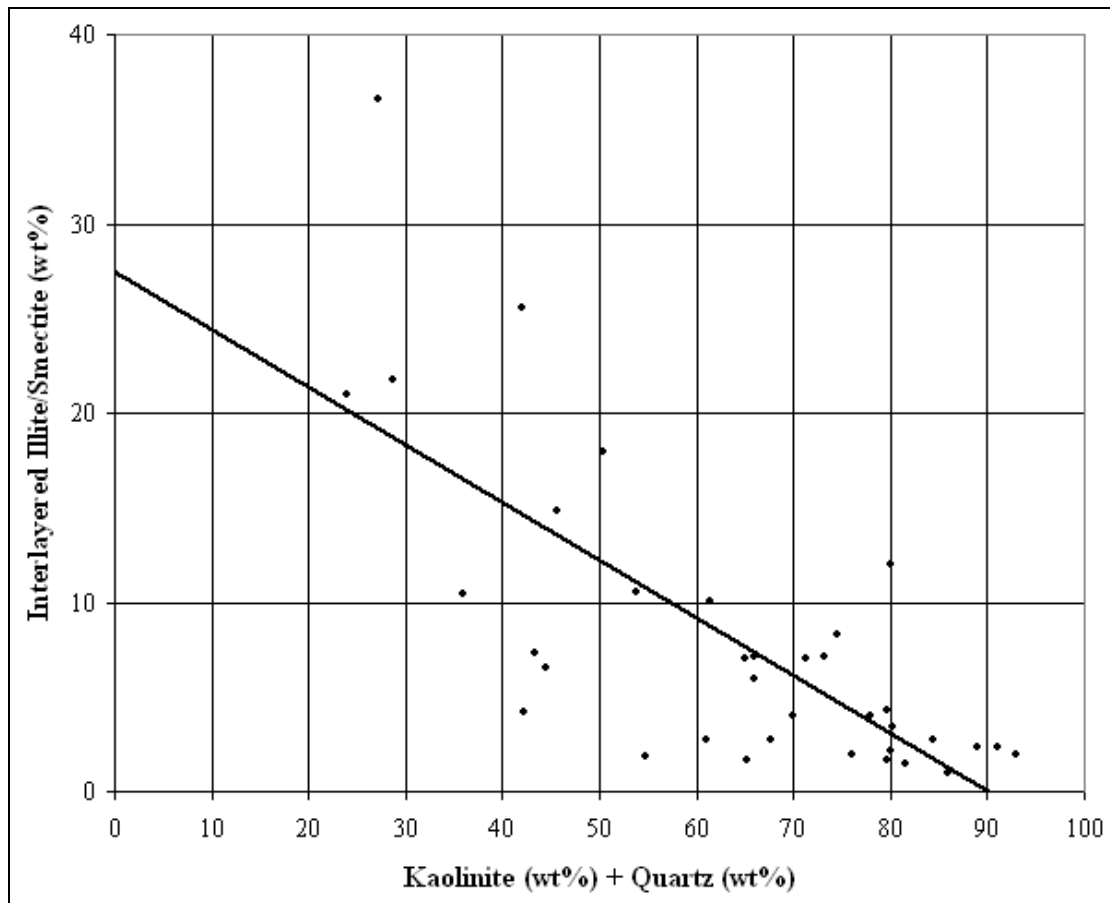


Figure 6.3.3(G). Relationship between illite/smectite and the quartz-kaolinite content.

Smectite formed as a result of the weathering of primary Al-Si minerals (e.g. K-feldspar, plagioclase etc.). Illite interstratification occurs with smectite as a result of an increase in temperature during diagenesis.

Chlorite

The term chlorite is applied to a large group of minerals with alternating layers similar to talc and brucite, however, there is a wide range of compositional variation involving substitution of Mg, Al, Fe²⁺, and Fe³⁺ and also of Al for Si (Nesse, 1991). The common chlorite compositions can be expressed as (Mg, Fe)₅Al(Si₃Al)O₁₀(OH)₈ with clinochlore and chamosite respectively as the Mg and Fe end members (Nesse, 1991).

Chlorite was identified in 16 samples of the No. 4 and No. 5 coal seams, and also in the surrounding siltstones and sandstones in a cluster of 7 boreholes in the Highveld Coalfield. Although kaolinite is generally present as a major to dominant mineral in coal and coal bearing strata, kaolinite was never identified in any of the samples that also contained chlorite. See the textbox below for a discussion of this aspect. Chlorite is present as a minor to major mineral in the rock with a weight percentage range of between 2 and 29 wt%, averaging at 11 wt%. Chlorite is absent in the Witbank Coalfield samples as illustrated in **Figure 6.3.3(E)**.

Quartz is mostly present as a major or dominant mineral in the samples that contain chlorite ranging between 14 and 66 wt%, averaging at 44 wt%. Although kaolinite is absent as a major or dominant mineral in the samples that contained chlorite, no other mineral is ever present in dominant concentrations except quartz. Plagioclase is present in all the samples ranging between 3 and 37 wt%, averaging at 12 wt%. K-feldspar is often present and range between 2 and 29 wt%, averaging at 11 wt%. Illite/smectite has also been found frequently in the samples between 7 and 37 wt%, averaging at 14%. Mica ranges between 3 and 29 wt%, averaging at 11 wt%. The carbonate minerals are present in variable quantities.

Chlorite is an authigenic secondary mineral (Ward, 2002). After a review has been made of several studies that refer to the occurrence of chlorite in some South African coal and coal bearing strata, it is suggested that chlorite formed from instable smectite/illite under elevated temperature as described below.

Hypothesis for chlorite formation in South African coalfields.

Chlorite is a product of low to medium grade metamorphism. However, the Ecca sedimentary rocks were not subjected to any regional metamorphism. Chlorite might also be formed from the recrystallization of clay minerals during contact metamorphism with dolerite intrusions. Dolerite sills extensively intruded the area in the Highveld Coalfield in this study where chlorite was identified.

Bühmann and Bühmann (1988) reported that the clay fraction is dominated by mica and chlorite in the Vryheid Coalfield in KwaZulu Natal; the KwaZulu Natal Coalfields have been subjected regionally to extensive dolerite intrusions in contrast to the localized dolerite intrusions of the Witbank and Highveld Coalfields that confirm the above point.

Cadle et al. (1990) state that a regional increase in the coal rank exists eastwards over the Karoo Basin coalfields, from sub-bituminous in the Free State Coalfield to antracitic and meso-antracitic in eastern-Natal. Snyman and Barclay (1989) also attributed this phenomenon to a regional increase in palaeogeothermal gradient, related to melting of the astenosphere and consequently large-scale magmatic activity, which culminated in a vast outpouring of lava during the Jurassic and the break-up of Gondwanaland. Bühmann and Bühmann (1988) also reported that in

samples that contained chlorite in the eastern Transvaal Coalfield (now called the Ermelo Coalfield), there is a general increase in the illite content of the illite/smectite interlayered clays. The increase in illite and decrease in smectite is evident of later increased temperature eastwards over the Karoo basin coalfields.

It is therefore suggested that chlorite forms from clays as a result of temperature elevation due to dolerite intrusions on a regional scale. This also explains the absence of kaolinite as the increase in temperature leads to chlorite and illite stability, and kaolinite and smectite instability.

The maximum stability of kaolinite is 270°C according to laboratory experiments. Bruvoll et al. (2004) gives the following reaction equation of illite and chlorite formation with increasing temperature:



Figure 6.3.3(H) below shows smectite and illite stability in clay experiments of Bruvol et al. (2004).

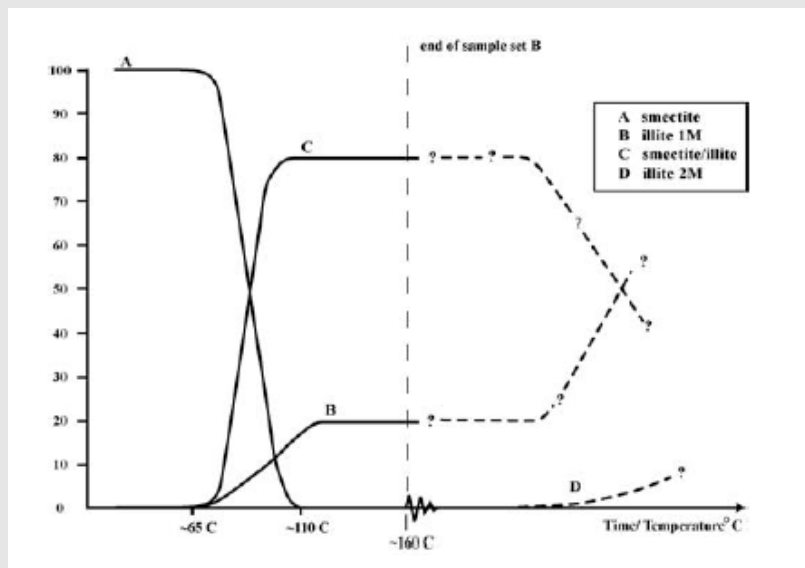


Figure 6.3.3(H). Smectite and illite stability in clay experiments (Bruvol et al., 2004) (The y-axis represents the wt% of the specific clay).

Mica

The mica identified in the coal and coal bearing strata will be present either as muscovite $(KAl_2(Si_3Al)O_{10}(OH,F)_2)$ or as glauconite $((K,Na)(Fe(III),Fe(II),Al,Mg)_2(Si,Al)_4O_{10}(OH)_2)$. Both these minerals are from the muscovite subgroup.

Mica is present in 104 of the 157 samples in total, ranging between 1 and 29 wt%, averaging at 7 wt%. It is slightly more frequent in clastic rocks than in coal.

As illustrated in **Figure 6.3.3(E)**, mica is more frequent in the Highveld Coalfield than in the Witbank Coalfield. It is also evident from **Figure 6.3.3(E)** that the mica content increases from the No. 2 upwards to the No. 4 and No. 5 coal seams. Where the presence of mica is due to marine transgressions, the mica present will be glauconite. Glauconite characteristically forms small rounded pellets in clastic sediments deposited under marine conditions where the presence of the glauconite also colors the sediments green (Nesse, 1991). Glauconite containing siltstones have often been identified above the No. 4 and No. 5 coal seams in the Highveld Coalfield in this study.

Feldspar

Feldspar in coal units is often of detrital origin as described by Ward (2002) and, given that the sedimentary source of the clastic units is felsic, this could also be applied to most of the feldspar in South African coals. In **Figure 6.3.3(I)** below it is evident that the average plagioclase content is higher in the Highveld Coalfield than in the Witbank Coalfield. Except for the No. 5 seam coal, the K-feldspar and plagioclase content is higher in the clastic rocks than in the coal seams.

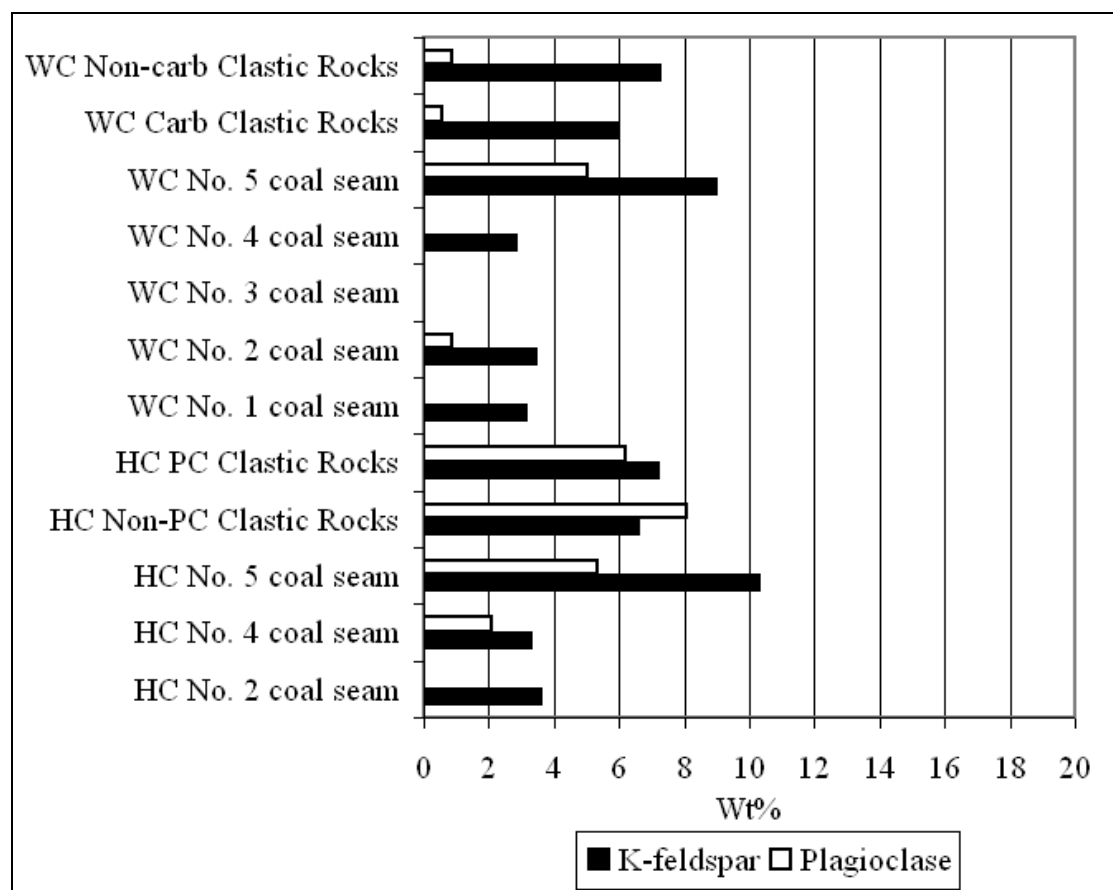


Figure 6.3.3(I). Average K-feldspar and plagioclase content in Highveld Coalfield (HC) and Witbank Coalfield (WC) samples (Carb = carbonaceous, PC = pyrite containing).

K-feldspar

K-feldspar is from the K(Na,Ba)-feldspar group of minerals and in the sediments would consist of orthoclase or microcline both with the formula KAlSi_3O_8 .

K-feldspar occurs frequently in both coal and clastic rocks as an accessory to a major mineral, although it is slightly more frequent in the clastic rocks. The K-feldspar content ranges between 1 and 32 wt%, averaging at 6 wt% in all the samples it was identified in.

Plagioclase

Plagioclase $((\text{Na,Ca})(\text{Si,Al})_4\text{O}_8)$ forms a solution series of Na and Ca between the two end member minerals albite and anorthite. Because the sedimentary rock originates from a felsic mother rock, the plagioclase present will be typically of an oligoclase composition with a $\text{Na}_{10}\text{Ca}_{90}$ – $\text{Na}_{30}\text{Ca}_{70}$ content.

Plagioclase is identified in 56 of the 157 samples in both coal and clastic rocks as an accessory to a major mineral. Plagioclase content ranges between 1 and 37 wt%, averaging at 7 wt% in all the samples it was identified in.

Pyrite and %S

Pyrite (FeS_2) is frequently present in all the coal seams, the carbonaceous clastic rocks and also in some pyrite containing clastic rocks. The euhedral pyrite in the non-carbonaceous clastic rocks may have an epigenetic origin.

Ward (2002) states that pyrite is often intimately associated with the organic matter in coal that represents pyrite formation during or very shortly after peat accumulation. However, pyrite also occurs as epigenetic veins that formed later in the coal's burial history (Ward, 2002).

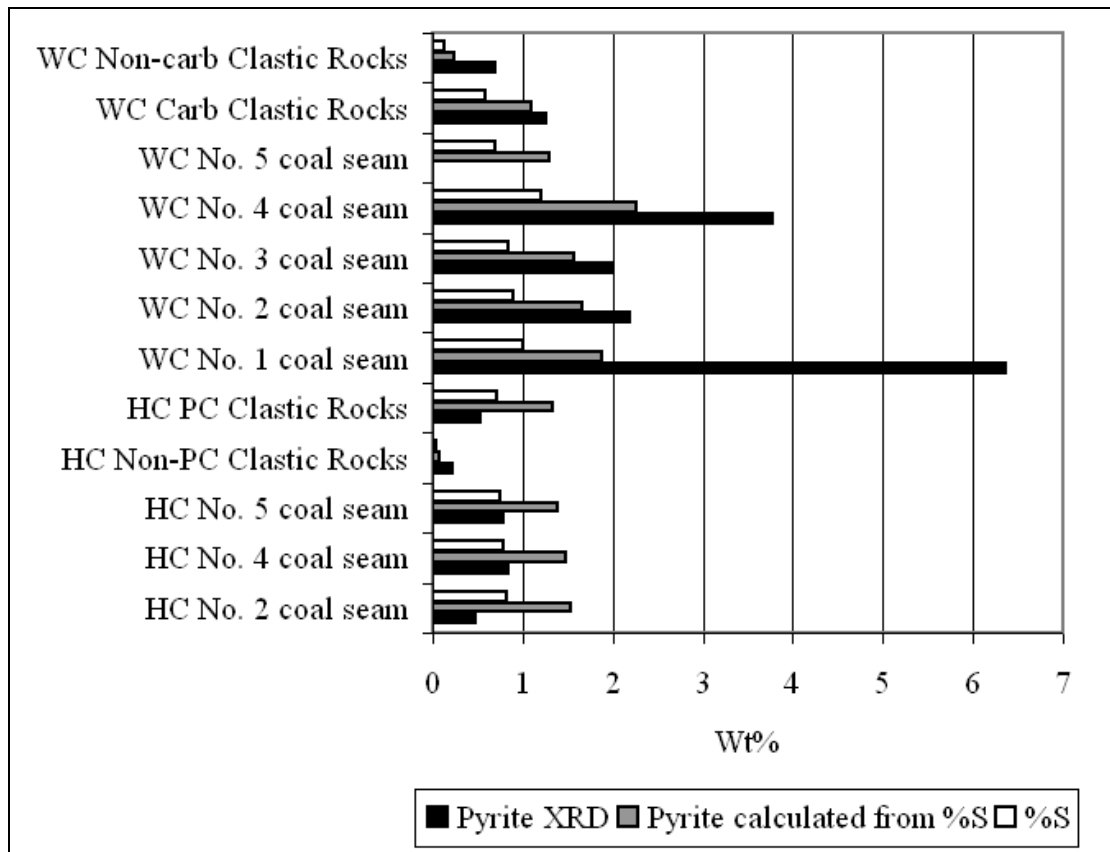


Figure 6.3.3(J). Average pyrite content as analysed by XRD and calculated from the total %S; (HC = Highveld Coalfield, WC = Witbank Coalfield, Carb = carbonaceous, PC = pyrite containing).

The average pyrite content for the Witbank and Highveld Coalfield samples is given in **Figure 6.3.3(J)**. It is evident from **Figure 6.3.3(J)** that the average pyrite content decrease from coal samples to carbonaceous clastic rocks to non-carbonaceous clastic rocks. Pyrite is also higher on average in the Witbank Coalfield samples than in the Highveld Coalfield samples.

Table 6.3.2(A) and **(B)** give the average pyrite content for the different coal seams and coal bearing strata for both the Witbank and Highveld Coalfields. The “calculated pyrite” was calculated from the total %S (the ratio between %S and pyrite is given below using the molar weight of Fe 55.847 g/mol and of S 32.066 g/mol).

Pyrite (wt%)	:	%S
1	:	0.5345
1.8708	:	1

From **Table 6.3.2(A)** and **(B)** it is clear that the pyrite calculated from the total %S content and pyrite analysed by XRD differ significantly especially in the coal seams.

The %S was also calculated from the amount of pyrite analysed by XRD. The calculated %S was then compared with the total %S determined by the Leco analyses shown in **Figure 6.3.3(K)**.

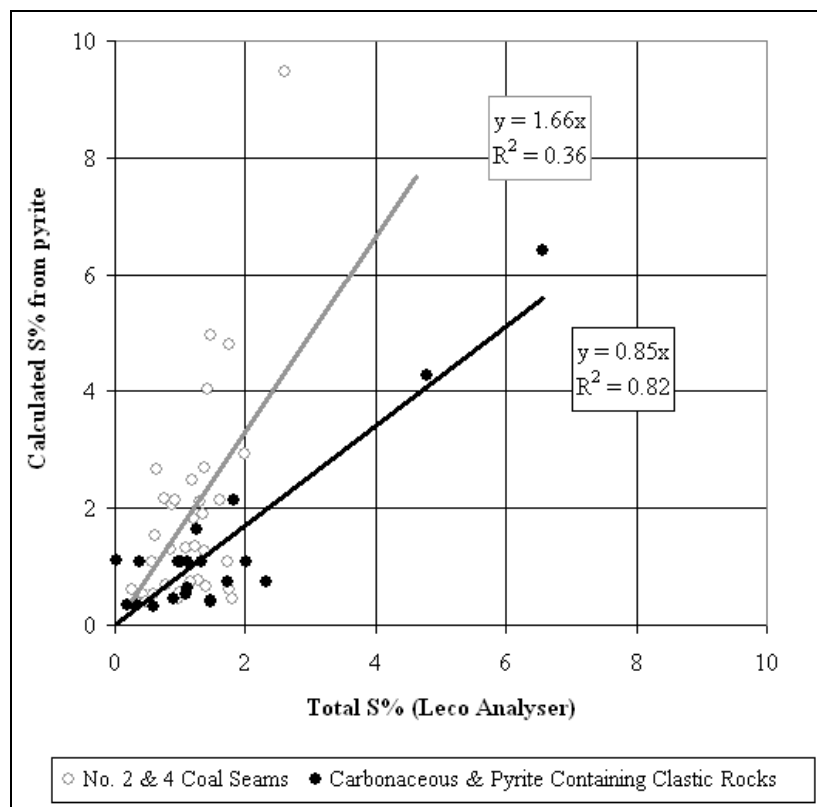


Figure 6.3.3(K). Calculated %S from XRD determined pyrite v. total %S determined by Leco analyser.

From **Figure 6.3.3(K)** it is evident that the pyrite content of the clastic rocks correlates better with the total %S, determined by the Leco analyzer, than the coal samples. This is because the mineralogical analyses of the samples are expressed in terms of the mineralogical ash content and not in terms of the total rock content as with the %S determined by the Leco analyzer. Therefore, the %S calculated from the XRD determined pyrite must actually be multiplied by the fraction of the total mineralogical ash content of the coal. Furthermore, it must be remembered that all mineral contents interpreted from XRD analyses are only semi-quantitative.

Because the clastic rocks have no or only a small carbonaceous content, good correlation were found between XRD analysis and the Leco Analyser. This has an important implication when samples are taken for geochemical modelling; together with XRD, the coal ash content of coal and some highly carbonaceous rocks must be determined if the mineral percentages need to be expressed in terms of the total rock content.

Carbonate minerals and NP

Calcite (CaCO_3), dolomite ($(\text{Ca,Mg})(\text{CO}_3)_2$) and siderite (FeCO_3) are present in coal seams and clastic rocks in trace to major concentration. Calcite ranges between trace amounts to 21 wt%, averaging at 5 wt%; dolomite ranges between trace amounts to about 23 wt%, averaging at 4 wt%; and siderite ranges between trace amounts and 27 wt%, averaging at 5 wt%. In the 157 samples, calcite is present in 87 samples, dolomite in 53 samples and siderite in 69 samples. Carbonate mineral content and NP are the highest in carbonaceous material.

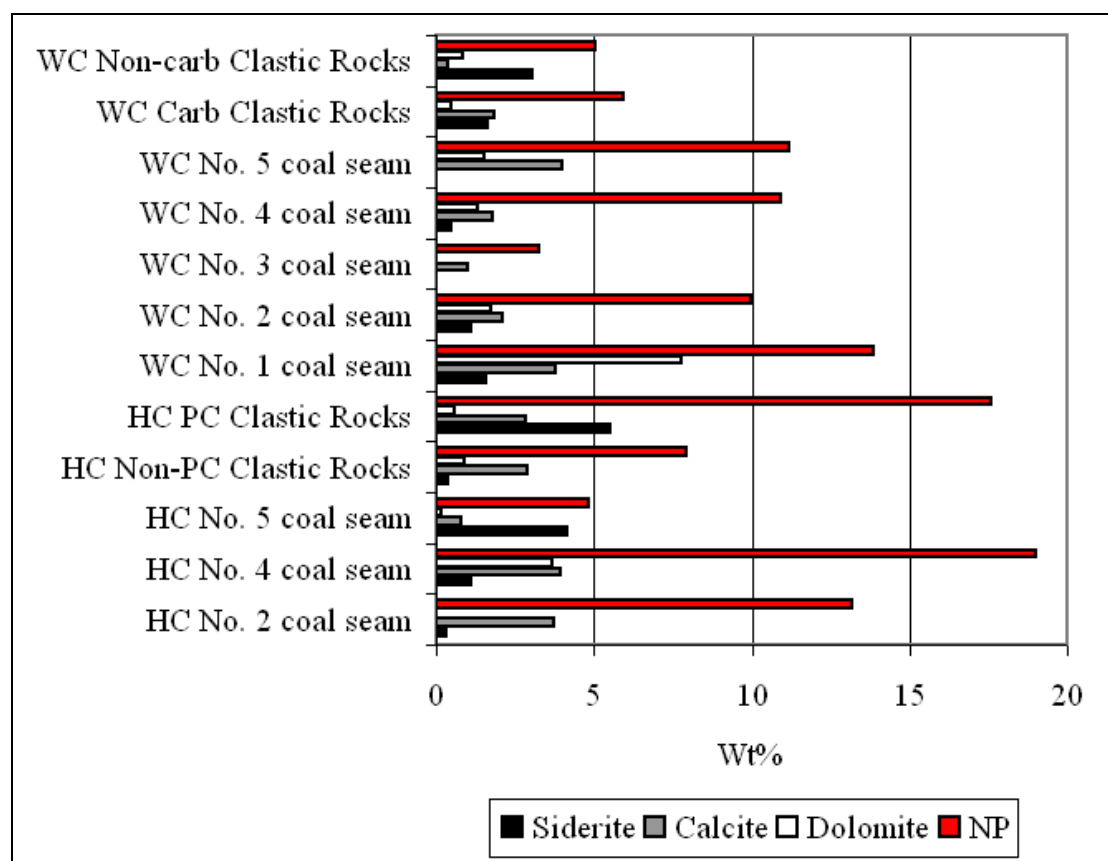


Figure 6.3.3(L). Distribution of carbonate minerals in the Witbank (WC) and Highveld Coalfields (HC) (Carb = carbonaceous, PC = pyrite containing).

From **Figure 6.3.3(L)** above it is evident that siderite is more frequent in carbonaceous clastic rocks than in coal seams or in non-carbonaceous clastic rocks. Calcite and dolomite are generally more frequent in coal seam samples than in clastic rocks.

In **Figure 6.3.3(M) to (O)** below, calcite, dolomite and siderite were plotted against the Neutralization Potential (NP). It is evident from these figures that the carbonate minerals only show weak positive correlation with the NP determined in the laboratory decreasing from calcite, dolomite to siderite.

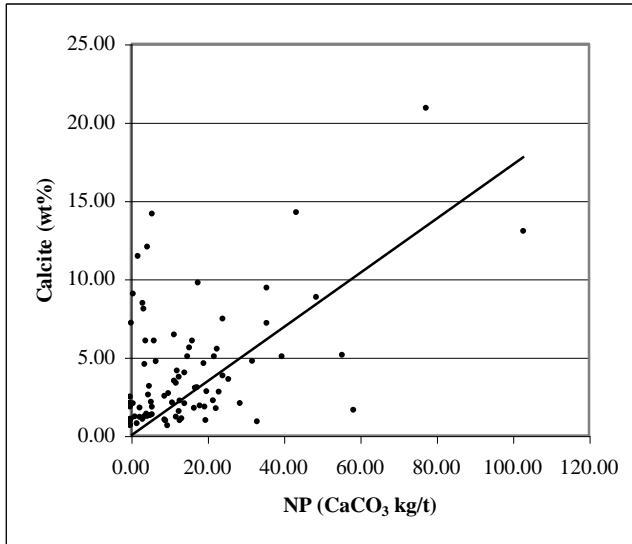


Figure 6.3.3(M). Calcite content against NP.

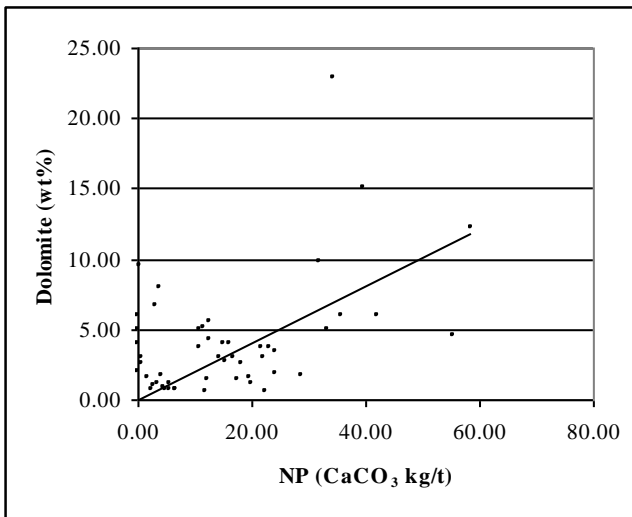


Figure 6.3.3(N). Dolomite content against NP.

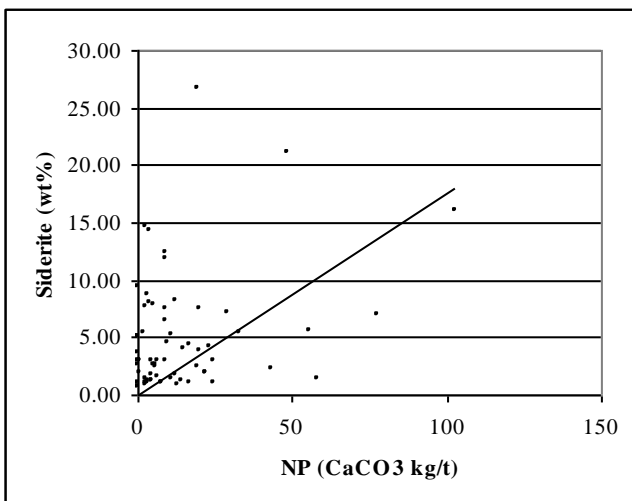


Figure 6.3.3(O). Siderite content against NP.

Carbonates can form both syn- and epigenetically. During the fermentation of organic material the activity of the CO₂ increases with resultant increase in carbonate

precipitation under the right pH conditions. Syngenetic siderite is described in more detail in **Section 2.6.3**. Epigenetically, carbonates are often present as cleat infillings in coal as described by Ward (2002).

Oxides, hydroxides, phosphates and sulphates

Anatase

Anatase is a titanium oxide (TiO_2) and has been identified by XRD as a trace to accessory mineral in some coal and clastic rocks. Anatase has been found in 39 of the 157 samples; 25 and 14 respectively from the Witbank and the Highveld Coalfields. In the Witbank Coalfield anatase was found in the northeastern part of the coalfield in 21 samples. Anatase was identified in only 4 samples in the western part of the coalfield. In the Highveld Coalfield anatase was present in the No. 2, No. 4 and No. 5 coal seams and in some of the surrounding clastic rocks.

The average content of anatase in samples was between trace and 1%. Only four samples have higher contents of respectively 2%, 3%, 6% and 7%. The first two samples are from the No. 1 coal seam in the eastern Witbank Coalfield and the latter two samples from the No. 4 coal seam in the samples taken from the eastern Highveld Coalfield.

Pinetown (2002) found that Ti, Al and Si show positive correlation in the Witbank Coalfield coal seams. This could be expected from sedimentary rocks with a felsic mother rock; anatase is found in felsic igneous rocks which are not easily altered or weathered in a sedimentary environment and are detrital minerals (Nesse, 1991).

Hematite and Goethite

Hematite (Fe_2O_3) was analyzed in 18 samples from coal seams and carbonaceous rocks in a cluster of 8 boreholes in the western Witbank Coalfield. In the rest of the samples, hematite was only found in one sandstone sample from the Highveld Coalfield and in one sample of the No. 2 coal seam from the north-eastern Witbank Coalfield. No siderite (FeCO_3) was analyzed in samples that contained hematite. Iron-hydroxides and -oxides can readily form from siderite weathering. The hematite occurred as a trace to major mineral, ranging from trace amounts to 13 wt%, averaging at 5 wt%.

Goethite (Fe(III)O(OH)) was analysed only in one sandstone sample of the Highveld Coalfield.

Phosphates

Apatite ($\text{Ca}_5(\text{PO}_4)_3(\text{OH},\text{F},\text{Cl})$) has been identified in 10 samples of the No. 2, No. 4 and No. 5 coal seams as well as in some carbonaceous clastic rocks from a cluster of 7 boreholes in the western Witbank Coalfield. The apatite content ranged between 1 and 6 wt%, averaging at 4 wt%.

Cairncross et al. (1990) has frequently identified the crandallite group of phosphates in the No. 2 coal seam of the Witbank Coalfield. Crandallite has also been identified by Pinetown (2002) as a major mineral in one sample of the No. 2 coal seam at the Leeufontein Mine (Witbank Coalfield) and as a dominant mineral in one sample from the No. 4 coal seam from an unknown locality in the Witbank Coalfield.

The crandallite group is a hydrated group of phosphates and also contains Al in its structure. Crandallite is formed by groundwater precipitation in sedimentary rocks and soils as a result of the breakdown of other phosphate minerals. The crandallite mineral itself is a calcium phosphate ($\text{CaAl}_3(\text{PO}_4)_2(\text{OH})_5 \cdot (\text{H}_2\text{O})$) but the Ca could be substituted by Ba (Gorceixite - $\text{BaAl}_3(\text{PO}_4)(\text{PO}_3\text{OH})(\text{OH})_6$) and Sr (Goyazite - $\text{SrAl}_3(\text{PO}_4)_2(\text{OH})_5 \cdot (\text{H}_2\text{O})$) and also some of the rare-earth elements (RAE).

Phosphorous minerals are mostly authigenic and formed from the P released into solution from the decaying plant material (Ward, 2002). Some phosphorous minerals may also be epigenetic and occur also as cleat fillings (Ward, 2002).

Alunite

Alunite has been identified as a trace to minor mineral in 7 samples of the No. 2 and No. 4 coal seams in a cluster of 5 boreholes in the western Witbank Coalfield and as a major mineral in one sandstone sample of the Highveld Coalfield.

In all the samples containing alunite the %S was found to be fairly high. In the 7 samples of the western Witbank Coalfield, the %S ranges between 0.61 and 2.61%, averaging at 1.49%. In these samples the XRD pyrite content was also above average, ranging between 3.6 and 17.7 wt%, averaging at 6.38 wt%. In the sandstone sample of the Highveld Coalfield the %S was at 0.23%.

The alunite group of sulphates is anhydrous and is divided into the alunite and the jarosite subgroups. The alunite subgroup consists among other minerals of alunite and natroalunite. The alunite mineral itself (as identified in the XRD analyses in this study) is a potassium-aluminous sulphate ($\text{KAl}_3(\text{SO}_4)_2(\text{OH})_6$). In natroalunite ($\text{NaAl}_3(\text{SO}_4)_2(\text{OH})_6$) Na replaces K.

The jarosite subgroup contains Fe^{3+} instead of Al and consists among other minerals of jarosite ($\text{KFe}_3(\text{SO}_4)_2(\text{OH})_6$) and natrojarosite ($\text{NaFe}_3(\text{SO}_4)_2(\text{OH})_6$).

These minerals often precipitate as secondary minerals from the effluent in acidic mine drainage environments where ferric iron compounds and sulphate are the products of pyrite oxidation and Na and K the products of feldspar, mica or clay dissolution.

6.4 Elemental composition of coal

As discussed in **Section 6.2**, no XRF or INAA analysis have been performed in this study and reference will be made to relevant major, minor and trace element analysis of other studies on South African coals.

Table 6.4(A) and **(B)** respectively give the typical variation of the major and trace elements in the No. 2 coal seam of the Northern Witbank Coalfield. The No. 2 coal

seam of the Witbank Coalfield is probably the most studied coal seam in the South African coalfields.

Table 6.4(A). Major element analyses from literature of the No. 2 coal seam with increasing ash content in the Northern Witbank Coalfield.

Major Elements (wt%)	Coal with < 40% ash ^a		ROM coal ^b		Coal with > 40% ash ^c	
	Coal	%	Coal	%	Coal	%
SiO ₂	6.51	41.84	10.30	48.02	35.85	54.91
TiO ₂	0.26	1.67	0.32	1.49	0.79	1.21
Al ₂ O ₃	4.74	30.46	6.70	31.24	15.89	24.34
FeO	1.01	6.49	1.10	5.13	2.66	4.07
MnO	0.01	0.06	0.01	0.05	0.03	0.05
MgO	0.22	1.41	0.30	1.40	1.38	2.11
CaO	1.20	7.71	1.40	6.53	7.51	11.50
Na ₂ O	0.01	0.06	0.02	0.09	0.09	0.14
K ₂ O	0.07	0.45	0.13	0.61	0.35	0.54
P ₂ O ₅	0.32	2.06	0.21	0.98	0.31	0.47
S	1.21	7.78	0.96	4.48	0.43	0.66
Total	15.56	100.00	21.45	100.00	65.29	100.00

^a 168 samples of the No. 2 coal seam from Cadle et al. (1989).
^b 41 samples of the No. 2 coal seam from Cairncross et al. (1990).
^c 31 samples of the No. 2 coal seam from Cadle et al. (1989).

Table 6.4(B). Trace element analyses (ppm) from literature of the No. 2 coal seam with increasing ash content in the Northern Witbank Coalfield.

Trace Elements (ppm)	Coal with < 40% ash ^a	ROM coal ^b	Coal with > 40% ash ^c	Average Earth Crust ^d	Trace Elements (ppm)	Coal with < 40% ash ^a	ROM coal ^b	Coal with > 40% ash ^c	Average Earth Crust ^d
As	5.8	4.6	3.5	2.0	Se	2.5	0.9	0.9	0.1
Ba	418.4	358.0	529.5	624.0	Sr	481.8	363.0	398.6	320.0
Bi	2.1	1.3	4.3	0.2	Ta	0.6	0.9	2.1	0.9
Br	2.4	0.8	1.3	1.6	Th	8.6	15.0	21.4	10.5
Co	7.6	7.9	7.0	17.3	U	2.7	4.0	6.1	2.7
Cr	22.0	28.0	101.4	92.0	V	23.6	27.0	87.6	97.0
Cs	1.2	1.4	4.2	4.9	W	3.6	3.9	7.7	1.9
Cu	6.9	9.7	34.9	28.0	Y	14.4	17.0	35.2	21.0
Ga	8.8	11.0	26.8	17.5	Zn	11.9	10.0	50.3	67.0
Ge	2.1	2.1	3.3	1.4	Zr	79.3	96.0	248.3	193.0
Hf	2.3	2.3	7.2	5.3	La ^e	22.8	26.0	36.3	31.0
Nb	8.2	7.9	23.2	12.0	Ce ^e	43.2	47.0	64.1	63.0
Ni	18.0	17.0	21.8	47.0	Nd ^e	19.2	20.0	29.3	27.0
Pb	11.9	10.0	20.1	17.0	Sm ^e	3.7	3.9	5.6	4.7
Rb	4.5	7.5	34.8	84.0	Eu ^e	0.6	0.6	0.9	1.0

Sb	0.3	0.5	0.4	0.4	Tb^e	0.6	0.6	0.9	0.7
Sc	5.2	6.5	10.0	14.0					
^a 168 samples of the No. 2 coal seam from Cadle et al. (1989).									
^b 41 samples of the No. 2 coal seam from Cairncross et al. (1990).									
^c 31 samples of the No. 2 coal seam from Cadle et al. (1989).									
^d Rudnick and Gao (2003)									
^e Rare Earth Elements (RAE)									

In **Table 6.4(A)** the “Coal” columns give the wt% of the major oxides as part of the total coal sample, and the total major oxide content of the coal is given at the bottom. The “%” columns give the wt% of the major oxides in terms of the total oxide content. The total major oxide content is related to the ash content of the coal as could be seen in **Table 6.4(A)** – the higher the ash content, the higher the total major element concentration. The following observations could be made from the major and trace elements presented above:

- SiO₂, CaO, MgO, Na₂O and K₂O correlate positively to the coal ash content.
- Al₂O₃ shows an increase in the total coal with increasing ash content but its percentage in terms of the total oxide content decreases with increasing ash content.
- P₂O₅, S and FeO show an increase in lower ash coal.
- All trace elements are elevated in the higher ash coal and depleted in the low ash coal except As, Br, Co, Sc and Sr.
- In low ash coal As, Bi, Br, Ge, Se, Sr and W are elevated above the average earth crust. These elements are also elevated in high ash coal except for Br. In high ash coal other elements that are elevated above the average earth’s crust are Cr, Cu, Ga, Hf, Nb, Pb, Sb, Ta, Th, U, Y, Zr and RAE except Eu.

The major genetic processes that played a role in the geochemical distribution of the major and trace elements given in **Table 6.4(A)** and **(B)** are the following:

- The mother rock type and the physical dispersion of the elements during weathering, plant growth and deposition of clastic rocks and coal.
- The physical and geochemical conditions during deposition.
- The hydro-chemistry of inflowing streams and marine transgressions
- Influence of post-depositional processes on mineralogy.

Mother rock type, the elemental composition of plant material and physical element dispersion in the sedimentary environment

The litho-stratigraphy consists of different sedimentary rocks: coal, carbonaceous clastic rocks, different clastic rocks – e.g. sandstone, shale, siltstone etc. All rocks had the same mother rock type; however, differences in the geochemistry of the different lithologies are a result of the differences in 1) the weathering rate, 2) the reworking of the sediments, 3) the geochemical and 4) the physical (subsidence v. stable shelf) depositional environment.

With reference to **Table 6.4(A)** and **(B)** above, the dispersion of the major and trace geochemistry in the coal environment is discussed below:

- Because of the northerly felsic source of the sediments, sandstones are often arkosic and major/minor minerals that would indicate a felsic mother rock like quartz and K-feldspar are present in the sedimentary rocks. The sedimentary rocks are therefore typically high in SiO₂ and Al₂O₃.

The accessory/trace mineral anatase indicates a felsic origin as anatase is an accessory/trace constituent of igneous rocks such as granite, granite pegmatite and felsic volcanic rocks (Nesse, 1991). Because anatase is relatively stable in the weathering environment, it is found as detrital grains in clastic rocks (Nesse, 1991). However, the positive correlation between Al and Ti as described by Pinetown (2003) does suggest that some Ti may occur in authigenetic kaolinite, as Fe and Ti can replace some of the Al in kaolinite.

- The average elemental composition of the earth's crust is of an intermediate composition as described by Rudnick and Gao (2003). In **Table 6.4(A)** SiO₂, Na₂O and K₂O show a lowered content in the coal with respect to the average earth's crust – this was also observed in the geochemical studies of Gaigher (1980). The average earth's crust for the above elements is respectively estimated at 66.62 wt%, 3.27 wt% and 2.80 wt% by Rudnick and Gao (2003).

These elements are supposedly lowered during coal deposition. The reason for the depletion of the sediment load from the clastic sediment source is described by Ward (2002) as the result of the following aspects: 1) The vegetation in and around the peat swamp acts as a filter, preventing some of the sediment carried in rivers and other water bodies from penetrating beyond the margins of the peat bed; 2) The acid or saline waters in the swamp may cause flocculation of clays and other suspended mineral particles, further reducing clastic dispersal.

- In **Table 6.4(A)** the elements Al₂O₃, CaO, FeO, TiO₂, P₂O₅, S show an elevated content with respect to the average earth's crust. The average earth's crustal composition is respectively at 15.4 wt%, 3.59 wt%, 5.04 wt%, 0.64 wt%, 0.15 wt%, 0.06 wt% (Rudnick and Gao, 2003). All of the above

elements will also be higher than the felsic mother rock of the Vryheid Formation.

Generally there is an increase in carbonate minerals and sulphides in the carbonaceous material (as shown in the mineralogical analyses in **Section 6.3.3** above) and therefore in the Ca, Fe and S content. The latter three elements and phosphorous are elevated in the coal since they are naturally elevated in plant material as described by Ward (2002).

It was shown in **Section 6.3.3** above that kaolinite was found to be the dominant mineral in the Witbank Coalfield coal samples in this study. Both Ti and Al are soluble under acidic conditions and leaching of the mineral content with humic and fulvic acids could elevate these elements in solution. During peatification Ti could precipitate together with Al as kaolinite in the coal environment as a slight substitution of Ti and Fe for Al is possible. Ti and Al show good correlation in elemental studies by Pinetown (2003).

- MgO and MnO show also slight depletion in terms of the average earth crust composition but are probably not significantly enriched or depleted in the high ash coal with relation to the mother source rock.

Mg is however lowered in the lower ash coal supposedly in the same manner as the SiO₂, Na₂O and K₂O are depleted during plant accumulation in marshes as described above.

The presence of MnS and MnCO₃ in South African coal bearing strata has not been described and therefore it is possible that Mn may be present in siderite. Most natural siderite is actually a solid solution containing some Ca, Mg and Mn in addition to Fe.

- Major elements will mostly be associated with mineral matter and their proportion to the total ash content could be calculated as was done in **Table 6.4(A)**. However, trace elements could be associated both with the organic and inorganic matter that makes interpretation more difficult. The trace elements in the total coal were presented in **Table 6.4(B)**. Most trace elements show elevation with increase in coal ash content. Observations and discussion in terms of the distribution of some trace elements are made with reference to **Table 6.4(B)**:

As is elevated in low ash coals and decreases with increasing ash content as shown in **Table 6.4(B)**. As has a chalcophile character and Ward (1999) states that As is generally strongly fractionated in pyrite in coal. Se is another element often found to be associated with S in coal (Ward, 1999) because of comparable ion-radii and valence. As in the case with As, Se is found in this study to be elevated in the low ash coal as shown in **Table 6.4(B)**.

Br is elevated in the low ash coal most probably due to its association with plant material (Hart et al., 1982). Br is also often elevated due to the marine

transgressions after the forming of the No. 2, No. 4 and No. 5 coal seams as is discussed in **Section 6.3.3** above. Cairncross et al. (1990) state that trace elements such as B, Cl, Li, and Br are elevated in the coal seams that have been contaminated by the overlying marine transgressions.

Sr and Ba are associated with both K and Ca containing minerals, however Sr is associated more with Ca minerals and Ba more with K minerals (De Bruijn, 2000). This possibly explains why Sr is elevated in the low ash coal and Ba in the higher ash coal. Sr, Ba and some of the RAE are also associated with the crandallite group phosphates as discussed in **Section 6.3.3** above. Pinetown (2003) found good positive correlation between Sr and P in the No. 2 coal seam of the Witbank Coalfield. In **Table 6.4(B)** both Sr and P are elevated in the low ash coal.

Pb could replace Sr, Ba and K in minerals (De Bruijn, 2000).

Ge and Ga are usually highly associated with respectively Si and Al due to comparable ion radii and valence. Ward et al. (1999) have also found that both trace elements are generally elevated in coal bearing strata due to association with organic material.

Rb is elevated in high ash coal, as it is highly associated with K-containing minerals as was also found in Pinetown (2003) and Ward et al. (1999). Cs often show association with Rb and K (De Bruijn, 2000).

Nb and Ta are elevated in the high ash coal and may occur in several minerals containing Ti, Zr, Si or Al.

Zr is elevated in the high ash coal probably due to the occurrence of zircon ($ZrSiO_4$) as a detrital mineral originating from the felsic mother rock. Hf is usually highly associated with Zr due to similar geochemical character (due to comparable ion radii and valence) as was also found in coal analyses by Ward et al. (1999).

The physical and geochemical conditions during deposition

Within a single mine-site, the differences in mineral type and content relate to the lateral and vertical differences of the palaeo-environment. Some parts of the palaeo-basin (now the coal reserve) were typically more subjected to stable reducing conditions than shallower parts during peatification. Epigenetically deposition of minerals also shows high variance throughout a coal reserve.

Less acidic conditions, a lowered water table and the fact that coals accumulated on the stable, passive margin of the Karoo Basin which prevented rapid subsidence, contributed to the fact that South African coals have elevated ash and high inertinite

maceral content (Cadle et al., 1990). Another contributor of high ash content in coal were the higher sediment load.

Some detrital minerals like quartz, that are not easily weathered, will not be as highly influenced by the geochemical environment as minerals whose stability is strongly influenced by the Eh and pH conditions such as pyrite. The different types of geochemical environments and the typical associated mineralogy were discussed in detail in **Section 2.5**.

Minerals that play a major role in acid generation (AMD) and neutralization are iron-sulphides and carbonate minerals. These minerals are reactive minerals in the coal mine environment and are very much influenced by the type of geochemical environment.

The geochemical environment of pyrite and siderite formation

In order to illustrate the stability fields of pyrite, siderite, FeS and other iron minerals, Eh-pH diagrams were drawn (**Figure 2.6.3(A) – (X)**) at different iron, TIC and sulphur activities using the Geochemist Workbench 6.0.3.

Siderite can potentially form when there is enough Fe^{2+} in solution (indicating reducing conditions) and high carbonate activity. When looking at the description of geochemical environments in **Table 2.5(A)**, it is shown that siderite can form in 1) the post-oxic zone before the transition to the sulfidic zone (and therefore the formation of pyrite), and also in 2) the anoxic-methanic zone (after pyrite formation). Some siderite can form at near-neutral conditions under high TIC conditions before pyrite formation, in anoxic conditions (see **Figure 2.6.3(A) – (B)**). However, with high sulphate content and under more alkaline or acidic conditions, siderite would not form in the post-oxic zone and a quicker transition to the anoxic-sulphidic zone would be made where sulphate would be reduced and pyrite would form. When the sulphur is significantly depleted by pyrite formation, siderite will form again in the anoxic zone.

To conclude, a significantly high Fe^{2+} and TIC content will not definitely lead to siderite formation, but a high Fe^{2+} and sulphur content would be very favourable for pyrite formation whatever the TIC content. Only with depletion of the sulphur content will siderite be significantly formed but it is possible that most Fe^{2+} would then already be used up by the formation of pyrite.

The bulk of the pyrite in coal measures is usually made out by framboids (Sawlowicz, 1993). Experiments by Butler and Rickard (2000) showed that the form of pyrite is often controlled by the saturation state of the pyrite.

The geochemical environment of calcite and dolomite formation

During the fermentation of organic material the activity of the CO_2 increases (see **Equation 2.6.2(A) – (C)**) with resultant increase in carbonate precipitation when the right pH conditions are reached. Acidic conditions prevail in swamps due to the

presence of humic/fulvic acids. However, it is possible for the carbonates that formed in the sedimentary environment not to react with these acids. Compton and Sanders (1993) made the interesting observation that in equilibrated acidic solutions, humic acids had no influence on calcite dissolution rates; if fresh sodium salts of humic acid were added significant inhibition of dissolution occurred (Morse and Arvidson, 2002).

The typical reactions of carbonate minerals formation and dissolution are given in **Section 2.7.2**. **Figure 2.7.1(A) – (F)** shows the stability fields of dolomite and calcite under different pH conditions and HCO_3^- activity at either 25 or 100°C.

The hydro-chemistry of inflowing streams and marine transgressions

Fluvial processes played the most significant role in coal seam formation and in most of the surrounding sedimentary strata in South Africa. However, marine transgressions also occurred above some of the coal predecessors influencing the trace element geochemistry. Where fluvial clastic rocks shielded the top of peat from the marine transgression, the sea water did not influence the trace chemistry; e.g. Cairncross et al. (1990) state that in the northern part of the Witbank Coalfield, the peat accumulation of the No. 2, No. 4 and No. 5 coal seams was overlain by fluvial deposited sandstones that shielded the underlying peat from being influenced by the marine transgression. Br will be elevated in rocks influenced by marine transgressions as it is higher in sea water than in fresh water. By using INAA Cairncross et al. (1990) found that Br is elevated in the top coal seams and in the surrounding clastic rock.

Post-depositional processes and epigenetic mineralization

Later infiltrations, for example into the cracks of the coal seams, led to discrete, albeit thin bands of mineral matter known as epigenetic mineral matter (Horsefall, 1993).

Epigenetic pyrite is generally observed as large crystals, massive forms with various overgrowths or as cleat- and fracture-filling pyrite (Ward, 2002). Epigenetic occurrences may represent remobilization of organic sulphur, sulphates or syngenetic sulphides within the coal, while other may be the result of factors outside the original depositional system, such as post-depositional fluid movement through the coal-bearing strata (Ward, 2002).

Generally other epigenetic minerals are carbonates that are commonly present as cleat-infillings and sometimes even phosphate minerals that have been remobilized within the seam (Ward, 2002). Authigenic illite and chlorite have also been reported to occur in cleats in coals from the Bowen Basin by Faraj et al. (1996) and it was indicated by isotopic studies that hot post-depositional fluids were present at between 70 – 170°C (Ward, 2002). The epigenetic deposition of chlorite has been discussed in **Section 6.3.3** above.

6.5 Conclusions

Coal mine spoils comprise of uneconomical coal seams, carbonaceous and non-carbonaceous clastic rocks. Very little mineralogical data have been published on other South African coalfields than the Witbank and Highveld Coalfields. The following conclusions on the mineralogy, geochemistry and the acid generating potential of spoils produced at South African coal mines could be made:

Silicate minerals

- In coal and clastic rocks of the Vryheid Formation, it was found that some trace to dominant minerals are often present on a regional scale that was also identified in other studies. These minerals include quartz, kaolinite, calcite, dolomite, mica, K-feldspar, plagioclase, siderite, pyrite, illite/smectite, smectite and anatase.
- Quartz was identified in all samples and is present as a major to dominant mineral in coal seams and in clastic rocks. Quartz is found to be the dominant mineral in all coal seams and clastic rocks of the Highveld Coalfield. Kaolinite is the dominant mineral in coal seams of the Witbank Coalfield. Kaolinite is also present in all samples either as a major or dominant mineral, except in a cluster of samples that contained chlorite in the northern Highveld Coalfield. It is suggested in this study that chlorite forms from clays as a result of temperature elevation due to dolerite intrusions. This also explains the absence of kaolinite as the increase in temperature leads to chlorite and illite stability, and kaolinite and smectite instability.
- K-feldspar, plagioclase, mica, illite/smectite and smectite are mostly present as minor minerals and sometimes as major minerals in samples.

The K-feldspar occurs frequently in both coal and clastic rocks, although it was identified more often in the clastic rocks. Because the sedimentary rock originates from a felsic mother rock, the plagioclase present will be typically of an oligoclase composition with a $\text{Na}_{10}\text{Ca}_{90} - \text{Na}_{30}\text{Ca}_{70}$ content.

Mica is more frequently present in coal and clastic rock samples of the Highveld Coalfield than in samples from the Witbank Coalfield. The No. 4 and No. 5 coal seams also contain more mica than the No. 2 coal seam in the Highveld Coalfield. Glauconite containing siltstones have often been identified above the No. 4 and No. 5 coal seams in the Highveld Coalfield in this study. Where the presence of mica is due to marine transgressions, the mica present will be glauconite.

Both smectite and illite/smectite is present in coal and in clastic units, however the illite/smectite content was found to be much higher in coal than in clastic rocks. A negative correlation between illite/smectite and the total quartz + kaolinite contents were shown; illite/smectite is associated with low-ash coal,

and quartz and kaolinite with high ash coal. Smectite formed as a result of the weathering of primary Al-Si minerals (e.g. K-feldspar, plagioclase etc.). Illite interstratification occurs with smectite as a result of an increase in temperature during diagenesis.

It is suggested that the presence of chlorite is due to the transition of smectite to illite and chlorite under elevated temperatures.

Oxides, hydroxides and sulphates

- Anatase is often present as a trace or as an accessory mineral in the coal bearing strata.
- Other trace to minor minerals is apatite, alunite, hematite and goethite. These minerals are observed only locally in borehole clusters and in certain parts of the coalfields.
- Hematite is expected to be the most stable form of the secondary iron minerals in the sedimentary rocks, however it was shown in **Section 2.5** that hematite (Fe_2O_3) forms not directly at low temperature but rather ferrihydrite ($\text{FeOOH}\cdot\text{H}_2\text{O}$). When ferrihydrite later accumulates in soils and sediments under dry conditions, it may eventually dehydrate and recrystallize to form more thermodynamically stable goethite (FeOOH) and later hematite (Fe_2O_3). This dehydration and recrystallization will especially occur with increase in temperature, e.g. during early sedimentary diagenesis, and therefore only hematite is frequently observed as the Fe-oxide present in the coal bearing strata.

Element dispersion in the coal forming environment

- The major/minor elements SiO_2 , Na_2O and K_2O are lowered in the No. 2 coal seam of the Witbank Coalfield with respect to the original felsic mother rock of the clastic sedimentary material. However, filtering of sediment occurred in marshes that prevent sediment to be carried in rivers and other water bodies from penetrating beyond the margins of the peat bed. The acid or saline waters in the swamp may also cause flocculation of clays and other suspended mineral particles, further reducing clastic dispersal.
- The elements Al_2O_3 , CaO , FeO , TiO_2 , P_2O_5 , S are elevated in the No. 2 coal seam of the Witbank Coalfield and more so in the low ash coal. Al and Ti are soluble in acidic conditions and could be released from the sediments to precipitate authigenetically as kaolinite in the coal; Fe and Ti can replace 2 mol of Al in kaolinite. Fe, P, S and Ca are released from the plant material and form authigenetic minerals in the coal.

- Trace elements are often associated with minerals phases in the coal ash content although many are derived from plant material. Most trace elements increase in the coal with increasing ash content, except As, Br, Co, Sc and Sr.

Marine transgressions occurred after the No. 2, No. 4 and No. 5 coal seams formed and glauconitic rocks have been identified in this study to occur above the No. 4 and No. 5 coal seams in the Highveld Coalfield. The marine transgressions also influenced the trace element geochemistry; for instance is elevated Br in rocks evident of the marine transgressions.

Pyrite and carbonate minerals and potential of spoils to generate AMD

- The average pyrite content decreases from coal samples to carbonaceous clastic rocks to non-carbonaceous clastic rocks. Pyrite is also higher in the Witbank Coalfield samples than in the Highveld Coalfield samples. Pyrite in non-carbonaceous clastic rocks was probably epigenetically deposited.
- No other iron sulphide mineral than pyrite has been identified in this study.
- Calcite and dolomite is higher in low to medium ash coal than in high ash coal or clastic rocks. In contrast siderite tends to be higher in high ash coal and in carbonaceous clastic rocks.
- Non-carbonaceous clastic rocks show NP and AP values of below 10 kg CaCO₃/t. XRD analyses also show little pyrite and carbonate mineral content for these rocks. Non-carbonaceous clastic rocks are the only material that shows a positive NNP.
- Carbonaceous clastic rocks from the Witbank and Highveld Coalfield show a negative NNP, comparable to the NP of some of the coal seams. The average AP and NP for the carbonaceous and pyrite containing clastic rocks are higher in the Highveld Coalfield samples but the NNP is less negative than that of the carbonaceous rocks of the Witbank Coalfield.
- Generally the NNP increases in the coal seams upwards from the No. 1 to the No. 4 coal seams in the Witbank Coalfield. This has been frequently observed in literature, e.g. Pinetown (2003) and Usher et al. (2001). XRD analyses confirmed that the calcite and dolomite mineral content decreases from the No. 1 up to the No. 4 coal seam. It was however observed that the siderite content increases from the No. 1 up to the No. 4 coal seam.
- Overall, both the AP and NNP are higher in the samples of the Witbank Coalfield than in the Highveld Coalfield. XRD analyses of the samples also show an average higher pyrite content for the Witbank Coalfield samples than for the Highveld Coalfield.

Implications for geochemical modelling of coal mine spoils

- If kinetic modelling is performed that includes the silicate mineral content, XRD analyses have to be performed on the coal and the coal bearing strata. Not only does the mineral content vary from mine to mine, but some minor minerals also occur only in parts of the coalfields.

The silicate mineral content must also be corrected to the amount of ash present in the coal or the other carbonaceous rock. For instance if plagioclase is 6% of the mineral ash content it will only be 3% of the total rock content if the coal has a 50% mineralogical content. Therefore the ash content must preferably be determined on the carbonaceous rocks on which XRD is performed.

- Unfortunately, it is not possible from the limited data of this study to give an indication of the amount of sampling that needs to be done at a mine. Samples would be required of the economical and the uneconomical coal seams as the geochemistry of the coal varies significantly with ash content. Samples also need to be taken from the carbonaceous clastic rocks as they would be a major contributor to acid generation in the spoils together with the uneconomical coal. Clastic rocks must be sampled as to determine whether they contain epigenetically pyrite or to what degree they can potentially neutralize acid.
- For geochemical modelling, the pyrite content can be calculated from the %S determined by the Leco analyzer or by the peroxide method. The siderite correction method must be used when determining the NP, as siderite is frequently identified in this study in the coal bearing strata. The calcite and dolomite can then be calculated from the determined NP. The ratio between calcite and dolomite can be calculated from the XRD analyses and/or from CIPW norms.

It would not be correct to use the XRD determined pyrite, calcite or dolomite wt% in geochemical modelling. XRD interpretation techniques are only semi-quantitative and less accurate when determining trace and accessory minerals in whole rock samples (samples containing a large variety of minerals).

6.6 References

Allaby, A. and Allaby, M. (2003). *Dictionary of Earth Sciences*. 2nd Edition, Oxford University Press.

Azzie, B.A. (2002). *Coal mine waters in South Africa: Their geochemistry, quality and classification*. Ph.D thesis, University of Cape Town, South Africa, 181 pp.

- Bruvoll, M., Jahren, J.S. and Per, A. (2004). *Smectite illitization in organic rich shale offshore mid-Norway*. In: *Illite diagenesis a quarter century after Hower et al.*. Clay Minerals Society, 41st Annual Meeting, Richland, WA, June 19-24.
- Bühmann, C. and Bühmann, D. (1988). *Sedimentary petrology of coal-bearing Ecca sediments*. Final Project Report (Unpublished), University of Natal, South Africa, 27 pp.
- Butler, I.B. and Rickard, D. (2000). *Framboidal pyrite formation via the oxidation of iron (II) monosulfide by hydrogen sulphide*. *Geochim. Cosmo. Acta*, 64(15), 2665-672.
- Cadle, A.B., Cairncross, B., Christie, A.D.M. and Roberts, D.L. (1990). *The Permian-Triassic coal-bearing deposits of the Karoo Basin, Southern Africa*. Information Circular No. 218, Economic Geology Research Unit, University of the Witwatersrand, Johannesburg.
- Cadle, A.B., Cairncross, B., Falcon, R.M.S., Manacyzynski, V. and Willis, J. (1989). *The Characterization of the No. 2 seam, Witbank Coalfield - a Collaborative Investigation*.
- Cairncross, B., Hart, R.J. and Willis, J. (1990). *Geochemistry and sedimentology of coal seams from Permian Witbank Coalfield, South Africa; a means of identification*. *Int. J. Coal Geol.*, 16, 309-325.
- Compton, R.G. and Sanders, G.H.W. (1993). *The dissolution of calcite in aqueous acid: the influence of humic species*. *J. Colloid Interface Sci.*, 158, 439-445.
- De Bruijn, H. (2000). *Introduction to Geochemistry*. Department of Geology, University of the Free State, Unpublished class notes.
- Faraj, B.S.M., Fielding, C.R. and Mackinnon, D.R. (1996). *Cleat mineralization of Upper Permian Baralaba/Rangal Coal Measures, Bowen Basin, Australia*. In: *Coalbed Methane and Coal Geology* (eds. Gayer, R. and Harris, I.). Geological Society, London, Special Publication 109, 151-164.
- Gaigher, J.L. (1980). *The mineral matter in some South African coals*. M.Sc. thesis, University of Pretoria, South Africa, 60 pp.
- Hart, R.J. and Leahy, R. (1983). *The geochemical characterization of coal seams from the Witbank Basin*. *Spec. Publ. Geol. Soc. S. Afr.*, 7, 169-174.
- Hart, R.J., Leahy, R. and Falcon, R.M.S. (1982). *Geochemical investigation of the Witbank Coalfield using instrumental neutron activation analysis*. *J. Radioanal. Chem.*, 71, 285-297.

Horsefall, D.W. (1993). *Coal preparation and usage – Coal processing for management*. Volume 1, Coal Publications.

Lawrence, R.W. and Wang, Y. (1997). *Determination of Neutralization Potential in the Prediction of Acid Rock Drainage*. 4th ICARD, Vancouver, p. 449-464.

Mills, C. (2003). *Acid-Base Accounting (ABA) Test Procedures*. Internet: <http://www.enviromine.com/ard/Acidbase/acidbase.htm>.

Morse, J.W. and Arvidson, R.S. (2002). *The dissolution kinetics of major sedimentary carbonate minerals*. Earth-Science Reviews, 58, 51-84.

Nesse, W.D. (1991). *Optical mineralogy*. 2nd Edition, Oxford, New York.

Pinetown, K.L. (2003). *Quantitative evaluation of minerals in coal deposits in the Witbank and Highveld Coalfields and the potential impact on acid mine drainage*. M.Sc. Thesis, Department of Geology, University of the Free State, South Africa.

Price, W.A. (1997). *DRAFT Guidelines and Recommended Methods for the prediction of Metal leaching and Acid Rock Drainage at Minesites in British Columbia*. British Columbia Ministry of Employment and Investment, Energy and Minerals Division, Smithers, BC, 143 p.

Rudnick, R.L. and Gao, S. (2003). *The Composition of the Continental Crust*. In: *The Crust* (ed. R.L. Rudnick), *Treatise on Geochemistry* (eds. H.D. Holland and K.K. Turekian). Elsevier-Pergamon, Oxford. 3, 1-64.

Sawlowicz, Z. (1993). *Pyrite framboids and their development: a new conceptual mechanism*. Int. J. Earth Sci., 82(1), 148-156.

Skousen, J., Renton, J., Brown, H., Evans, P., Leavitt, B., Brady, K., Cohen, L. and Ziemkiewicz, P. (1997). *Neutralisation Potential of Overburden Samples containing Siderite*. Journal of Environmental Quality, Vol. 26(3), 673-681.

Snyman, C.P. and Barclay, J. (1989). *The coalification of South African coal*. Int. J. Coal Geol., 13, 375-390.

Sobek, A.A., Schuller, W.A., Freeman, J.R. and Smith, R.M. (1978). *Filed and Laboratory Methods Applicable to Overburden and Minesoil*. Report EPA-600/2-78-054, U.S. National Technical Information Service Report PB-280 495.

Soregaroli, B.A. and Lawrence, R.W. (1998). *Update on Waste Characterization Studies*. Proc. Mine Design, Operations and Closure Conference, Polson, Montana.

Usher, B.H., Cruywagen, L-M., De Necker, N. and Hodgson, F.D.I (2001). *On-site and laboratory Investigations of Spoil in Open-cast Collieries and the development of*

Acid-Base Accounting Procedures. WRC Report no., Water Research Commission, Pretoria.

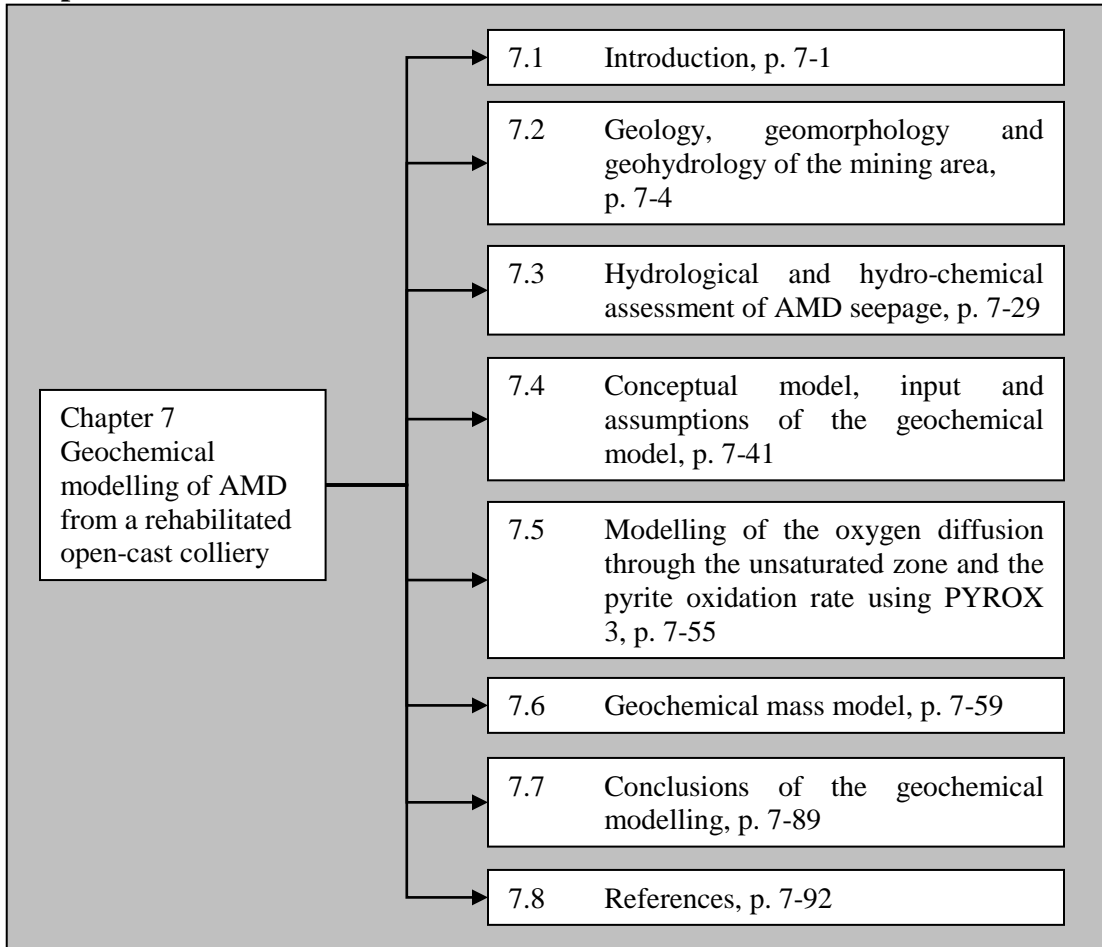
Ward, C.R. (2002). *Analysis and significance of mineral matter in coal seams*. Int. J. Coal Geol., 50, 135-168.

Ward, C.R., Spears, D.A., Booth, C.A., Staton, I., and Gurba, L.W. (1999). *Analysis and significance of mineral matter in coal seams*. Int. J. Coal Geol., 40, 281-308.

Ward, C.R. and Taylor, J.C. (1996). *Quantitative mineralogical analysis of coals from the Callide Basin, Queensland, Australia using X-ray diffractometry and normative interpretation*. Int. J. Coal Geol., 30, 211-229.

7 Case study – Geochemical modelling of Acid Mine Drainage (AMD) from a rehabilitated open-cast colliery

Chapter Structure



7.1 Introduction

The case study mine is a small defunct coal mine situated in the northern Klip River Coalfield in the KwaZulu-Natal province of South Africa. Mining ceased in 1992 and although two coal seams are economically mined in the coalfield, namely the Top and Bottom Seams, only the former was mined at the case study mine. The mining at the colliery comprised of two shallow open-cast pits (floor depth <15 m below surface) on the northern and southern sides of a river. The pits were backfilled with waste rock and thereafter covered with 1 m of topsoil which was vegetated with grass.

Samples taken of pit water have shown elevated sulphate (> 2500 mg/l) and acidity (pH < 4.5) contents. Seepage in the form of base flow from the mining pits into the river has resulted in a worsening water quality of the river, and salt encrustations are present on the riverbanks. A photo taken from the river towards the southern pit is depicted in

Figure 7.1(A) below. The boreholes in the photo are from the left OBH-9, IBH-6 and 16. The former two boreholes were drilled just outside the pit perimeter and the latter within the southern pit perimeter, with the pit just behind the horizon.



Figure 7.1(A). The river next to the case study colliery. The presence of ferrihydrite (coloring the water orange and often called “yellow-boy”) is a tell-tale sign that Acid Mine Drainage seeps through the berm into the river.

The small northern pit does not have sufficient monitoring data and this case study only investigated the larger southern pit. Monitoring data, which includes groundwater quality and borehole water level information, were made available for this study.

7.1.1 Objectives

The first overall objective will be to apply the theory of the modelling of AMD, as discussed in **Chapter 2** to **4**, through numerical software programs on the available monitoring data. This entails the modelling of the interaction of the gaseous, solid and liquid phase.

The second objective is to determine whether the available data was sufficient in order to model the case study mine geochemically and which assumptions were viable, and to

make recommendations for future studies. Hydro-chemical and water level monitoring information were the only data available for this case study.

The above objectives are set specifically to aid in the setting up of geochemical models for application to AMD prediction in South Africa. A description of input required for the modelling of the physico-chemical processes in coal mine waste and recommendations for future studies based on experience gained from this study are given in **Chapter 8**. There is an increased need to determine the environmental impact of collieries as coal mining will reach its maximum extent in many South African coalfields in the following decades.

Only the larger southern pit of the colliery is modelled as the pit has detailed monitoring data – the northern pit has less data available and is also more complex because of its more heterogeneous backfill.

7.1.2 Methodology

The methodology used will incorporate the study and presentation of some baseline information that is necessary for 1) the development of a conceptual model of the site and 2) input into the geochemical models.

A brief geological and geohydrological description of the larger mining area will be made in **Section 7.2**. This will include an assessment of the *water level distribution* and also an assessment of the average *background chemistry* of the unpolluted Karoo aquifer for input in the geochemical model.

In **Section 7.3** a hydrological and hydro-chemical assessment is made of the AMD seepage. The hydro-chemical assessment of the pit water will be used as input for the geochemical model. In **Section 7.3** results from the Visual HELP 2.2 software program are given that include the steady state moisture content of the unsaturated zone as well as the deep percolation (recharge) towards the saturated zone. The moisture content in the unsaturated zone plays an important role in oxygen diffusion into the pit.

The geochemical interactions in the mine spoils will be modelled in **Section 7.4 – 7.6** as follows:

- In **Section 7.4** a conceptual model of the AMD generation at the case study mine is given. All input and assumptions of the geochemical models are also discussed in this section.
- The oxygen diffusion into the pit and the oxidation rate of pyrite will be modelled using the software PYROX 3. PYROX 3 numerically solves the oxygen diffusion equation in porous material expressed as **Equation 3.2.4.1(D)**. The software is

discussed in more detail in **Section 7.5**.

- A geochemical mass model of the pit will simulate all the geochemical reactions in the pit in **Section 7.6**. The software The Geochemist's Workbench 6.0.3 will be used and a steady state oxygen concentration will be used as input into the model.

An assessment was made in **Section 7.7** of the shortcomings of the input of the model. This assessment is done in order to determine the data necessary for a typical geochemical model of an open-cast colliery. Recommendations for future geochemical modelling studies are made in **Section 8.2 and 8.3** as part of the conclusions of this study.

7.2 Geology, geomorphology and geohydrology of the mining area

7.2.1 Regional geology and geomorphology of the Klip River Coalfield

The study area is situated in the Klip River Coalfield of KwaZulu-Natal. The coal bearing area of Northern KwaZulu-Natal is subdivided into three geographically distinct coalfields: the Klip River Coalfield, the Utrecht Coalfield and the Vryheid Coalfield.

The largest and historically the most important is the Klip River Coalfield stretching over a total area of 6000 km² of which roughly 50% can be considered as potentially coal bearing (Bell and Spurr, 1986). **Figure 7.2.1(A)** shows the approximate locality of the case study mine in the coalfield.

The eastern escarpment of the Drakensberg Mountain Plateau, that trend approximately north to south, bound the Klip River Coalfield in the north to west. Below the escarpment is a plateau with an average elevation of between 1200 mamsl and 1350 mamsl (Bell and Spurr, 1986). Rising above the general country level are low dolerite ridges and flat-topped hills that locally attain elevations of 1700 mamsl (Bell and Spurr, 1986). Drainage in the area is dominated by two main river systems, the Buffalo River in the north and the Sundays River in the south and west. Both these drain to the south into the Tugela River complex (Bell and Spurr, 1986).

The geology of the Klip River Coalfield comprises sedimentary rocks of the Karoo Super Group with voluminous occurrences of Karoo dolerite present on a regional scale throughout the study area (Tankard et al., 1982). A geological cross-section through the Klip River Coalfield, indicating the extensive intrusion of dolerite sills, is given in **Figure 7.2.1(B)**.

Dwyka tillite and shale of glacial origin were deposited on a pre-Karoo floor and with the advance of a warmer climate the Ecca Group was deposited after the retreat of the ice sheets (Tankard et al., 1982). The coal bearing Vryheid Formation was deposited on top

of the Dwyka except for the eastern and southeastern portions of the Karoo basin, incorporating the Ermelo and the three Natal coalfields which were much deeper at the time of the retreat of the Dwyka glaciers (Snyman, 1998). Consequently, in the latter areas the Pietermaritzburg Formation was deposited as a shelf facies in the continental Ecca Sea before the Vryheid Formation was later deposited in its characteristic fluviodeltaic environment (Snyman, 1998). The gradational change from Pietermaritzburg Formation shales to sandstones of the lower Vryheid Formation represents a regressive deltaic depositional event in which delta-front sands prograded over prodelta shales and mudstones (Bell and Spurr, 1986). A litho-stratigraphical profile of the Karoo Super Group in the Klip River Coalfield is given in **Figure 7.2.1(D)**.

Only two economic coal seams are distinguished viz. the Top and Bottom Seams which are correlated with the Gus and Alfred Seams respectively of the other Kwazulu-Natal Coalfields (Snyman, 1998). A third uneconomical coal seam, the No. 3 seam, is sporadically developed below the Bottom Seam. The average thicknesses of the coal seams for the northern area of the Klip River Coalfield (the region in which the case study mine falls) are given in **Figure 7.2.1(C)**.

Nine types of dolerite sills have been distinguished, the four major ones from the oldest, being the Zuinguin, Utrecht, Ingogo and Talana sills (Snyman, 1998). In the Klip River Coalfield the maximum displacement of strata by dolerite sills is reported to be 137 m (Snyman, 1998). These dolerite sills are depicted in the geological cross-section through the Klip River Coalfield in **Figure 7.2.1(B)**.

No pre-Karoo rocks are exposed within the area, the nearest granite outcrop being in the Nondweni region east of the coalfield (Bell and Spurr, 1986).

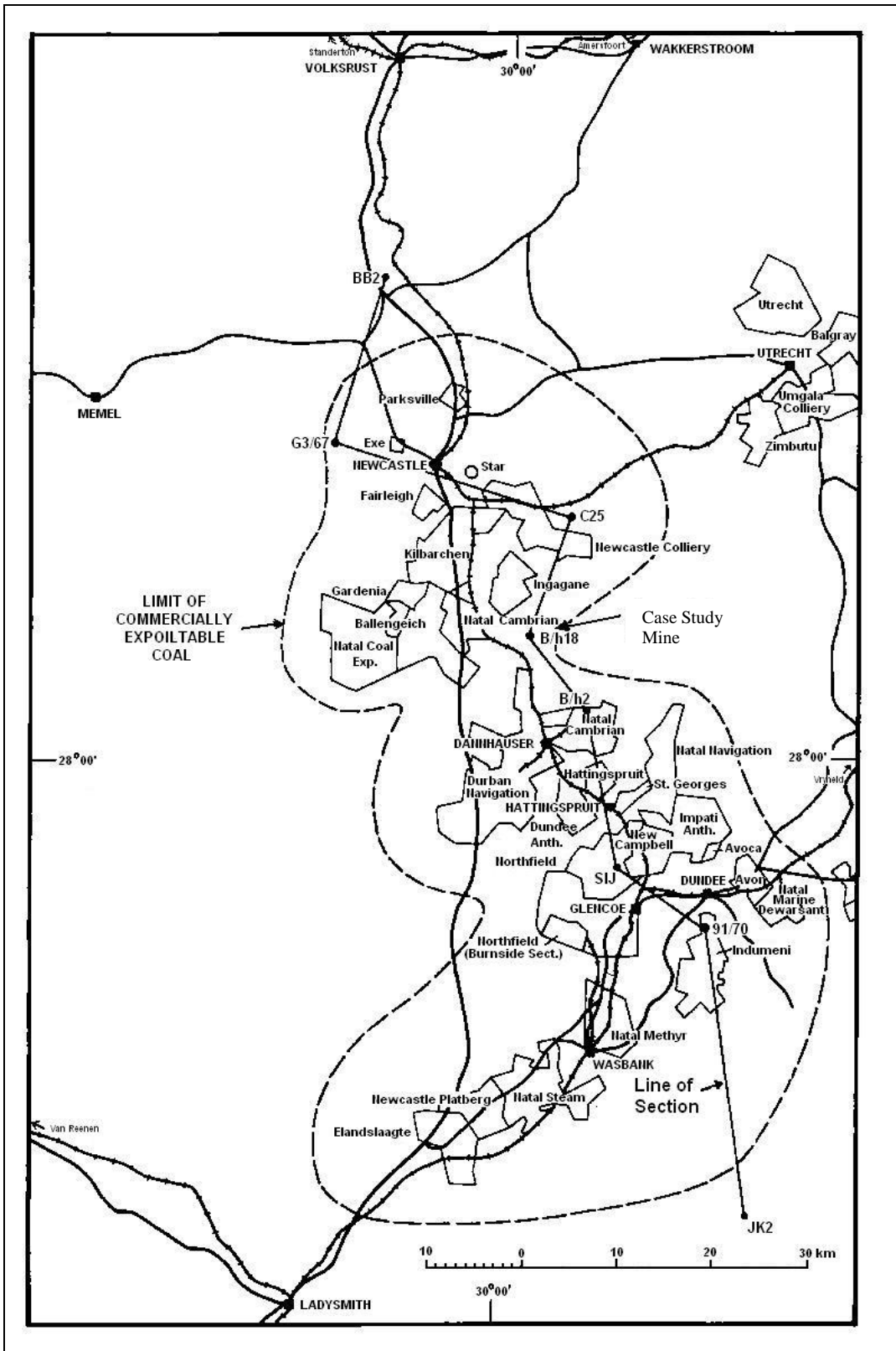


Figure 7.2.1(A). The Klip River Coalfield (after Bell and Spurr, 1986).

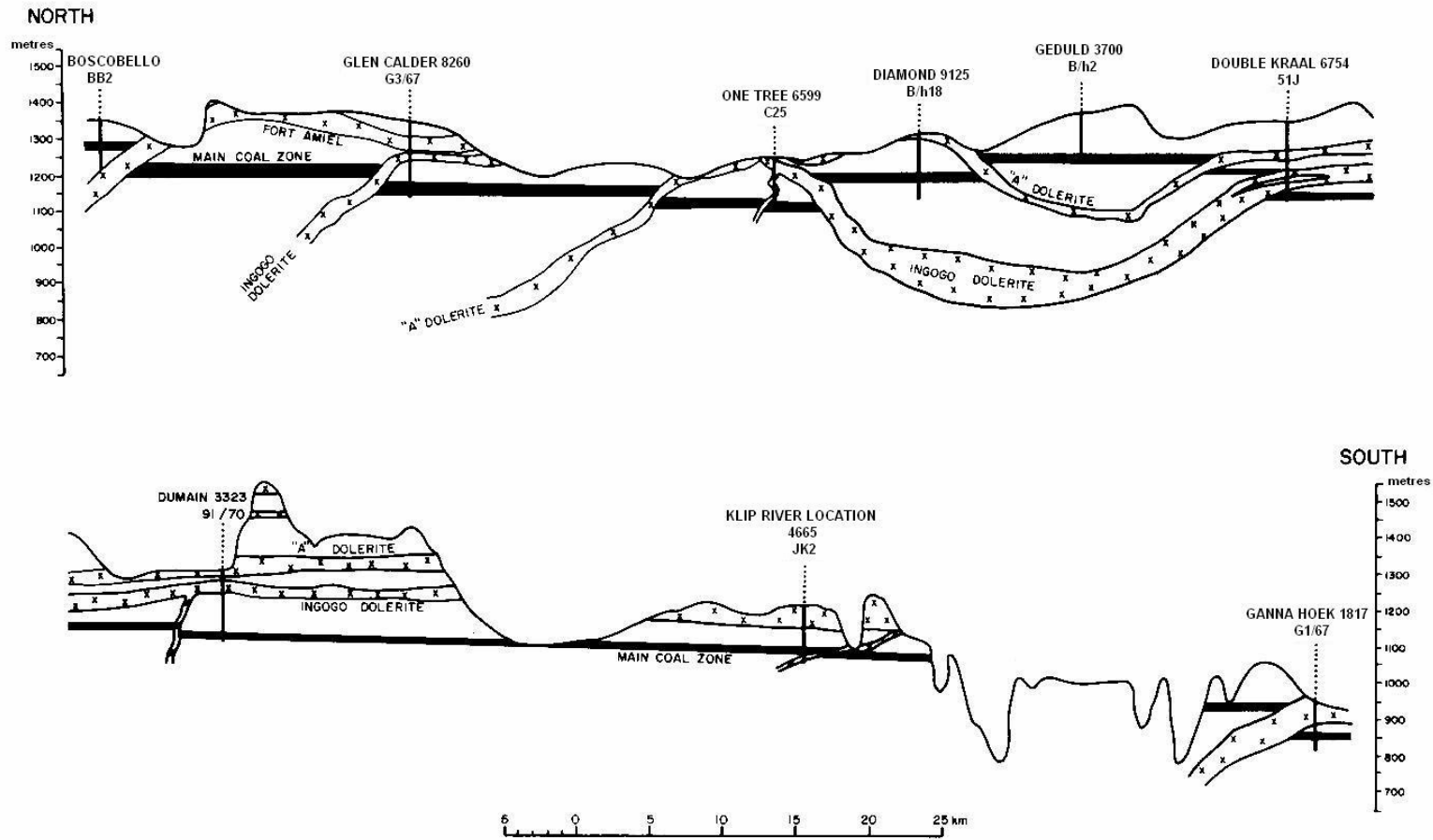
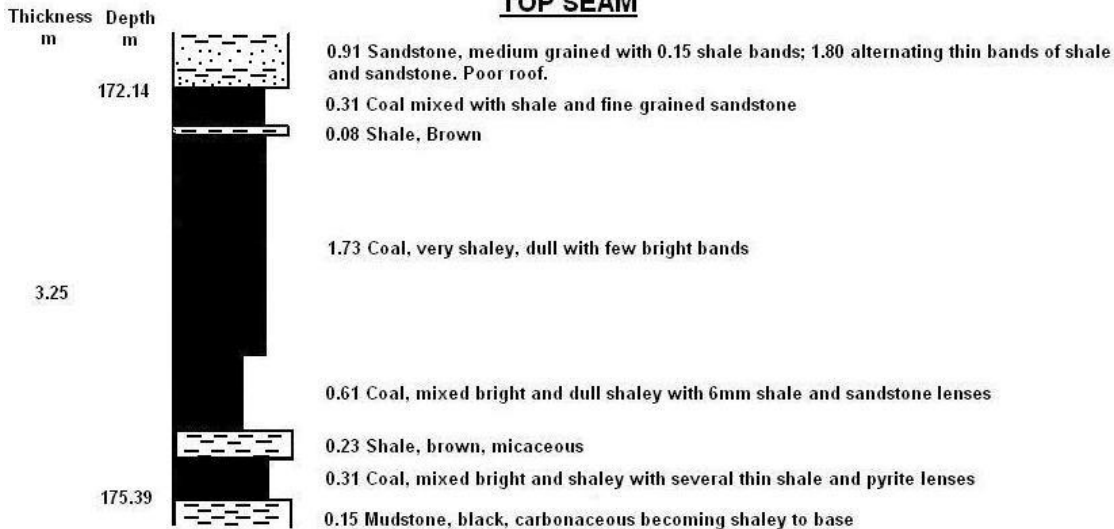


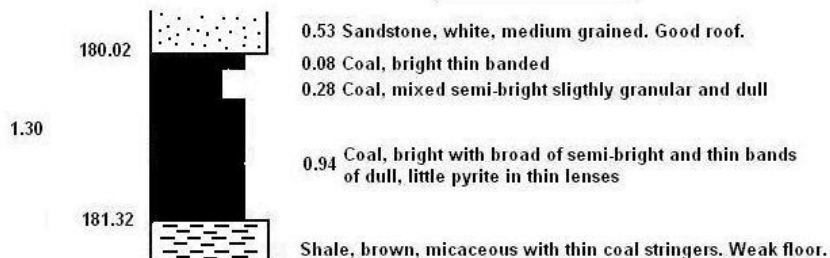
Figure 7.2.1(B). Geological cross-section through the Klip River Coalfield (after Bell and Spurr, 1986).

NORTH AREA

TOP SEAM



BOTTOM SEAM



NO.3 SEAM

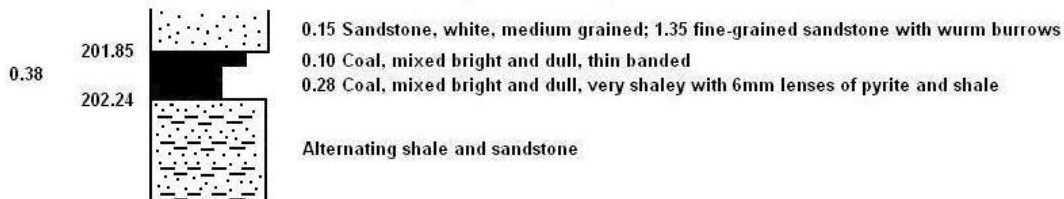


Figure 7.2.1(C). Coal seam thickness in the northern Klip Rivier Coalfield (after Bell and Spurr, 1986).

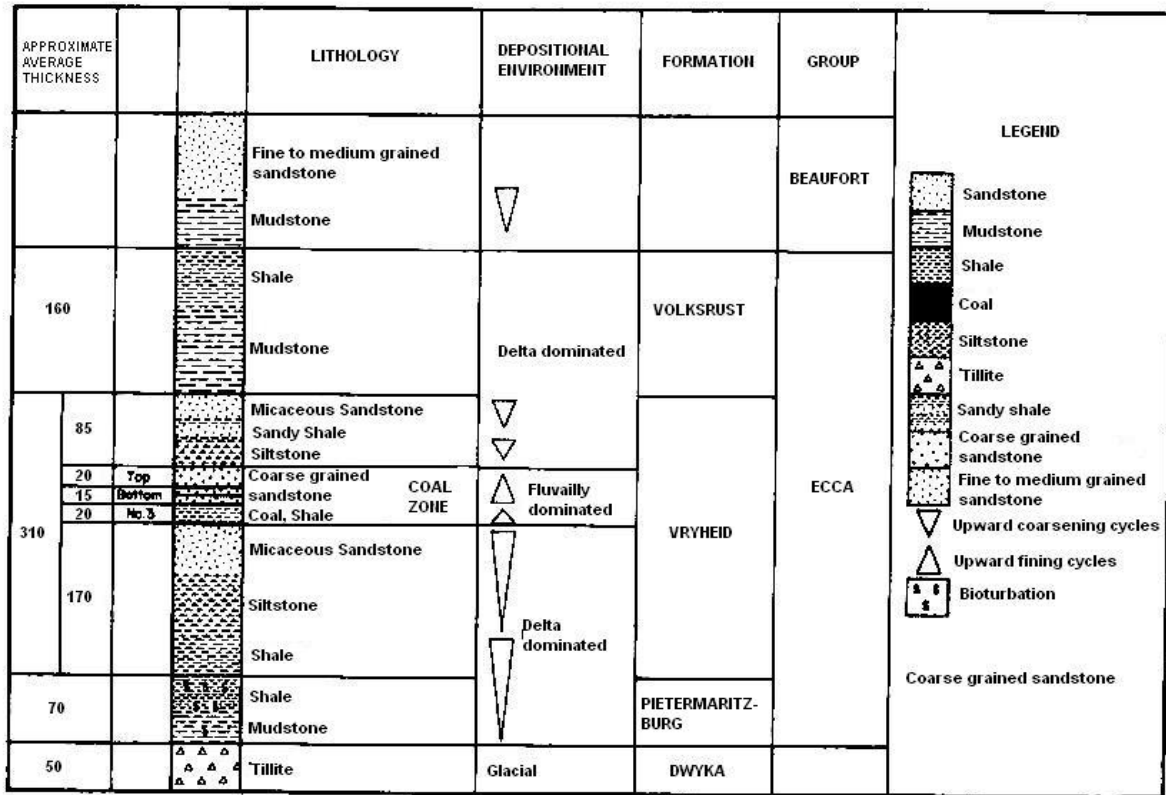


Figure 7.2.1(D). Litho-stratigraphical profile of the Karoo Super Group in the Klip River Coalfield (after Bell and Spurr, 1986).

7.2.2 Local geomorphology and geology

Some of the maps and their description that forms part of **Section 7.2.2** are attached in **Appendix A**. **Appendix A** is treated as confidential as the position and the name of the mine may not be revealed due to sensitivities with relation to the closure of the mine.

The case study mine consists of a northern and southern pit of respectively 7.4 ha and 22.4 ha. The location of the case study mine in the upper sub-drainage region of the adjacent river is shown in **Figure 7.2.2(A)** below.

The local Karoo aquifer that surrounds the southern pit is indicated in **Figure 7.2.2(A)** and covers an area of about 289 ha; for easy reference it will be called the “Southern Aquifer”. The boundaries of the Southern Aquifer consist of a groundwater divide in the south and streams in the west, north and east. From water level interpretations, it is evident that the river and its tributaries serve as drains to the aquifer (“gaining rivers”).

Figure 7.2.2(B) and **(C)** in **Appendix A** further depict the location of the case study mine with relation to the local geology and topography.

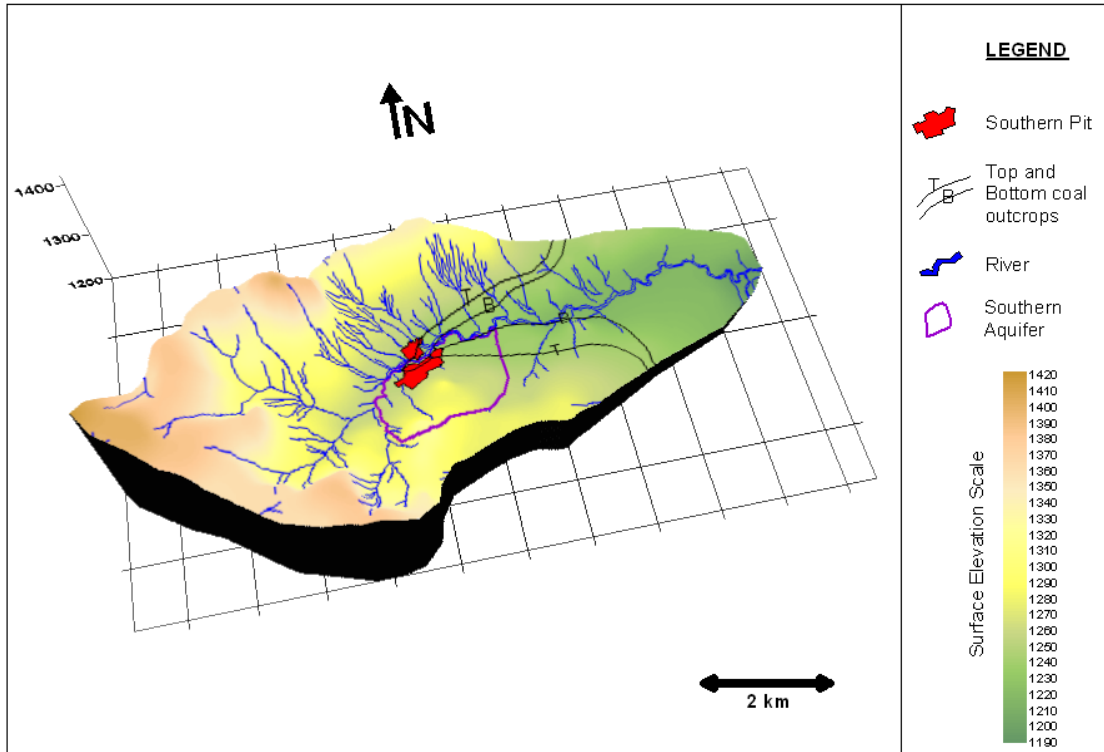


Figure 7.2.2(A). The location of the case study mine in the river sub-drainage region.

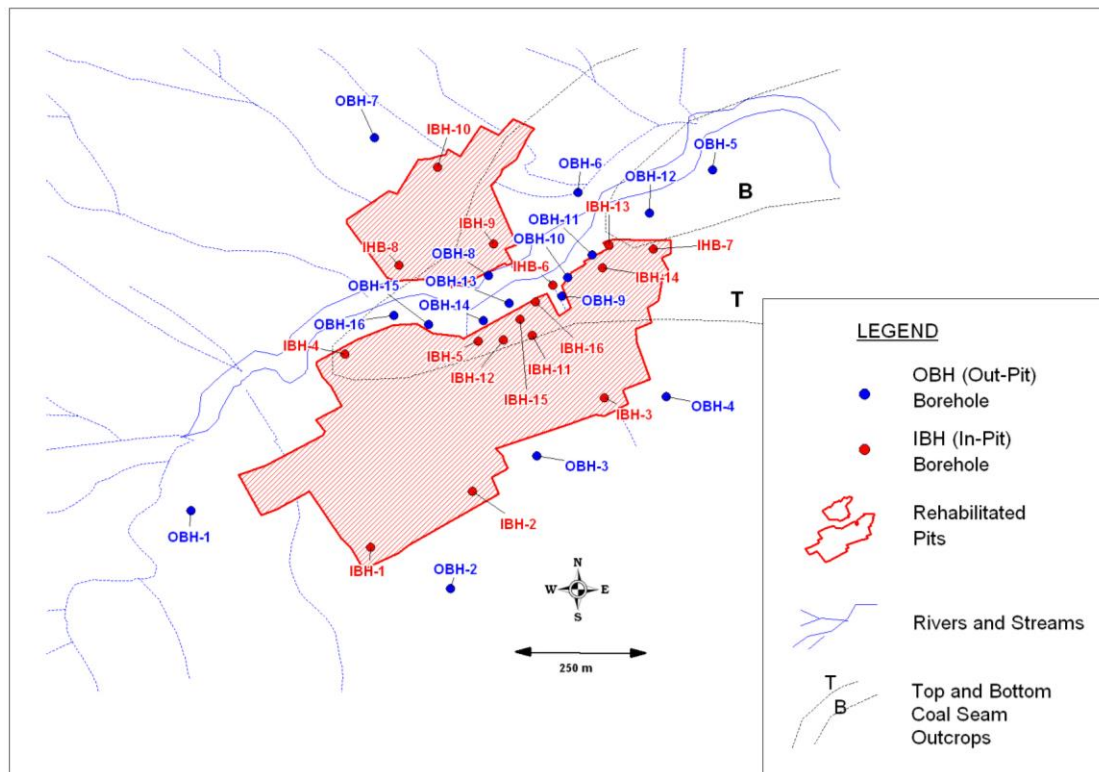


Figure 7.2.2(D). Position of boreholes at the case study mine.

A total of 16 boreholes were drilled into the pits (called IBH or “in-pit” boreholes). From these a total of 13 boreholes were drilled into the southern pit except for IBH-6 that was actually drilled just outside the pit perimeter. Another 16 boreholes were all drilled outside the pits (called OBH or “out-pit” boreholes) whereof 13 were drilled next to the southern pit and 3 next to the northern pit. The position of all the boreholes in the study area is given in **Figure 7.2.2(D)** above.

The Top Seam were intersected in 7 out-pit boreholes: OBH-1, 6, 7, 8, 9, 10 and 11; the thickness of the coal was respectively at 2 m, 2 m, 3 m, 2 m, 2 m, 1 m and 2 m, with the depth to the top of the seam at respectively 8 m, 5 m, 11 m, 10 m, 8 m, 11 m and 9 m. The Bottom Seam was intersected in OBH-12 with a thickness of 0.5 m with the top of the seam at a depth of 18.5 m below surface.

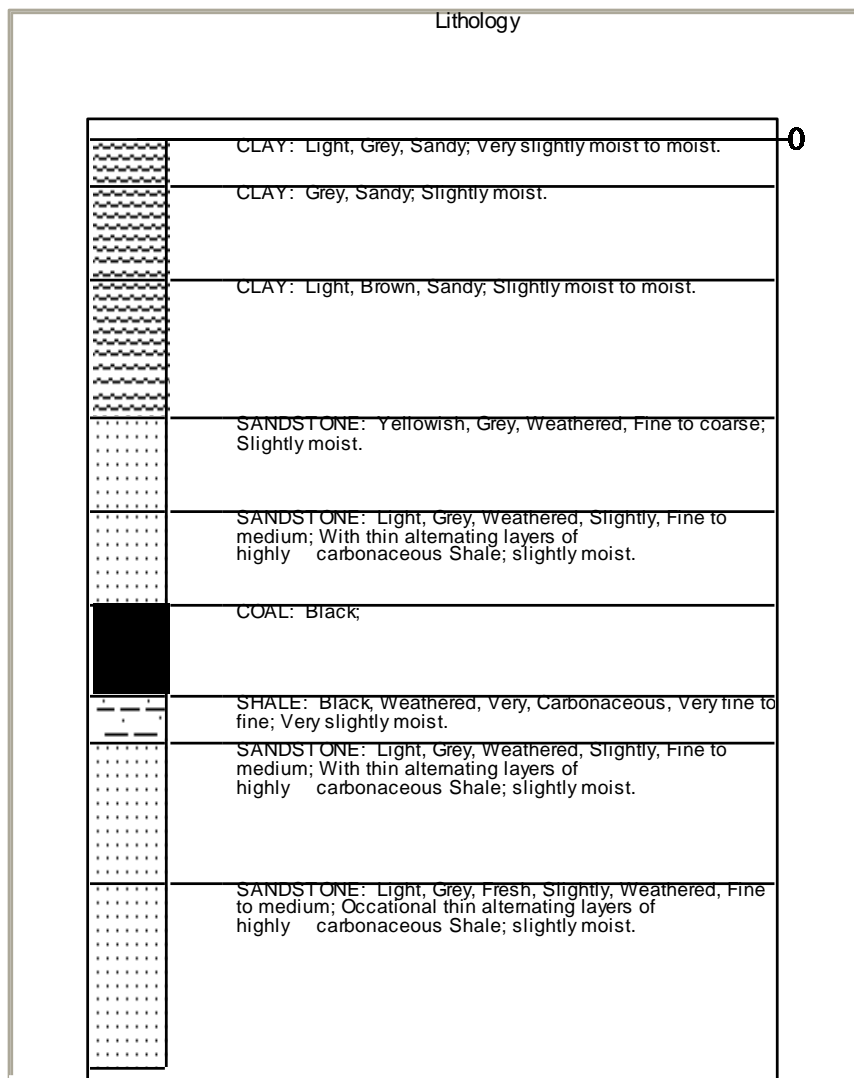


Figure 7.2.2(E). Representative lithological profile (OBH-8). (Coal seam thickness = 2 m, Depth to top of coal = 11 m).

Air rotary percussion drilling was used for the OBH boreholes and the thickness of the intersected lithologies cannot be accurately logged and must be estimated from the blown-out rock-chips. However, accuracy is not of importance to illustrate the main lithologies present and a representative lithological profile of the area (as logged by the geohydrological consultants JMA Consulting (Pty) Ltd) is given by borehole OBH-8 above in **Figure 7.2.2(E)**.

The lithological profile depicted in **Figure 7.2.2(E)** above shows that sandstone is the dominant sedimentary rock unit. Sandstone adjacent to the coal seam includes alternating layers of carbonaceous shale. The Top Seam is about 2 m thick and a carbonaceous shale layer of 1 m thickness is regionally present beneath the coal seam as is also shown in **Figure 7.2.1(C)**.

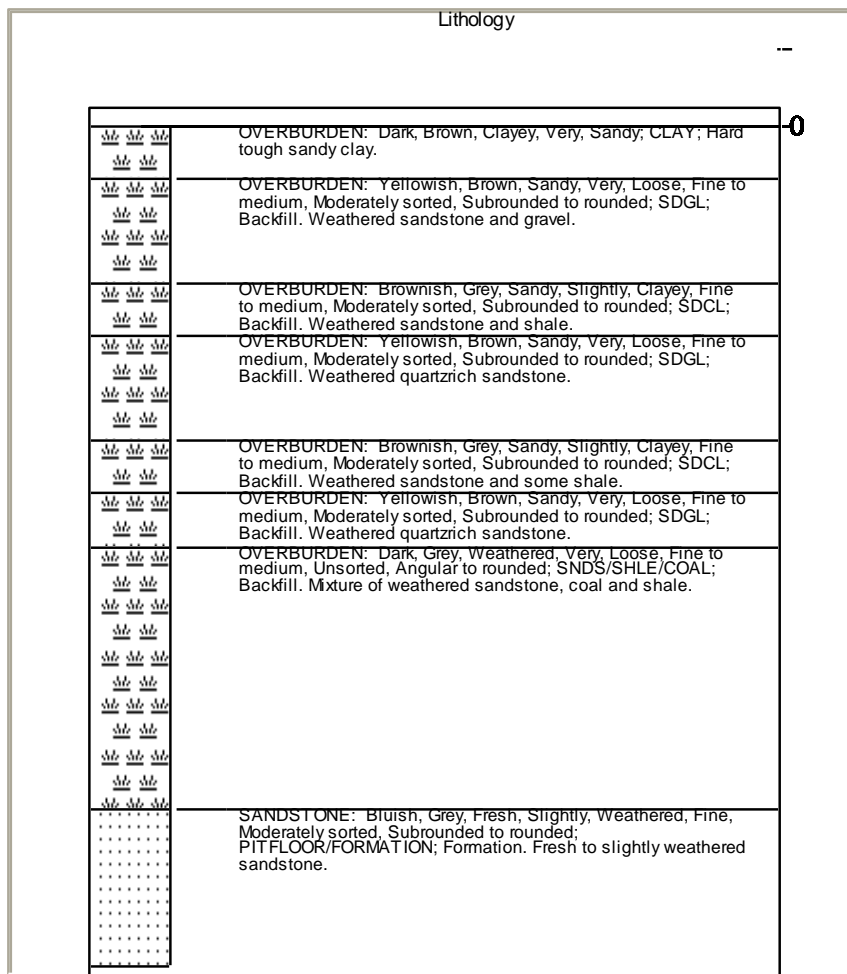


Figure 7.2.2(F). IBH-15 in the Southern Pit.

The backfill in the rehabilitated pit consists of waste rock and a small quantity of discard and the material is capped with 1 m thick sandy-loam soil layer. The boreholes drilled

into the backfilled pit showed a mixture of backfill material, viz. clay, sandstone, shale (often carbonaceous) and coal.

A vertical profile given for the backfill as depicted in **Figure 7.2.2(F)** above, shows that weathered sandstone and shale form the bulk volume of the backfill. The pit floor consisting of sandstone is at a depth of 13 m. The backfill (except for the upper soil layer) of this specific borehole contains a significant pyrite content as shown by the Acid Base Accounting (ABA) analyses in **Section 7.4.3.2**. The backfill is covered with a 1 m thick loamy soil (clay and sand).

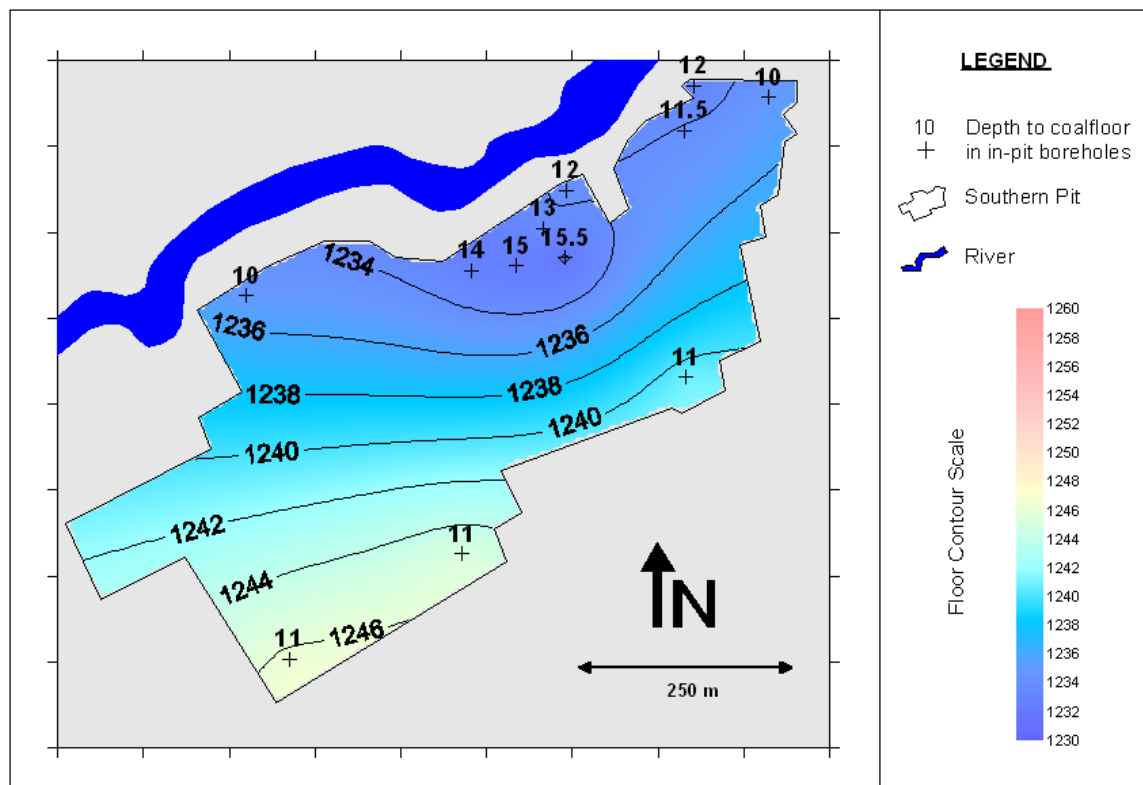


Figure 7.2.2(G). Floor contour of the case study mine.

The pit floor contour is shown in **Figure 7.2.2(G)** and was interpolated from the borehole data using the Kriging method in Surfer 8. The software also calculated the dip of the coal floor towards the northwest at between 0.24% and 5.34%, averaging at 2.90%.

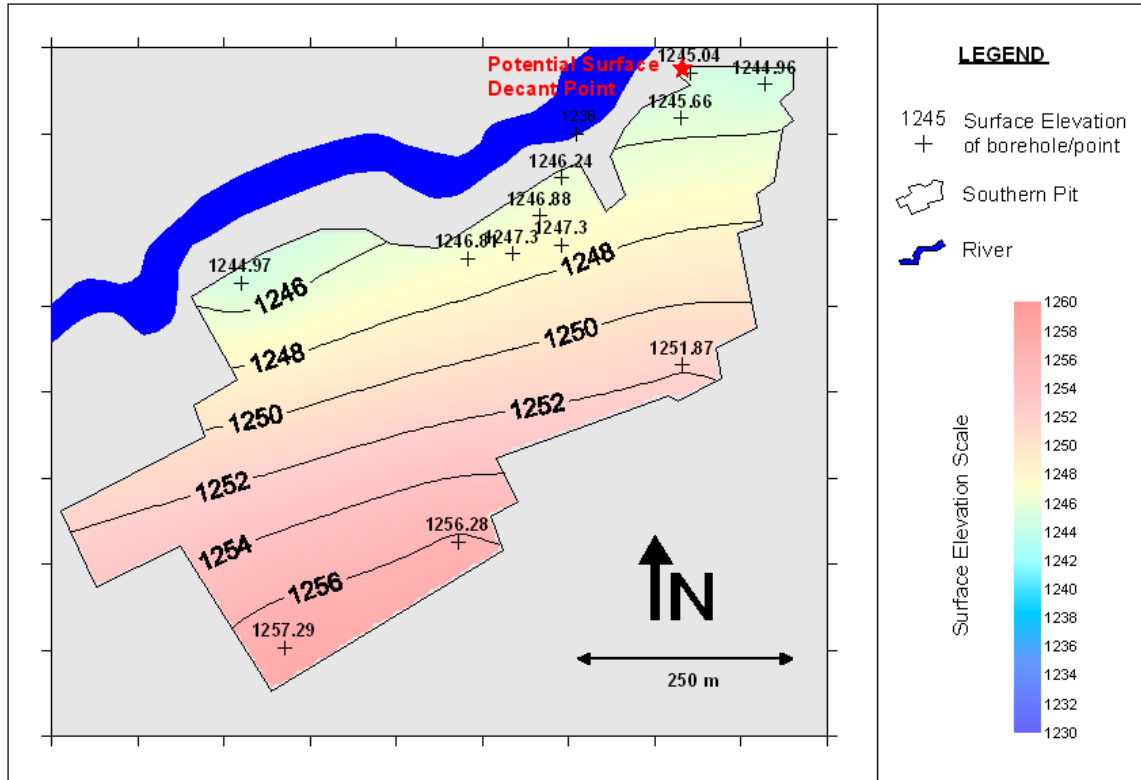


Figure 7.2.2(H). Surface contours of the case study mine.

Figure 7.2.2(H) depicts the surface contours of the Southern Pit. The depth of the pit (calculated by Surfer 8 by subtracting the pit floor contour from the surface contour) ranges between 9.97 m and 15.45 m, averaging at 11.74 m. The software calculated the slope of the topography at between 0.57% and 3.25%, averaging at 2.48%. The theoretical surface decant point is at 1245 mamsl, however, no surface decant have been observed and all out-flowing pit water is in the form of base-flow towards the adjacent river.

7.2.3 Groundwater level information

The average water level for each borehole during seven monitoring runs, as measured by the geohydrological consultants JMA Consulting (Pty) Ltd, from July 2003 to October 2004, is summarized in **Table 7.2.3(A)** below:

Table 7.2.3(A). Average water level data in the case study mine pits and the surrounding aquifer from July 2003 to October 2004.

Bh No.	Altitude + Collar Height (mamsl)	Depth to Water level (m) (collar)	Water level Elevation (mamsl)	Bh No.	Altitude + Collar Height (mamsl)	Depth to Water Level (m) (collar)	Water level Elevation (mamsl)
IBH-1	1,257.62	9.77	1,247.85	OBH-1	1,254.48	7.00	1,247.48
IBH-2	1,256.68	10.74	1,245.94	OBH-2	1,266.85	10.63	1,256.22
IBH-3	1,252.18	10.35	1,241.83	OBH-3	1,258.81	13.00	1,245.81
IBH-4	1,245.65	5.49	1,240.16	OBH-4	1,253.23	8.78	1,244.45
IBH-5	1,247.09	9.15	1,237.94	OBH-5	1,237.67	3.43	1,234.24
IBH-6	1,245.06	8.00	1,237.06	OBH-6	1,240.96	4.77	1,236.19
IBH-7	1,245.21	9.20	1,236.01	OBH-7	1,257.11	6.34	1,250.77
IBH-8	1,243.38	5.52	1,237.86	OBH-8	1,245.84	8.92	1,236.92
IBH-9	1,245.94	6.00	1,239.94	OBH-9	1,246.49	10.00	1,236.49
IBH-10	1,247.47	8.53	1,238.94	OBH-10	1,245.93	9.80	1,236.13
IBH-11	1,247.74	9.21	1,238.54	OBH-11	1,245.68	9.72	1,235.97
IBH-12	1,247.60	10.00	1,237.60	OBH-12	1,239.51	4.41	1,235.10
IBH-13	1,245.32	9.42	1,235.90	OBH-13	1,244.99	8.48	1,236.51
IBH-14	1,245.97	9.73	1,236.24	OBH-14	1,245.79	9.00	1,236.79
IBH-15	1,247.36	9.50	1,237.86	OBH-15	1,246.19	8.00	1,238.19
IBH-16	1,246.66	9.53	1,237.13	OBH-16	1,246.19	7.48	1,238.71

Mine water level

The pit floor is flooded up to 1236 – 1240 mamsl. From these water level data, the thickness of the saturated zone within the pit was calculated (by subtracting the pit floor from the Krigged interpolated water level in Surfer 8) as to range between 0.41 m to 5.24 m, averaging at 2.94 m. Therefore, the average water level depth in the Southern Pit is at 8.80 m. Boreholes IBH-1 to 3 were drilled through the pit floor and show water levels between 1242 – 1248 mamsl in the sandstone below the pit. **Figure 7.2.3(A)** below gives the correlation between the pit water level and the topography.

Water level in the surrounding Karoo aquifer

The average water levels of IBH and OBH boreholes were plotted against the surface elevation in **Figure 7.2.3(A)**. The IBH boreholes showed an expected weaker regression (0.714) against the topography elevations than the OBH boreholes (0.921).

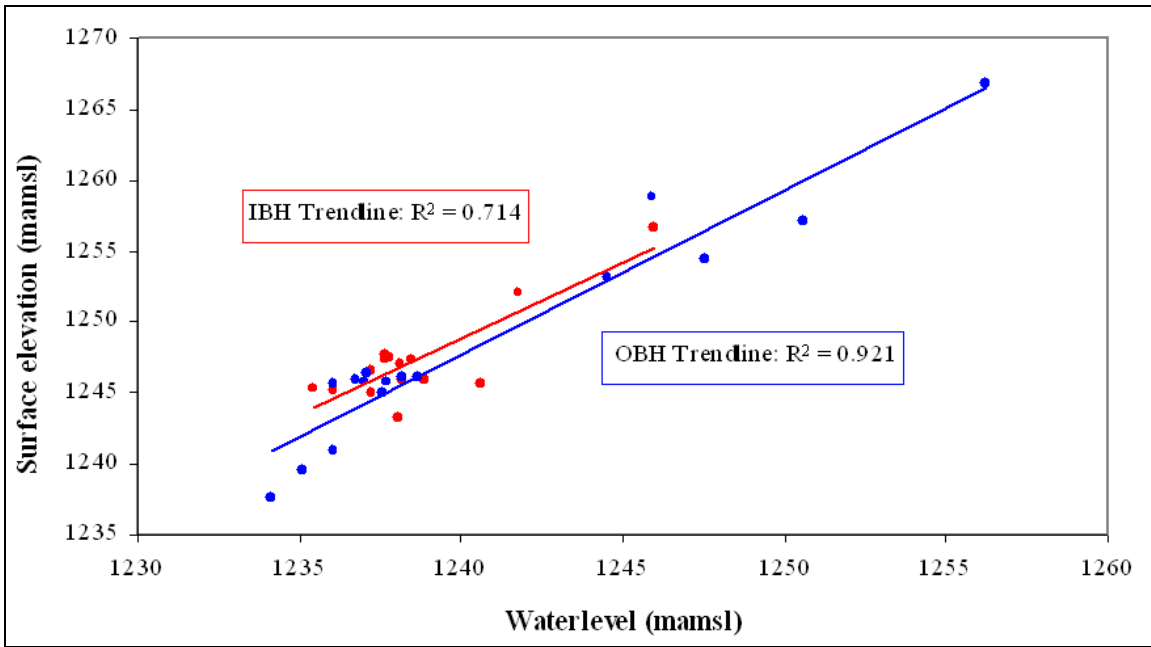


Figure 7.2.3(A). Correlation between water level and topography in all boreholes.

Not only do IBH boreholes have a lowered water level, but also all the OBH boreholes in the vicinity of the pit. When OBH boreholes whose water levels are influenced by the pit are omitted, the regression between the surface elevation (mamsl) and the water level elevation (mamsl) increases to 0.994 as shown in **Figure 7.3.2.2(B)**. The boreholes omitted, namely OBH-3, 4, OBH-8 to 11 and OBH-13 to 16, are all situated closer than 20 m to the pits. The selected boreholes, OBH-1, 2, 5, 6, 7 and 12, are situated between 60 m to 175 m from the pits.

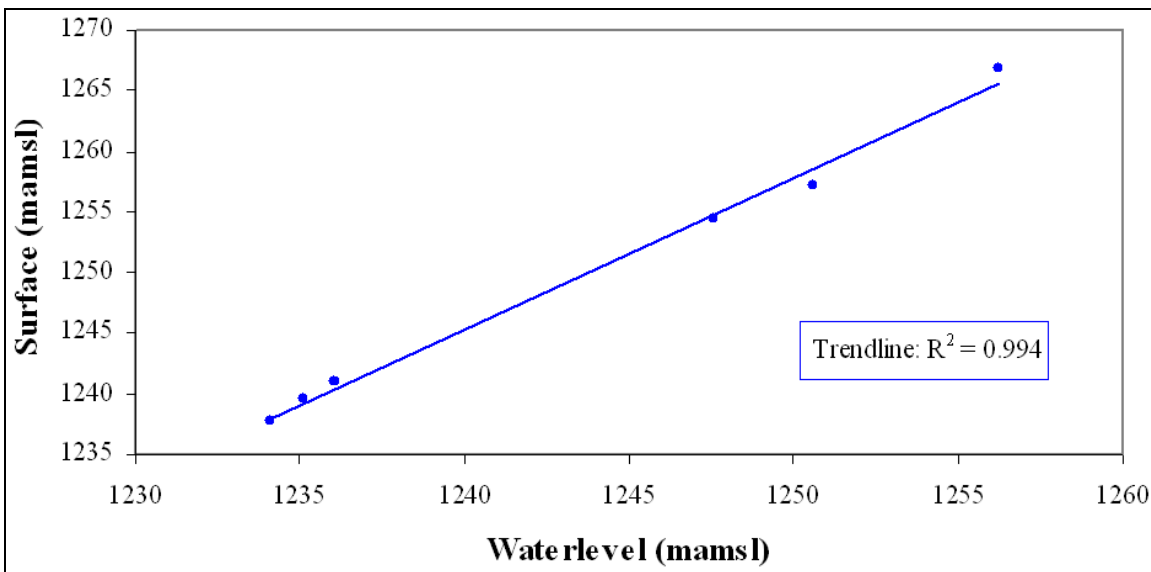


Figure 7.2.3(B). Correlation between water level and topography in selected OBH boreholes.

7.2.4 Background groundwater chemistry

A representative background groundwater chemistry of the Karoo aquifer could only be found from some of the OBH boreholes since all the IBH boreholes are elevated in the products of acid mine drainage. The background groundwater quality will be needed as input for the geochemical model in **Section 7.4**.

A total of 78 samples were taken from the 16 OBH boreholes over 7 sample runs. One sample run on OBH-1 to 7 was performed during 1996 and six on all boreholes from 2003. However, not all boreholes were sampled and not all parameters were analyzed for every time. The chemical analyses of the 78 samples are given in **Table 7.2.4(A)** below:

Table 7.2.4.(A). Hydro-chemical samples taken from the OBH boreholes.

Date of sampling	Borehole Nr.	pH	EC (mS/m)	TDS (mg/l)	Ca (mg/l)	Mg (mg/l)	Na (mg/l)	K (mg/l)	Si (mg/l)	Total Alkalinity as CaCO ₃ (mg/l)	Cl (mg/l)	SO ₄ (mg/l)	N (mg/l)	F (mg/l)	Al (mg/l)	Fe (mg/l)	Mn (mg/l)
19960528	OBH-1	7.00	66.0	432.0	50.0	25.0	67.0	4.4	0.9	370.0	10.0	<3.0	0.30	0.30		0.570	0.316
20030714	OBH-1	7.80	64.6	314.0	24.0	30.0	62.0	2.7	14.7	324.0	12.0	<5.0	<0.20	0.30	0.335	14.000	0.200
20031006	OBH-1	7.80		374.0	35.0							12.0	<0.20			18.000	0.220
20040119	OBH-1	7.80	65.0	368.0	37.0	31.0	60.0	2.2	17.6	352.0	11.0	<5.0	<0.20	0.30	<0.100	13.000	0.172
20040405	OBH-1	7.70		400.0	53.0							<5.0	<0.20			14.000	0.119
20040721	OBH-1	7.80	68.1	402.0	55.0	28.0	67.0	2.0	17.0	376.0	10.0	<5.0	<0.20	<0.20	0.584	14.000	0.179
20041021	OBH-1	7.50		350.0	40.0							<5.0	<0.20			15.000	0.141
19960528	OBH-2	6.35	44.0	290.0	34.0	17.0	23.0	10.0	0.9	160.0	31.0	24.0	0.50	<0.20		9.600	1.051
20030714	OBH-2	6.90	10.6	66.0	6.0	<2.0	11.0	4.5	8.1	40.0	<5.0	<5.0	<0.20	<0.20	<0.100	23.000	1.020
19960527	OBH-3	7.05	71.0	472.0	34.0	17.0	111.0	5.5	0.9	295.0	36.0	66.0	0.40	0.40		0.360	0.102
20030714	OBH-3	8.00	117.0	610.0	54.0	31.0	142.0	7.9	4.8	240.0	219.0	13.0	<0.20	<0.20	0.325	33.000	0.839
20031006	OBH-3	7.60		696.0	56.0							9.0	<0.20			16.000	0.711
20040120	OBH-3	7.40	107.0	634.0	50.0	35.0	122.0	7.2	5.6	216.0	213.0	<5.0	<0.20	<0.20	<0.100	9.840	0.479
20040406	OBH-3	7.00		608.0	45.0							17.0	<0.20			1.260	0.654
20040721	OBH-3	7.30	128.0	704.0	64.0	36.0	145.0	15.0	8.8	320.0	197.0	<5.0	<0.20	<0.20	5.300	143.000	3.830
20041021	OBH-3	7.60		582.0	53.0							6.0	<0.20			13.000	0.426
19960527	OBH-4	6.65	209.0	1138.0	196.0	66.0	98.0	13.6	0.9	285.0	375.0	14.0	0.30	0.60		7.600	1.225
20030714	OBH-4	6.90	184.0	1154.0	144.0	65.0	114.0	11.1	16.1	204.0	447.0	7.0	<0.20	<0.20	<0.100	48.000	0.446
20031006	OBH-4	6.90		1510.0	79.0							10.0	<0.20			46.000	0.504
20040120	OBH-4	7.00	182.0	1358.0	135.0	73.0	121.0	12.2	17.1	272.0	442.0	<5.0	<0.20	<0.20	<0.100	49.000	0.403
20040406	OBH-4	6.80		1180.0	128.0							32.0	<0.20			11.000	0.357
20040721	OBH-4	7.50	191.0	1240.0	152.0	73.0	130.0	12.1	15.7	308.0	428.0	<5.0	<0.20	<0.20	<0.100	32.000	0.345
20041021	OBH-4	7.30		1066.0	131.0							7.0	<0.20			30.000	0.310
19960527	OBH-5	7.05	153.0	838.0	100.0	38.0	108.0	6.6	0.9	275.0	275.0	20.0	0.30	0.30		0.610	0.361
20030714	OBH-5	7.70	135.0	704.0	70.0	37.0	108.0	6.8	17.9	260.0	257.0	<5.0	<0.20	<0.20	<0.100	14.000	0.245
20031006	OBH-5	7.70		852.0	83.0							7.0	<0.20			18.000	0.290

Table 7.2.4.(A). Hydro-chemical samples taken from the OBH boreholes...continued

Date of sampling	Borehole Nr.	pH	EC (mS/m)	TDS (mg/l)	Ca (mg/l)	Mg (mg/l)	Na (mg/l)	K (mg/l)	Si (mg/l)	Total Alkalinity as CaCO ₃ (mg/l)	Cl (mg/l)	SO ₄ (mg/l)	N (mg/l)	F (mg/l)	Al (mg/l)	Fe (mg/l)	Mn (mg/l)
20040120	OBH-5	7.70	131.0	844.0	87.0	49.0	121.0	6.5	17.1	276.0	260.0	<5.0	<0.20	<0.20	<0.100	7.280	0.207
20040406	OBH-5	7.60		750.0	79.0							<5.0	<0.20			2.370	0.137
20040721	OBH-5	7.90	134.0	756.0	100.0	36.0	128.0	5.9	16.2	288.0	257.0	<5.0	<0.20	<0.20	<0.100	8.110	0.225
20041021	OBH-5	7.70		736.0	99.0							<5.0	<0.20			10.000	0.211
20030729	OBH-9	3.60	412.0	4256.0	488.0	259.0	208.0	18.5	7.0	<5.0	34.0	2743.0	0.30	<0.20	<0.100	117.000	20.000
20031003	OBH-9	3.60		3842.0	449.0							2453.0	0.40			114.000	12.000
20040119	OBH-9	4.50	368.0	4044.0	480.0	240.0	203.0	14.0	7.3	<5.0	44.0	2420.0	<0.20	<0.20	<0.100	157.000	11.000
20040406	OBH-9	3.00		3782.0	449.0							2260.0	<0.20			122.000	9.150
20040721	OBH-9	3.70	367.0	3770.0	441.0	243.0	217.0	12.6	5.1	<5.0	62.0	2532.0	<0.20	<0.20	<0.100	148.000	9.020
20041021	OBH-9	3.90		2988.0	485.0							115.0	<0.20			64.000	7.910
20030729	OBH-10	2.90	508.0	5190.0	460.0	324.0	264.0	16.5	13.6	<5.0	39.0	3439.0	<0.20	<0.20	0.135	343.000	45.000
20031003	OBH-10	2.90		5176.0	462.0							3257.0	0.50			250.000	28.000
20040119	OBH-10	4.30	443.0	5190.0	552.0	269.0	231.0	16.2	12.0	<5.0	48.0	3293.0	<0.20	<0.20	0.256	388.000	30.000
20040406	OBH-10	2.60		4498.0	453.0							2977.0	<0.20			288.000	17.000
20040721	OBH-10	2.70	483.0	4670.0	489.0	287.0	246.0	15.2	8.5	<5.0	38.0	3279.0	<0.20	<0.20	0.125	333.000	25.000
20041021	OBH-10	3.80		4790.0	490.0							64.0	<0.20			257.000	23.000
20030729	OBH-11	2.90	512.0	5136.0	500.0	336.0	298.0	14.7	6.5	<5.0	41.0	3428.0	0.40	<0.20	<0.100	215.000	41.000
20031003	OBH-11	3.20		5306.0	481.0							3080.0	0.30			231.000	38.000
20040120	OBH-11	3.50	485.0	5454.0	480.0	346.0	264.0	14.5	11.7	<5.0	59.0	3487.0	<0.20	<0.20	<0.100	379.000	44.000
20040406	OBH-11	2.70		5166.0	477.0							3117.0	<0.20			349.000	46.000
20040721	OBH-11	2.60	533.0	5038.0	465.0	345.0	287.0	13.7	8.1	<5.0	59.0	3200.0	<0.20	<0.20	0.168	336.000	38.000
20041021	OBH-11	3.10		5276.0	515.0							69.0	<0.20			253.000	41.000
20030729	OBH-12	7.70	106.0	606.0	82.0	34.0	86.0	5.5	15.1	296.0	143.0	9.0	<0.20	<0.20	0.104	7.890	0.282
20031003	OBH-12	7.70		652.0	66.0							<5.0	<0.20			13.000	0.291
20040120	OBH-12	7.60	101.0	616.0	76.0	32.0	101.0	6.1	15.1	292.0	164.0	<5.0	<0.20	<0.20	<0.100	14.000	0.174
20040406	OBH-12	7.60		468.0	45.0							<5.0	<0.20			1.560	0.070

Table 7.2.4.(A). Hydro-chemical samples taken from the OBH boreholes...continued

Date of sampling	Borehole Nr.	pH	EC (mS/m)	TDS (mg/l)	Ca (mg/l)	Mg (mg/l)	Na (mg/l)	K (mg/l)	Si (mg/l)	Total Alkalinity as CaCO ₃ (mg/l)	Cl (mg/l)	SO ₄ (mg/l)	N (mg/l)	F (mg/l)	Al (mg/l)	Fe (mg/l)	Mn (mg/l)
20040721	OBH-12	7.80	70.1	362.0	13.0	23.0	87.0	4.7	0.3	88.0	160.0	<5.0	<0.20	<0.20	<0.100	15.000	0.069
20041021	OBH-12	7.70		420.0	55.0							<5.0	<0.20			13.000	0.107
20030729	OBH-13	3.50	454.0	4934.0	460.0	336.0	197.0	13.0	7.6	<5.0	16.0	3166.0	0.30	<0.20	0.158	233.000	35.000
20031003	OBH-13	3.20		4596.0	449.0							3202.0	0.30			221.000	26.000
20040119	OBH-13	4.30	386.0	4232.0	480.0	312.0	224.0	10.5	6.4	<5.0	10.0	2733.0	<0.20	<0.20	<0.100	227.000	17.000
20040406	OBH-13	2.80		3908.0	437.0							2373.0	<0.20			174.000	19.000
20040721	OBH-13	3.20	432.0	4444.0	457.0	292.0	207.0	10.2	5.5	<5.0	33.0	2820.0	<0.20	<0.20	0.148	235.000	20.000
20041021	OBH-13	3.50		4108.0	481.0							2757.0	<0.20			204.000	7.600
20030729	OBH-14	3.10	470.0	4882.0	480.0	324.0	167.0	9.6	12.8	<5.0	13.0	3275.0	0.40	<0.20	0.101	181.000	26.000
20031003	OBH-14	3.20		4960.0	457.0							3368.0	0.50			260.000	27.000
20040119	OBH-14	3.90	365.0	4050.0	400.0	252.0	190.0	10.1	7.0	<5.0	16.0	2693.0	<0.20	<0.20	0.245	259.000	9.600
20040406	OBH-14	3.00		3804.0	441.0							2251.0	<0.20			257.000	9.700
20040721	OBH-14	3.10	374.0	3746.0	381.0	245.0	166.0	7.3	3.7	<5.0	19.0	2535.0	0.30	<0.20	0.169	0.793	8.810
20041021	OBH-14	3.80		3554.0	353.0							2612.0	<0.20			250.000	11.000
20030729	OBH-15	3.20	391.0	3968.0	440.0	276.0	109.0	6.8	9.9	<5.0	10.0	2620.0	0.40	<0.20	0.148	177.000	19.000
20031003	OBH-15	2.80		4068.0	465.0							2703.0	<0.20			158.000	10.000
20040119	OBH-15	3.70	360.0	3790.0	460.0	264.0	164.0	8.0	12.5	<5.0	12.0	2701.0	<0.20	<0.20	0.127	227.000	9.840
20040406	OBH-15	3.40		3694.0	461.0							2152.0	<0.20			200.000	13.000
20040721	OBH-15	3.40	355.0	3648.0	417.0	228.0	139.0	6.6	3.8	<5.0	24.0	2641.0	<0.20	<0.20	0.181	189.000	5.070
20041021	OBH-15	3.60		3696.0	481.0							2646.0	<0.20			247.000	4.100
20030729	OBH-16	8.10	99.4	726.0	94.0	47.0	55.0	4.7	6.9	224.0	7.0	317.0	<0.20	0.30	0.231	34.000	1.750
20031003	OBH-16	6.70		1022.0	117.0							509.0	<0.20			1.290	1.010
20040119	OBH-16	7.10	107.0	850.0	96.0	60.0	77.0	4.2	10.7	176.0	7.0	419.0	<0.20	0.40	<0.100	33.000	0.331
20040406	OBH-16	7.40		658.0	80.0							292.0	<0.20			27.000	0.667
20040721	OBH-16	7.90	95.3	680.0	67.0	57.0	64.0	3.2	4.6	188.0	6.0	353.0	<0.20	<0.20	0.237	14.000	0.194
20041021	OBH-16	7.90		706.0	64.0							317.0	0.30			11.000	0.078

7.2.4.1 Classification of samples taken from the OBH boreholes

Before the selection of the background hydro-chemistry, a classification of the samples from OBH boreholes was done on the basis of the pH, sulphate and chloride analyses. It seems reasonable to use these parameters for classification of the samples since acidity and sulphate are direct products of pyrite oxidation and would indicate any significant AMD related impact; chloride shows variation in the shallow aquifer as a result of evaporation and transpiration (Bredenkamp et al., 1995; Woodward and Chevallier, 2002; Appello and Postma, 1993).

Only 42 of the 78 samples have been analyzed for all three of the above hydro-chemical parameters. **Table 7.2.4.1(A)** indicates the variations in the water quality of the OBH boreholes. Note that only the 42 samples with full analysis are counted in the columns and that the numbers in brackets indicate the total amount of samples taken from the specific borehole.

Table 7.2.4.1(A). Variation in 42 OBH hydro-chemical samples.*

pH		Neutral to alkaline pH > 6			Acidic pH < 4.5
		High Cl (> 143 mg/l)	Low Cl (< 36 mg/l)		Low Cl (< 62 mg/l)
Sulphate		Low SO ₄ (< 32 mg/l)	Low SO ₄ (< 66 mg/l)	Intermediate SO ₄ (317 - 419 mg/l)	High SO ₄ (2420 - 3487 mg/l)
Number of OBH Borehole Samples*	OBH-1 (7)		4		
	OBH-2 (2)		2		
	OBH-3 (7)	3	1		
	OBH-4 (7)	4			
	OBH-5 (7)	4			
	OBH-9 (6)				3
	OBH-10 (6)				3
	OBH-11 (6)				3
	OBH-12 (6)	3			
	OBH-13 (6)				3
	OBH-14 (6)				3
	OBH-15 (6)				3
	OBH-16 (6)			3	
	Total = 42 (78)	14	7	3	18

* Only 42 samples with measured Cl, SO₄ and pH are listed, numbers in brackets indicate the total amount of samples taken from the borehole.

From the above table the following observations could be made:

- A classification of the hydro-chemical samples in terms of pH, chloride and sulphate seems reasonable since samples from the same boreholes plot within the same groups over all the sample runs (except one sample of OBH-3).
- None of the OBH samples have a pH of between pH 4.5 and pH 6.4 which is attributed to the lack of buffering capacity in this pH range.
- A total of 24 samples have a pH of above pH 6.4. None of these samples show chloride values of between 36 mg/l and 143 mg/l and the samples were classified as having either a low or high chloride content.

All samples (14) with high chloride (> 143 mg/l) have a low sulphate (< 32 mg/l) content which indicate that these boreholes have not been impacted by drainage from the mine. Boreholes that fall in this group are OBH-3, -4, -5 and -12 and are situated southeast and east of the pit. This group was identified as unpolluted aquifer water with chloride and sodium as the respective dominant anion and cation. The samples were regarded not as recently recharged water due to their high chloride content.

Ten samples with a low chloride content (< 36 mg/l) are further classified in terms of their sulphate content:

- Seven samples with a low sulphate content (< 66 mg/l) indicate that they have not (significantly at least) been impacted by drainage from the mine. This group was identified as unpolluted and as more recently recharged water (compared to the high chloride water discussed above). Boreholes that fall within this group are OBH-1 and OBH-2 as well as one sample of OBH-3. These boreholes are situated southeast and east of the pit.
- Three samples that have an intermediate sulphate content (317 mg/l - 419 mg/l) are all from borehole OBH-16 which is situated in the berm between the pit and the adjacent river. This borehole shows definite impact from drainage from the pit.
- A total of 18 samples have a pH of below pH 4.5. These samples all have a high sulphate content (2420 mg/l to 3487 mg/l) which shows that they have been directly impacted by the acidic drainage from the mine. Boreholes that fall within this group are OBH-9, 10, 11, 13, 14 and 15 and all of them are situated in the berm between the Southern Pit and the adjacent river. This is an indication of the poor drainage quality through the berm towards the river.

After the OBH samples have been classified in terms of their water quality, it became evident that the background chemistry can only be from the two unpolluted groups (pH > 6, low sulphate) with respectively low chloride and high chloride content. The cation/anion dominance of these two unpolluted groups was assessed below at the hand of Piper and extended Durov plots.

The unpolluted, high chloride group (OBH-3, -4, -5 and -12)

Piper- and Extended Durov plots of the samples are depicted as **Figure 7.2.4.1(A)** and **(B)** below:

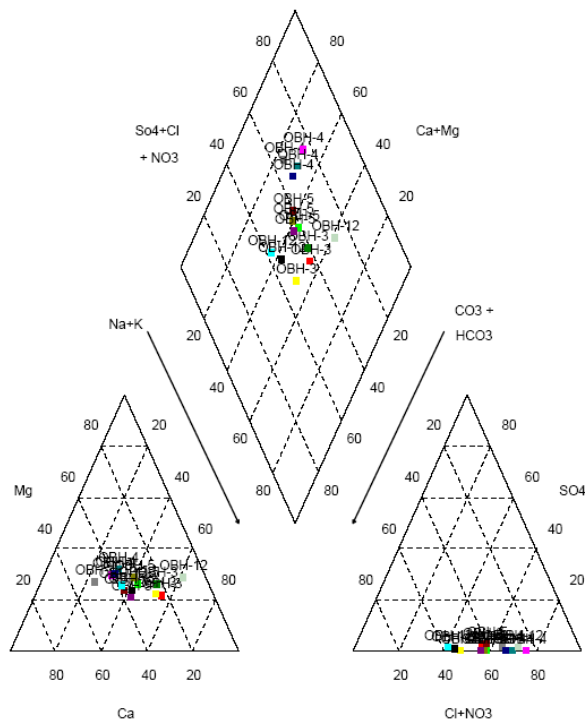


Figure 7.2.4.1(A). Piper diagram of the unpolluted, high chloride group.

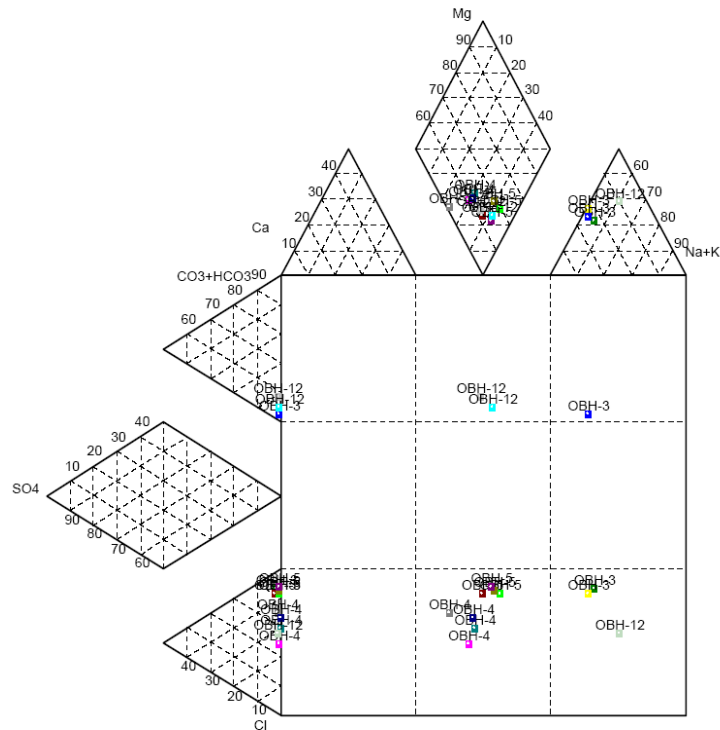


Figure 7.2.4.1(B). Extended durov plot of the unpolluted, high chloride group.

Samples show chloride as the dominant anion (the chloride equivalence ranges between 60% - 80% and the bicarbonate between 20% - 40%) except for borehole OBH-12 that shows both chloride and bicarbonate as dominant anions (chloride 40% - 50% and bicarbonate 50% - 55%). In all samples sulphate, fluoride and nitrate in equivalent units are less than 2% of the total anions. All of these borehole samples can be classified as background groundwater since no evidence could be found of any mining related (or other) impact.

These samples show either calcium (20% – 50%) or sodium (20% - 55%) as the dominant cations (in equivalent units), while magnesium (20% - 35%) is also a major cation specie. In all samples potassium in equivalent units made up less than 2% of the cations.

The unpolluted, low chloride group (OBH-1, -2, and -3)

Piper- and Extended Durov plots of the samples are depicted as **Figure 7.2.4.1(C)** and **(D)** below:

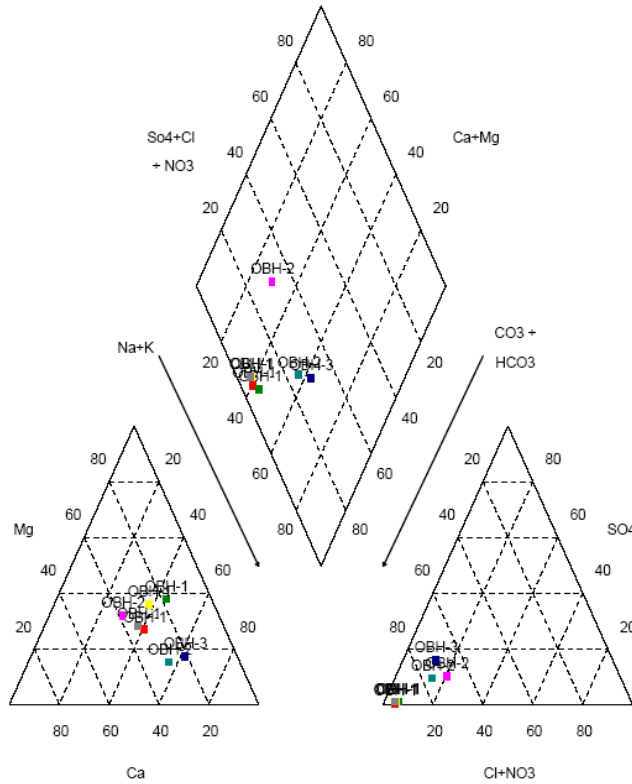


Figure 7.2.4.1(C). Piper diagram of the unpolluted, low chloride group.

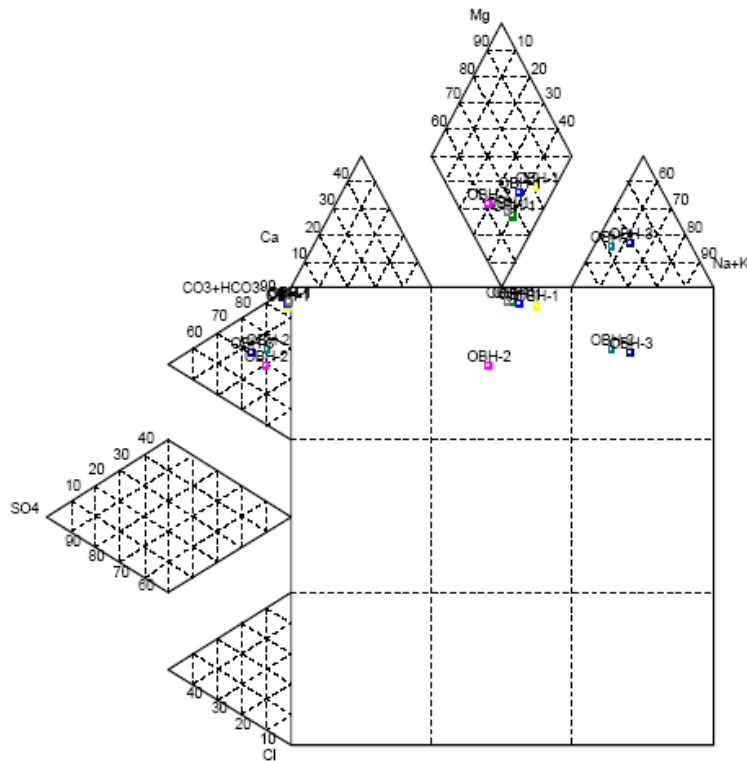


Figure 7.2.4.1(D). Extended durov plot of the unpolluted, low chloride group.

Samples from OBH-1 show similar chemistry in all sample runs and plot within the same area on the chemistry diagrams above. The samples of OBH-1 show bicarbonate as the dominant anion (93% - 95%) in equivalent units. Chloride is a minor anion (4% - 5%) and in all samples sulphate, fluoride and nitrate in equivalent units are less than 2% of the anions. The samples show sodium (36% - 42%), magnesium (27% - 38%) and calcium (19% - 33%) as major cations in equivalent units, while potassium is less than 2% of the cations. All the samples of OBH-1 can be classified as background groundwater since no evidence could be found of any mining related (or other) impact.

Samples from OBH-2 and 3 show sulphate as a minor anion (6% - 10%). However these samples except for one sample of OBH-2 were discarded as background chemistry because sulphate is the dominant anion. The other sample of OBH-2 was included in the background chemistry together with OBH-1 because its sulphate concentration was below detection limit (both < 5 mg/l) and the anion dominance is rather similar to that of OBH-1 with bicarbonate as the dominant anion. The Piper plot will be slightly inaccurate for this sample as the anion dominance was calculated from the detection limit of 5 mg/l for both sulphate and chloride while it will probably be less in reality.

7.2.4.2 Background groundwater chemistry of the Karoo aquifer

In the above section two groups have been identified that are representing the background groundwater chemistry. The ranges in the hydro-chemistry for each group are given in **Table 7.2.4.2(A)** and **(B)** below:

Table 7.2.4.2(A). Background groundwater with high chloride.

Parameters	Minimum (mg/l)	Maximum (mg/l)	Average (mg/l)
pH*	6.7	8.0	7.4
EC (mS/m)	70.1	209.0	139.2
TDS	362.0	1358.0	826.0
Ca	13.0	196.0	94.5
Mg	23.0	73.0	44.9
Na	86.0	145.0	115.1
K	4.7	15.0	8.7
Si	0.3	17.9	10.8
Total Alkalinity as CaCO ₃	88.0	320.0	258.6
Cl	143.0	447.0	274.1

SO ₄	5.0	20.0	7.7
NO ₃ as N	<0.2	0.3	<0.2
F	<0.2	0.6	<0.2
Al [#]	0.1	5.3	0.6
Fe [#]	0.6	143.0	27.8
Mn [#]	0.1	3.8	0.7

* log(geometric mean[H⁺]), # Sample acidified before filtration.

Table 7.2.4.2(B). Background groundwater samples with low chloride (four samples of borehole OBH-1^a and one sample of OBH-2).

Parameters (mg/l)	Minimum (4 OBH-1 samples) ^a (mg/l)	Maximum (4 OBH-1 samples) ^a (mg/l)	Average (4 OBH-1 samples) ^a (mg/l)	Sample OBH-2 (20030714) (mg/l)
pH ^b	7.0	7.8	7.6	6.9
EC (mS/m)	64.6	68.1	65.9	10.6
TDS	314.0	432.0	379.0	66.0
Ca	24.0	55.0	41.5	6.0
Mg	25.0	31.0	28.5	2.0
Na	60.0	67.0	64.0	11.0
K	2.0	4.4	2.8	4.5
Si	0.9	17.6	12.6	8.1
Total Alkalinity as CaCO ₃	324.0	376.0	355.5	40.0
Cl	10.0	12.0	10.8	5.0
SO ₄	3.0	5.0	4.5	5.0
NO ₃ as N	<0.2	0.3	<0.2	<0.2
F	<0.2	0.3	0.3	<0.2
Al ^c	0.1	0.6	0.3	0.1
Fe ^c	0.6	14.0	10.4	23.0
Mn ^c	0.2	0.3	0.2	1.0

^a The four OBH-1 samples were taken at 19960528, 20030714, 20040119, 20040721 respectively and have a complete set of chemical analyses.

^b log(geometric mean[H⁺]).

^c Sample acidified before filtration.

The following observations are made from **Table 7.2.4.2(A)** and **(B)**:

- Major cations present in the Karoo background groundwater are sodium, magnesium, calcium and potassium. Major anions are alkalinity and chloride. The background groundwater quality was classified as having either a low or high Cl

content. The two types of background groundwater could be distinguished in terms of their anion concentrations and also their anion dominance using a piper plot.

- The background samples were selected in order not to include any impact/contamination by any unnatural source: 1) no sample has elevated sulphate that would indicate any AMD related impact, 2) nitrate (as N) and fluoride are below 1 mg/l in the background hydro-chemistry and no agricultural/human impact are therefore also evident.
- Aluminium, iron and manganese values are variable in the background hydro-chemistry and especially iron is often elevated. This is a result of the acidification of the samples before they went to the laboratory where they were filtrated and analysed. The elevation in iron in the backgroundwater is not due to any mining related impact; to illustrate this point, a sample of OBH-3 shows iron at 143 mg/l and sulphate at <5 mg/l. Acidification of samples before filtration (and not vice versa which would be the correct method) results in the mobilization of these metals from the suspended soil particles.

7.3 Hydrological and hydro-chemical assessment of AMD seepage

7.3.1 Soil moisture distribution and AMD seepage volume from the unsaturated zone

Software used

The software Visual HELP 2.2 (HELP = Hydrological Evaluation of Landfill Performance), was used in order to calculate the soil moisture distribution and recharge through the unsaturated zone.

HELP is a versatile U.S. EPA model for predicting landfill hydrologic processes and testing the effectiveness of landfill designs, enabling the prediction of landfill design feasibility. HELP has become a requirement for obtaining landfill operation permits in the U.S.A. HELP could also be used in estimating groundwater recharge.

Input

The Visual HELP 2.2 model uses 1) the local climatic data (rainfall, temperature, solar radiation and evaporation information) and 2) the layer properties (slope, hydraulic conductivity, and porosity, field capacity and wilting point) to determine the daily amount of evaporation, runoff, recharge/infiltration and the moisture retention curve.

The rainfall and temperature data were obtained from the nearest weather station in Newcastle. The rainfall data is also depicted in **Figure 7.3.2(E)**. The solar radiation was determined by the Visual HELP 2.2 program for the given latitude. Evaporation and humidity data was taken from the Visual HELP 2.2 database for the Estcourt area in Natal. The slope of the site was determined in **Section 7.2.2** above. The porosity, field capacity and wilting point of the material was taken from Wates and Rykaart (1999) for sandy loam soil and compacted coal discard and is specified for each layer in **Table 7.3.1(A)**.

The average depth of the profile was set at 12 m below surface. Only 20 vertical layers can be defined in Visual HELP 2.2. All layers were classified as vertical percolation layers in the Visual HELP 2.2 model which means that they are unsaturated and water is allowed to percolate through them.

Because the program calculates the moisture content per layer, layers must be thinner in the section where the value of the moisture contents is the most variable - the moisture content will vary more in the topsoil layer due to evapotranspiration. Therefore, the 1 m compacted sand-loam was defined as 8 separate layers with a thickness of 0.125 m each. The waste rock and discard immediately underneath the soil were defined in 4 separate layers of 0.25 m thick each, and the underlying discard was separated in 6 more layers

with a thickness of 1.5 m each and a final layer of 1 m thick to give the profile a total vertical depth of 12 m deep.

Results from the Visual HELP 2.2 simulation

The Visual HELP 2.2 model was run over 10 years in order to obtain representative steady state output. **Table 7.3.1(A)** gives the calculated runoff, evaporation and seepage through the waste rock.

Table 7.3.1(A). 10 Year average annual runoff, evaporation and seepage.

Parameter	Water make/loss per m ² (mm)	% of average precipitation
Precipitation	846.11	100.00
Run-off	2.37	0.28
Evapotranspiration	668.62	79.02
Seepage to water table	173.42	20.50
Change in water storage	1.69	0.20

The moisture content of the layers was computed as nearly steady-state values by the program. **Table 7.3.1(B)** below gives the moisture content and also summarizes the other specified characteristics for every layer.

Table 7.3.1(B). Layer characteristics of the Visual HELP 2.2 profile.

Layer	Depth to bottom (m)	Thickness (m)	Porosity	Field Capacity	Wilting Point	Steady state water content (%)	Saturated Hydraulic Conductivity (m/d)
1	0.125	0.125	0.330	0.235	0.120	20.180	0.314
2	0.250	0.125	0.330	0.235	0.120	20.710	0.314
3	0.375	0.125	0.330	0.235	0.120	18.630	0.314
4	0.500	0.125	0.330	0.235	0.120	20.400	0.314
5	0.625	0.125	0.330	0.235	0.120	23.470	0.314
6	0.750	0.125	0.330	0.235	0.120	23.470	0.314
7	0.875	0.125	0.330	0.235	0.120	23.470	0.314
8	1.000	0.125	0.330	0.235	0.120	23.480	0.314
9	1.250	0.250	0.300	0.090	0.025	8.980	3.860
10	1.500	0.250	0.300	0.090	0.025	8.980	3.860
11	1.750	0.250	0.300	0.090	0.025	8.980	3.860
12	2.000	0.250	0.300	0.090	0.025	8.980	3.860
13	3.500	1.500	0.300	0.090	0.025	8.970	3.860
14	5.000	1.500	0.300	0.090	0.025	8.970	3.860
15	6.500	1.500	0.300	0.090	0.025	8.970	3.860

16	8.000	1.500	0.300	0.090	0.025	8.970	3.860
17	9.400	1.500	0.300	0.090	0.025	8.960	3.860
18	11.000	1.500	0.300	0.090	0.025	8.950	3.860
19	12.000	1.000	0.300	0.090	0.025	8.970	3.860

The following comments and conclusions are made with regard to **Table 7.3.1(A)** and **(B)**:

- The first meter consists of sandy loam that was separated into 8 layers. The first 0.5 m is subjected to evapotranspiration and the steady state moisture content is just below the field capacity and ranges between 18.63 and 20.71. From 0.5 m to 1 m the steady state moisture content in the soil is almost at field capacity (0.235).
- The steady state moisture content for the underlying waste rock and discard is also almost at field capacity (0.09).
- The moisture content is an important parameter in terms of the oxygen diffusion through the unsaturated zone. It is important to note that the topsoil layer plays the most important part in the storage of moisture and in obstructing oxygen infiltration. The total porosity of the soil is at 0.34 and the bulk soil volume will contain 18.63% - 23.50% of water. The coal discard has a porosity of 0.30, but in contrast will only contain about 9% water in its bulk volume.
- Most precipitation is lost as evapotranspiration or ends up as seepage to the water table in the pit.

7.3.2 Hydro-chemistry of generated AMD

The IBH boreholes are the only source of direct hydro-chemical information of acidic generated drainage. No surface decant point is present that could be used to measure the “average” decant quality emanating from the pit. Although surface water samples have historically been taken in the adjacent river, the river is not an accurate measurement of the drainage quality from the pit because of the unknown dilution of mine water seepage into the river.

Samples have been taken from IBH boreholes during seven sample runs. However, some boreholes have been found dry or obstructed at times and were not sampled. In total only 66 samples were taken from in-pit boreholes. The analyses of the samples are listed in **Table 7.3.2(A)** below:

Table 7.3.2(A). Hydro-chemical samples taken from the IBH boreholes.

Date of sampling	Borehole Nr.	pH	EC (mS/m)	TDS (mg/l)	Ca (mg/l)	Mg (mg/l)	Na (mg/l)	K (mg/l)	Si (mg/l)	Total Alkalinity as CaCO ₃ (mg/l)	Cl (mg/l)	SO ₄ (mg/l)	N (mg/l)	F (mg/l)	Al (mg/l)	Fe (mg/l)	Mn (mg/l)
20031006	IBH-1	2.70		5238.0	481.0							3532.0	0.40			252.000	41.000
19960527	IBH-2	3.65	563.0	3971.0	2.0	1.0	51.0	10.4	0.9		<5.0	1967.0	0.40	3.50		28.000	60.000
20030714	IBH-2	3.60	764.0	10570.0	475.0	568.0	278.0	10.8	2.5	<5.0	19.0	6964.0	0.50	0.30	159.000	1554.000	46.000
20031006	IBH-2	2.80		8986.0	502.0							5722.0	<0.20			966.000	46.000
19960527	IBH-3	6.75	615.0	4744.0	595.0	240.0	620.0	13.5	0.9	365.0	32.0	2875.0	3.80	1.40		5.200	7.100
20030714	IBH-3	3.90	610.0	7408.0	462.0	595.0	280.0	14.9	8.0	<5.0	49.0	4955.0	0.60	<0.20	0.240	494.000	62.000
20031006	IBH-3	6.80		5216.0	385.0							3220.0	0.30			244.000	2.520
20040120	IBH-3	6.40	482.0	4942.0	348.0	283.0	621.0	13.9	5.5	80.0	10.0	3424.0	0.40	<0.20	0.248	688.000	12.000
20040406	IBH-3	7.10		4998.0	349.0							3038.0	<0.20			25.000	0.588
20040721	IBH-3	6.20	482.0	4846.0	329.0	287.0	634.0	10.8	6.1	32.0	15.0	3311.0	<0.20	<0.20	5.630	300.000	2.170
19960528	IBH-4	6.00	627.0	5260.0	1005.0	285.0	178.0	14.1	0.9	88.0	17.0	3405.0	0.40	2.30		386.000	43.000
20030715	IBH-4	8.40	83.5	498.0	12.0	34.0	111.0	1.9	2.5	176.0	56.0	152.0	<0.20	<0.20	0.130	3.380	0.336
20031006	IBH-4	7.80		660.0	35.0							295.0	<0.20			6.200	0.600
20040119	IBH-4	8.30	88.7	546.0	10.0	41.0	122.0	2.2	0.9	136.0	59.0	231.0	<0.20	<0.20	0.183	2.620	0.335
20040405	IBH-4	8.60		604.0	4.0							193.0	<0.20			0.593	0.194
20040721	IBH-4	7.50	115.0	742.0	52.0	49.0	142.0	6.8	1.9	236.0	51.0	318.0	<0.20	<0.20	0.103	7.630	1.390
20041021	IBH-4	8.20		558.0	11.0							153.0	<0.20			2.260	0.110
19960527	IBH-5	5.55	683.0	5959.0	1005.0	360.0	171.0	17.3	0.9	60.0	15.0	3790.0	0.40	1.70		380.000	46.000
20030715	IBH-5	7.60	494.0	5028.0	385.0	345.0	611.0	11.3	4.5	168.0	12.0	3182.0	<0.20	<0.20	33.000	328.000	1.580
20031003	IBH-5	3.60		9540.0	401.0							6528.0	0.40			611.000	113.000
20040119	IBH-5	4.50	580.0	7410.0	499.0	494.0	305.0	18.3	10.5	<5.0	44.0	4621.0	<0.20	<0.20	0.245	623.000	65.000
20040405	IBH-5	3.40		7558.0	401.0							4374.0	<0.20			615.000	69.000
20040721	IBH-5	3.50	608.0	7220.0	474.0	544.0	329.0	18.5	9.5	<5.0	59.0	4916.0	<0.20	<0.20	1.390	564.000	72.000
20041021	IBH-5	3.10		7126.0	432.0							4810.0	<0.20			648.000	73.000
19960527	IBH-6	5.75	716.0	6142.0	1010.0	335.0	216.0	22.0	0.9	80.0	36.0	4210.0	0.60	1.30		446.000	52.000
20030715	IBH-6	7.30	64.6	438.0	42.0	31.0	41.0	2.6	0.5	48.0	23.0	230.0	<0.20	1.10	8.690	136.000	3.850

Table 7.3.2(A). Hydro-chemical samples taken from the IBH boreholes...continued

Date of sampling	Borehole Nr.	pH	EC (mS/m)	TDS (mg/l)	Ca (mg/l)	Mg (mg/l)	Na (mg/l)	K (mg/l)	Si (mg/l)	Total Alkalinity as CaCO ₃ (mg/l)	Cl (mg/l)	SO ₄ (mg/l)	N (mg/l)	F (mg/l)	Al (mg/l)	Fe (mg/l)	Mn (mg/l)
20031003	IBH-6	6.60		478.0	449.0							283.0	<0.20			30.000	1.220
20040119	IBH-6	6.20	75.8	538.0	44.0	38.0	56.0	3.3	0.5	16.0	29.0	311.0	<0.20	1.20	2.070	52.000	1.920
20040406	IBH-6	7.00		498.0	20.0							235.0	0.40			2.850	0.820
20040721	IBH-6	7.70	63.8	370.0	21.0	31.0	69.0	2.8	0.5	108.0	31.0	173.0	0.60	0.90	0.472	16.000	0.346
20041021	IBH-6	7.60		320.0	13.0							115.0	0.30			20.000	0.278
19960527	IBH-7	6.00	780.0	6610.0	1000.0	350.0	357.0	16.0	0.9	175.0	21.0	4067.0	0.80	2.70		400.000	76.000
20030716	IBH-7	3.90	341.0	3140.0	268.0	313.0	164.0	6.4	0.2	<5.0	126.0	2018.0	<0.20	<0.20	0.559	144.000	6.360
20031006	IBH-7	3.60		3656.0	273.0							2131.0	0.30			90.000	5.990
20040120	IBH-7	4.20	335.0	3504.0	362.0	279.0	145.0	6.7		<5.0	85.0	2305.0	<0.20	<0.20	0.200	214.000	6.250
20040406	IBH-7	3.90		3222.0	289.0							1939.0	<0.20			70.000	4.710
20040721	IBH-7	6.00	294.0	2806.0	245.0	243.0	199.0	6.5	0.9	16.0	73.0	1867.0	<0.20	<0.20	0.259	85.000	2.040
20041021	IBH-7	5.10		2482.0	178.0							1472.0	<0.20			45.000	1.480
20030729	IBH-11	2.80	502.0	4974.0	500.0	348.0	252.0	15.3	12.9	<5.0	32.0	3234.0	0.30	<0.20	0.175	359.000	38.000
20031003	IBH-11	2.90		5312.0	473.0							3320.0	0.30			274.000	45.000
20040119	IBH-11	3.40	460.0	5176.0	525.0	321.0	322.0	15.1	13.8	<5.0	41.0	3426.0	0.30	<0.20	0.036	399.000	37.000
20040406	IBH-11	2.80		4836.0	401.0							3191.0	<0.20			314.000	18.000
20030729	IBH-12	2.90	636.0	7244.0	460.0	504.0	250.0	22.0	11.8	<5.0	27.0	4553.0	0.40	<0.20	0.241	735.000	58.000
20031003	IBH-12	3.40		9926.0	476.0							6383.0	0.60			1046.000	72.000
20040119	IBH-12	3.90	563.0	7026.0	533.0	420.0	230.0	29.0	11.6	<5.0	39.0	4155.0	<0.20	<0.20	1.240	716.000	43.000
20040405	IBH-12	2.90		6186.0	201.0							3826.0	<0.20			602.000	35.000
20040721	IBH-12	3.30	581.0	6972.0	491.0	436.0	270.0	26.0	6.0	<5.0	31.0	4701.0	<0.20	<0.20	0.210	696.000	39.000
20041021	IBH-12	3.50		6750.0	423.0							4242.0	0.40			740.000	38.000
20030729	IBH-13	2.90	512.0	5040.0	520.0	336.0	252.0	11.6	23.0	<5.0	58.0	3234.0	0.40	<0.20	0.285	304.000	39.000
20031006	IBH-13	3.00		5130.0	425.0							3347.0	0.30			281.000	37.000
20040120	IBH-13	3.80	390.0	3992.0	463.0	283.0	168.0	9.8	13.8	<5.0	102.0	2486.0	<0.20	<0.20	0.369	235.000	16.000
20040721	IBH-13	3.00	360.0	3242.0	385.0	228.0	185.0	7.8	7.2	<5.0	124.0	2097.0	<0.20	<0.20	0.340	134.000	7.960

Table 7.3.2(A). Hydro-chemical samples taken from the IBH boreholes...continued

Date of sampling	Borehole Nr.	pH	EC (mS/m)	TDS (mg/l)	Ca (mg/l)	Mg (mg/l)	Na (mg/l)	K (mg/l)	Si (mg/l)	Total Alkalinity as CaCO ₃ (mg/l)	Cl (mg/l)	SO ₄ (mg/l)	N (mg/l)	F (mg/l)	Al (mg/l)	Fe (mg/l)	Mn (mg/l)
20041021	IBH-13	4.20		3156.0	361.0							2053.0	<0.20			122.000	4.500
20030729	IBH-14	2.90	452.0	4234.0	440.0	276.0	282.0	12.8	3.3	<5.0	44.0	2766.0	<0.20	<0.20	0.182	307.000	28.000
20031006	IBH-14	3.10		4384.0	345.0							2689.0	0.40			250.000	20.000
20040119	IBH-14	4.00	393.0	4190.0	390.0	252.0	200.0	10.6	3.9	<5.0	92.0	2361.0	<0.20	0.30	0.103	450.000	18.000
20040721	IBH-14	3.80	349.0	3460.0	271.0	238.0	260.0	8.0	2.3	<5.0	101.0	2061.0	<0.20	<0.20	0.183	310.000	13.000
20041021	IBH-14	4.10		2578.0	173.0							1567.0	0.60			210.000	8.330
20030729	IBH-15	3.10	509.0	5510.0	460.0	396.0	243.0	14.3	16.6	<5.0	17.0	3617.0	0.30	<0.20	0.173	243.000	43.000
20040119	IBH-15	3.20	494.0	5462.0	552.0	349.0	206.0	15.0	36.0	<5.0	35.0	3407.0	<0.20	<0.20	0.154	364.000	47.000
20040721	IBH-15	2.90	460.0	4604.0	489.0	345.0	253.0	15.4	1.1	<5.0	21.0	3281.0	0.30	<0.20	0.331	124.000	29.000
20041021	IBH-15	5.60		4424.0	480.0							2527.0	0.40			135.000	31.000
20030729	IBH-16	2.80	512.0	5236.0	480.0	384.0	234.0	14.9	18.1	<5.0	17.0	3617.0	0.50	<0.20	0.192	301.000	43.000
20040119	IBH-16	3.50	479.0	5356.0	565.0	337.0	204.0	17.6	36.0	<5.0	35.0	3234.0	<0.20	<0.20	0.225	378.000	44.000
20040721	IBH-16	2.70	508.0	5080.0	489.0	360.0	264.0	18.4	18.3	<5.0	29.0	3498.0	<0.20	<0.20	0.407	348.000	37.000
20041021	IBH-16	2.90		4758.0	464.0							3107.0	<0.20			378.000	28.000

A Piper and an Extended Durov diagram of all the IBH-samples are depicted in **Figure 7.3.2(A)** and **(B)** below:

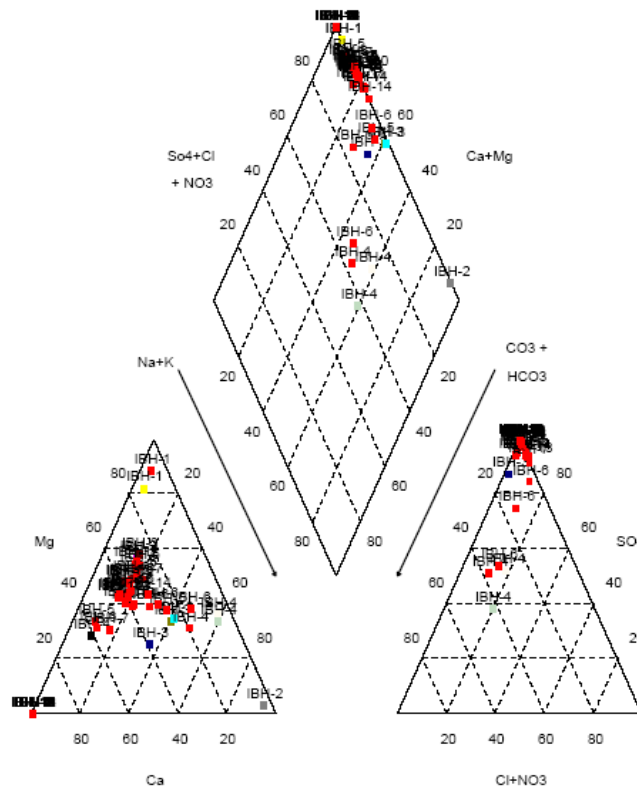


Figure 7.3.2(A) Piper diagram of IBH borehole samples

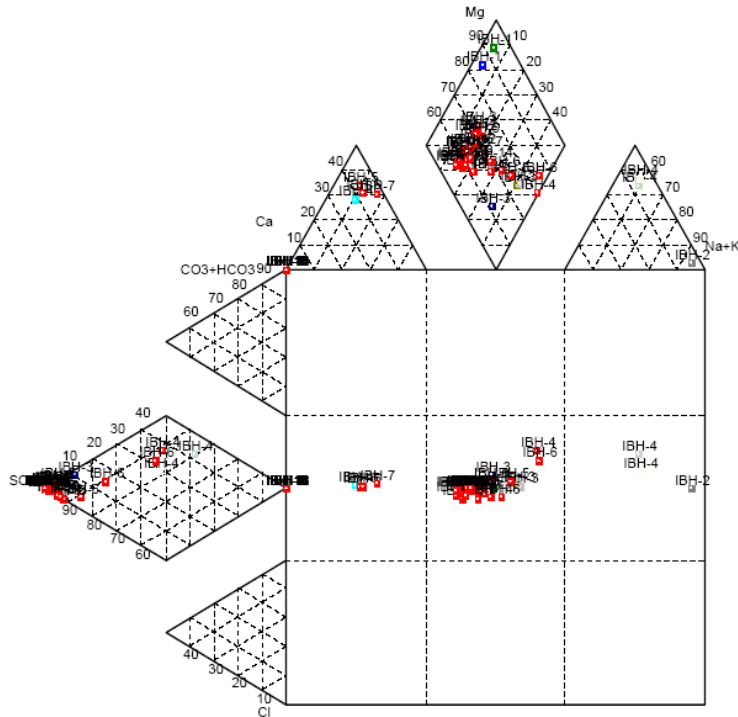


Figure 7.3.2(B) Extended Durov plot of IBH borehole samples

From **Figure 7.3.2(A)** and **(B)** it is evident that sulphate is the dominant anion in all samples. All samples except IBH-4 and 6 show high sulphate content, low to intermediate chloride content with fluoride and bicarbonate usually below detection limit. IBH-4 and 6 show lower sulphate concentrations and low to intermediate alkalinity content. IBH-4 is situated in the north-western side of the pit near the pit-perimeter. Less flow occurs from the pit through this upper part of the berm and some ingress of river water may even occur during rainfall events. IBH-6 is situated just outside the pit perimeter (see **Section 7.2.2**) and has also been less influenced by the pit water.

Figure 7.3.2(C) below depicts the changes in the sulphate concentration over the various sample runs. The average sulphate concentration is indicated by the black line. **Figure 7.3.2(D)** below shows the relation between the average pH, TDS and sulphate content. The rainfall data of Newcastle and the average TDS and sulphate of the mining pit are shown in **Figure 7.3.2(E)**. All “average” concentrations were calculated by excluding the samples of IBH-4 and –6 as these boreholes are influenced by river water.

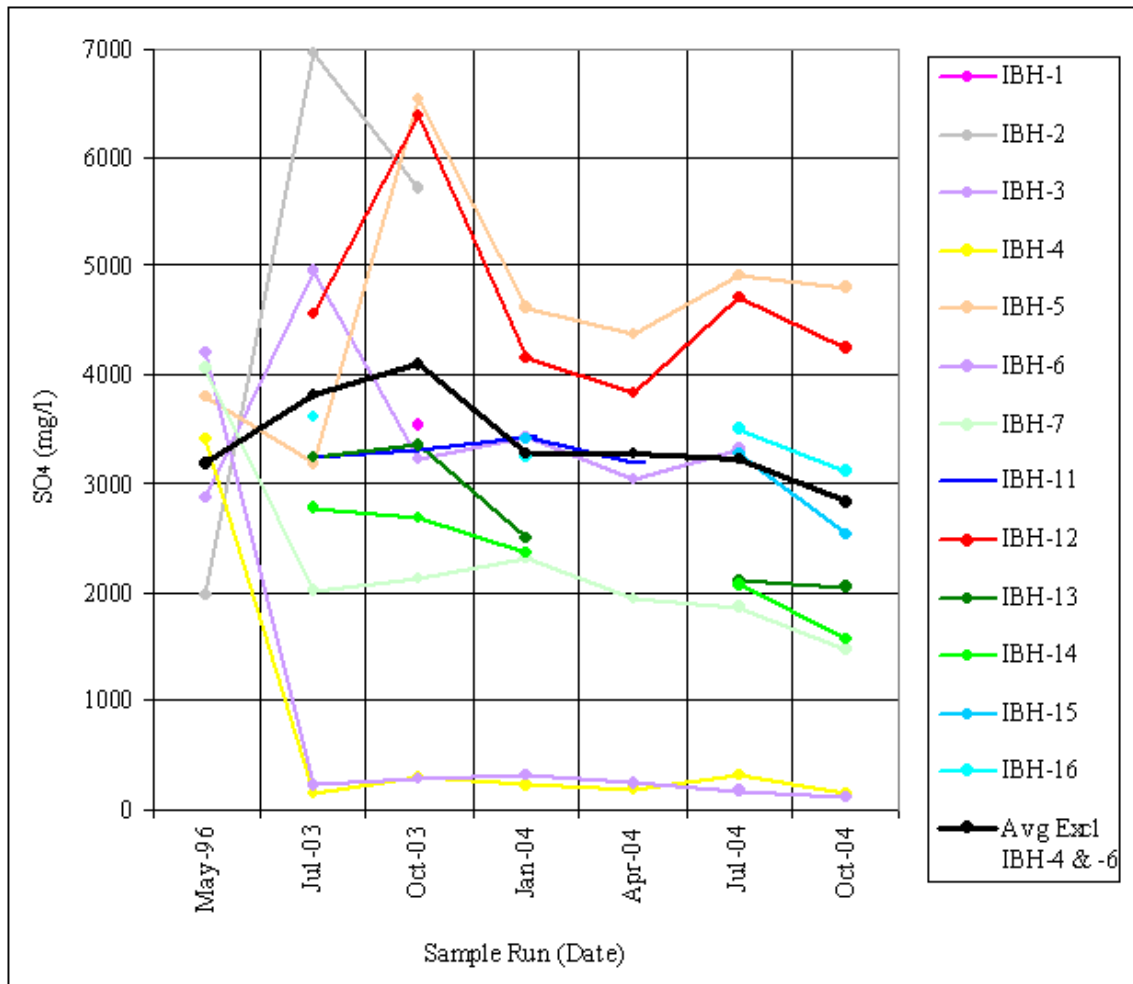


Figure 7.3.2(C). Sulphate concentration change over different sample runs in the mine water (IBH boreholes).

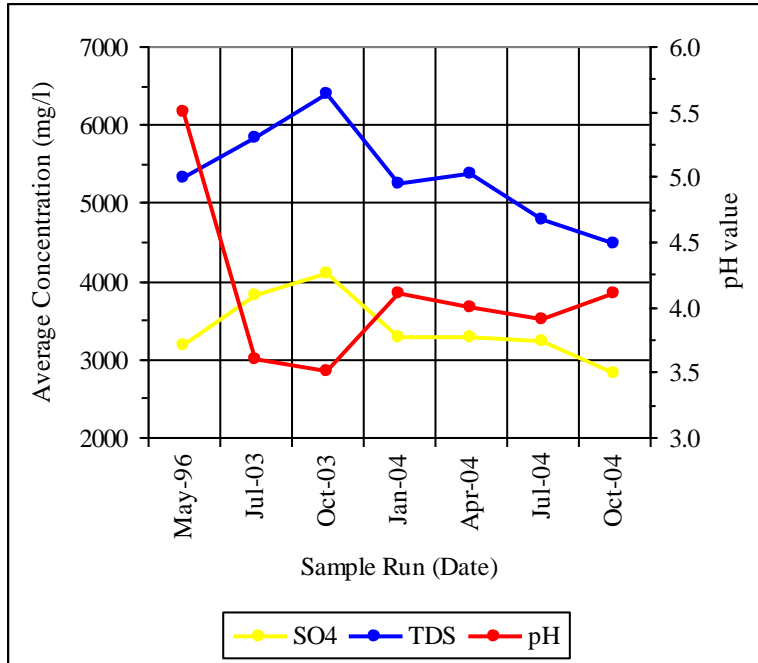


Figure 7.3.2(D).
Average sulphate, TDS and pH changes over the different sample runs in the IBH boreholes (excluding IBH-4 and IBH-6).

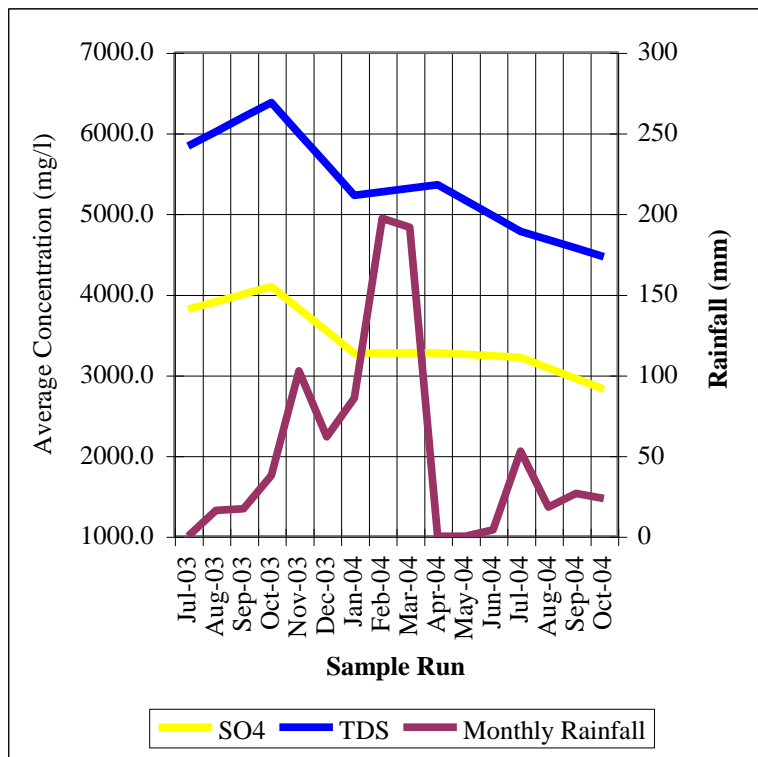


Figure 7.3.2(E).
Average sulphate and TDS concentration in IBH boreholes (excluding IBH-4 and IBH-6) compared to the monthly rainfall of Newcastle.

Table 7.3.2(B) below gives the average concentration of all the hydro-chemical parameters over the various sample runs.

Table 7.3.2(B). Average concentrations of major hydro-chemical parameters over the different sample runs in the IBH boreholes (excluding IBH-4 and IBH-6).

Constituent (mg/l)	May-96	Jul-03	Oct-03	Jan-04	Apr-04	Jul-04	Oct-04
pH ¹	5.5	3.6	3.7	4.1	4.0	3.9	4.1
EC (mS/m)	660.3	533.2		464.0		455.3	
TDS	5321.0	5838.4	6376.4	5228.7	5360.0	4778.8	4467.7
Ca	650.5	445.0	417.9	470.8	328.2	396.6	358.7
Mg	237.8	406.5		335.3		335.1	
Na	299.8	284.6		266.8		299.3	
K	14.3	13.4		15.1		13.9	
Si	0.9	10.1		16.4		6.4	
Total Alkalinity (as CaCO ₃) ²	151.0	<21.3		<13.0		<9.8	
Total Alkalinity (as CaCO ₃) ³	66.0	<7.1		<7.0		<7.3	
Total Alkalinity (as CaCO ₃) ⁴	18.0	<5.6		<5.6		<6.2	
Cl	18.3	40.1		53.7		56.6	
SO ₄	3174.8	3814.0	4096.9	3268.8	3273.6	3216.5	2825.4
NO ₃ (as N)	1.4	0.4	0.4	0.2	0.2	0.2	0.3
F	2.3	0.2		0.2		0.2	
Al ⁵		19.4		0.3		1.1	
Fe ⁵	203.3	476.9	446.0	451.9	325.2	320.1	325.4
Mn ⁵	47.3	36.5	42.5	32.0	25.5	25.3	26.3

¹ log(Geometric Mean[H⁺]), ² Arithmetic Mean, ³ Geometric Mean, ⁴ Harmonic Mean, ⁵ Sample acidified before filtration.

In **Table 7.3.2(B)** the arithmetic, geometric and harmonic means were calculated for alkalinity. Alkalinity has an inverse relationship with acidity which in turn does not have a normal distribution. Therefore the arithmetic mean could not be used for pH or alkalinity and both the geometric and harmonic mean is reported for alkalinity. Most alkalinity in the pit water is further below detection limit (<5 mg/l) and since the value of

5 mg/l has been used to calculate the mean alkalinity, the actual mean is indicated to be lower than the calculated value.

From **Table 7.3.2(B)** and **Figure 7.3.2(C) - (E)**, the following observations could be made:

- From **Figure 7.3.2(C)** it is evident that the sulphate content in most boreholes increased over the first three monitoring runs (May-96, Jul-03, Oct-2003). The sulphate content of most boreholes decreased thereafter up until the last sample run (Oct-04). This trend is clearly shown by the calculated average sulphate.
- It is also observed from **Figure 7.3.2(C)** that boreholes that are situated close to each other in the pit, show the same level of sulphate content and their trend also mimic each other more closely. Such groups of boreholes identified are IBH-7, -13 and -14; IBH-5 and -12; IBH-11, -15 and -16.
- **Figure 7.3.2(D)** shows the average sulphate and its respective positive and negative correlation with the average TDS and pH.
- It is clear from **Figure 7.3.2(E)** that no obvious (positive or negative) relationship exist between rainfall and the salt load from the pit.
- The average concentrations of all the hydro-chemistry parameters were given in **Table 7.3.2(B)**. The following trends could be observed from the chemistry data:
 - Sulphate, iron and TDS show an overall increase of values until October 2003 and a subsequent decrease afterwards until October 2004.
 - Sodium and potassium show a fairly constant concentration over the sample runs.
 - Alkalinity and calcium show an overall decrease over the sample runs most probably because of the depletion of calcite.
 - Magnesium however shows a peak concentration in July 2003 where-after it decreases. This trend can be attributed to the slower reaction of dolomite in the backfill with respect to calcite.
 - Chloride shows an overall increase over the sample runs.
 - No definite trends could be observed for manganese, aluminium, silicon and EC.

- Nitrate and fluoride decreased in concentration over the sample runs and remained at low concentrations in the mine water.
- The different trends in the hydro-chemistry observed above will be discussed in further detail in the geochemical model in **Section 7.4**.

7.4 Conceptual model, input and assumptions of the geochemical model

7.4.1 Introduction and objectives

The aim of the geochemical model was to simulate the physico-chemical processes in AMD generation from the case study mine. The geochemical model was run over 40 years and therefore does not aim to make extrapolated long-term predictions beyond this time which cannot be calibrated. The objectives for the geochemical model are as follows:

- Constructing a conceptual model of the AMD generation from the mine.
- Defining the assumptions made in terms of the numerical model setup and the input used.
- Listing the input used for the model setup.
- Modelling of oxygen influx through the unsaturated zone.
- Modelling of the oxidation of pyrite in contact with oxygen and water in the unsaturated pit material.
- Modelling of the neutralization reactions of the carbonate and silicate minerals.
- Calibration with observed pit water quality.

The interaction of the gas, water and solid phases in the AMD environment are inter-dependent and can only be numerically solved. In this study PYROX 3 and the Geochemist's Workbench Standard 6.0.3 (GWB) were used for the geochemical modelling. The model codes are discussed in **Section 7.5** and **7.6**.

The shortcomings experienced in this study will help to make useful recommendations for future geochemical modelling studies in South Africa and are summarized in **Chapter 8**.

7.4.2 Conceptual model and methodology

A general conceptual model of the physico-chemical processes in coal mine waste material was already given in **Section 1.4**. The conceptual model plays an important role in the decision of the model setup as discussed in **Section 2.2** and **2.3**.

A conceptual model of the physico-chemical processes in the case study mine is depicted as **Figure 7.4.2(A)** below:

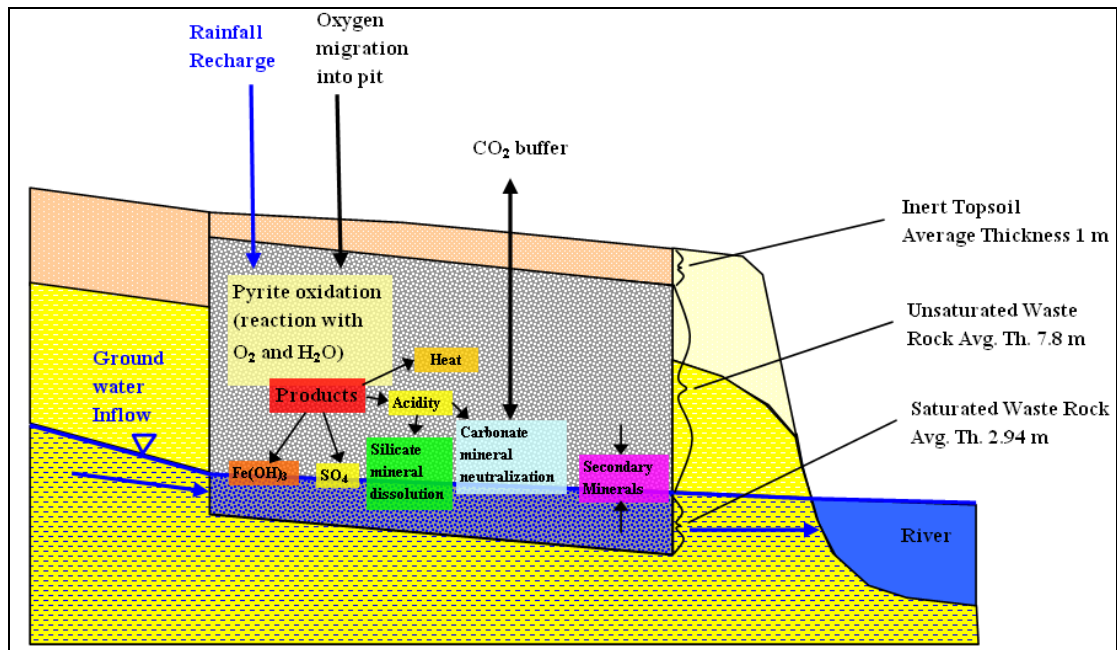


Figure 7.4.2(A). Conceptual model of the major processes of AMD generation at the case study mine.

The conceptual model for the AMD generation is discussed below:

- Because the average mine water pH was above pH 3 (ranging between pH 3.6 – 4.1 in the last six monitoring runs (see **Table 7.3.2(A)**), no pyrite oxidation by ferric iron was assumed to take place because all ferric iron will form ferrihydrite, commonly referred to as “yellowboy.” Ferrihydrite is also visually evident in the AMD from the case study mine as shown in **Figure 7.1(A)**. (See **Section 2.6.3** and **2.6.4** and also the modelling assumptions in **Section 7.4.3** below for more detail).

Bacteria often create micro-environments in coal mine spoils where they catalyse ferrous iron oxidation. If the pH is lower than pH 3, pyrite will be oxidized by the produced ferric iron and hot-spots of increased pyrite oxidation in the spoils will be created. However, no outliers in the pH, sulphate or temperature were detected in the 16 in-pit boreholes that would indicate any such hot-spots. Therefore, no bacterial activity was considered in this study and only the abiotic oxidation of pyrite by oxygen was modelled. Because the pH in the geochemical model also never reached values of below pH 3, no oxidation of pyrite by ferric iron was modelled.

- The oxygen concentration over the vertical profile (from surface to the bottom of the pit) decreased downwards because of its consumption by pyrite oxidation. Because oxygen was present in the pit water (although at low concentrations), oxygen migration into the unsaturated zone was not seen as the rate limiting step of the overall pyrite oxidation process but rather the oxidation of ferrous iron in solution (see **Section 2.6.4**).

- Pyrite oxidation is an exothermic process and is generally a source of heat in pit material. No evidence of increased heat was however observed in the pit water (as discussed in **Section 7.4.3.7**). All heat must therefore be lost to the surrounding environment. Pressure differences in the gas phase due to temperature differences is the driving force for gas convection. Because no evidence of heat differences was observed, oxygen diffusion was seen as the main process of oxygen migration into the pit material. (Other advection processes such as barometric pumping were not considered.)
- Pyrite oxidation introduces acidity into the pit water which will be consumed by calcite and dolomite. These carbonate minerals will release calcium, magnesium and alkalinity into solution. In the case of an open system, the carbonate alkalinity will equilibrate with the CO₂ in the atmosphere. However, if the system is closed the CO₂ species will increase in solution with measurable alkalinity in the pit water. Different modelling scenarios were run for the open and closed CO₂ systems.
- Silicate minerals in the spoil material will slowly dissolve in the acidic pit water consuming some acidity and thereby introducing elements such as aluminium, silica, sodium and potassium into the pit water.
- Some of the sulphate that is released by the oxidation of pyrite will precipitate with calcium as gypsum. Gypsum is also visually evident in the AMD from the mine as shown in **Figure 7.1(A)**.
- The most significant secondary minerals that precipitate from solution were ferrihydrite and gypsum as discussed above. Other secondary minerals included Al-hydroxides, Al-sulphates, Fe-sulphates and some clays.

Figure 7.4.2(B) was constructed in order to illustrate the detailed model methodology. The overall methodology that was followed in the setup, execution, validation and calibration of the geochemical model is discussed below:

(The actual input, how it was calculated and the modelled assumptions are discussed in Section 7.4.3)

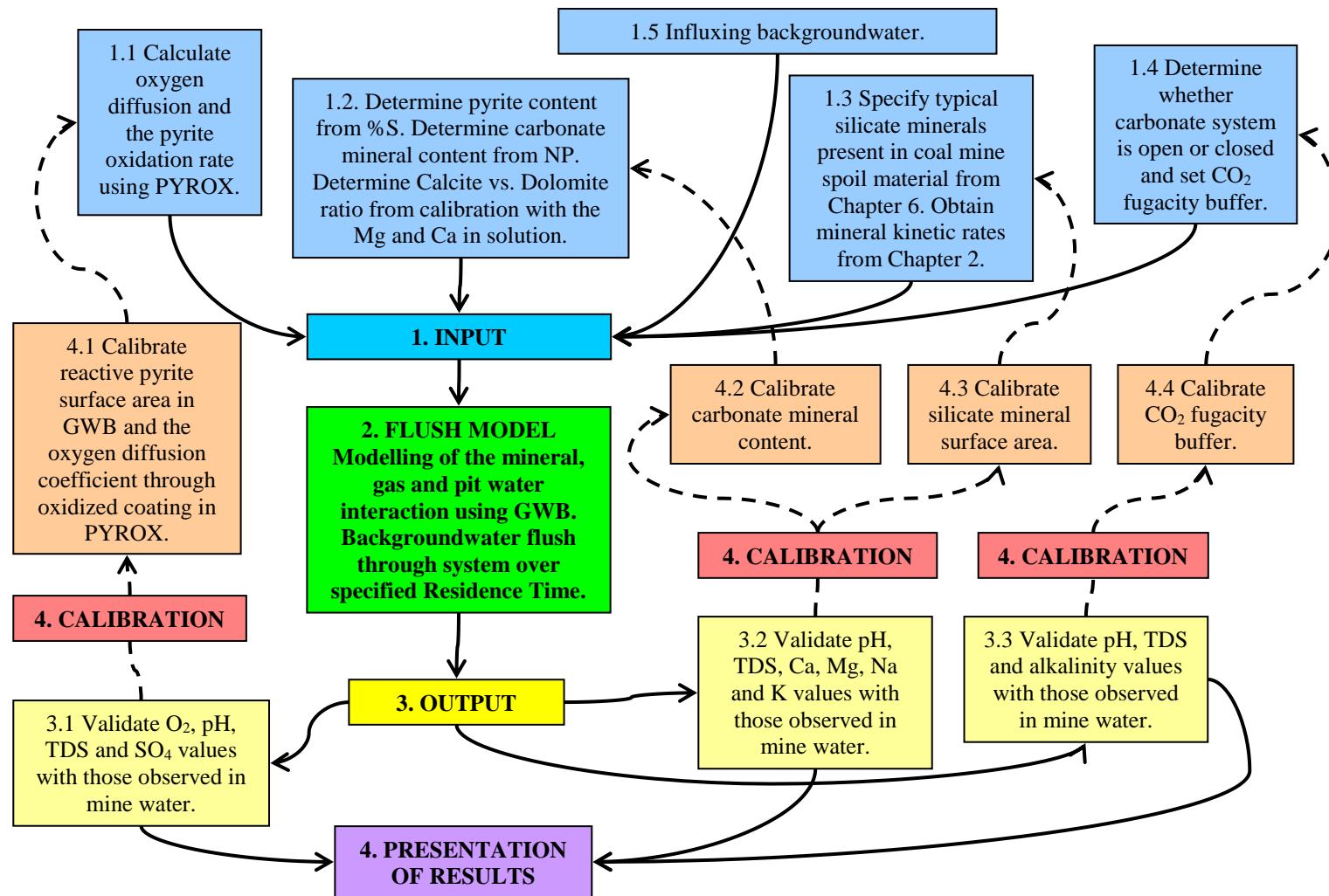


Figure 7.4.2(B). Geochemical model methodology followed for the case study mine.

- The pyrite oxidation rate was determined in the PYROX 3 model (1.1 in **Figure 7.4.2(B)**).

The pyrite mineral surface was in reality not completely available for oxidation as the mineral is partly in contact with other mineral surfaces. When specifying the total pyrite mineral surface in a geochemical model the pyrite reaction rate will be overestimated. This was overcome in PYROX 3 by adjusting the oxygen diffusion coefficient through the oxidized coating of the pyrite grain (3.1 and 4.1 in **Figure 7.4.2(B)**) until the oxygen concentration was calibrated to the observed concentration in the field. The reactive pyrite surface area in GWB was then adjusted (3.1 and 4.1 in **Figure 7.4.2(B)**) until the pyrite reaction rate was similar to that modelled in PYROX 3.

- The pyrite and carbonate mineral contents in the spoil material were respectively calculated from the average %S and NP in the spoil material (1.2 in **Figure 7.4.2(B)**). The calcite to dolomite ratio was calibrated in the model to the Mg and Ca concentrations observed in the mine water (3.2 and 4.2 in **Figure 7.4.2(B)**).
- Typical silicate minerals present in the Vryheid Formation, as determined in **Chapter 6**, were defined in the model (1.3 in **Figure 7.4.2(B)**) and their respective surface areas were calibrated to the mine water chemistry (4.3 in **Figure 7.4.2(B)**). All kinetic rate data of the minerals were obtained from **Chapter 2**.
- Modelling scenarios were run for both the open and the closed CO₂ systems (1.4 in **Figure 7.4.2(B)**). The CO₂ buffer was also calibrated (3.3 and 4.4 in **Figure 7.4.2(B)**) to between an open and closed system in order that the results would fit the measured alkalinity in the pit water.
- Recently recharged background groundwater (see **Section 7.2.4** and **7.4.3.6**) was specified as the inflowing water into the pit (1.5 in **Figure 7.4.2(B)**). The water was flushed through the unsaturated zone for every residence time specified in the model.

7.4.3 Model input and assumptions

7.4.3.1 Oxygen fugacity and pyrite oxidation rate

ASSUMPTION 1

Oxygen was the only oxidizing agent of pyrite in the mine spoils.

Pyrite oxidation takes place in the unsaturated spoil material. Because the average mine water pH is above pH 3 (ranging between pH 3.6 - 4.1 in the last six monitoring runs – see **Table 7.3.2(A)**), no pyrite oxidation by ferric iron takes place because all ferric iron will form ferrihydrite. Only at pH conditions of about below pH 3 does the activity of ferric iron becomes high enough so that oxidation of pyrite by ferric iron becomes the main mechanism for acid production, with bacterial oxidation of ferrous iron providing the ferric iron (Nordstrom, 1982; Kleinman et al., 1981). (See **Section 2.6.4** for more detail on the pyrite oxidation mechanisms).

Bacteria often create micro-environments in coal mine spoils where they catalyse ferrous iron oxidation. However, no outliers in the pH, sulphate or temperature were detected in the 16 in-pit boreholes that would indicate any such hot-spots. No bacterial activity was therefore considered in this study and only the abiotic oxidation of pyrite by oxygen was modelled.

The oxygen diffusion coefficient through the oxidized pyrite coating was adjusted in PYROX 3 until the oxygen concentration in the model was calibrated to field observations. The measured oxygen concentration in the mine water, as measured in July 2003 in IBH-11 to 16, was between 1.75 mg/l and 3 mg/l, averaging at about 2.6 mg/l. This is about 31% of the oxygen concentration of water in direct contact with the atmosphere.

The oxygen concentration in the GWB model was adjusted to a fugacity buffer of 0.08 (40% of 0.2; 40% is the average fraction of oxygen in the calibrated vertical profile modelled by PYROX 3) and the pyrite oxidation rate was calibrated to that modelled in PYROX 3 by adjusting the reactive pyrite surface area.

Both open and closed scenarios for oxygen were also run and in both scenarios the initial oxygen fugacity was set to 0.2, but only in the open scenario was a fixed oxygen buffer specified.

7.4.3.2 Pyrite and carbonate mineral content in mine spoils

ASSUMPTION 2

Pyrite is the only sulphide mineral and calcite and dolomite the only carbonate minerals present in the mine spoils.

From **Chapter 6** it was evident that no other sulphide mineral than pyrite was present in the Vryheid Formation. In the geochemical model it was assumed that pyrite is the only sulphide mineral and calcite and dolomite the only carbonate minerals present in the mine spoils. The concentration of these minerals in the mine spoils was calculated from the Acid-base accounting (ABA) analyses performed on the spoils.

A total of 10 samples have been taken from boreholes IBH-12 and IBH-15 at depths of respectively 5 – 15 m and 3 – 13 m for ABA analyses. These two boreholes were drilled into the northwestern part of the rehabilitated pit; refer to **Figure 7.2.2(D)** for the position of the boreholes.

The boreholes drilled into the rehabilitated mine showed a mixture of rocks (coal, sandstone, shale) and unconsolidated material (sand, gravel, clay) present in each sample. The determination of the acidification potential of the backfill will give a qualitative indication of the long-term impact on water that seeps from the open-cast mine. Acid-base accounting (ABA) was performed on these ten samples using the Modified Sobek (Lawrence) Method and the results are shown in **Table 7.4.3.2(A)** below:

Table 7.4.3.2(A). Acid-base accounting analyses of the mine spoils.

Sample	Sample Description	Paste pH	Total S (wt%)	AP (kg CaCO ₃ /t)	NP (kg CaCO ₃ /t)	NNP (kg CaCO ₃ /t)	AP:NP Ratio	Rock Type
IBH 12 5-6 m	Sand and Gravel	6.64	0.177	5.53	0.00	-5.53	-	I
IBH 12 6-9 m	Coal, Sandstone and Sand	6.30	0.971	30.34	1.00	-29.34	1 : 0.03	I
IBH 12 9-11 m	CB Sh*, Sand and Gravel	5.72	3.453	107.91	0.00	-107.91	-	I
IBH 12 11-14 m	Coal, Shale and Sandstone	6.08	1.736	54.25	0.00	-54.25	-	I
IBH 12 14-15 m	CB Sh* and Sandstone	7.01	0.328	10.25	0.75	-9.40	1 : 0.07	I
IBH 15 3-4 m	Shale and Sandstone	6.93	0.933	29.16	9.40	-19.66	1 : 0.33	I
IBH 15 4-6 m	Sand, Gravel and Sandstone	7.20	0.245	7.66	0.00	-7.66	-	I
IBH 15 6-7 m	Sandstone and Shale	7.60	0.899	28.09	4.25	-23.84	1 : 0.15	I
IBH 15 7-8 m	Sand, Gravel and Sandstone	6.85	0.170	5.31	0.00	-5.31	-	I
IBH 15 8-13 m	Coal, Shale and Sandstone	6.79	1.065	33.28	2.75	-30.53	1 : 0.08	I
Minimum		5.72	0.170	5.31	0.00	-107.91	-	I
Maximum		7.60	3.453	107.91	9.40	-5.31	1 : 0.33	I
Average		6.71	0.998	31.18	1.83	-29.35	-	I
Weighted Average		6.60	1.17	36.48	1.56	-34.92	-	I

*CB Sh = Carbonaceous Shale

From **Table 7.4.3.2(A)** the following observations were made:

- The paste pH's of the 15 samples ranged between pH 5.72 and pH 7.60, with a weighted average of pH 6.60.
- The total %S of all the spoils ranged from 0.170% to 3.453%, with a weighted average value of 1.17%. The Acid Potential (AP) is calculated from the %S and gives the gross potential for acidification per volume material. The unit of kg CaCO₃/t is used in order to indicate the amount of calcite that can be neutralized by the acid produced by the pyrite. The range in AP is between 5.31 kg CaCO₃/t and 107.91 kg CaCO₃/t with a weighted average value of 36.48 kg CaCO₃/t. A total of seven samples (75% of the samples) have high AP values of above 9.38 kg CaCO₃/t (or a S% of above 0.30%).
- The Neutralization Potential (NP) gives an indication of the total base potential available to neutralize acidification. To express it in terms of calcite, the units of kg CaCO₃/t are used. The range in NP is between 0.00 kg CaCO₃/t and 9.40 kg CaCO₃/t, with an average of only 1.83 kg CaCO₃/t.
- The Net Neutralization Potential (NNP) is the total of NP – AP. A positive value means that the material has an excess base potential, while a negative value indicates excess acid potential. The range in NNP is between –107.91 kg CaCO₃/t and –5.31 kg CaCO₃/t, averaging at –29.35 kg CaCO₃/t. The negative range in NNP indicates the dominating acid producing potential of the rocks. A NNP of lower than –20 kg CaCO₃/t is often considered as definitely acid producing (see **Section 6.2** for discussion of the ABA screening methods) and 6 of the 10 samples have a NNP of –20 kg CaCO₃/t or lower.
- From the results in **Table 7.4.3.2(A)** it can be seen that the samples from the backfill are all classified as “likely AMD generating” rock. A total of 7 of the 10 samples also show %S of more than 0.30% (see **Section 6.2** for discussion of the ABA screening methods). Therefore, the bulk of the open-cast material shows definite acidification potential. Actual field data confirmed the presence of acidic drainage from the mine.

If it is assumed that all the sulphur in the rock can be attributed to the pyrite present, then the pyrite content could easily be calculated as follows:

Calculation of Pyrite(wt%) from %S

%S = weight percentage S = S(wt%)

According to the following equation, 2 mol S are required for every 1 mol of pyrite:



Therefore, the mol S in 1 kg rock = $(\%S \times 10)g / 32.066 \text{ g/mol} = (0.3118 \times \%S) \text{ mol}$
 and mol Pyrite in 1 kg rock = $0.3118 \times \%S / 2 = 0.1559 \times \%S \text{ mol}$

Pyrite (wt%) = $[0.1559 \times \%S \text{ mol} \times (55.845 + 32.066 \times 2) \text{ g/mol} / 10] \text{ wt\%}$

Pyrite (wt%) = $1.8708 \times \%S \text{ wt\%}$

It is important to note that little Neutralization Potential was identified in the ABA samples above. From the 10 samples, 5 have been analyzed with zero NP. This indicates that the buffering minerals like calcite and dolomite are nearly depleted in the sampled backfill due to reaction with the acid drainage produced.

The NP has the units kg CaCO₃/t and therefore the calcite weight percentage is simply calculated by dividing the NP with a factor of 10. The final amount of carbonate minerals present in the pit material were calibrated to the pit water quality. The calcite to dolomite ratio was calibrated to the calcium and magnesium content in the pit water. The mass of the calcite and dolomite used in the model were back-calculated to the amount of NP which is 1.15 kg CaCO₃/t as shown in **Table 7.4.3.2(B)** below.

The pyrite content calculated from the ABA results and the final content incorporated into the geochemical models are given in **Table 7.4.3.2(B)** below.

Table 7.4.3.2(B). Calculated and calibrated pyrite and carbonate minerals content.

In-pit material	%S (wt%)	Pyrite Content (wt%)	NP (kg CaCO ₃ /t)	Calcite Content (wt%)	Dolomite Content (wt%)
Measured in 2003					
Weighted Average IBH-12	0.78	1.46	0.38	0.038	-
Weighted Average IBH-15	1.55	2.90	2.72	0.272	-
Average IBH-12 and -15	1.17	2.19	1.56	0.156	-
Selected mineral content					
Average for whole pit as input for GWB	1.55	2.90	1.15	0.050	0.060

Since no direct experimental measurements of the mineral surface areas were available, the geometric surface area (as discussed in **Section 2.3.2**) was used in the model. For all the minerals, apart from pyrite and clays, an average grain diameter of 0.0033 cm was assumed.

Carbonate minerals can be either assigned in the mass model as kinetic minerals or be set to equilibrate with the calcium or magnesium content in the modelled solution. The carbonate minerals were added as kinetic minerals but it was found that their reactive surface area and reaction rates were large enough so that they were in equilibrium with the calcium and magnesium content anyway.

The *initial* pyrite radius in PYROX 3 was taken as 0.00005 m that equates to a surface area of 119.71 cm²/g for the spherical pyrite grains. In PYROX 3 the oxygen diffusion coefficient was used to calibrate the model. Because the pyrite mass, the pyrite oxidation rate and the oxygen fugacity were known, the reactive surface area could then be calibrated in GWB as discussed in **Section 7.5.4**.

A summary of the surface areas assigned to the minerals is given below:

Mineral	Surface Area (cm²/g)
Dolomite	635
Calcite	671
Pyrite	119.71 (initial SA in PYROX 3)
Pyrite	24 (calibrated reactive SA in GWB)

All other kinetic rate data for the minerals was obtained from **Section 2.6.5 – 2.7.3** and are also given in the GWB input files in **Section 7.6.2**.

7.4.3.3 Silicate minerals

ASSUMPTION 3

Silicate minerals in the spoil material were similar to those generally observed in the No. 4 coal seam strata of the Witbank Coalfield.

No whole rock analysis was performed on the mine spoil material. Little information on the geochemistry/mineralogy of the coal seams of the Klip River coalfield exists in literature in contrast with the more economical and well studied coal seams of the Witbank and Highveld coalfields.

The Top and Bottom coal seams equate stratigraphically with the No. 4 seam of the Witbank and Highveld coalfields as shown by Snyman (1998).

It is realistic to expect that most of the detrital minerals of the coal bearing strata of the Vryheid Formation in the various coalfields are the same since the clastic sediments of the Vryheid Formation originate from a similar northerly situated predominantly granitic source (Cairncross et al, 1990). Resultant arkosic sandstones are present throughout the Witbank, Highveld and Natal Coalfields (Cairncross et al, 1990; Cadle et al, 1990).

Because of the arkosic nature of the sandstones, minor K-feldspar and plagioclase are expected with the quartz in the sandstone. The quartz, K-feldspar and plagioclase originate from the original felsic source. Plagioclase will be higher in sodium than in calcium content and the mineral will be of Oligoclase (An₁₀ – An₃₀) composition. Kaolinite, illite and smectite (nontronite) are clay minerals that are also often present in the sandstones.

Since no direct experimental measurements of the mineral surface areas were available, the geometric surface area (as discussed in **Section 2.3.2**) was used in the model. For all the minerals, apart from pyrite and clays, an average grain diameter of 0.0033 cm was assumed. For the clays an average grain diameter of 0.0002 cm was taken.

Although the mineral mass percentages are not known in the mine spoil material it is important to assign some silicate minerals in the geochemical mass model; if this is not done very unrealistic pH values are modelled over the long term.

The silicate minerals were initially added in the GWB model at the same proportions as observed in the No. 4 coal seam strata of the Witbank coalfield. The reactive surface area of the feldspar and of some clay minerals were then calibrated to the potassium and sodium content as measured in the mine water.

The surface areas assigned to the silicate minerals in the model are given below:

Mineral	Surface Area (cm²/g)
K-feldspar	711
Oligoclase(Ab ₇₅ An ₂₅)	695
Illite	4680
Quartz	686
Nontronite-Na	10400
Kaolinite	11600

All other kinetic rate data for the minerals was obtained from **Section 2.8.3** and are given in the GWB input files in **Section 7.6.2** below.

The GWB does not have the thermodynamical data of oligoclase in its database thermo.com.v8.r6+.dat. Oligoclase with the composition $Ab_{75}An_{25}$ was added to the database as follows:

```
Oligoclase(ab75an25)           type= Feldspar
  formula= Na0.75Ca0.25Al1.25Si2.75O8
  mole vol.= 0.000 cc   mole wt.= 266.219 g
  6 species in reaction
-5.0000 H+           1.2500 Al+++           0.7500 Na+
 2.5000 H2O          2.7500 SiO2(aq)         0.2500 Ca++
 0 0 8.306 0
 0 0 0 0
```

7.4.3.4 CO₂ buffer

Modelling scenarios were run for both the open and closed CO₂ systems. In the closed system no CO₂ buffer was specified and in the open system a CO₂ buffer of -3.5 log fugacity was used. A scenario was also run where the modelled alkalinity was calibrated to the measured carbonate alkalinity in the mine water by adjusting the CO₂ buffer. This calibrated CO₂ system was close to the open CO₂ system.

7.4.3.5 Model and residence time

ASSUMPTION 4

The residence time was taken as the time for water to seep through the reactive mineralogy in the unsaturated zone.

The residence time in steady state was determined by dividing the volume of water in contact with reactive minerals by the inflow/outflow through the unsaturated zone (as modelled in **Section 7.3.1** using Visual HELP 2.2):

$$\begin{aligned}
 R_t &= \text{Volume Water} \div \text{Inflow/Outflow} \\
 &= 156,689 \text{ m}^3 \div 38,847 \text{ m}^3/\text{a} \\
 &= 4 \text{ a}
 \end{aligned}$$

In the geochemical model, a total of 10 residence times were modelled that is equivalent to about 40 years.

The model time (Year 0) started at the beginning of 1993. Mining has ceased at the end of 1992. The model time started at Year 0 and ended at Year 40.

7.4.3.6 Inflowing water quality

ASSUMPTION 5

The water quality of the rainfall recharge before filtrating through the unsaturated zone is the same as the background groundwater containing low chloride (as classified in Section 7.2.4).

Most of the water that flows into the pit is rainfall recharge. The water quality of the low chloride containing background water represents recently recharged water. The average of four samples of OBH-1 (given in **Section 7.2.4**) was slightly modified and was taken as to represent the inflowing water into the pit. This water quality is given in **Table 7.4.3.6(A)** below:

Table 7.4.3.6(A). Inflowing water quality used in model

Parameters (mg/l)	Inflowing water quality (mg/l)
pH	7.6
EC (mS/m)	65.9
TDS	379.0
Ca	41.5
Mg	28.5
Na	64.0
K	2.8
Si	12.6
Alkalinity as HCO ₃ ⁻	355.5
Cl	10.8
SO ₄	4.5
Al [#]	0.01
Fe [#]	0.01

7.4.3.7 Modelling temperature

ASSUMPTION 6

No heat build-up occurs in the spoil rock and therefore the oxygen convection was negligible.

Pyrite oxidation is an exothermic process and is a source of heat in the spoil material. No evidence of increased heat was observed from the multi-parameter profiles of the

IBH boreholes drilled in July 2003. The temperature at the bottom of the pit ranged between 20°C and 22°C and in the OBH boreholes drilled in July 2003 ranged between 19°C and 22.7°C. Therefore, the same temperature was observed in boreholes inside and outside of the pit. Temperature variation over the dimensions of the spoil material was therefore not further considered in the modelling exercise. All modelling was performed at a constant temperature of 22°C.

7.4.3.8 Secondary minerals

ASSUMPTION 7

The kinetic rates for secondary mineral dissolution and precipitation were not specified as it was assumed that they react fast enough.

It was assumed that secondary minerals react fast enough and no kinetic rate data for them were specified. Furthermore, there was a lack in kinetic data for most secondary minerals and hardly any precipitation rate data is generally available for minerals as discussed in **Section 2.3.2**.

The following secondary minerals were allowed to precipitate in the unsaturated zone:

Ferrihydrite	$\text{Fe}(\text{OH})_3$
Alunite	$\text{KAl}_3(\text{OH})_6(\text{SO}_4)_2$
Jarosite	$\text{KFe}_3(\text{OH})_6(\text{SO}_4)_2$
Gypsum	$\text{CaSO}_4 \cdot 2\text{H}_2\text{O}$
Nontronite-Ca	$\text{Ca}_{0.165}\text{Fe}_2\text{Al}_{0.33}\text{Si}_{3.67}\text{H}_2\text{O}_{12}$
Nontronite-Mg	$\text{Mg}_{0.165}\text{Fe}_2\text{Al}_{0.33}\text{Si}_{3.67}\text{H}_2\text{O}_{12}$
Tridymite	SiO_2
Gibbsite	$\text{Al}(\text{OH})_3$
Diaspore	AlHO_2

In all scenarios secondary minerals were allowed to precipitate from solution but different scenarios were run that removed them from solution after precipitation or allowed them to back-react with the mine water.

7.5 Modelling of the oxygen diffusion through the unsaturated zone and the pyrite oxidation rate using PYROX 3

7.5.1 Objective

The objective for using PYROX 3 was to model the oxygen diffusion through the unsaturated zone and to calculate the subsequent pyrite oxidation rate. The output was then used to calibrate certain parameters in the geochemical mass model.

7.5.2 Model Code

PYROX 3 was kindly made available for this study by John Molson from the University of Waterloo. The computer code modelled 1) the diffusion of oxygen through the unsaturated zone of pyrite containing spoils, 2) the oxygen consumed by pyrite oxidation, and 3) the subsequent sulphate, iron and acidity production.

PYROX 3 numerically solved the oxygen diffusion equation in porous material expressed as **Equation 3.2.4.1(D)** using the Galerkin finite element method. The model used the following semi-empirical equation (**Equation 3.2.4.2(F)**) for modelling the effective oxygen diffusion coefficient through the unsaturated zone:

$$D_e(x, t) = 3.98 \times 10^{-9} \times \left(\frac{\theta_a(x, t) - 0.05}{0.95} \right)^{1.7} \times (T(x) + 273.15)^{1.5}$$

where

- D_e = Effective Diffusion Coefficient for oxygen ($\text{m}\cdot\text{s}^{-1}$),
 T = Temperature ($^{\circ}\text{C}$),
 θ_a = Air filled porosity ($\text{m}^3\cdot\text{m}^{-3}$).

In PYROX 3 the pyrite grains were assumed to be spherical particles and the surface area was calculated from the pyrite radius as specified by the user. Through the model each spherical pyrite grain was then modelled as a shrinking core with a subsequent thickening oxidized coating. An explanation of the mathematical expressions used by PYROX 3 can be found in Wunderley et al (1996).

7.5.3 The model input file

No kinetic rate for pyrite dissolution needed to be specified in PYROX 3 as opposed to GWB. In PYROX 3 the pyrite oxidation rate is determined by the rate oxygen is delivered to the reaction site. The pyrite grain radius and the oxygen diffusion coefficient through the oxidized pyrite coating were used to calibrate the model

The pyrite radius was however kept constant at 0.00005 m which equates to a surface area of 119.71 cm^2/g for the spherical pyrite grains. The base of the oxygen profile in

the model was calibrated to the oxygen concentration measured in the mine water by adjusting the oxygen diffusion coefficient through the oxidized coating.

The pyrite fraction in the soil was taken as zero and in the spoil material as 0.0155 as calculated in **Table 7.4.3.2(B)** above. The total porosity and the moisture content were taken from **Section 7.3.1**. The temperature was obtained from **Section 7.4.3.7** above.

The final input file is given below with explanatory notes next to the input:

<u>Input file for PYROX 3</u>	
0.00005 0.99	; Pyrite radius (m); Starting radius (0 - 1)
1.45d-17	; O ₂ diffusion coefficient of oxidized coating (m ² /s)
1.d-3 100	; length of time steps (year); End time
10 1 5 10 15 20 25 30 35 40 45	; Number of print times; Print Times
8.8 440	; Depth of unsaturated zone (m) ; Number of nodes in unsaturated zone.
0.0000 0.33 0.22 22 1880.2x 50	; Pyrite fraction in topsoil; Total porosity; Moisture content; Temperature (°C); Bulk density (kg/m ³)
0.0155 0.30 0.09 22 1880.2x 390	; Pyrite fraction in spoil material; Total porosity; Moisture content; Temperature (°C); Bulk density (kg/m ³)

7.5.4 Model calibration and results

The bottom of the oxygen profile in the model was calibrated to the oxygen concentration measured in the mine water by adjusting the oxygen diffusion coefficient through the oxidized coating.

The oxygen concentration in the mine water (measured ±10 years after closure in July 2003 in IBH-11 to 16) ranged between 1.75 and 3 mg/l, averaging at about 2.6 mg/l. This is about 31% of the oxygen concentration in water that is in direct contact with the atmosphere.

The PYROX 3 model was calibrated until the oxygen concentration at the bottom of the pit was 31% of the atmospheric oxygen concentration after about 10 years as shown in **Figure 7.5.4(A)** and **(B)** below:

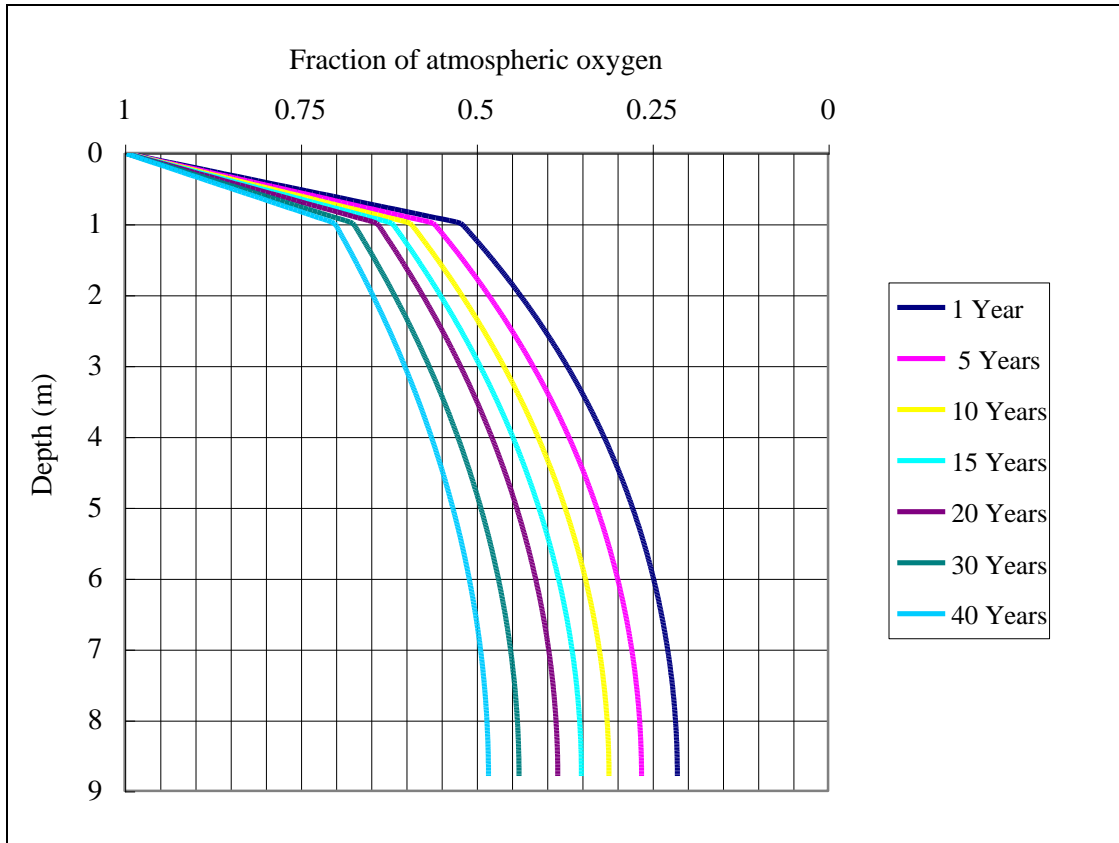


Figure 7.5.4(A). Fraction of atmospheric oxygen in the unsaturated zone as modelled by PYROX 3.

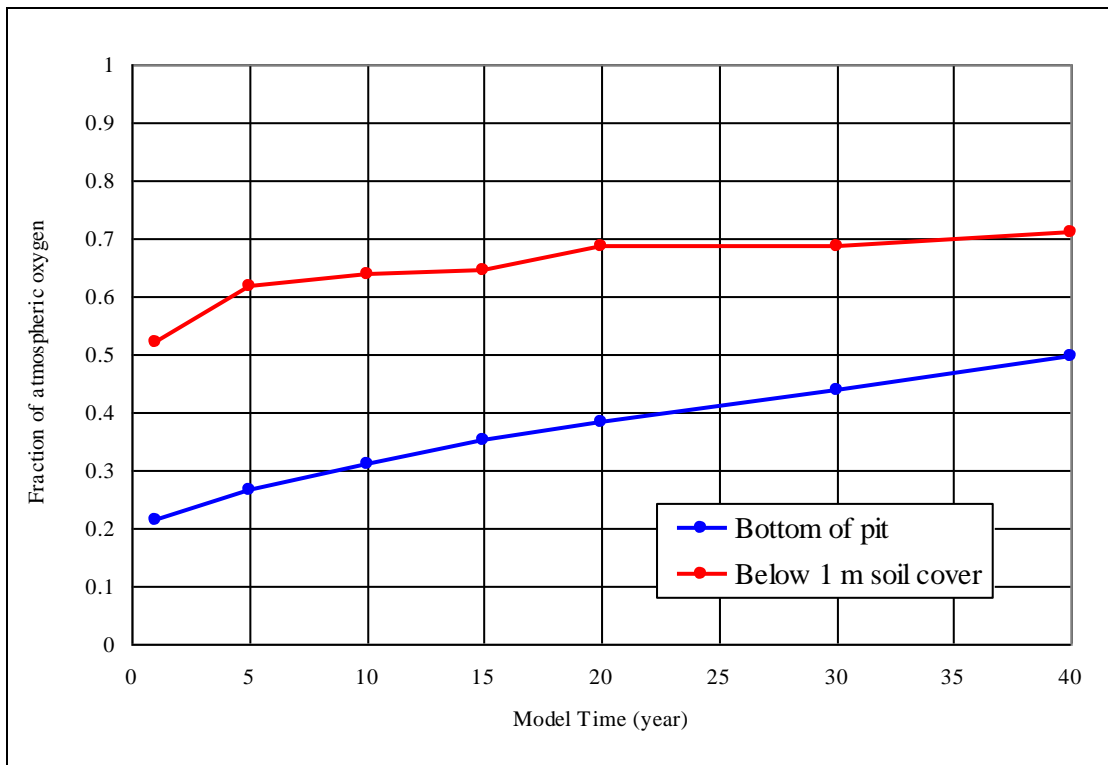


Figure 7.5.4(B). Fraction of atmospheric oxygen in the unsaturated zone as modelled by PYROX 3.

The pyrite mass reacted in the PYROX 3 model are summarized in **Table 7.5.4(A)** and depicted in **Figure 7.5.4(C)** below:

Table 7.5.4(A). Mass pyrite reacted in PYROX 3.

Model Time (year)	Pyrite reacted in 5 model years (g/kg)	Cumulative pyrite mass reacted (g/kg)
5	4.624	4.624
10	4.133	8.757
15	3.852	12.609
20	3.625	16.233
25	3.177	19.410
30	3.524	22.934
35	3.125	26.059
40	2.997	29.056

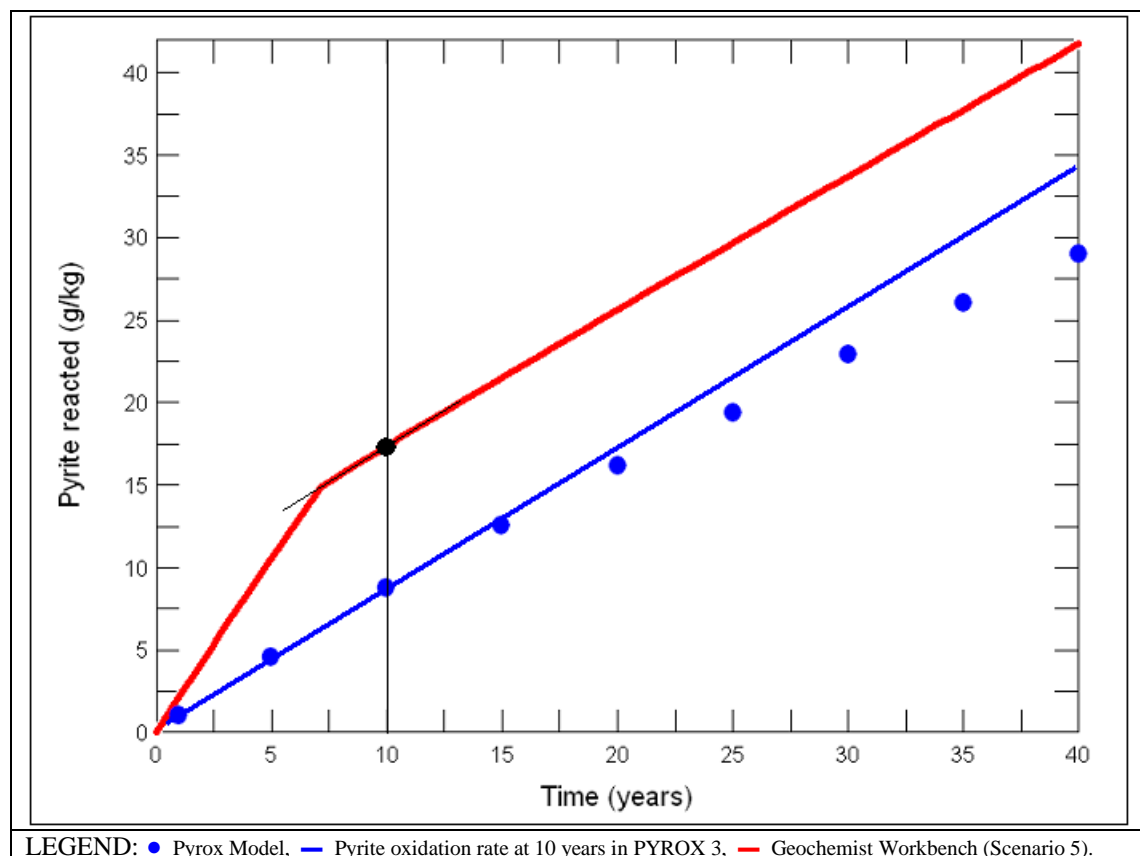


Figure 7.5.4(C). The pyrite reacted in PYROX 3 and GWB Scenario 5 (at 10 years the pyrite oxidation rate is 0.83 g/year).

From **Figure 7.5.4(A)** to **(C)** and **Table 7.5.4(A)** the following observations are made:

- As the thickness of the oxidized coating of the pyrite grains increased over time, the oxygen concentration in the unsaturated zone increased as shown in **Figure 7.5.4(A)**. PYROX 3 evidently modelled a transient oxygen diffusion state. However, the increasing oxygen concentration in the pit became smaller

as shown in **Figure 7.5.4(B)** and oxygen diffusion will eventually reach near steady-state conditions.

- The pyrite oxidation rate decreased slightly in PYROX 3 because of the increase in the thickness of the oxidized coating. This was shown by the decrease in the gradient between the oxygen below the soil cover and the oxygen at the bottom of the unsaturated zone as depicted in **Figure 7.5.4(B)**. A change in the pyrite oxidation rate therefore resulted in a change in the oxygen profile. The PYROX 3 model was calibrated until the oxygen concentration at the bottom of the pit was 31% of the atmospheric oxygen concentration after about 10 years as shown in **Figure 7.5.4(A)** and **(B)**. The pyrite oxidation rate in GWB was calibrated by adjusting the reactive pyrite surface area until it was equal to the pyrite oxidation rate modelled by PYROX 3 at 10 years. Because the pyrite oxidation rates in GWB and PYROX 3 are equal at 10 years, the same mass pyrite per unit time reacted at that point in both models and the same amount of oxygen was consumed.
- One of the shortcomings in PYROX 3 was that the pyrite oxidation was only dependent on the availability of oxygen at the reaction sites. The rate of pyrite oxidation by oxygen was also negatively dependent on the hydrogen activity as shown in **Section 2.6.5**. If the hydrogen activity is low, as in the first seven years in the GWB mass model (Scenario 5), the pyrite oxidation rate will be higher with a larger resultant oxygen gradient than modelled in PYROX 3.
- Because the pH stayed the same *after* the first seven years in the mass model (Scenario 5), the pyrite oxidation rate was also almost constant thereafter in the GWB model. However, in the PYROX 3 model the oxidation rate of pyrite decreased as the thickness of the oxidized coating increased.
- The pyrite oxidation rates in the PYROX 3 and GWB models, as well as the vertical oxygen profile in PYROX 3, were calibrated with the measured field data obtained 10 years after mining. In GWB the oxygen buffer and the reactive pyrite surface area were fixed throughout the model. Therefore, GWB assumed a steady state oxygen profile whereas the PYROX 3 models a transient state oxygen profile. If the oxygen diffusion in the acidified pit is actually in steady state, then the single calibration at 10 years would be sufficient for the geochemical mass model. A steady state was assumed in the remainder of the study as only a single dissolved oxygen measurement was available.

7.6 Geochemical mass model

7.6.1 The Geochemist's Workbench (GWB)

The GWB is a set of interactive software tools for solving problems in aqueous geochemistry. The edition used in this study was the Geochemist's Workbench

Standard 6.0.3. The GWB software used for the modelling was React 6.0.3. Gtplot 6.0.3 was used to plot all the output data against the modelling time and Act 6.0.3 was used to plot the output data on speciation graphs.

The interactions between the mineral, water and gas phases were modelled by the React 6.0.3 software. The activity of ionic species as discussed in **Section 2.2.1** was calculated by the model and all chemical reactions were solved through the equilibrium model (**Section 2.2.2**). Additionally, the kinetic rate law for mineral dissolution (**Section 2.3.2**) could be incorporated into the model. The sets of non-linear mole-balance and mass-action equations were solved iteratively by a Newton-Raphson formulation as explained in more detail in Bethke (1996).

7.6.2 Setup of the geochemical mass model

Seven modelling scenarios were performed in order to illustrate the most likely conditions in the spoil material. The following discusses the different inputs used for the modelling scenarios:

<u>Scenarios modelled in the GWB</u>	
Scenario 1	Assumes no contact with atmospheric oxygen. Full CO ₂ contact with the atmosphere was assumed.
Scenario 2	Assumes full contact with atmospheric oxygen. Full CO ₂ contact with the atmosphere was assumed.
Scenario 3	The oxygen buffer was calibrated to field measurements. Full CO ₂ contact with the atmosphere was assumed.
Scenario 4	Same oxygen buffer as in Scenario 3. No CO ₂ contact with the atmosphere was assumed.
Scenario 5	Same oxygen buffer as in Scenario 3. The modelled alkalinity was calibrated to field measurements by adjusting the CO ₂ buffer.
Scenario 6	Same oxygen and CO ₂ buffer as in Scenario 3. No primary silicate minerals.
Scenario 7	Same oxygen and CO ₂ buffer as in Scenario 5. Secondary minerals allowed to back-react with mine water.
Scenarios 1 to 7	All scenarios have the same pyrite, calcite and dolomite content. All scenarios contain the same mass of primary silicate minerals except Scenario 6 that contained no silicates. The same influxing water quality was also used for all scenarios. In all scenarios the calibrated reactive pyrite surface area was applied as discussed in Section 7.4.3.2 .

The modelling scripts of the seven scenarios modelled as well as some explanation commentary is given below:

SCENARIO 1 – NO O₂ CONTACT WITH ATMOSPHERE

This scenario assumed no contact with the atmosphere. The *initial* oxygen fugacity in the pit was at atmospheric level (oxygen fugacity = 0.2) but the oxygen buffer was not fixed. Full CO₂ contact with the atmosphere was assumed. The script for Scenario 1 is given below:

```
# React script – Scenario 1

data = "C:\Program Files\Gwb\Gtdata\Johan-thermo.com.v8.r6+.dat" verify
time start = 0 years, end = 40 years
temperature = 22
swap O2(g) for O2(aq)
swap CO2(g) for HCO3-
1 kg H2O
.08 fugacity O2(g)
-3.5 log fugacity CO2(g)
1500 mg/kg Ca++
200 mg/kg Mg++
5.5 pH
1 mg/kg SiO2(aq)
.1 mg/kg Fe++
400 mg/kg Na+
10 mg/kg Cl-
3000 mg/kg SO4--
15 mg/kg K+
.1 mg/kg Al+++
balance off
react 10 kg of H2O
react 415 mg of Ca++
react 285 mg of Mg++
react 640 mg of Na+
react 28 mg of K+
react 126 mg of SiO2(aq)
react 3555 mg of HCO3-
react 108 mg of Cl-
react 45 mg of SO4--
react .1 mg of Al+++
react .1 mg of Fe++
kinetic Pyrite 605.71 gram
kinetic Dolomite 12.52 gram
kinetic Calcite 10.43 gram
```

```

kinetic K-Feldspar 607.8 gram
kinetic Oligoclase(ab75an25) 1620.8 gram
kinetic Illite 2431.2 gram
kinetic Quartz 8103.99 gram
kinetic Nontronite-Na 405.2 gram
fix fugacity of CO2(g)
kinetic Kaolinite 7090.99 gram
kinetic Pyrite rate_con = 6.457e-13 surface = 24 power(H+) = -.11 power(O2(aq)) = .5
kinetic Dolomite rate_con = 6.457e-8 surface = 635 power(H+) = .5
kinetic Calcite rate_con = 5.012e-5 surface = 671 power(H+) = 1
kinetic K-Feldspar rate_con = 8.71e-15 surface = 711 power(H+) = .5
kinetic Oligoclase(ab75an25) rate_con = 2.138e-14 surface = 695 power(H+) = .457
kinetic Illite rate_con = 1.413e-16 surface = 4680 power(H+) = .37
kinetic Quartz rate_con = 1.023e-18 surface = 686
kinetic Nontronite-Na rate_con = 1.047e-15 surface = 10400 power(H+) = .34
kinetic Kaolinite rate_con = 4.898e-16 surface = 11600 power(H+) = .777

suppress ALL
unsuppress Alunite Calcite Diaspore
unsuppress Dolomite Fe(OH)3 Gibbsite Gypsum
unsuppress Illite Jarosite K-Feldspar Kaolinite
unsuppress Nontronite-Ca Nontronite-Mg Nontronite-Na Oligoclase(ab75an25)
unsuppress Pyrite Quartz Tridymite
alter Oligoclase(ab75an25) 0 0 8.306 0 0 0 0
dump
flow-through
flush
printout basis = short
dxplot = .01
dxprint = .01

```

SCENARIO 2 – FULL O₂ EQUILIBRIUM WITH ATMOSPHERE

This scenario assumed full contact with the atmosphere. The initial oxygen fugacity in the pit was at atmospheric level and the oxygen fugacity was fixed at 0.2. Full CO₂ contact with the atmosphere was assumed. The following line was added to the Scenario 1 script:

```

# Scenario 2 - Changes to Scenario 1 script:

fix fugacity of O2(g)

```

SCENARIO 3 – O₂ CALIBRATED MODEL

In this scenario the oxygen buffer was adjusted to the average oxygen fugacity in the unsaturated zone as modelled by PYROX 3. Full CO₂ contact with the atmosphere was assumed. The following lines were added to the Scenario 1 script:

```
# Scenario 3 - Changes to Scenario 1 script:
```

```
.08 fugacity O2(g)  
fix fugacity of O2(g)
```

SCENARIO 4 – NO CO₂ CONTACT WITH ATMOSPHERE

The same calibrated oxygen buffer was used as in Scenario 3. In this scenario no CO₂ contact was assumed with the atmosphere. The CO₂ "swapped" for bicarbonate in the program script of Scenarios 1, 2, 3, 5 and 6, was "unswapped" and an initial concentration was given to bicarbonate. The CO₂ buffer was automatically removed when CO₂ is "unswapped". The following lines were added to the Scenario 1 script:

```
# Scenario 4 - Changes to Scenario 1 script:
```

```
.08 fugacity O2(g)  
fix fugacity of O2(g)
```

```
unswap HCO3-  
250 mg/kg HCO3-
```

SCENARIO 5 – CO₂ CALIBRATED MODEL

The same calibrated oxygen buffer was used as in Scenario 3. The alkalinity was calibrated to the alkalinity in field observations by adjusting the CO₂ buffer. The following lines were added to the Scenario 1 script:

```
# Scenario 5 - Changes to Scenario 1 script:
```

```
.08 fugacity O2(g)  
fix fugacity of O2(g)
```

```
0.0031 fugacity CO2(g)
```


SCENARIO 6 - NO PRIMARY SILICATES

The same calibrated oxygen buffer was used as in Scenario 3. Full CO₂ contact with the atmosphere was assumed. The mass of the primary silicate minerals in the scenarios was all set to zero.

```
# Scenario 6 - Changes to Scenario 1 script:
```

```
.08 fugacity O2(g)
```

```
fix fugacity of O2(g)
```

```
kinetic K-Feldspar 0 gram
```

```
kinetic Oligoclase(ab75an25) 0 gram
```

```
kinetic Illite 0 gram
```

```
kinetic Quartz 0 gram
```

```
kinetic Nontronite-Na 0 gram
```

```
kinetic Kaolinite 0 gram
```

SCENARIO 7 – CO₂ CALIBRATED MODEL, SECONDARY MINERAL ALLOWED TO BACK-REACT IN MINE WATER

The same calibrated oxygen buffer was used as in Scenario 3. The alkalinity was calibrated to the alkalinity in field observations by adjusting the CO₂ buffer as in Scenario 5. The secondary minerals were allowed to back-react with the mine water. The following lines were added to the Scenario 1 script:

```
# Scenario 7 - Changes to Scenario 1 script:
```

```
# Delete “through-flow” in Scenario 1 script manually.
```

```
.08 fugacity O2(g)
```

```
fix fugacity of O2(g)
```

```
0.0031 fugacity CO2(g)
```

7.6.3 Modelling results

The results of the GWB model for Scenarios 1 – 6 are shown in **Figure 7.6.3(A) – (P)** below:

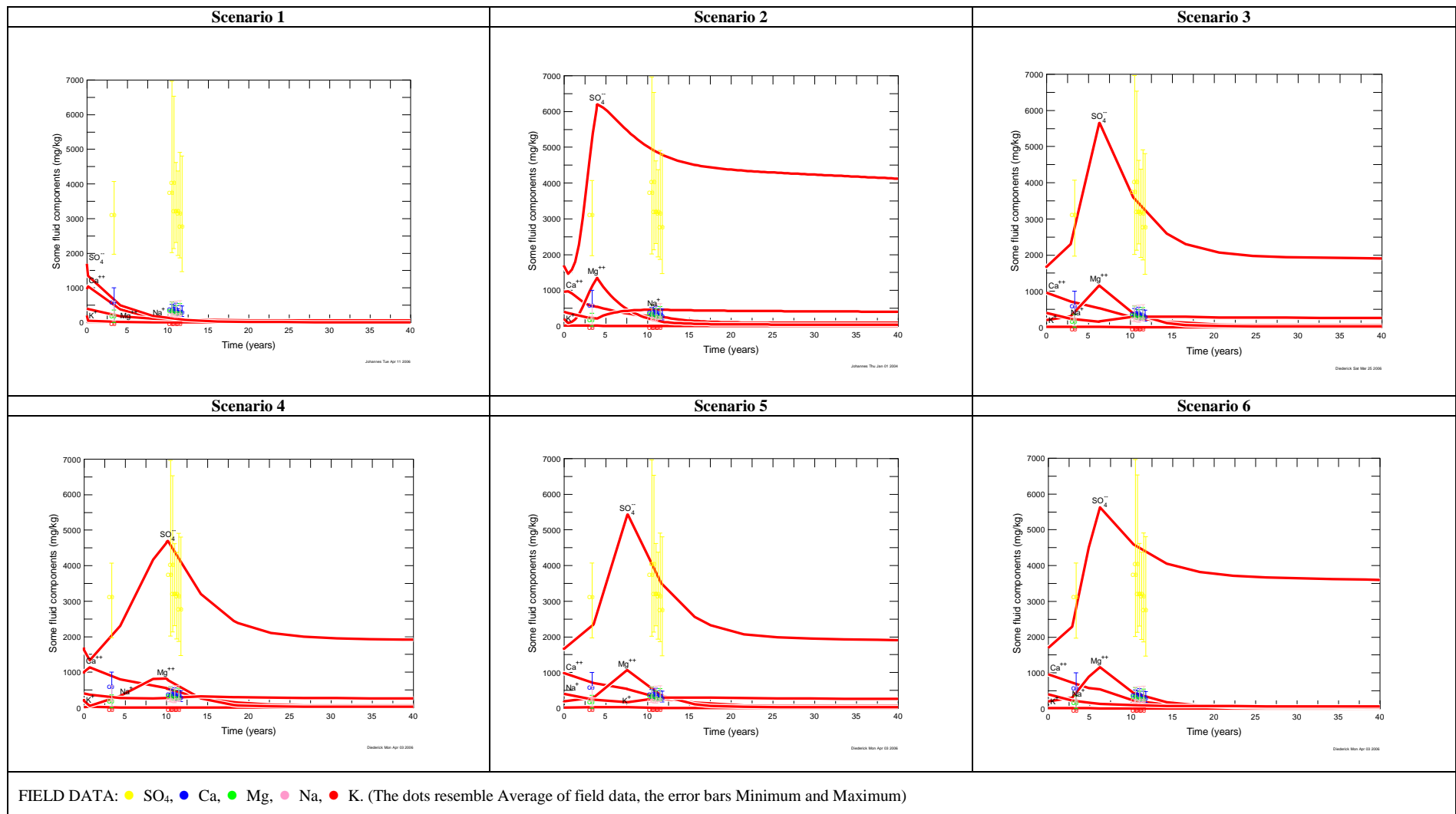


Figure 7.6.3(A). Modelled major element concentrations for Scenarios 1 – 6.

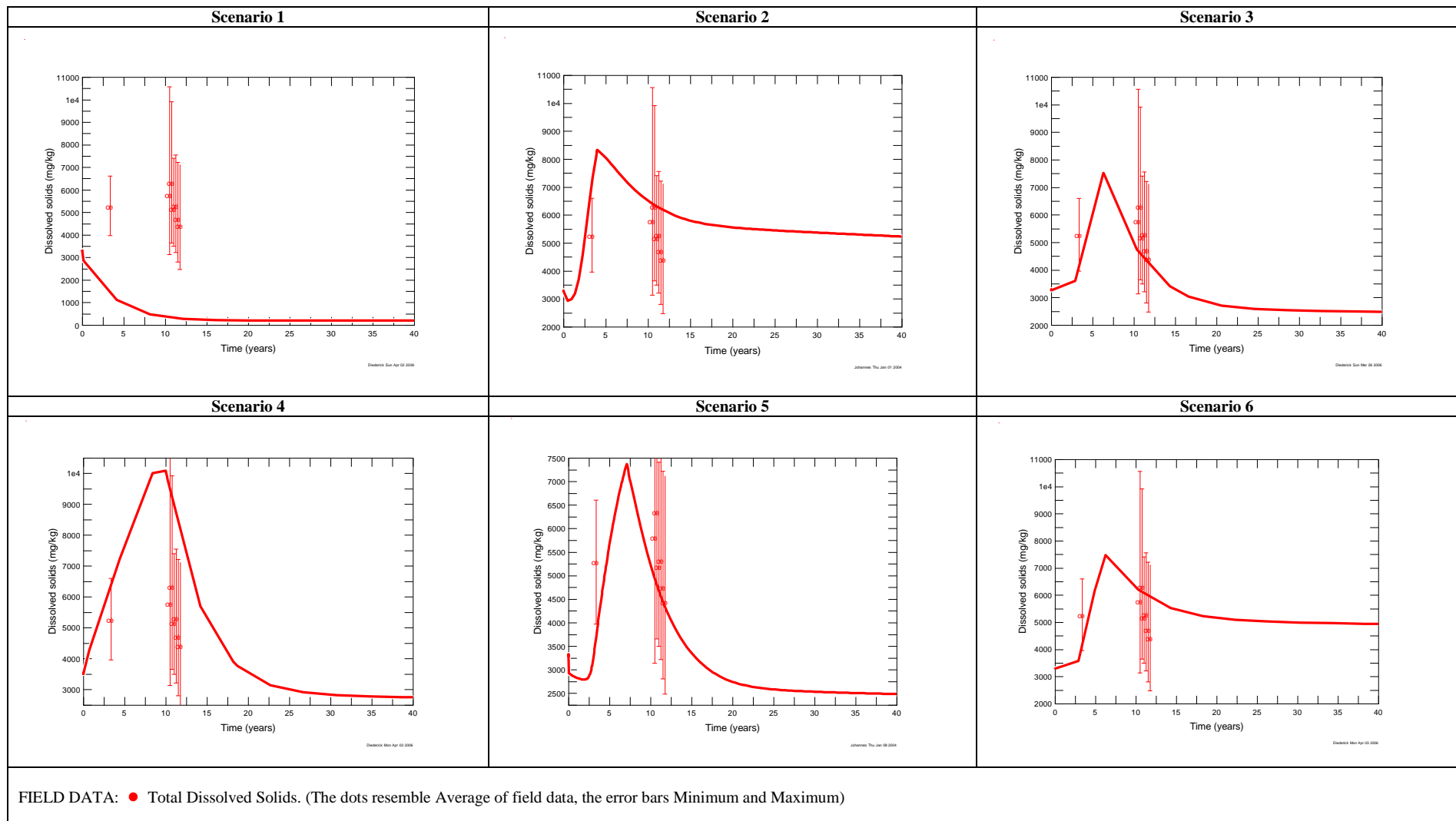


Figure 7.6.3(B). Modelled Total Dissolved Solids for Scenarios 1 – 6.

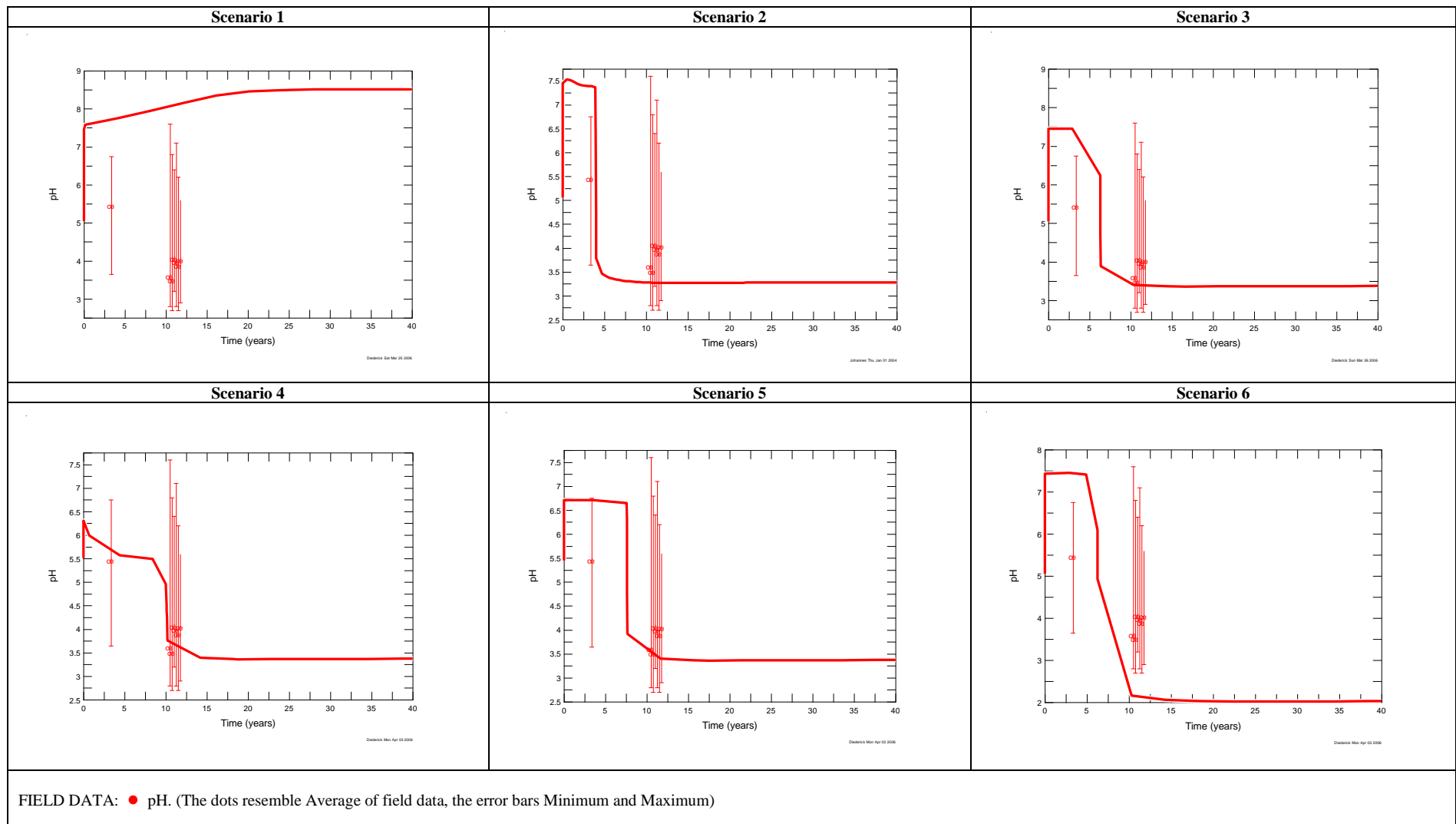


Figure 7.6.3(C). Modelled pH for Scenarios 1 – 6.

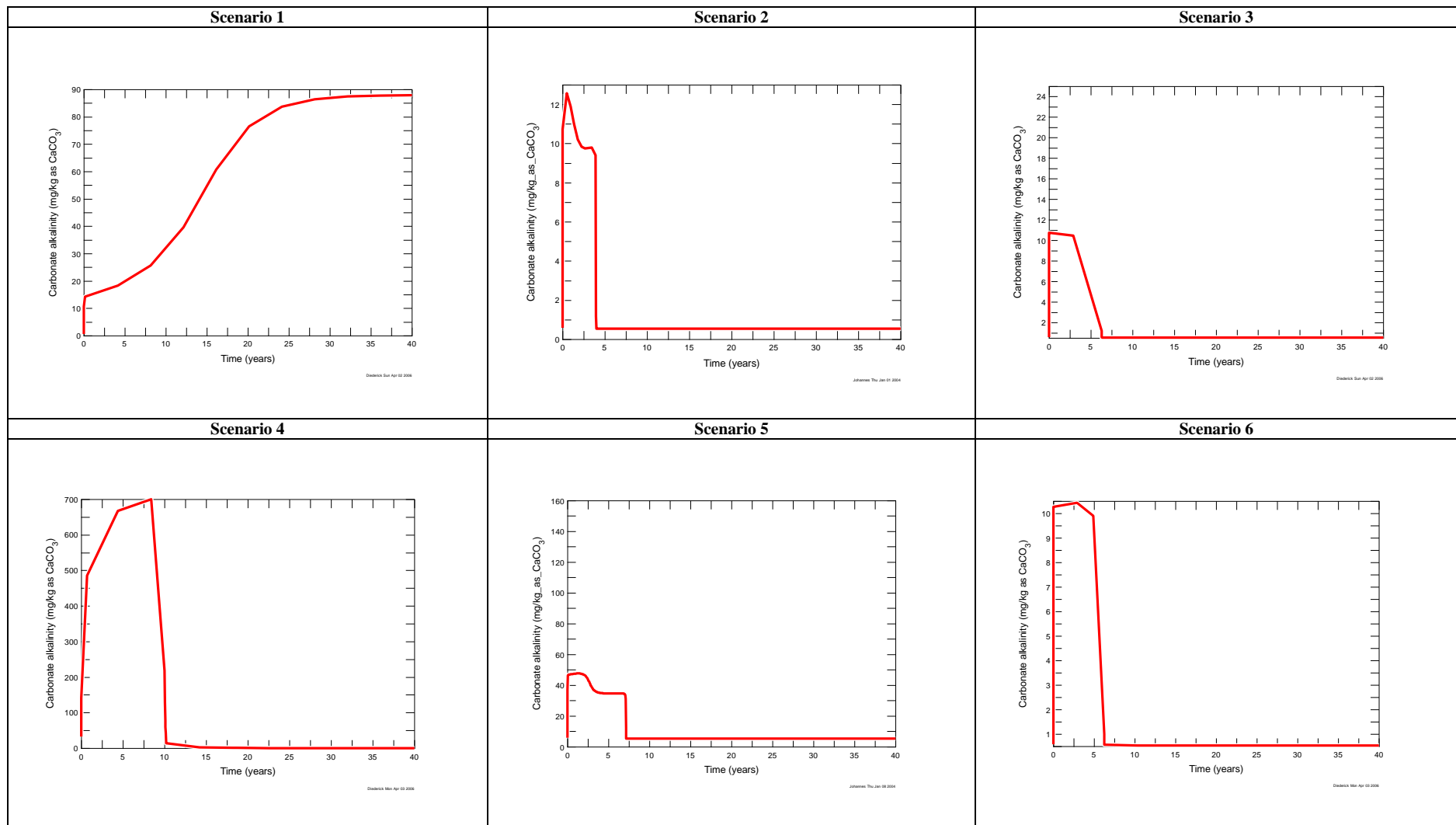


Figure 7.6.3(D). Modelled Carbonate Alkalinity for Scenarios 1 – 6.

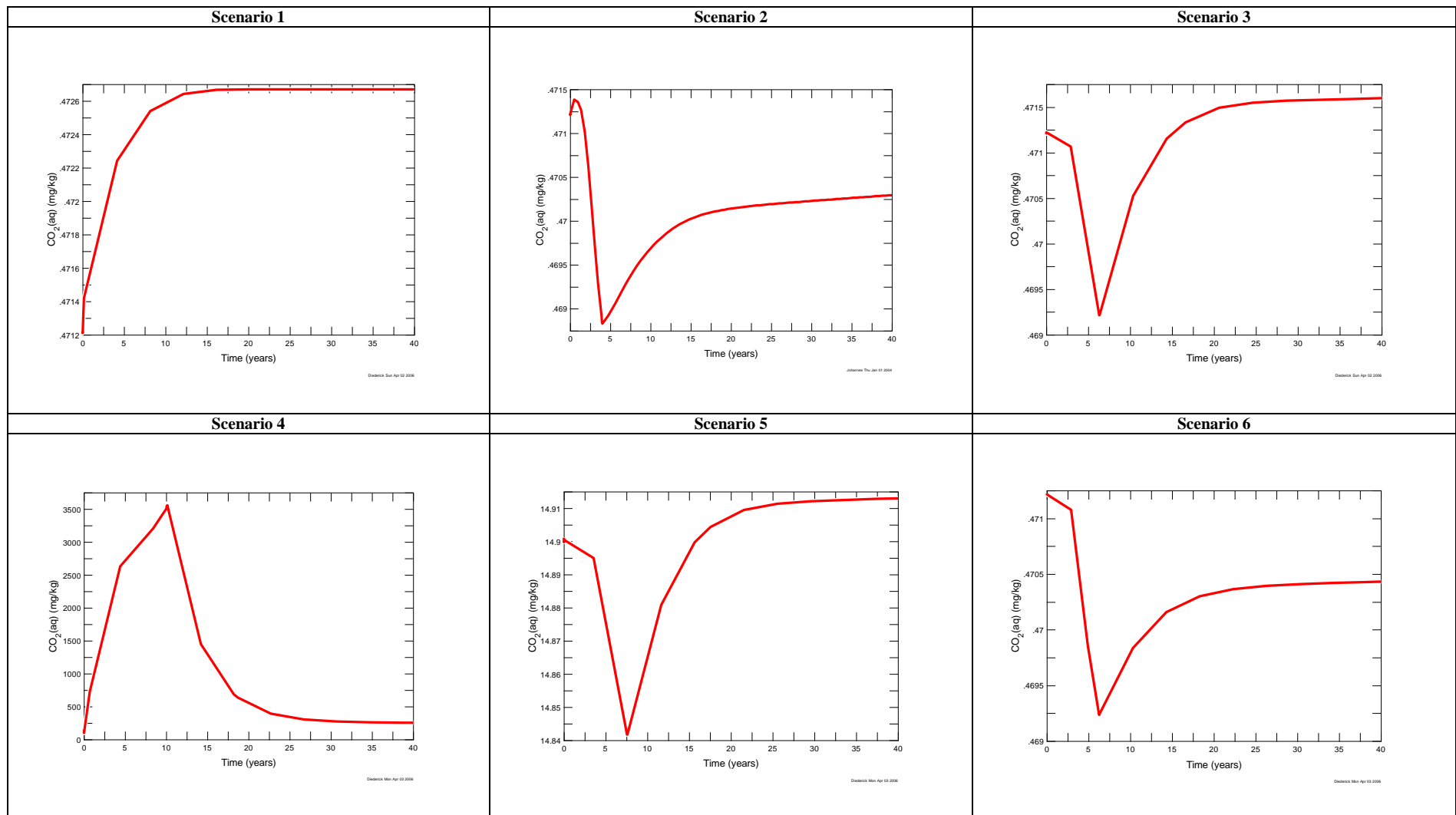


Figure 7.6.3(E). Modelled CO₂(aq) for Scenarios 1 – 6.

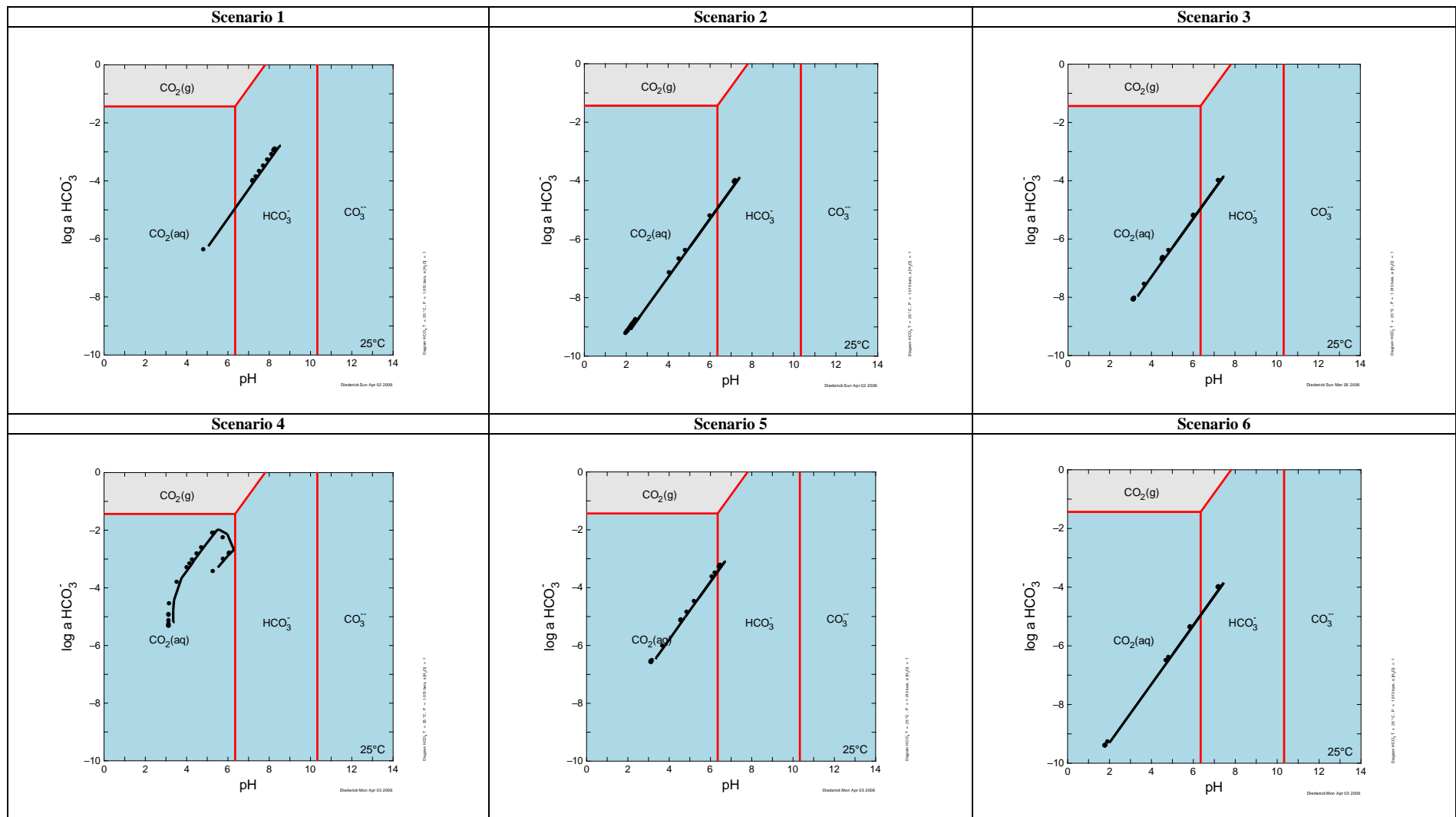


Figure 7.6.3(F). Modelled activity of HCO_3^- for Scenarios 1 – 6 with “Reaction Trace” plotted.

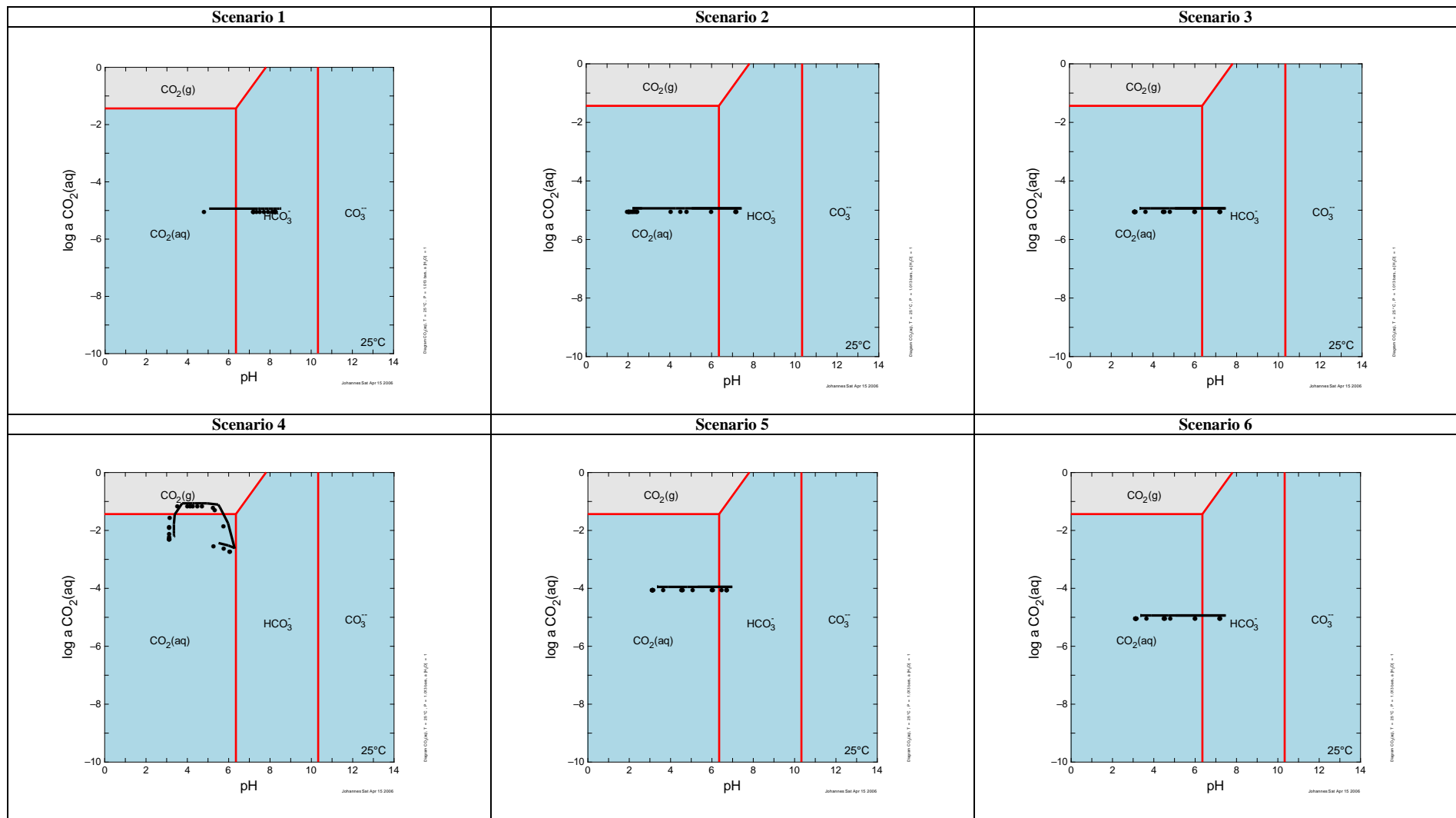


Figure 7.6.3(G). Modelled activity of $\text{CO}_2(\text{aq})$ for Scenarios 1 – 6 with “Reaction Trace” plotted.

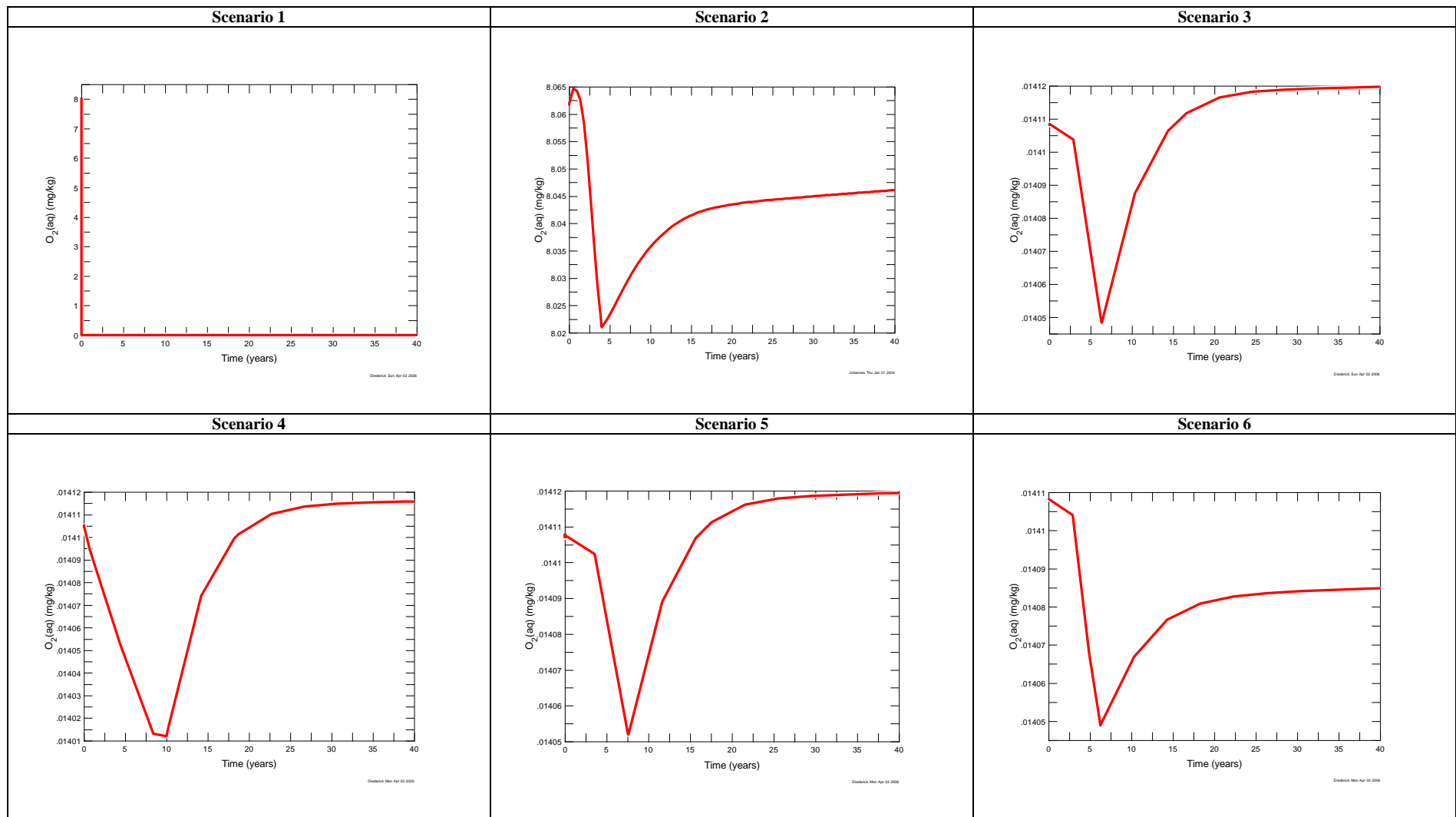


Figure 7.6.3(H). Modelled $O_2(aq)$ for Scenarios 1 – 6.

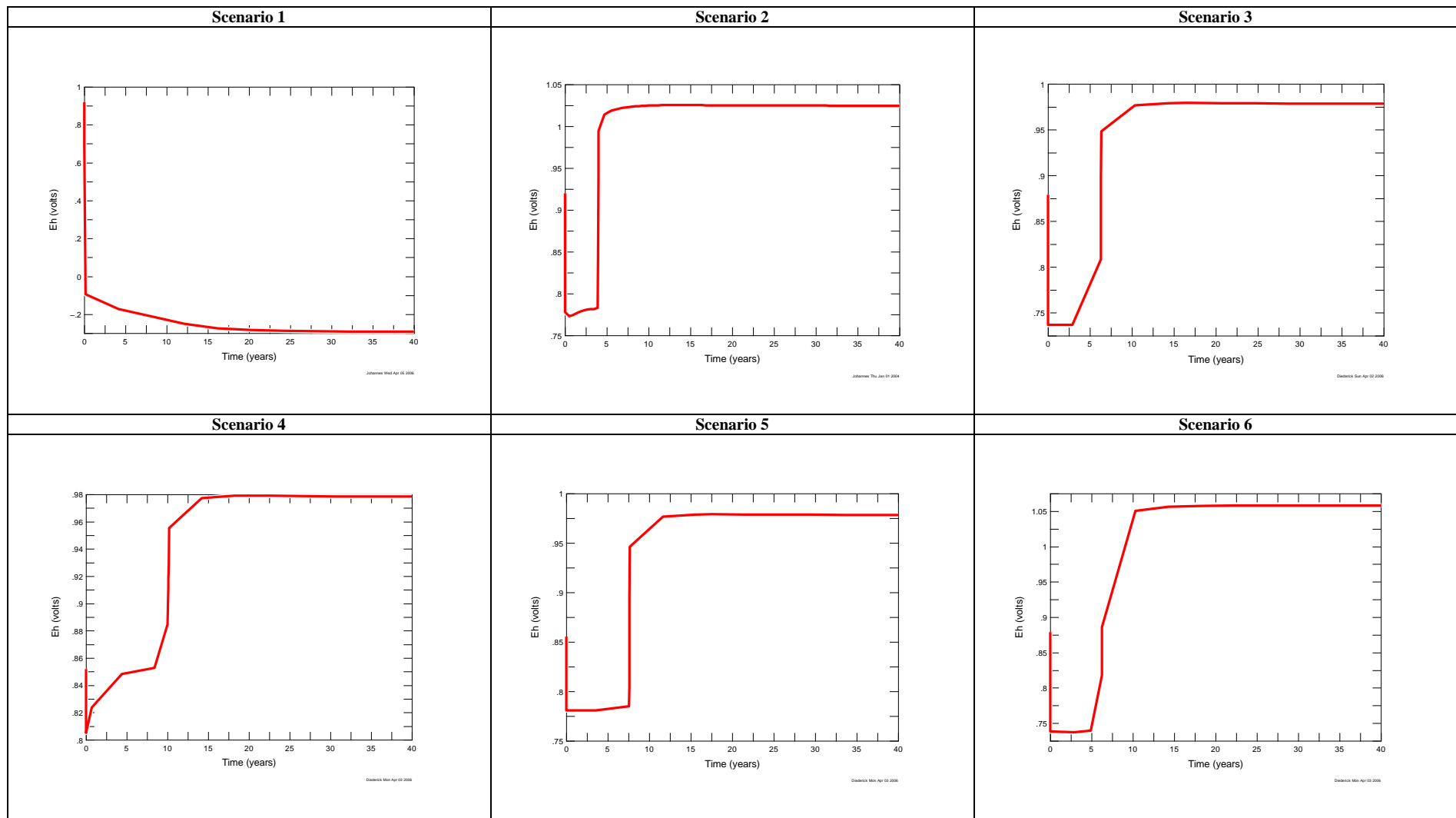


Figure 7.6.3(I). Modelled Eh (V) for Scenarios 1 – 6.

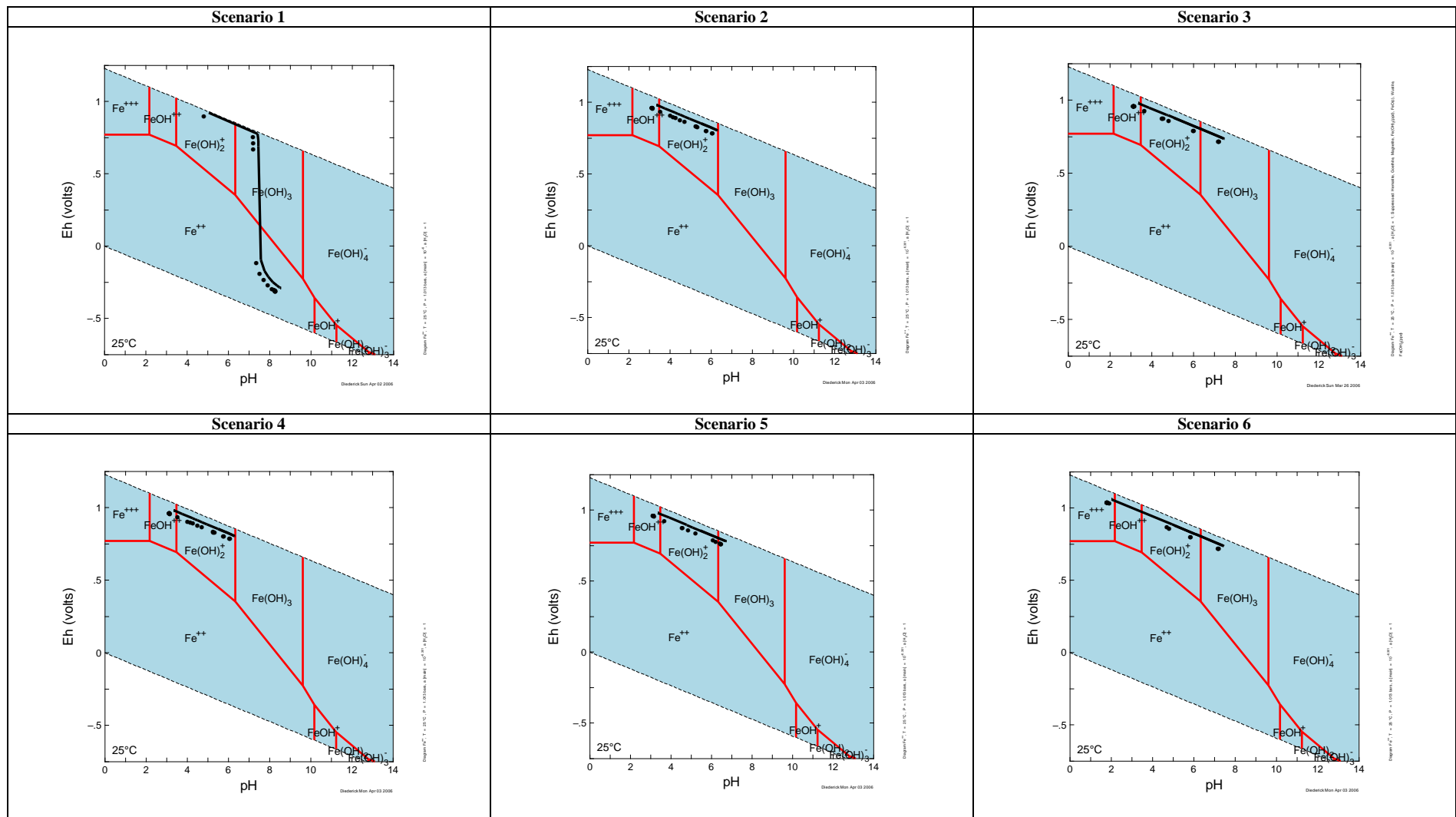


Figure 7.6.3(J). Modelled Eh-pH conditions for Scenarios 1 – 6 (log a_{Fe} = -6.301) with “Reaction Trace” plotted.

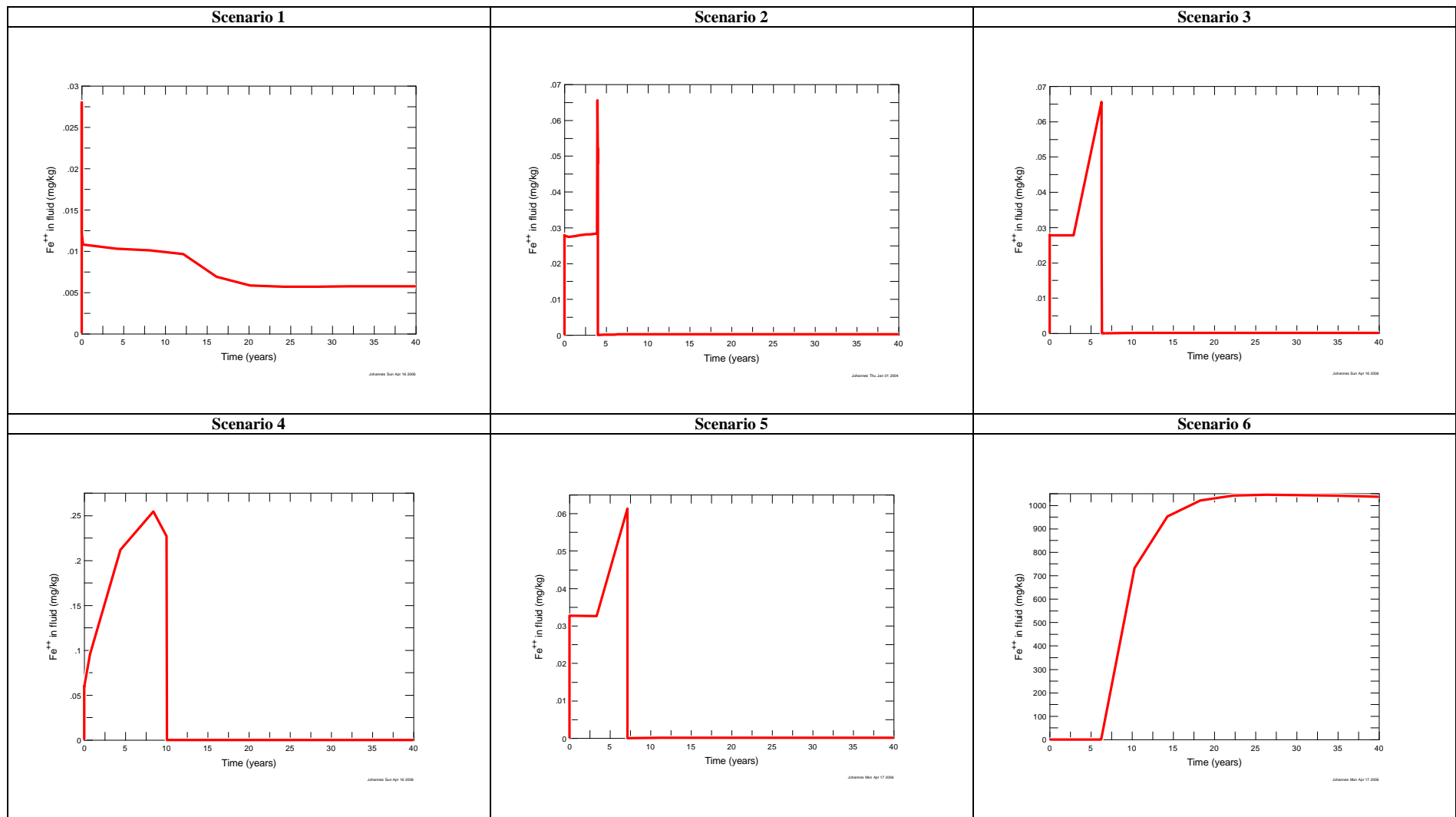


Figure 7.6.3(K). Modelled total Fe in solution for Scenarios 1 – 6.

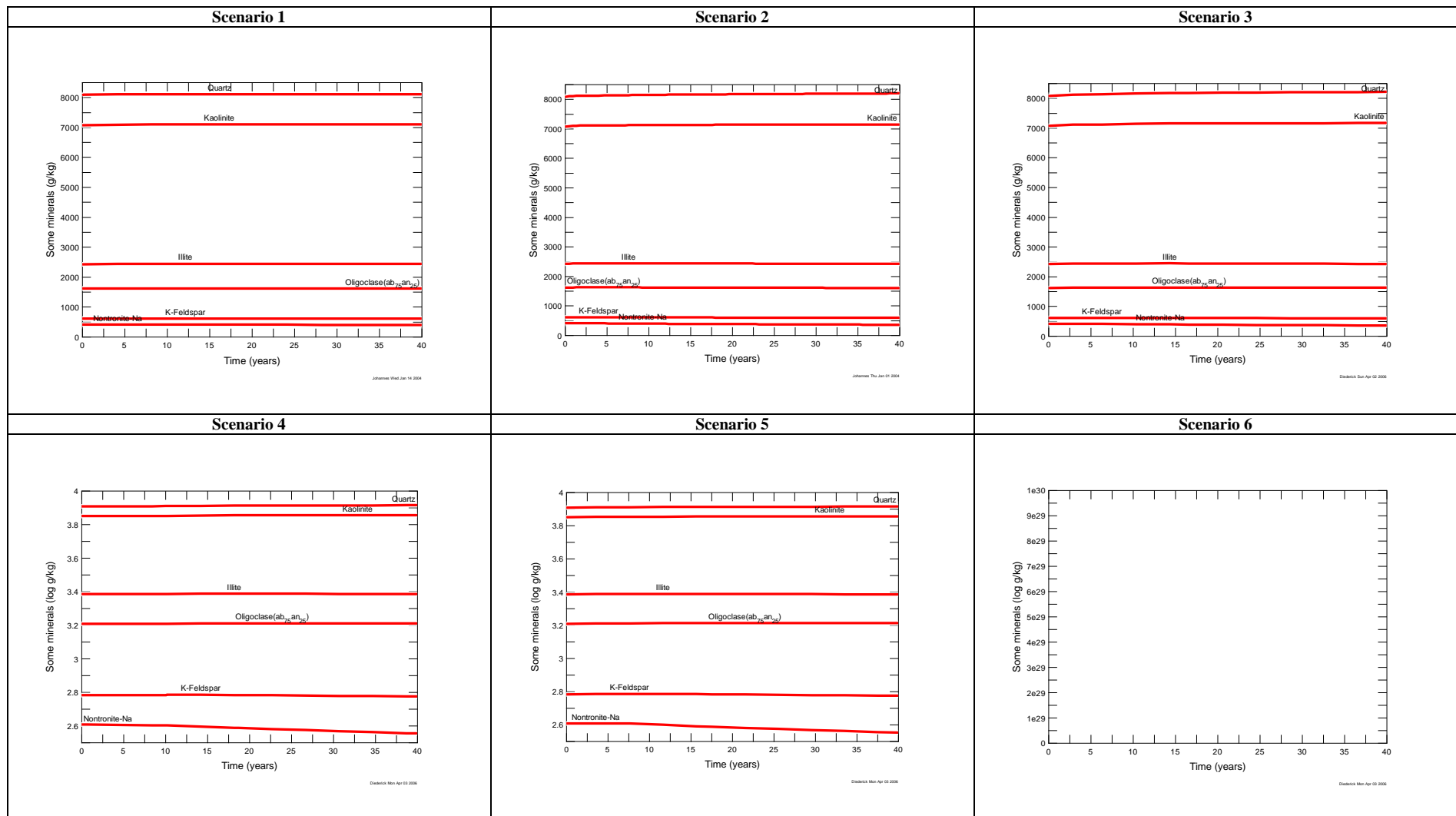


Figure 7.6.3(L). Modelled primary silicates concentrations for Scenarios 1 – 6.

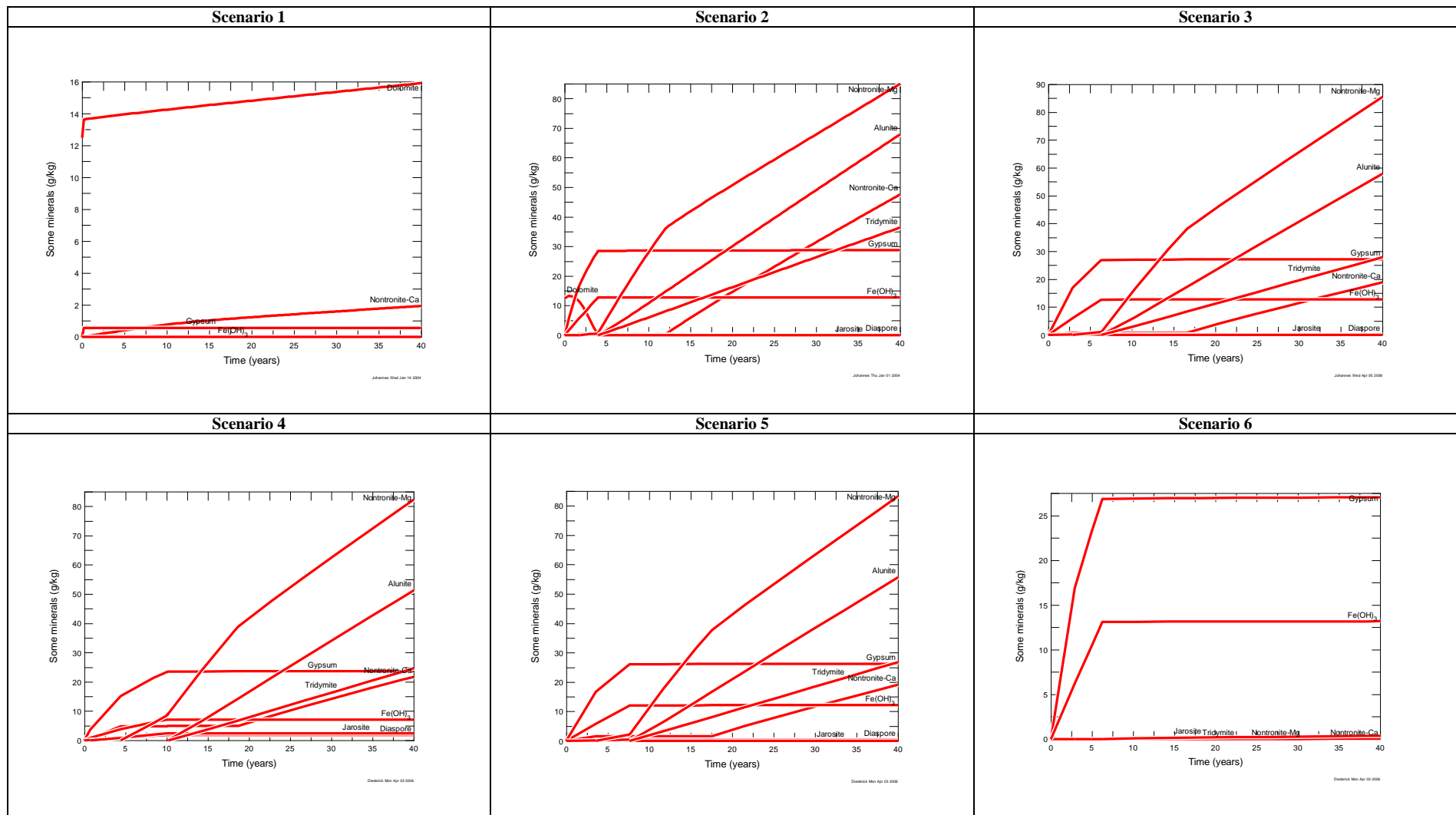


Figure 7.6.3(M). Modelled secondary minerals for Scenarios 1 – 6.

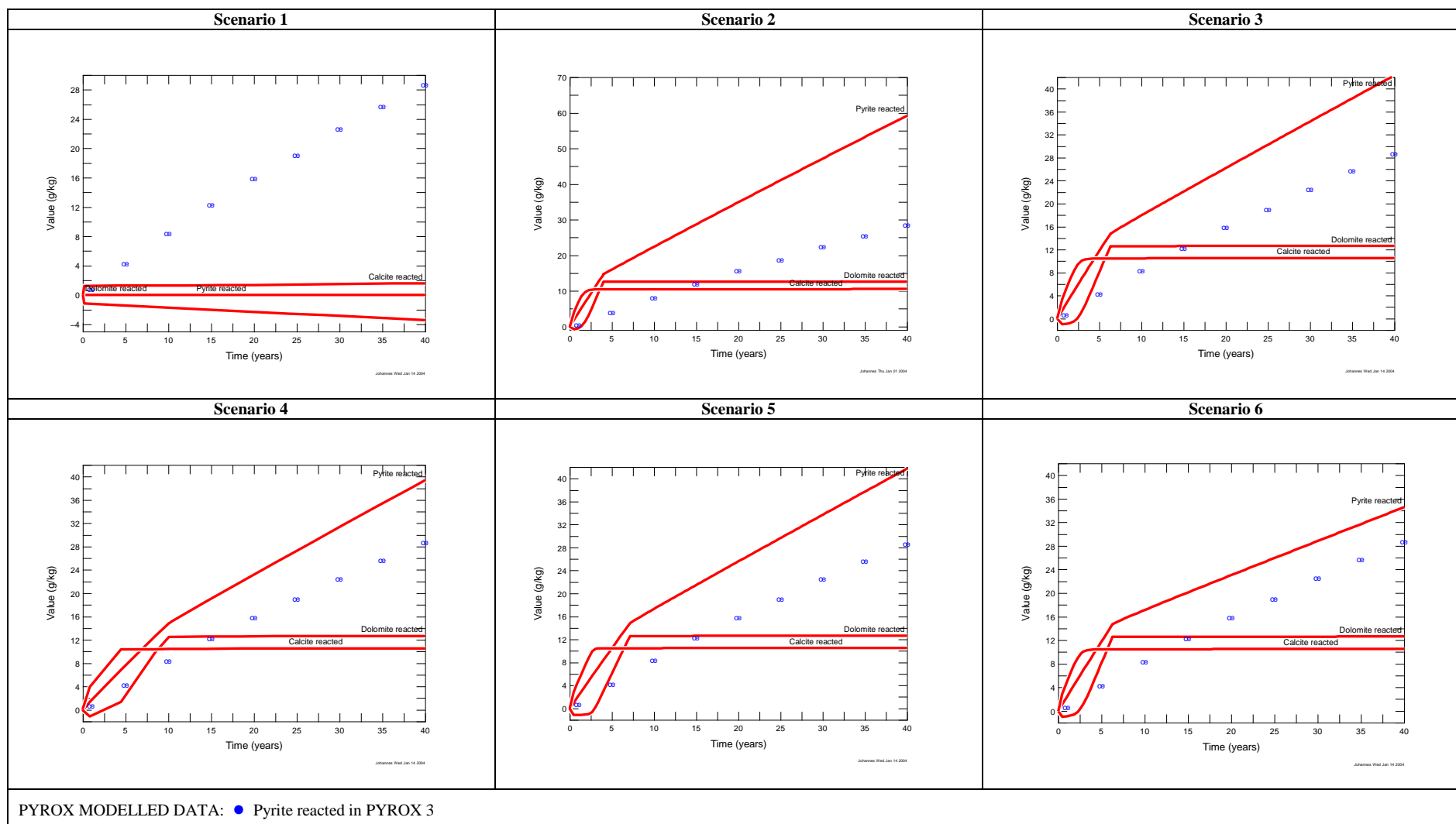


Figure 7.6.3(N). Modelled pyrite, calcite and dolomite reacted for Scenarios 1 – 6.

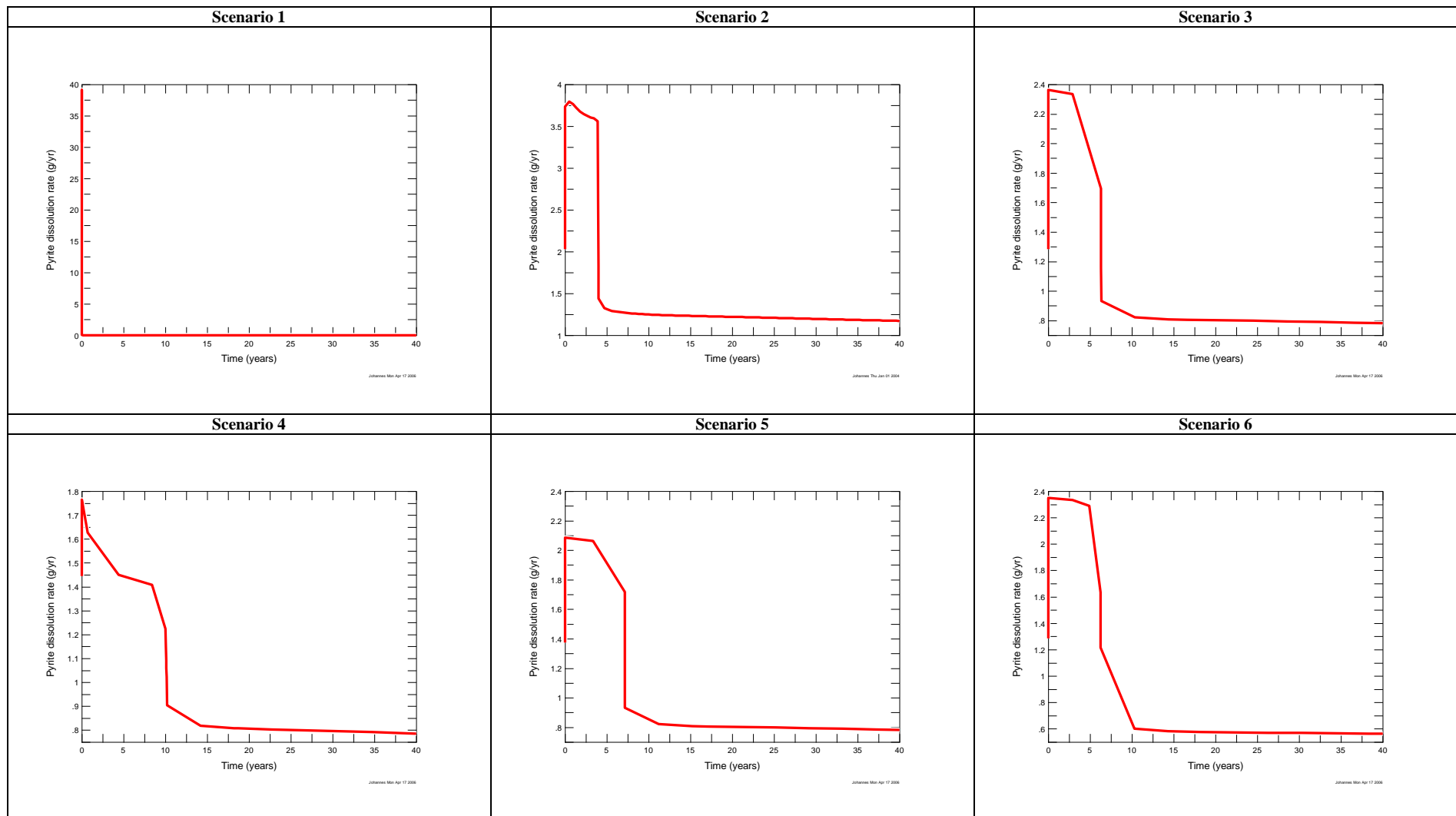


Figure 7.6.3(O). Pyrite dissolution rate for Scenarios 1 – 6.

Additional results for Scenario 5 and 6 are given in **Figure 7.6.3(P) – (R)** below:

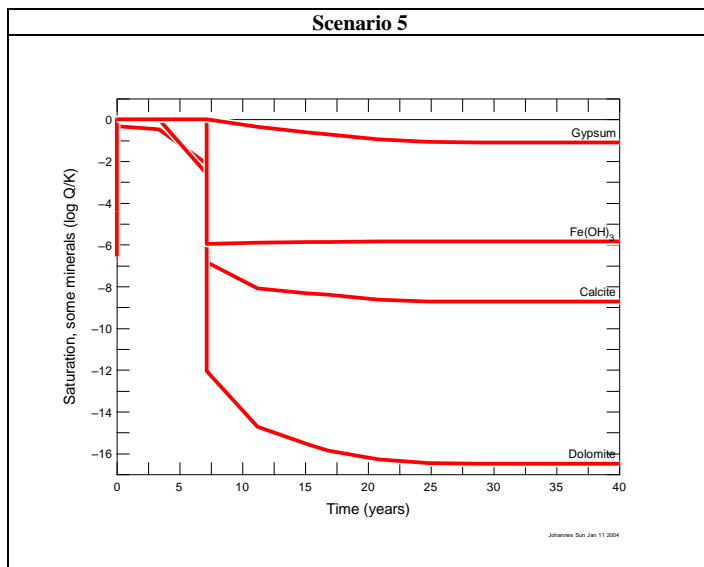


Figure 7.6.3(P). Saturation index for some minerals in Scenario 5.

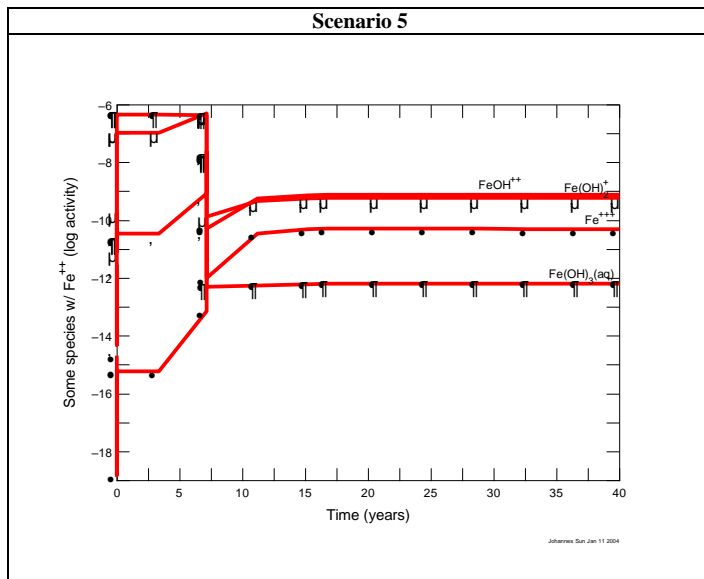


Figure 7.6.3(Q). Activity of Fe-species in Scenario 5.

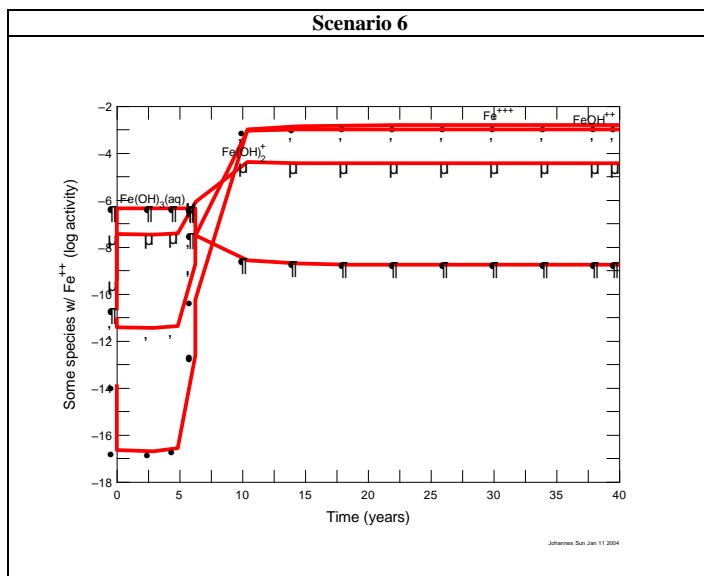


Figure 7.6.3(R). Activity of Fe-species in Scenario 6.

Results for Scenario 7 are depicted in **Figure 7.6.3(S)** and **(T)** below:

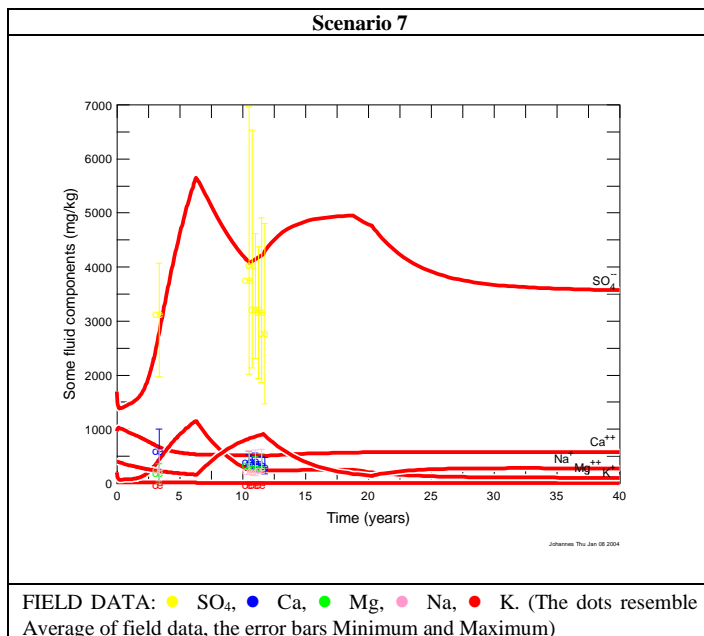


Figure 7.6.3(S). Major parameters in Scenario 7.

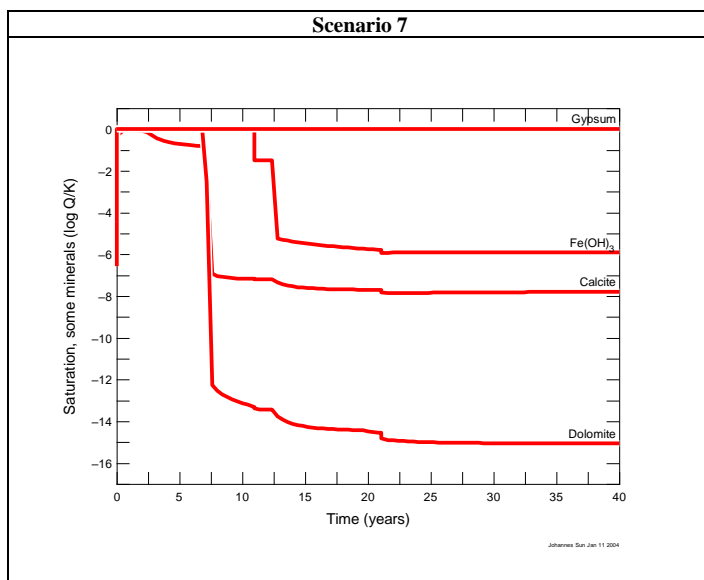


Figure 7.6.3(T). Saturation index for some minerals in Scenario 7.

The modelled water quality from Scenario 5 is given in **Table 7.6.3(A)** below:

Table 7.6.3(A). Modelled water quality from Scenario 5.

Year	Model Time	pH	TDS (mg/l)	Ca (mg/l)	K (mg/l)	Mg (mg/l)	Na (mg/l)	SO ₄ (mg/l)	Alk (CaCO ₃) (mg/l)	Fe (mg/l)
Modelled water quality										
1994*	1.00	7.1	2818.0	939.6	16.1	49.1	324.4	1417.0	47.7	0.030630
1995	2.00	7.1	2792.0	870.0	16.7	55.7	282.9	1495.0	47.0	0.030650
1997	4.00	6.9	4494.0	636.7	18.4	497.2	213.2	3072.0	35.0	0.033230
1999	6.00	6.9	6592.0	549.8	19.9	940.7	172.4	4853.0	34.7	0.033680
2001	8.00	3.6	6647.0	459.5	0.2	866.3	221.1	5006.0	5.3	0.000067
2003	10.00	3.4	5231.0	318.4	0.1	487.5	279.6	3951.0	5.3	0.000112
2005	12.00	3.4	4239.0	228.1	0.0	268.6	297.8	3207.0	5.3	0.000131
2007	14.00	3.4	3587.0	172.4	0.0	143.4	299.0	2717.0	5.3	0.000142
2009	16.00	3.4	3169.0	139.0	0.0	73.4	292.3	2403.0	5.3	0.000149
2011	18.00	3.4	2902.0	104.4	0.0	45.1	282.7	2207.0	5.3	0.000150
2013	20.00	3.4	2743.0	79.2	0.0	34.1	275.9	2092.0	5.3	0.000148
2015	22.00	3.4	2652.0	66.3	0.0	28.5	271.2	2025.0	5.3	0.000147
2017	24.00	3.4	2599.0	59.8	0.0	25.7	268.0	1987.0	5.3	0.000146
2019	26.00	3.4	2567.0	56.7	0.0	24.4	265.6	1963.0	5.3	0.000145
2021	28.00	3.4	2547.0	55.2	0.0	23.7	263.8	1947.0	5.3	0.000144
2023	30.00	3.4	2532.0	54.5	0.0	23.4	262.3	1936.0	5.3	0.000143
2025	32.00	3.4	2520.0	54.2	0.0	23.3	261.0	1927.0	5.3	0.000143
2027	34.00	3.4	2510.0	54.1	0.0	23.2	259.7	1919.0	5.3	0.000142
2029	36.00	3.4	2500.0	54.0	0.0	23.2	258.5	1912.0	5.3	0.000142
2031	38.00	3.4	2491.0	54.0	0.0	23.2	257.4	1905.0	5.3	0.000142
2033	40.00	3.4	2482.0	54.0	0.0	23.2	256.2	1898.0	5.3	0.000141

* 1993 is taken as Year 0. Mining ended at the end of year 1992.

The results and conclusions of the geochemical mass model given in **Figure 7.6.6(A) – (T)** and in **Table 7.6.3(A)** are discussed below:

Scenarios calibrated to field data

- Overall, the most realistic scenarios modelled were Scenario 3 and 5. In these scenarios the rate of pyrite reaction was calibrated to that modelled in PYROX 3. Scenario 3 assumed full contact with the CO₂ in the atmosphere and in Scenario 5 the CO₂ buffer was adjusted (modelled alkalinity calibrated to the carbonate alkalinity) so that the CO₂ system was slightly more closed than Scenario 3.

Major component concentration and TDS in the modelled solution

- In Scenario 1 the sulphate content decreased quickly in solution as shown in **Figure 7.4.6(A)** because of the absence of oxygen to sustain pyrite oxidation. In Scenario 2 the sulphate reached high values because of the high pyrite oxidation rate. These two scenarios indicate that either a completely open or closed system with regard to the oxygen buffer was unrealistic, however, the open system indicated that the system in reality was not too far from an open system with regard to the oxygen buffer.
- In Scenarios 3 – 6 the oxygen buffers were calibrated and more realistic sulphate values were obtained. Because of slower acidification in Scenario 4 compared to Scenario 3, the pyrite oxidation rate was lower with a resultant lowered peak sulphate concentration in the modelled solution. The same was true for Scenario 5 and Scenario 3, only to a lesser degree.

The same long-term sulphate concentration of 1900 mg/l was modelled for Scenario 3 – 5 because of similar long-term pH conditions and oxygen buffers. Scenario 6 showed lowered pH conditions and higher long-term sulphate concentrations than Scenarios 3 – 5. The lowered pH condition in Scenario 6 was attributed to the fact that no acidity was consumed by silicate minerals.

- The calcium and magnesium concentrations in the modelled solutions were highly dependent on the calcite and dolomite dissolution. In Scenarios 2 – 6 calcium decreases in solution as calcite was depleted in the first few model years. Dolomite reacted slower than calcite and therefore magnesium reached its peak concentration only between Year 5 and 10. In Scenario 1 the magnesium decreased in solution because dolomite formed as a secondary mineral.
- The measured sodium content in the actual mine water was fairly high (near 300 mg/l – see **Table 7.3.2(A)**) when compared to the calcium and magnesium concentrations. Sodium containing silicates (Na-smectite and oligoclase) was introduced into the model. In contrast to oligoclase, Na-nontronite (a smectite clay) dissolution contributed significantly to the sodium concentration in the modelled solution.
- The potassium measured in the mine water stayed constant at about 14 mg/l (see **Table 7.3.2(A)**). However, the geochemical model showed that the potassium in concentration will eventually mostly be used up by the precipitation of secondary potassium containing iron and aluminium sulphates.
- The modelled TDS in Scenario 1 decreased to below 400 mg/l. In Scenario 2 it reached high values (> 8000 mg/l) because of the high sulphate content. In Scenario 4 the TDS was higher than in Scenario 3 because of the high alkalinity in the closed system (see **Figure 7.6.3(B)**). The TDS during the first

few modelling years in Scenario 5 was higher than in Scenario 3 because the CO₂ system was slightly more closed. After the first seven modelling years, the TDS in Scenario 6 was higher than in Scenario 3 because of the higher sulphate content as shown in **Figure 7.6.3(B)**.

Alkalinity, the CO₂ buffer and pH

Alkalinity has an inverse relationship with acidity which in turn does not have a normal distribution. Therefore, the arithmetic mean must be used with care when calculating the average pH or alkalinity; both the geometric and harmonic mean must be considered when assessing the average alkalinity value of a data set. For the mine water the geometric mean (as also used for pH) was taken as the most realistic.

- In Scenario 5 the modelled pH was higher during the first seven years (\pm pH 7) than the pH measured in the mine water in 1996 (average pH 5.5). However, the long-term pH modelled after seven years (pH 3.4) was closer but slightly lower than the pH measured in the field (pH 3.6 – 4.1) (see **Figure 7.4.6(C)** and **(D)**).

The pH modelled during the first seven years in Scenario 5 was lower than in Scenario 3 because the CO₂ system was slightly more closed than in Scenario 5 with resultant higher carbonic acid in solution.

In contrast to Scenario 3, Scenario 4 was modelled in a closed CO₂ system. The pH modelled in Scenario 4 (pH 5.6) after seven years was very close to the pH measured in the mine water in 1996 (average pH 5.5).

- Amongst Scenarios 3, 4 and 5, Scenario 5 modelled the carbonate alkalinity during the near neutral stage (\pm 40 mg/l), the closest to the geometric mean of the total alkalinity (66 mg/l) measured during 1996 in the mine water (see **Table 7.3.2(A)**). Scenario 3 modelled the carbonate alkalinity (11 mg/l) closer to the harmonic mean of the total alkalinity measured (18 mg/l) during 1996 in the mine water.

The carbonate alkalinity modelled in Scenario 4 reached a maximum of almost 700 mg/l in solution. The arithmetic mean of alkalinity measured in 1996 was 151 mg/l.

After the first seven years the alkalinity was decreased drastically to 5.3 mg/l in Scenario 5 and to < 1 mg/l in Scenarios 3 and 4. The arithmetic, geometric and harmonic means of the alkalinity measured in the mine water between 2003 and 2004 ranged between 21.3 – 9.8, 7.3 – 7.0 and 5.6 – 6.2, respectively. These averages were actually lower in reality because 5 mg/l were taken as the alkalinity value of samples with alkalinity values below detection limit.

- Alkalinity has an inverse relationship with acidity which in turn does not have a normal distribution. Therefore, the arithmetic mean must be used with care

when calculating the average pH or alkalinity; both the geometric and harmonic mean must be considered when assessing the average alkalinity value of a data set. For the mine water the geometric mean (as also used for pH) was taken as the most realistic.

- Scenario 5 (almost an open CO₂ system) predicted the carbonate alkalinity in the mine water the most accurately while Scenario 4 (closed CO₂ system) simulated the pH during the first seven years the best. Scenario 5 modelled the carbonate alkalinity fairly low in the mine water which was validated by the geometric mean of the measured total alkalinity in the field data. Scenario 4 again modelled the pH closer to the measured pH in the pit water, however the modelled carbonate alkalinity was much higher than that measured in the field.

This is a good example of the disequilibrium that is often present in pollution drainage. The reason for the above disequilibrium is discussed below:

When the mine water is still near-neutral (> pH 5.5), the carbonate minerals are rapidly consumed by the acidity released from the pyrite oxidation. Even when a solution is in contact with the atmosphere the rapid increase in CO₂(aq) does not equilibrate with the CO₂(g) immediately but builds up in solution that leads to a slightly lowered pH because of the increased carbonic acid. Therefore, although Scenario 5 is the most overall realistic scenario, the pH in the mine water does not behave as predicted by Scenario 5 in the first seven years but rather as predicted by the closed CO₂(aq) system in Scenario 4. This CO₂(aq) build-up has also been described by Bethke (1996).

CO₂(aq) is however a much more stable phase (below pH 6.4) than carbonic acid. Appelo and Postma (1993) state that at 25°C, CO₂(aq) is about 250 times more abundant in solution than H₂CO₃(aq). Therefore when CO₂ increases rapidly in solution, it will not only be out of equilibrium with CO₂(g) but also with the bicarbonate and carbonate contents in solution.

Therefore, the mine water during the first seven years has an increased CO₂(aq) content that is not in full equilibrium with CO₂(g) in the atmosphere and the (bi)carbonate content in solution. This leads to a slight decrease in the expected pH and alkalinity.

- In Scenario 1 the modelled system was closed to atmospheric oxygen. No pyrite oxidation was therefore present after the initially present oxygen, at a fugacity of 0.2, was depleted. This led to an increase in alkalinity and pH over the model time as the carbonate system equilibrated with the carbonate mineral content and the atmospheric CO₂ (see **Figure 7.4.6(C)** and **(D)**).
- Scenario 2 and 3 showed almost similar pH conditions since both were in full contact with the atmospheric CO₂. In Scenario 2 the pyrite oxidation rate was

slightly higher and the carbonate minerals were depleted more rapidly than in Scenario 3 (see **Figure 7.4.6(C)** and **(D)**).

- Scenario 6 had the same setup as Scenario 3 except that it contained no primary silicates. This resulted in a lower long term pH of pH 2 and alkalinity of below 1 mg/l (see **Figure 7.4.6(C)** and **(D)**). This showed the importance of silicate minerals for acid consumption over the long term in an AMD system.
- **Figure 7.4.6(G)** shows that the activity of CO₂ for Scenarios 1, 2, 3, 5 and 6 stayed constant over the model time as a constant CO₂ buffer was specified. In Scenarios 2, 3, 5 and 6 the stable CO₂ species changed from bicarbonate to CO₂(aq) as the modelled solution acidified. In Scenario 1 the stable species became bicarbonate as the pH in the model increased. Scenario 4 initially showed such a high CO₂(aq) build-up that CO₂(g) became the stable species. As soon as the carbonate mineral content got depleted, CO₂(aq) once again became the stable species.
- **Figure 7.4.6(E)** shows that the mass CO₂(aq) almost stayed constant in solution in Scenarios 1, 2, 3, 5 and 6 but increases to 3500 mg/kg in Scenario 4. In Scenario 5 the mass CO₂(aq) was higher in solution than in Scenario 3 because Scenario 5 was slightly more closed to the atmospheric CO₂ buffer.
- **Figure 7.4.6(F)** shows that the bicarbonate activity became lower in Scenarios 2 – 6 because of increased acidity, whereas the opposite was true for Scenario 1.

Pyrite in the model

- Experiments by Williamson and Rimstidt (1994) showed that the oxidation of pyrite by oxygen was exponentially dependent on the dissolved oxygen activity by an exponent of 0.50 and on the hydrogen activity by an exponent of -0.11 (see **Section 2.6.5**). The negative dependence of the oxidation rate of pyrite on the hydrogen activity was also illustrated by “Equation 2.6.4(A)” as depicted in **Figure 2.6.5(A)**.

The pyrite oxidation rate as modelled by PYROX 3 at 10 years (0.83 g pyrite/year), was calibrated to the field measurements of oxygen 10 years after mining. The pyrite oxidation rate in GWB was calibrated to the rate in PYROX 3 by adjusting the reactive pyrite surface area to 24 cm²/g. Because the pyrite oxidation rates in GWB and PYROX 3 were equal at 10 years, the same mass pyrite per unit time reacted at that point in both models and the same amount of oxygen was consumed. GWB assumed a steady state oxygen profile whereas the PYROX 3 model inherently assumed a transient state oxygen profile.

- The oxidation rate of pyrite is shown in **Figure 7.4.6(O)**. The oxygen activity in solution was constant in Scenario 2 – 6. Therefore, the dissolution rate was only influenced in the model by the pH. As the pH decreased over the model time, the pyrite oxidation rate also decreased. This was also evident in **Figure 7.4.6(N)** that shows the total pyrite reacted over the model time. The gradient of the “pyrite reacted” decreased after the first few years (seven years in Scenario 5) as the modelled mine water acidified.

Because the pH in Scenario 3 was higher than in Scenario 5, the pyrite oxidation was initially higher in Scenario 3 than in Scenario 5, which was in turn higher than that of Scenario 4. The long-term pyrite oxidation rate was almost the same in the acidic modelled mine water (in Scenario 3 – 5) but higher than the very acidic Scenario 6.

Because of the eventual zero fugacity of oxygen in Scenario 1, the pyrite oxidation rate was zero.

Calcite and dolomite

- The calcite in Scenarios 3 – 6 was depleted before dolomite (see **Figure 7.4.6(N)**). This was because dolomite is more stable than calcite at near neutral conditions and calcite is more stable at alkaline conditions as was shown in **Section 2.7.1**.

In Scenario 5 the calcite was depleted after 3 years and the dolomite after 7 years. In Scenarios 3 and 6 the calcite and dolomite were depleted more rapidly because the CO₂ system was open and in Scenario 4 these minerals are depleted more slowly because of the closed CO₂ system. In Scenario 2 the calcite and dolomite were both depleted more rapidly than in Scenario 5 because of the higher release in acidity.

In Scenario 1 the calcite only initially reacted to neutralize the initial acidity produced from the pyrite oxidation. Dolomite precipitated out of solution since it was stable at near-neutral conditions and because the initial water as well as the inflowing water contained Mg.

- The dissolution and the later depletion of calcite and dolomite had a significant effect on many aspects of the model. Except for the direct effect that calcite and dolomite had on parameters such as pH, TDS, alkalinity and magnesium and calcium ion activities, it also influenced the pyrite oxidation rate indirectly through its buffering of the pH. After the carbonate mineral depletion a decrease in the pH as well as in the pyrite oxidation rate occurred.

The calcite and dolomite decrease also had a significant effect on the gypsum saturation as discussed further below.

Primary silicate dissolution

- In all scenarios that modelled a low long-term pH the quartz mass actually increased (see **Figure 7.6.3(L)**), not only because of the increased Si released into the solution by Na-smectite dissolution, but also because quartz is more stable in acidic conditions as discussed in **Section 2.8.2**. The kaolinite mineral mass also slightly increased in these scenarios as Si and Al were released into solution and kaolinite is generally stable over a very wide pH range.
- In Scenarios 1 – 3 the primary silicate minerals illite, oligoclase and K-feldspar stayed at almost constant concentrations over the model run. The Na-nontronite was the only primary silicate mineral that showed significant dissolution. The dissolution of Na-nontronite also kept the sodium levels in the solution at realistic concentrations.

Secondary minerals

- The models consisted of 1) a near neutral stage where calcite and dolomite buffered the solution and of 2) an acidic stage where the carbonate minerals were depleted and silicate minerals consumed some of the acidity. These two stages had a significant influence on the model pH and the ions in solution.
- Secondary minerals that significantly formed during the near neutral stage were gypsum and $\text{Fe}(\text{OH})_3$ (see **Figure 7.6.3(M)**). These two minerals are described in more detail below.
- During the acidic stage silicate minerals started to dissolve and a variety of ions (Ca, Na, Mg, K, Si, Al and Fe) were released into the solution with a resultant variety of secondary minerals that precipitated. During the acidic stage diasporite, alunite, jarosite, Ca-nontronite, Mg-nontronite and tridymite precipitated.

Saturation of gypsum

- In **Figure 7.6.3(P)** it was shown that during the first seven years of Scenario 5, gypsum was in equilibrium with the modelled solution. After the depletion of calcite and dolomite no more calcium was released into solution and the gypsum became undersaturated. During the acidic stage Ca rather precipitated as Ca-nontronite.
- Input for Scenario 7 was the same as for Scenario 5 except that gypsum was allowed to back-react with the modelled solution so that it could be in full equilibrium ($Q/K = 1$) over the modelled time as shown in **Figure 7.6.3(T)**. However, this led to unrealistic high sulphate values in the modelled solution as shown in **Figure 7.6.3(S)**.

Modelled Eh, Fe in solution, and Fe(OH)₃ saturation

- As the carbonate minerals became depleted, the pH and the pyrite oxidation rate decreased (see **Figure 7.6.3(O)**) while the Eh and the oxygen concentration increased in the model (see **Figure 7.6.3(H) and (I)**). In Scenario 1 the Eh became negative because of no contact with the atmosphere as shown in **Figure 7.6.3(J)**.
- Eh-pH diagrams were also drawn in order to illustrate the most stable iron species in solution. At near-neutral pH, the most stable iron species in solution was Fe(OH)₃. However, with decreased pH the stable species became Fe(OH)₂⁺, Fe(OH)²⁺ and eventually Fe³⁺ as shown in **Figure 7.6.3(J)**. **Figure 7.6.3(Q)** showed that during the near neutral stage (Year 0 – 7) modelled in Scenario 5, Fe(OH)₃ had the highest log activity of about -6.3. During the acidic stage (after Year 7), Fe(OH)₂⁺ and Fe(OH)²⁺ became the dominant species and Fe(OH)₃ was undersaturated as shown in **Figure 7.6.3(P)**. Oxidation of pyrite by ferric iron will however not occur under these conditions because only at pH levels of below pH 3 does the ferric iron activity become high enough to oxidize pyrite (see **Section 2.6.4**). In Scenario 6 the pH reached the lowest level compared to the other scenarios and Fe(OH)²⁺ and Fe³⁺ were the dominant iron species (see **Figure 7.6.3(R)**); the total iron increased to high concentrations as shown in **Figure 7.6.3(K)**.

7.7 Conclusions of the geochemical modelling

The following conclusions are made in terms of the geochemical modelling:

Modelling input and results

- Overall, the most realistic scenarios modelled were Scenarios 3 and 5. In these scenarios the rate of pyrite reaction was calibrated to that modelled in PYROX 3. Scenario 3 assumed full contact with the CO₂ in the atmosphere and in Scenario 5 the CO₂ buffer was adjusted (modelled alkalinity calibrated to the carbonate alkalinity) so that the CO₂ system was slightly more closed than Scenario 3.
- Because the average mine water pH was above pH 3 (ranging between pH 3.6 – 4.1 in the last six monitoring runs), no pyrite oxidation by ferric iron was assumed to take place because all ferric iron will form ferrihydrite, commonly referred to as “yellowboy.” Ferrihydrite is also visually evident in the AMD from the case study mine. Only at pH conditions below pH 3 will the ferric iron activity become high enough to oxidize pyrite.

Bacteria often create micro-environments in coal mine spoils where they catalyse ferrous iron oxidation. If the pH is lower than pH 3, pyrite will be oxidized by the produced ferric iron and hot-spots of increased pyrite

oxidation in the spoils will be created. However, no outliers in the pH, sulphate or temperature were detected in the 16 in-pit boreholes that would indicate any such hot-spots. Therefore, no bacterial activity was considered in this study and only the abiotic oxidation of pyrite by oxygen was modelled. Because the pH in the geochemical model also never reached values of below pH 3, no oxidation of pyrite by ferric iron was modelled.

- The oxygen concentration over the vertical profile (from surface to the bottom of the pit) decreased downwards because of its consumption by pyrite oxidation. Because oxygen was present in the pit water (although at low concentrations), oxygen migration into the unsaturated zone was not seen as the rate limiting step for the pyrite oxidation process. The rate limiting step of the overall pyrite oxidation rate was the oxidation of ferrous iron in solution.
- Pyrite oxidation is an exothermic process and is a source of heat in the pit material. No evidence of increased heat was however observed in the pit water. All heat must therefore be lost to the surrounding environment. Pressure differences in the gas phase due to temperature differences are the driving force for gas convection. Because no evidence of heat differences were observed, oxygen diffusion is seen as the main process of oxygen migration into the pit material. (Other advection processes such as barometric pumping was not considered).
- The pyrite mineral surface was in reality not completely available for oxidation as the mineral is partly in contact with other mineral surfaces. When using the total pyrite mineral surface in a geochemical model the pyrite reaction will therefore be overestimated. This was overcome in PYROX 3 by adjusting the oxygen diffusion coefficient through the oxidized coating of the pyrite grain until the oxygen concentration was calibrated to the observed concentration in the field. The reactive pyrite surface area in GWB was then adjusted until the pyrite reaction rate was the same as that modelled in PYROX 3.
- In the geochemical mass model seven scenarios were run that modelled closed, open and intermediate systems with regard to the oxygen and CO₂ buffer. It was found that the waste material was *almost open* to atmospheric oxygen and CO₂. These characteristics can be attributed to the shallowness of the pit (<15 m).
- The models consisted of 1) a near neutral stage (Year 0 – 7) where calcite and dolomite buffered the solution and of 2) an acidic stage (after Year 7) where the carbonate minerals were depleted and silicate minerals consumed some of the acidity. These two stages had a significant influence on the modelled pH and the ions in solution.

- It was observed however that the modelled solution calculated the pH conditions slightly higher than measured in the mine water during the near neutral stage. It was determined that with the rapid release of acidity and the subsequent carbonate mineral consumption, the mine water had an increased CO₂(aq) content that was not in full equilibrium with CO₂(g) in the atmosphere and the (bi)carbonate content in solution. This led to a slight decrease in the expected pH. The long-term pH modelled was only slightly lower than the pH measured in the field.
- The major parameters in the modelled solution were modelled quite accurately.

In the most realistic scenarios (Scenarios 3 and 5) the sulphate reached values of up to 5500 mg/l during the near neutral stage and decreased thereafter to a long-term concentration of 1900 mg/l.

The calcium and magnesium concentrations in the modelled solution were highly dependent on the calcite and dolomite dissolution in the model. Calcite was depleted during the first few model years. Dolomite reacted more slowly than calcite and magnesium reached its peak concentration a few years later than calcium.

Gypsum stayed at equilibrium during the near neutral stage significantly affecting the calcium concentration in solution. As the calcite and dolomite minerals were depleted gypsum became undersaturated.

The measured sodium content in the mine water was fairly high when compared to the calcium and magnesium concentrations. Sodium containing silicates (Na-smectite and oligoclase) were introduced into the model. In contrast to oligoclase, Na-nontronite (a smectitic clay) dissolution contributed significantly to the sodium concentration in the modelled solution.

- In the most realistic scenarios it was observed that during the near neutral stage Fe(OH)₃ had the highest activity of all iron species in solution. During the acidic stage Fe(OH)₂⁺ and Fe(OH)²⁺ became the dominant species and Fe(OH)₃ became undersaturated. Oxidation of pyrite will however not occur under these conditions because only at pH levels of below pH 3 does the ferric iron activity become high enough to oxidize pyrite.

Shortcomings experienced in the field measurements for model calibration/validation

Listing the major shortcomings experienced would be useful for future studies. The data that will be typically required for future studies is discussed in **Section 8.2**.

The silicate mineral content used in the model were assumed from equivalent coal bearing strata of the Witbank Coalfield as no XRD analyses on the spoil material were

performed. XRD analyses in order to determine the major silicates present would have been very helpful in this study.

A more complete monitoring data set of the leachate chemistry would be invaluable for model validation and calibration.

The oxygen content in the boreholes was only measured once and more oxygen measurements for model calibration is a necessity.

7.8 References

- Appelo, C.A.J., and Postma, D. (1993). *Geochemistry, groundwater and pollution*. Balkema, 536 p.
- Bell, K. and Spurr, M.R. (1986). *The Klip River Coalfield of Northern Natal*. In: Mineral deposits of Southern Africa, vol. II. (eds: Anhaeusser, C.R. and Maske, S.). Geological Society of South Africa, Johannesburg, pp. 2033 – 2046.
- Bethke, C.M. (1996). *Geochemical reaction modeling*. Oxford, 397 p.
- Bredenkamp, D.B., Botha, L.J., Van Tonder, G.J., and van Rensburg, H.J. (1995). *Manual on quantitative estimation of groundwater recharge and aquifer storativity*. WRC Report No. TT 73/95, Water Research Commission, Pretoria, 363 p.
- Cadle, A.B., Cairncross, B., Christie, A.D.M. and Roberts, D.L. (1990). *The Permo-Triassic coal-bearing deposits of the Karoo Basin, Southern Africa*. Information Circular No. 218, Economic Geology Research Unit, University of the Witwatersrand, Johannesburg.
- Cairncross, B., Hart, R.J. and Willis, J. (1990). *Geochemistry and sedimentology of coal seams from Permian Witbank Coalfield, South Africa; a means of identification*. Int. J. Coal Geol., 16, 309-325.
- Kleinmann, R.L.P., Crerar, D.A. and Pacelli, R.R. (1981). *Biogeochemistry of acid mine drainage and a method to control acid formation*. Mining Engineering, 33, 300-303.
- Nordstrom, D.K. (1982). *Aqueous pyrite oxidation and the consequent formation of secondary iron minerals*. In: *Acid sulfate weathering* (eds. Kittrick, J.A., Fanning, D.S. and Hossner, L.R.), Soil Science Society of America, pp. 37-63.
- Snyman, C.P. (1998). *Coal*. In: *The mineral resources of South Africa* (eds: Wilson, M.G.C. and Anhaeusser, C.R.). Handbook, Council for Geoscience, Pretoria, vol. 16, p. 40 –45.
- Tankard, A.J., Jackson, M.P.A., Eriksson, K.A., Hobday, D.K., Hunter, D.R., and Minter, W.E.L (1982). *Crustal evolution of Southern Africa – 3.8 Billion Years of*

Earth History. Springer-Verlag, New York, 523 p.

Wates, J.A. and Rykaart, E.M. (1999). *The performance of natural soil covers in rehabilitating open-cast mines and waste dumps in South Africa*. WRC Report No. 575/1/99, Water Research Commission, Pretoria.

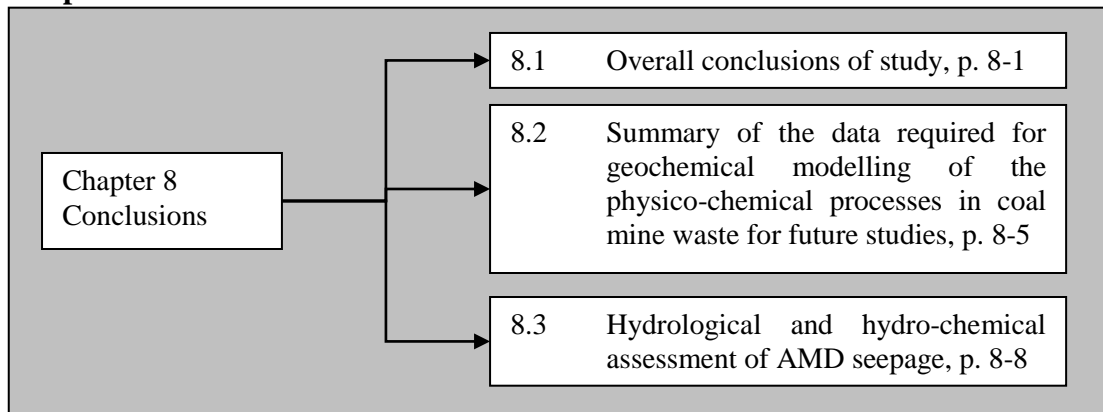
Williamson, M.A. and Rimstidt, J.D. (1994). *The kinetics and electrochemical rate-determining step of aqueous pyrite oxidation*. *Geochim. Cosmo. Acta*, vol. 58, pp. 5443-5454.

Woodward, A.C. and Chevallier, L. (2002). *Hydrogeology of the main Karoo Basin: Current knowledge and future research needs*. WRC Report No. TT 179/02, Water Research Commission, Pretoria, 466 p.

Wunderley, M.D., Blowes, D.W., Frind, E.O., and Ptacek, C.J. (1996). *Sulphide mineral oxidation products in mine tailings impoundments: A numerical model*. *Water Resources Research*, vol. 10, pp. 3173 – 3187.

8 Conclusions

Chapter Structure



8.1 Overall conclusions of study

The study covers a wide range of aspects that relate to the production of AMD in the coal mine environment.

PART I included all the literature research done in this study on the physico-chemical processes in coal mine waste including governing mineral reactions, mineral kinetics, thermodynamics, as well as gas migration and heat flow in coal mine waste. PART II included the description of coal discard and spoil quality in South Africa and the modelling of the physico- chemical processes in a case study.

The major conclusions made from the study are as follows:

Mineralogy

- Pyrite was precipitated in an anoxic-sulphidic geochemical environment during coal formation. Because of mining, pyrite is exposed to the oxic environment where it oxidizes and produces acid. The overall pyrite reaction series is among the most acid-producing of all weathering processes in nature.
- The carbonate system is by far the most important buffer for water systems in nature. This is because carbonate minerals are 1) widely present in sedimentary rocks and 2) have a relative high reaction rate when under-saturated.

Carbonate minerals play the most important role in the neutralization of acid mine drainage from coal mines in South Africa. In the Karoo Super Group (that contains all South African coal) carbonate minerals are present in-situ in the coal bearing strata.

- Silicate minerals consume acid as they dissolve because of the hydrolysis of silica tetrahedral consuming acid. The lower the Si/O ratio in the silicate

structures, the higher the charge on the silicate tetrahedral and the greater the potential to neutralize acid.

Silicate minerals will not play a significant role in the neutralization of acidic drainage over the short term (during the life of the mine) but they would definitely play a role over the long term as was also shown in the case study.

Oxygen migration into coal mine wastes

- Diffusion is described by Fick's Law that states that flux is directly proportional to the gradient across a surface and inversely proportional to the resistance to flow.

After their initial placement gaseous diffusion is the main process providing oxygen within coal mine waste rock. Diffusion remains active thereafter as long as the oxidation process contributes to the depletion of the oxygen concentration in the gas phase within the pile.

Molecular diffusion is a spontaneous process. It increases with increasing temperature and are resisted in the unsaturated zone by the mineral matrix, water-filled pores, other gas molecules and by bacteriological and pyrite consumption.

- Advection in spoil material is described using Darcy's Equation for advective airflow. This equation is partially differentiated to the direction of the potentiometric gradient, but the dimension of time could also be added to compensate for barometric pressure.

Advection is a passive mechanism of air migration into coal mine waste. Various mechanisms for gaseous advection exists in waste material:

- Convection due to heat gradient.
- Convection due to changes in gas composition.
- Barometric pumping.
- Change in saturation.

Heat flow

- Heat has an indirect influence on every aspect of Acid Mine Drainage (AMD) production in coal mine waste material e.g. the microbial activity, gas migration, the rate of chemical reactions etc. The distribution of heat flow is an integral part of gas flow as it not only influences the kinetic energy of gas molecules during diffusion but differences in temperature also leads to resultant gas convection.
- Heat flow occurs in mine waste material by means of conduction, convection, radiation and latent heat.

Coal discard

- More than 1000 Mt of discard and a total of 52.8 Mt of dumped slurry are present in the South African coalfields. Coal discard analysed in this study, showed a high net acid generation potential, whether it was subjected to spontaneous combustion or not. It can be concluded that coal discard has a high potential to generate AMD.

Mine spoils

- Coal mine spoils comprise of uneconomical coal seams, carbonaceous and non-carbonaceous clastic rocks.
- The average pyrite content decreases from coal samples to carbonaceous clastic rocks to non-carbonaceous clastic rocks. Pyrite is also higher in the Witbank Coalfield samples than in the Highveld Coalfield samples. Pyrite in non-carbonaceous clastic rocks was probably epigenetically deposited.
- No other iron sulphide mineral than pyrite has been identified in this study.
- Calcite and dolomite is higher in low to medium ash coal than in high ash coal or clastic rocks. In contrast siderite tends to be higher in high ash coal and in carbonaceous clastic rocks.
- In coal and clastic rocks of the Vryheid Formation it was found that some trace to dominant minerals were present that were also identified in other studies. These minerals include quartz, kaolinite, calcite, dolomite, mica, K-feldspar, plagioclase, siderite, pyrite, illite/smectite, smectite and anatase.

Modelling of the physico-chemical processes in coal mine waste material

- The oxygen diffusion part of the problem was solved using PYROX 3. In order to model the drainage quality from the pit, the Geochemist's Workbench 6.0.3 (GWB) was used.
- The pyrite oxidation rate in GWB was calibrated by adjusting the reactive pyrite surface area until it was equal to the pyrite oxidation rate modelled by PYROX 3.
- One of the shortcomings in PYROX 3 was that the pyrite oxidation is only dependent on the availability of oxygen at the reaction sites and not on the hydrogen activity in the solution.
- In the geochemical mass model seven scenarios were run that modelled closed, open and intermediate systems with regard to the oxygen and CO₂ buffer. It was found that the waste rock material was almost open to the

atmospheric O₂ and CO₂ buffers. This could be attributed to the shallowness of the pit (<15 m). The waste material was only slightly closed to the atmosphere with calibrated CO₂ and O₂ buffers of respectively $f_{\text{CO}_2} = 0.0031$ and $f_{\text{O}_2} = 0.08$.

- The model consisted of 1) a near neutral stage where calcite and dolomite buffered the solution and 2) an acidic stage where the carbonate minerals were depleted and silicate minerals consumed some of the acidity. These two stages had a significant influence on the modelled pH and the activity of ions in solution.
- It was observed that sulphate reaches its peak concentration (5500 mg/l) in the near neutral stage just before the acidification of the pit water, whereafter it decreases steadily before reaching a long-term concentration of nearly 1900 mg/l.

The calcium and magnesium concentrations in the modelled solution were highly dependent on the calcite and dolomite dissolution in the model. Calcite was depleted in the first few model years, however, dolomite reacted slower and magnesium therefore reached its peak concentration later than calcium in solution.

Gypsum stayed at equilibrium during the near neutral stage significantly affecting the calcium in solution. As soon as the carbonate minerals were depleted, gypsum however became undersaturated.

- During the neutral stage Fe(OH)₃ had the highest activity of all iron species. Fe(OH)₃ became undersaturated while Fe(OH)₂⁺ and Fe(OH)²⁺ were the dominant species during the acidic stage. However, the ferric iron activity becomes only high enough at pH levels of below pH 3 in order to oxidize pyrite.
- Bacteria often create micro-environments in coal mine spoils where they catalyse ferrous iron oxidation. If the pH is lower than pH 3 pyrite will be oxidized by the produced ferric iron and hot-spots of increased pyrite oxidation in the spoils will be created. However, no outliers in the pH, sulphate or temperature were detected in the 16 in-pit boreholes that would indicate any such hot-spots. Therefore, no bacterial activity was considered in this study and only the abiotic oxidation of pyrite by oxygen was modelled. Because the pH in the geochemical model also never reached values of below pH 3, no oxidation of pyrite by ferric iron was modelled. Furthermore, any biotic pyrite oxidation rate in the field could not be easily measured and implementation thereof in a numerical geochemical model is remote. The biggest shortcoming of geochemical modelling is therefore the impossibility of including the full heterogeneity of the pit into a model. This shortcoming is however also applicable to field work – measurement of the

physical and geochemical heterogeneity in the subsurface remains a challenge, and even more so for any biotic activity and metabolism.

8.2 Summary of the data required for geochemical modelling of the physico-chemical processes in coal mine waste for future studies

A comprehensive list of methods available to determine the physico-chemical conditions and properties of waste material are listed in **Table 8.2(A)** below. However, the final input that will be required for a geochemical model of the site will depend on the aim of the modelling exercise and the conceptual model of the site.

Table 8.2(A). Main characterization and interpretation methods available to determine the physico-chemical conditions and properties of waste material (edited from Lefebvre et al., 2001).

Characterization and interpretation methods	Physico-chemical properties				
	Waste material	Pyrite oxidation and other mineral reactions	Fluid flow	Heat transfer	Gas diffusion
1. Field measurements and monitoring					
1.1) Leachate chemistry	x	X			
1.2) Leachate flow			X		
1.3) Temperature in boreholes		X	X	X	x
1.4) Oxygen in boreholes		X	X		X
1.5) Pressure in boreholes			X		
1.6) Permeability tests			X		
2. Laboratory measurements					
2.1) Grain size	X	X	x		
2.2) Total rock surface area	X	X			
2.3) Water content	x	x	X	X	X
2.4) Pyrite concentration	X	X			X
2.5) Rock mineralogy	X	X		X	
2.6) Acid-base accounting	X	X			
3. Analytical models or simple numerical interpretations					
3.1) Temperature profiles		X	x	X	x
3.2) Oxygen profiles		X			X
3.3) Cyclic temperature			X	X	
3.4) Barometric pressure			X		
3.5) Water balance		X	X	x	

Key to symbols as related to the determination of the classes of physical properties: **X** – direct relationship; X – significant indirect relationship; x – qualitative or very indirect relationship; no symbol denotes insignificant usefulness.

The main methods available to determine the physico-chemical conditions and properties of waste material listed in **TABLE 8.2(A)** are briefly discussed as follows:

- Collecting of the geochemical modelling input consists of the following aspects:
 - 1) Field measurements and monitoring.
 - 2) Laboratory measurements.
 - 3) Analytical and numerical interpretations.
- The coal mine waste material has the following classes of physico-chemical properties and processes: the physical and geochemical properties of the waste rock, the oxidation process of pyrite, fluid (water and gas) flow, heat flow and oxygen diffusion.
- Monitoring of the leachate quality (1.1 in **Table 8.2(A)**) from the waste rock gives valuable information on the composition of the source. It is critical to monitor the quality of the leachate in order to validate and to calibrate the model. With no monitoring data no proper geochemical modelling can be performed.
- Leachate flow measurements (1.2 in **Table 8.2(A)**) in the field can be valuable in order to calibrate the calculated water balance (3.5 in **Table 8.2(A)**). However, sometimes it may be impossible to make direct flow measurements because of subsurface seepage from the site whereas in other instances it could be done fairly accurately (e.g. such as surface decant measurements at open-cast mines). For modelling of the leachate quality that results from the mineral reactions in the waste rock, it is important to model the overall water balance (3.5 in **Table 8.2(A)**) of the waste material. The water balance is also used for modelling of the heat distribution through the waste material
- Temperature measurements (1.3 in **Table 8.2(A)**) and calculated temperature profiles (3.1 in **Table 8.2(A)**) are used to specify the temperature at which mineral reactions takes place throughout the waste material. Temperature measurements and cyclic temperature variation (3.3 in **Table 8.2(A)**) are also critical in order to monitor the heat distribution through the dump and modelling of the convective gas flow. Although temperature is not the driving force of diffusion (as in convective flow), some modelling parameters in diffusion must also be calculated using temperature measurements.
- Oxygen measurements (1.4 in **Table 8.2(A)**) are critical to calculate the oxygen profiles (3.2 in **Table 8.2(A)**) through the waste material. This will be used as important input for calculating the pyrite oxidation process.

- Pressure and permeability measurements in boreholes (1.5 and 1.6 in **Table 8.2(A)**) are important to determine the advective air flow through the waste material.
- Grain size analyses and determination of the total rock surface area (2.1 and 2.2 in **Table 8.2(A)**) are both valuable for estimation of the mineral surface area. In this study the reactive pyrite surface area was estimated through modelling. However, experimental work would be valuable to verify model calibrations.
- The water content of the waste rock (2.3 in **Table 8.2(A)**) is used in the calculation of the diffusion, heat and fluid flow through the unsaturated zone. Water has a high heat capacity and influences heat distribution significantly. The water content in the unsaturated zone has a significant effect on the effective oxygen diffusion coefficient. Because of the influence on the oxygen and temperature profiles it also has an important indirect influence on the pyrite oxidation rate.
- The pyrite concentration (2.4 in **Table 8.2(A)**) of the waste material must be determined and will be used as important input in the determination of the pyrite oxidation rate and the gas diffusion rate in the waste material. ABA (Acid-base accounting) (2.6 in **Table 8.2(A)**) can be used to predict the net acid generation potential of coal mine waste. In this study the pyrite and carbonate minerals were respectively calculated from the %S and the NP of the ABA results. If possible this must be validated by X-ray diffractometry (XRD) results. Care must be taken in direct use of XRD results as XRD only gives semi-quantitative estimation of the minerals present in the rock.
- The total waste rock mineralogy (2.5 in **Table 8.2(A)**) is important to know when the aim of the model is to model the quality of the leachate from the waste material. The carbonate and also some silicate minerals buffer the leachate pH and have therefore an indirect influence on the pyrite oxidation rate since the pyrite oxidation rate is actually also dependent on the hydrogen activity. Minerals also have different specific heat conductivities and will have an important effect on the heat distribution in the waste material.

No geochemical model is unique as described by Bethke (1996) and every modeller has a different conceptualization of the geochemical problem. As stated previously field measurement of the total heterogeneity of the waste material is also not practically possible. In South Africa field measurements are furthermore often limited by the project budget.

8.3 Recommendations for future studies

The modelling approach used in this study can not be directly applied to other sites where different oxygen transport conditions are present. The mine-site modelled in this study was almost open to the atmospheric O₂ and CO₂. The temperature measured in boreholes inside and outside the pit was the same and it was assumed therefore that little oxygen convection took place. These characteristics can be attributed to the shallowness of the pit (<15 m).

Numerous other coal mine waste sites exist that have larger pyrite contents (e.g. discard dumps) where higher temperature gradients are present with possible significant convective flow. Spoils may also have a smaller ratio between acid generation and neutralization potentials than discard material. Therefore, longer periods of pH buffering will occur in spoil material.

Other sites will also have much different geometries (e.g. discard dumps) and thicker soil covers. There exists therefore a large research field for future modelling studies in South Africa when considering the different external (precipitation, site geometry etc.) and internal properties (mineralogy, gas migration etc.) of different sites.

Further research on the physico-chemical properties of coal mine waste may include the use of different modelling techniques and approaches. Advective flow can be modelled using variations of the TOUGH2 model that was originally developed by Pruess (1991). TOUGH2 is a numerical simulator used for multiphase fluid and heat flow. Fieldwork in advective flow studies can include pressure measurements down boreholes and barometric measurements at sites.

In future studies where the focus is also on diffusion modelling, more detailed field measurements must be performed than in this study and research funds must therefore be obtained. For instance, oxygen measurements must be taken more regularly or oxygen and temperature probes can be installed within the boreholes or in the waste material. Almost no mines in South Africa include oxygen and temperature measurements in their monitoring programs.

A list of the shortcomings experienced in the field measurements for model calibration/validation in this study are given in **Section 7.7**.

Modelling of coal mine waste sites will become increasingly more important as more mines close in especially the Witbank and Highveld coalfields. In South Africa the number of operating coal mines has declined from 112 in 1986, to 65 in 2004. Modelling of AMD at coal mining sites will have fundamental applications to make informed choices in water quality implications in South Africa.

8.4 References

Bethke, C.M. (1996). *Geochemical reaction modeling*. Oxford, 397 p.

Lefebvre, R., Hockley, D., Smolensky, J., and Gélinas, P. (2001). *Multiphase transfer*

processes in waste rock piles producing acid mine drainage - 1: Conceptual model and system characterization. Journal of Contaminant Hydrology, vol. 52, pp. 137-167.

Pruess, K. (1991). *TOUGH2 – A general purpose numerical simulator for multiphase fluid and heat flow.* LBNL-29400, UC-251, Earth Sciences Division, Lawrence Berkeley National Laboratory, Berkeley, CA, 1991.

ABSTRACT

In the first part of this study the typical physico-chemical processes involved in Acid Mine Drainage (AMD) generation were discussed. This included a detailed description of mineralogical reactions, oxygen migration processes and heat conduction typically found in coal mine wastes. In the second part of the study the mineralogy as well as the AMD generation potential of coal mine spoils and discard in South Africa was assessed. A geochemical model of the AMD generation at a rehabilitated backfilled open-cast mine was constructed that simulated the oxygen diffusion process.

Coal mine wastes produce Acid Mine Drainage (AMD) due to the ingress of oxygen and the subsequent oxidation of pyrite in the waste rock. As coal mine wastes consume oxygen, oxygen molecules will spontaneously diffuse into the coal mine waste rock along the concentration gradient. Oxygen migration into coal mine wastes also occurs through the passive process of advection. Mechanisms for advection include 1) air convection due to heat differences or changes in gas composition, 2) barometric pumping or 3) changes in water saturation.

Heat is generated in coal mine waste mostly through pyrite oxidation and spontaneous combustion of coal. Heat flow occurs by means of conduction, convection, radiation and latent heat. Heat has an indirect influence on every aspect of Acid Mine Drainage (AMD) including microbial activity, gas migration, the rate of chemical reactions etc.

Coal discard analysed in this study showed a high net acid generation potential, whether subjected to spontaneous combustion or not. Overall it can be concluded that coal discard has a high potential to generate AMD in South Africa. In spoil material it was found that some trace to dominant minerals were present that were also identified in other studies. These minerals include quartz, kaolinite, calcite, dolomite, mica, K-feldspar, plagioclase, siderite, pyrite, illite/smectite, smectite and anatase. The average pyrite content decreased from coal samples to carbonaceous clastic rocks to non-carbonaceous clastic rocks. The net acid generation potential was found to increase upwards from the No. 1 to the No. 4 coal seam.

In the case study, one dimensional modelling of oxygen diffusion through waste material was performed using the PYROX 3 model of the University of Waterloo. The interaction between the gas, mineral and water phases was modelled using The Geochemist's Workbench 6 (GWB).

Consumption of oxygen by pyrite resulted in a decrease in oxygen concentration towards the bottom of the pit. Oxygen was however present in the saturated zone at the bottom of the pit and oxygen migration into the unsaturated zone was therefore not seen as the rate limiting step for the overall pyrite oxidation process.

The pyrite oxidation rate was determined in PYROX after calibrating the oxygen concentration in the model to field conditions. By adjusting the reactive pyrite surface area in GWB the pyrite oxidation rate was calibrated to the rate modelled in PYROX.

In the geochemical mass model seven scenarios were run that modelled closed, open and intermediate systems with regard to the oxygen and CO₂ buffer. It was found that the geochemical system was nearly open to atmospheric oxygen and CO₂, which can be attributed to the shallowness of the pit (average depth of 12 m).

During the first few years a near neutral stage (pH 5.5 - 7.5) existed where calcite and dolomite buffered the solution. After depletion of the carbonate minerals an acidic stage (pH 3.0 - 4.0) followed where silicate minerals consumed some of the acidity. These two stages had a significant influence on the mineral reactions in the waste material and the ion concentrations in the pit water.

The abiotic rate of pyrite oxidation by oxygen is positively dependent on the dissolved oxygen activity and negatively dependent on the hydrogen activity. As the pH decreased over the model time, the pyrite oxidation rate also decreased.

The concentrations of all the major parameters and of iron in the pit water were modelled. It was observed that sulphate reached its peak concentration during the near neutral stage just before the acidification of the pit water and thereafter it decreased steadily before reaching a long-term concentration.

During the neutral stage Fe(OH)₃ had the highest activity of all iron species. Fe(OH)₃ became undersaturated while Fe(OH)₂⁺ and Fe(OH)²⁺ were the dominant species during the acidic stage. Oxidation of pyrite by ferric iron did however not occur as the ferric iron activity became only high enough at pH levels of below pH 3.

This study showed that the AMD process can be successfully modelled using numerical modelling. In South Africa the number of operating coal mines have declined significantly over the past two decades and numerous coal discard dumps are present throughout coalfields. Modelling of AMD at coal mining sites will become increasingly more important for management decisions as more mines close in the Witbank and Highveld coalfields.

OPSOMMING

In die eerste gedeelte van hierdie studie is die fisies-chemiese prosesse wat 'n rol speel in die produksie van suur-mynwater bespreek. Hierdie gedeelte sluit 'n gedetailleerde beskrywing van die mineralogiese reaksies, die suurstofmigrasie prosesse en die hitte-generasie wat tipies gevind word in steenkoolmyn afvalprodukte. In die tweede gedeelte van hierdie studie word die mineralogie sowel as die suur-mynwater produksie potensiaal van die steenkoolmyn afvalprodukte in Suid-Afrika ondersoek. 'n Geochemiese model van die suur-mynwater produksie by 'n gerehabiliteerde oopgroefmyn is gebruik om die diffusie van suurstof in die myn in te simuleer.

Steenkoolmyn afvalprodukte genereer suur-mynwater weens die infiltrasie van suurstof en die gevolglike oksidasie van piriet in die afvalmateriaal. Soos wat die materiaal suurstof verbruik sal suurstofmolekules spontaan diffundeer in die materiaal in, in reaksie op die konsentrasiegradiënt wat geskep word. Suurstofinfiltrasie kan ook passief plaasvind naamlik deur adveksie. Meganismes van adveksies sluit in 1) lugkonveksie weens hitte- of lugsamestellingsverskille, 2) barometriese drukking of 3) veranderinge in waterversadiging.

Hitte word geproduseer in steenkoolmyn afvalmateriaal deur die oksidasie van piriet, en deur die spontane verbranding van steenkooluitskot. Hittevloei vind plaas deur geleiding, konveksie, radiasie en latente hitte. Hitte het 'n indirekte invloed op elke aspek van die produksie van suur-mynwater, insluitend mikrobiële aktiwiteit, gasmigrasie, chemiese reaksie tempo's ens.

Steenkooluitskot van die veredelingsproses het in hierdie studie 'n hoë potensiaal getoon om suur-mynwater te genereer. Dit was selfs ook die geval vir steenkooluitskot wat onderhewig was aan spontane verbranding.

In steenkoolmyn afvalgesteentes is spoor tot dominante minerale teenwoordig wat ook in ander studies geïdentifiseer was. Hierdie minerale sluit in kwarts, kaolinite, kalsiet, dolomiet, mika, K-veldspaat, plagioklaas, sideriet, piriet, illiet/smekiet, smekiet en anataas. Die gemiddelde piriet inhoud neem af vanaf steenkool na koolstofhoudende klasties gesteentes na nie-koolstofhoudende klastiese gesteentes. Dit is gevind dat die netto suur-mynwater produksie potensiaal toegeneem het opwaarts vanaf die Nr. 1 na die Nr. 4 steenkoolsoom.

In die gevallestudie is een-dimensionele suurstofdiffusie deur die steenkoolmyn afvalmateriaal gemodelleer met behulp van die PYROX 3 model van die Universiteit van Waterloo. Die interaksie tussen die gas-, mineraal- en waterfase is gemodelleer met The Geochemist's Workbench 6 (GWB).

Verbruik van suurstof deur piriet lei tot 'n afname in die suurstofkonsentrasie nader aan die vloer van die myn. Suurstof was wel gevind in die waterversadigde sone op die vloer en suurstofmigrasie in die onversadigde sone is dus nie beskou as die tempobepalende stap vir suurmynwater produksie nie.

Die piriet oksidasietempo is bepaal in PYROX deur dit met die gemete suurstofkonsentrasie in die versadigde sone te kalibreer. Die reaktiewe piriet oppervlakarea in GWB was aangepas totdat die piriet oksidasietempo gekalibreer was met dié van PYROX.

In die geochemiese massamodel was sewe scenarios uitgevoer om geslote, oop en intermediêre sisteme ten opsigte van suurstof en CO₂ buffers te modelleer. Dit is bevind dat die geochemiese sisteem amper oop was vir atmosferiese suurstof en CO₂, wat toegeskryf kan word aan die feit dat die myn redelik vlak is (gemiddelde diepte 12 m).

Gedurende die eerste paar jare in die model het 'n ampere neutrale-fase (pH 5.5 - 7.5) voorgekom waarin kalsiet en dolomiet in kontak met die oplossing as buffers opgetree het. Na die totale verbruiking van die karbonaatminerale het 'n suurfase (pH 3.0 - 4.0) gevolg waarin silikaatminerale van die suur begin verbruik het. Hierdie twee fases in die geochemiese model het 'n betekenisvolle invloed gehad op die mineraalreaksies in die afvalmateriaal en die ionkonsentrasies in die gemodelleerde mynwater.

Die tempo van die abiotiese oksidasie van piriet deur suurstof is positief afhanklik aan die suurstof aktiwiteit en negatief afhanklik aan die waterstof aktiwiteit in die oplossing. Soos die pH oor die gemodelleerde tyd afneem sal die piriet oksidasietempo ook afneem.

Die konsentrasies van al die hoof parameters asook die van yster in die mynwater is gemodelleer. Sulfaat bereik sy piek konsentrasie gedurende die neutrale-fase voor versuring van die mynwater plaasvind. Gedurende die suurfase neem die sulfaatkonsentrasie geleidelik af totdat dit stabiliseer en 'n langtermyn konsentrasie bereik.

Gedurende die neutrale-fase het Fe(OH)₃ die hoogste aktiwiteit bereik van al die ysterspesies. Fe(OH)₃ word egter onderversadig terwyl Fe(OH)₂⁺ and Fe(OH)²⁺ die dominante spesies is gedurende die suurfase. Volgens die model vind die oksidasie van piriet deur Fe³⁺ nie plaas aangesien Fe³⁺ se aktiwiteit eers hoog genoeg is onder pH vlakke van pH 3.

Hierdie studie het getoon dat die prosesse wat 'n rol speel in die produksie van suurmynwater suksesvol numeries gemodelleer kan word. In Suid-Afrika het die hoeveelheid operasionele steenkoolmyne betekenisvol afgeneem gedurende die afgelope twee dekades en talle steenkooluitskothope is ook teenwoordig in die steenkoolvelde. Soos wat meer steenkoolmyne sluit sal die modellering van suurmynwater by steenkoolmyne toenemend meer belangrik word vir bestuursbesluitneming.

Terme hierbo gebruik:

- 1) Steenkoolmyn afvalprodukte = Coal mine waste
- 2) Steenkooluitskot van die veredelingsproses = Coal mine discard
- 3) Steenkoolmyn afvalgesteentes = Coal mine spoils

“Steenkoolmyn afvalprodukte” is 'n omvattende term wat beide die steenkooluitskot van die veredelingsproses sowel as steenkoolmyn afvalgesteentes insluit.

KEYWORDS

Acid Mine Drainage

Geochemical Modelling

Physico-chemical processes

Coal Mine Spoil

Coal Discard

Diffusion

Advection

Coal Mineralogy

Mineral Dissolution

Kinetic Mineral